

2023-08

Development of a Drilling Simulator to Achieve Drilling Optimization

Etaje, Darlington Christian

Etaje, D. C. (2023). Development of a drilling simulator to achieve drilling optimization (Doctoral thesis, University of Calgary, Calgary, Canada). Retrieved from <https://prism.ucalgary.ca>.

<https://hdl.handle.net/1880/116890>

Downloaded from PRISM Repository, University of Calgary

UNIVERSITY OF CALGARY

Development of a Drilling Simulator to Achieve Drilling Optimization
by

Darlington Christian Etaje

A THESIS

SUBMITTED TO THE FACULTY OF GRADUATE STUDIES
IN PARTIAL FULFILMENT OF THE REQUIREMENTS FOR THE
DEGREE OF DOCTOR OF PHILOSOPHY

GRADUATE PROGRAM IN CHEMICAL AND PETROLEUM ENGINEERING

CALGARY, ALBERTA

AUGUST, 2023

© Darlington Christian Etaje 2023

Abstract

In summary, drilling simulation, a set of physic-based models run through time or depth steps to mirror events in the drilling rig, is the backbone of all field testing of technologies or procedures. If a model has been validated using drilling simulation, the risk of wasted field trial is lowered significantly. This is why the formulation of models that make up drilling simulation is key and this is what this thesis has focused on.

20 functions were used to simulate the processes described in this research. Finite element formulation of space models linked with time-based models have been developed for the 2-node system in X (axial loading and axial torsion), Y (transverse bending of Z), and Z (transverse bending of Y) directions. Laplace transform was used to solve the time based partial differential equation paving way for the development of velocity, acceleration, force, and torque equations. Drill ahead modeling using build and walk relation to resultant forces was validated. Stick slip mitigation using the optimized RPM objective function was used to optimize the mechanical efficiency of drilling. Particle swarm optimization was the process used for optimization where each solution is considered a particle in search of the global minimum. An expression of the optimized RPM was developed and simulated with field data. Confined compressive strength of the field data was compared with the CCS obtained from the simulation but there was no perfect match yet. Further runs of the simulation would show more lessons as to how to improve the results.

It can be concluded that the MSE minimization process should rather be called MSE optimization process as the decision to raise or lower MSE should be based on the data supplied to the particle swarm optimizer since the objective function is built with constraints to lower drill string vibrations. When tested with field data, the objective function and optimizer built in this research was found to increase MSE but lower the downhole stick slip index by 28 percent. The downhole stick slip index was below 0.5.

Preface

The title of this study is “Development of a Drilling Simulator to Achieve Drilling Optimization.” This means the principles and processes that run a drilling simulator were defined and developed in this thesis; the results of these processes were then subject to optimization process to obtain better results for a certain problem in oil and gas drilling. Physics based models were the principles utilized starting from the finite element governing equations being solved to get expressions for the elemental displacements, force, and torque and other time-based variables. Once the solutions were validated, it became necessary to validate the process by comparing drilling parameters from the models to field parameters of same scenarios and they were found to be trending accordingly. This confirmation gives an opportunity to use the drilling simulation principles to tackle any drilling problem. In this case, minimizing the mechanical specific energy, MSE, was investigated. It is expected that the energy to drill will be reduced if there is no energy loss to excessive vibration. When developing the objective function for the particle swarm optimization, penalties were given to increase the optimized RPM when the stick slip limits were exceeded. This process led to a decrease in stick slip there by actualizing the MSE needed for drilling.

Acknowledgement

I would like to express my appreciation to Professor Roman Shor for his supervision, guidance, and advice throughout my studies and research work, with his endurance, knowledge and expertise that have allowed me to find success in my endeavors. I also appreciate all other professors and support staff of the department of Chemical and Petroleum Engineering.

I am very thankful for the Department of Chemical and Petroleum Engineering, University of Calgary for giving me the chance and resources to pursue my studies.

I wish to thank my family, particularly my wife, Victoria Elekwa Etaje, for their constant support and inspiration throughout my studies. I appreciate my parents, my kids, my wife's parents and siblings and all organizations I associate with in Canada and Nigeria.

Lastly, I give my thanks to Almighty God for giving me the wisdom and capability to overcome all hurdles.

Table of Contents

Abstract	ii
Preface.....	iii
Acknowledgement	iv
List of Figures	viii
List of Tables	xiii
List of Abbreviations	xiv
Chapter 1 Introduction	1
1.1 Introduction to Drilling	1
1.2 Brief Introduction to Drilling Systems.....	2
1.3 Problems During Drilling Processes and Operations.....	3
1.4 Why Drilling Simulators are Needed.	5
1.5 Relating Drilling Simulators to Optimization	5
1.6 Goal of Research	6
1.6.1 Research Questions	6
1.6.2 Outcomes and Impact of the Research	6
1.6.3 Outline of Thesis	7
Chapter 2 Literature Review	8
2.1 Lumped Parameter Model	9
2.2 Soft and Stiff String Model	11
2.3 Static and Transient Model	12
2.4 Linear and Non-Linear Model.....	13
2.5 Discrete and Coupled Model.....	15
2.6 Gap in Knowledge	17
2.7 Conclusion.....	17
Chapter 3 Modeling Well Path Designing for Drilling Simulation	18
3.1 Understanding the Minimum Curvature Method	19
3.2 Six Directions Considered for Well Path Design in a Drilling Simulator	21
3.3 Calculating Course Length as Implemented in the Drilling Simulator	22

3.4 Interpolating a Well Path.....	24
3.5 Constructing Path for Multi-Lateral Well (MLW).....	28
3.6 Practicing Well Path Design on Well 4.....	33
3.7 Conclusion.....	37
Chapter 4 Drill String Displacement Estimation Using Finite Element Method.....	38
4.1 The Governing Equation and Stiffness Matrix for Bending in the XY and XZ Planes	39
4.2 The Governing Equation and Stiffness Matrix for Axial Loading.....	47
4.3 The Governing Equation and Stiffness Matrix for Axial Torsion	50
4.4 Full Element Stiffness Matrix of 3D Beams	54
4.5 Global and Local Members of the Drill String	58
4.5.1 Unrestrained and Restrained Degree of Freedom	59
4.5.2 Switching from Bit Axis to Global Axis Using the Transformation Matrix	64
4.6 Formulas Leading to the Force and Moment Calculations	68
4.6.1 Fixed End Moments of the Drill String	69
4.6.2 Calculating Joint Load of the Drill String	70
4.7 Conclusion.....	71
Chapter 5 Optimizing the Finite Element Drilling Simulation.....	72
5.1 The Drilling Dynamics.....	72
5.1.1 Estimating the Mass Matrix and The Damping Matrix	72
5.1.2 The Time Dependent Governing Solutions for Y and Z Direction	75
5.1.3 The Time Dependent Governing Solutions for X Direction (Axial and Torsion)	80
5.1.4 Validation of the Finite Element Process	83
5.2 Torque Calculations	84
5.3 Needed Output from Finite Element Method.....	87
5.4 Coefficient of Friction Estimation.....	89
5.4.1 Graphical Representation of Coefficient of Friction While Drilling	91
5.5 Drill Ahead Modeling Based on Finite Element.....	93
5.5.1 Important Parameters for Drill Ahead Modeling	94
5.5.2 Supporting Variables for the Drill Ahead Process	97
5.6 Validation Process for the Drilling Simulation.....	98
5.6.1 CCS Validation	99
5.6.2 Acceleration Validation	100

5.7 Optimization to Reduce Energy Loss	101
5.8 Conclusion.....	102
Chapter 6 Computational Results of Drill String Dynamics.....	103
6.1 Transverse Element FEM Validation.....	105
6.2 Axial Element FEM Validation.....	109
6.2 Time Based Assembly Process	111
6.2.1 Movement Away from the Reference Point	112
6.2.2 Pull of Interest	113
6.2.3 The Finite Element Simulation Flow	115
6.2.4 Important Assembly Results	118
6.2.5 Neutral Point of Tension/Compression and Neutral Point of Bending	120
6.3 Drilling Parameter Validation	120
6.3 Downhole Measurement Validation.....	125
6.3.1 CCS Measurement	125
6.4 Drilling Forecasting Validation.....	127
6.5 Drilling Optimization Testing	133
6.6 Identifying Minimum MSE Using Particle Swarm Optimization PSO	138
6.7 Conclusion.....	147
Chapter 7 Conclusion.....	149
7.1 A Review of Drilling Simulation	149
7.2 Key Activities of the Research.....	150
7.3 Expanding the Research	151
References	153
Appendix.....	158
Appendix 1 How to Interpolate Measured Depth, Inclination and Azimuth	158

List of Figures

Figure 1. 1 Activities in the Upstream, Midstream, and Downstream Sector of the Oil and Gas Industry (Eland, 2021)	1
Figure 1. 2 Stages of the Drilling Process (Shor, 2019)	2
Figure 1. 3 Common Drilling Problems (Pegasus Vertex, 2022)	4
Figure 2. 1 A Summary of Models and Solutions for Drill String Dynamics (Pastusek, et al., 2019)	8
Figure 2. 2 Simplified Lumped Model of the Drilling System (Richardson, Germay, & Detournay, 2007)	9
Figure 2. 3 Section of the Bottom-Hole Profile Located (Richardson, Germay, & Detournay, 2007)	10
Figure 2. 4 Soft String Model Continuous Contact Phenomenon	11
Figure 2. 5 Comparing Contact Points for Soft String and Stiff String Models (Sahal & Al-Zubaidi, 2021)	12
Figure 2. 6 Well bore stability based on hydrate saturation (Wang, 2022)	14
Figure 2. 7 Processes involved in the adaptive drilling optimization system (Daireaux, et al., 2021)	16
Figure 2. 8 Advisory mode interface (Daireaux, et al., 2021)	16
Figure 3. 1 Inputs and Outputs of a Well Path Equation	18
Figure 3. 2 Comparing Well Path Inputs and Outputs Schematically	18
Figure 3. 3 Schematics for Minimum Curvature Method (Amorin & Broni-Bediako, 2010)	20
Figure 3. 4 The Six Directions of 3D Space Well Path	21
Figure 3. 5 Type I, II, & III Well Profiles for 2D Construction (Inglis, 2013)	22
Figure 3. 6 Exemplifying Key Difference Between 2D and 3D Course Length	24
Figure 3. 7 Forward Direction Azimuth Scenario	26
Figure 3. 8 Backward Direction Azimuth Scenario	27
Figure 3. 9 Schematic for Fishbone Multi-Lateral	28
Figure 3. 10 Zooming in on First Two Lateral Deviation for Fishbone	28

Figure 3. 11 Schematics for Root Shaped Multi-Lateral Well	29
Figure 3. 12 Zooming in on the First Two Laterals for Root Multi-Lateral Wells.....	29
Figure 3. 13 Deviation of Azimuth in Multi-Lateral Well.....	32
Figure 3. 14 Reverse Azimuth Change in Multi-Lateral Wells	32
Figure 4. 1 Unit Loading in Y Direction.....	39
Figure 4. 2 The Bending of a Beam	39
Figure 4. 3 Forces and Moments in a 2 Node Element.....	40
Figure 4. 4 The Boundaries of a Two Node Element	42
Figure 4. 5 Variation of Translation Interpolation Functions for 2 Node Element	44
Figure 4. 6 Variation of Rotation Interpolation Functions for 2 Node Element.....	45
Figure 4. 7 4 DOFs in Beam Element.....	45
Figure 4. 8 Unit Loading in Z Direction	47
Figure 4. 9 Axial Loading in x Direction.....	47
Figure 4. 10 Axial Boundaries of a Two Node Element.....	48
Figure 4. 11 Two DOFs in Axial Loaded Beam Element.....	50
Figure 4. 12 Axial Torsion Phenomenon.....	51
Figure 4. 13 Variations in Interpolation Functions for Axial Loads and Torsion in x Direction ..	54
Figure 4. 14 Global Axes System of the Drill String.....	54
Figure 4. 15 Global Reference Labelling of Drill String	55
Figure 4. 16 Global and Local Axis System in Drill String.....	58
Figure 4. 17 Boundary Conditions of the Drill String	59
Figure 4. 18 Assigning Member Nomenclature for Vertical Well (Xiaozhen, 2013)	60
Figure 4. 19 Labelled Drill String with Unrestrained DOF Shown.....	61
Figure 4. 20 Structural Description of Global Stiffness Matrix.....	63
Figure 4. 21 The Four Quadrants of the Global Stiffness Matrix for the Complete Structure	64
Figure 4. 22 Inclined Members of the Drill String	64
Figure 4. 23 Categorizing Total K into Unrestrained and Restrained DOF	68
Figure 4. 24 Process of Obtaining Fixed End Moments of the Drill String	69
Figure 4. 25 Process for Finite Element Drill String Dynamics Process.....	71

Figure 5. 1 Forces and Moment in Y and Z Direction.....	76
Figure 5. 2 Convergence of Displacement in Y or Z Direction.....	80
Figure 5. 3 Forces of Axial Loading in X Direction.....	81
Figure 5. 4 Convergence of Displacement in X Direction.....	83
Figure 5. 5 The Concept of Torque Losses Downhole (Beeh, 2017)	84
Figure 5. 6 Understanding the Concept of Drag (Beeh, 2017)	86
Figure 5. 7 Magnitude of Torque and Drag Based on Drilling Type	87
Figure 5. 8 Interactions Between Gravitational Pull and Tension Stretch in the Drill String (Liu, Ma, Chen, & Yang, 2018).....	87
Figure 5. 9 Steps for Calculating Normal Force from Outputs of Finite Element Method	88
Figure 5. 10 Friction Coefficient Values in Cased and Open Holes (SoftDrill NL, 2023)	89
Figure 5. 11 Steps for Calculating Friction Factor from Outputs of Finite Element Method.....	90
Figure 5. 12 Bucking and Tensile Limit Safety Windows (Brekke, 2016)	91
Figure 5. 13 Structure of the Buckling Tensile Plot	93
Figure 5. 14 Obtaining Neutral Point from Axial Forces	93
Figure 5. 15 The 3 Key Steps of The Finite Element Implementation on Drill String.....	94
Figure 5. 16 Initial Schematic of Drill Ahead Path	95
Figure 5. 17 Schematics for Resultant Force for Drill Ahead Modelling.....	96
Figure 6. 1 Diameter of BHA Used for Test Data	103
Figure 6. 2 Bit Depth vs Measured Depth of Sample Data	104
Figure 6. 3 Drilling Data for Bit Depth vs Measured Depth	104
Figure 6. 4 Series of Validation and Testing for the FEM Based Drilling Simulation	105
Figure 6. 5 Four Feet Beam Element.....	105
Figure 6. 6 Cantilever with Uniformly Distributed Load (Budynas-Nisbett, 2011).....	106
Figure 6. 7 Comparing the Actual and Trial Solutions for the Transverse Displacements	107
Figure 6. 8 Comparing the Actual and Trial Derivatives of the Transverse Displacements	107
Figure 6. 9 Residual of the Transverse Governing Equation.....	108
Figure 6. 10 Residuals for 500 and 50 Divisions of the 4ft Beam Domain.....	108
Figure 6. 11 Axial Load on a Fixed Beam.....	109
Figure 6. 12 Displacement Graph for Axial Loading	110

Figure 6. 13 Residual Plot for Axial Loading for 50, 100, and 500 Divisions	110
Figure 6. 14 The Drilling Simulation Process	111
Figure 6. 15 Calculation of Rotation, Torque and Force	112
Figure 6. 16 Effect of The Assembly Boundary Conditions on Displacements	113
Figure 6. 17 Displacement from Reference Location	115
Figure 6. 18 Simulation Flow Chart for XYZ Finite Element Modeling	116
Figure 6. 19 Time Adjusted Displacements, Torques, and Forces	117
Figure 6. 20 Displacement Values for Transverse Y Direction.....	117
Figure 6. 21 Displacement Values for Transverse Z Direction	118
Figure 6. 22 Displacement Values for X Direction—Loading, Torsion.....	118
Figure 6. 23 Global Number of the Drill string	119
Figure 6. 24 Identifying Actual Drilling in Inclination Azimuth Plot	120
Figure 6. 25 Plot of Drilled Path vs Well Plan	121
Figure 6. 26 Initial Values of the Field Data	121
Figure 6. 27 Measured Hookload vs Calculated Hookload	122
Figure 6. 28 Impact on Weight on Bit on Hook load during Simulation.....	123
Figure 6. 29 Forces and Torques in Axial Nodes	123
Figure 6. 30 ROP Calculated vs ROP Data	124
Figure 6. 31 Measured Depth from Data vs Axial Translation from Simulation	124
Figure 6. 32 Effect of Rotational Speed on Surface Torque	125
Figure 6. 33 Calculated CCS vs CCS from Data	126
Figure 6. 34 MSE vs CCS vs Depth	127
Figure 6. 35 Plot of Azimuth Differential vs Inclination Differential	127
Figure 6. 36 Forces in X, Y, and Z Directions.....	128
Figure 6. 37 Comparing XYZ Forces with WOB.....	129
Figure 6. 38 Comparing the Resultant Force with WOB.....	129
Figure 6. 39 Torques in X, Y, and Z Directions	130
Figure 6. 40 Comparing XYZ Torques with Surface Torque.....	130
Figure 6. 41 Comparing Resultant Torque to Surface Torque.....	131
Figure 6. 42 Perfection of Inclination Predicted Compared with Field Data	132
Figure 6. 43 Perfection of Azimuth Predicted Compared with Field Data.....	132

Figure 6. 44 Boundary Conditions Illustration for MSE Minimization.....	135
Figure 6. 45 Optimized RPM vs Length of BHA Component	137
Figure 6. 46 Depth of Cut Effect on RPM	138
Figure 6. 47 Drilling Vibration Severity Snapshot (Dushaishi, Nygaard, Hoel, Andersen, & Hellvik, 2015)	138
Figure 6. 48 Formula for Mean of Datapoints Per Stick Slip Severity	139
Figure 6. 49 Behavior of Stick Slip Severity at 0.5, 1.0 and 1.5 Levels	140
Figure 6. 50 Effect of Penalties in the Objective Function on Optimized RPM	141
Figure 6. 51 Surface Plot of Optimized RPM and Stick Slip Index	142
Figure 6. 52 Increasing Optimized RPM with Increasing RPM Input	142
Figure 6. 53 Effect of Depth of Cut on DSSI	143
Figure 6. 54 Looping the PSO and the Optimized RPM Objective Function.....	143
Figure 6. 55 Pseudo Code for Particle Swarm Optimization.....	144
Figure 6. 56 Comparing RPM from Data to RPM Recommended by the Optimization Process.....	145
Figure 6. 57 Comparing ROP from Data to ROP from Optimization Process	146
Figure 6. 58 Comparing MSE from Data and MSE from Optimization Process	146
Figure 6. 59 Proof of Reduction in Stick Slip Vibration	147
Figure 6. 60 List of Functions Needed for Simulation and Testing.....	148
 Figure 7. 1 Relations Between Drilling Simulation and Drilling Field Testing	 149
Figure 7. 2 An Overview of Drilling Simulation.....	150
Figure 7. 3 Six Node System	152

List of Tables

Table 3. 1 Inputs Needed to Calculate 2D Well Profile Types.....	23
Table 3. 2 Generic Form for a Build Only Well.....	30
Table 3. 3 Main Lateral Data	30
Table 3. 4 Lateral 1 Data.....	31
Table 3. 5 Lateral 2 Data.....	31
Table 3. 6 Lateral 3 Data.....	31
Table 3. 7 Lateral 4 Data.....	31
Table 3. 8 Total Well Path for Lateral 4	33
Table 3. 9 Summary of Data for Well 4 and its Laterals	34
Table 3. 10 Well 4B Data Summary Sheet.....	34
Table 3. 11 Unknown Azimuth in Well 4B Data.....	35
Table 3. 12 Error in Azimuth Calculation in Well 4B Data	35
Table 3. 13 Error in Measured Calculation in Well 4B Data.....	36
Table 3. 14 Error in Measured Depth Calculations for Well 4B	36
Table 4. 1 Boundary Conditions Table for 2 Node Element	42
Table 4. 2 Expressions of Interpolation Functions for Linear 2 Node Beam	43
Table 4. 3 Axial Loading Boundary Conditions Table for 2 Node Element	49
Table 4. 4 Axial Loading Expressions of Interpolation Functions for Linear 2 Node Beam	49
Table 4. 5 Axial Torsion Boundary Conditions Table for 2 Node Element	52
Table 4. 6 Axial Torsion Expressions of Interpolation Functions for Linear 2 Node Beam	52
Table 4. 7 Displacement Labelling for 4 Independent Processes of 3D Beams	55
Table 4. 8 Process Per Row of 12 by 12 Stiffness Matrix for Drill String	56
Table 4. 9 Expressions of Stiffness in 3 D 12 by 12 Matrix	57
Table 4. 10 Connectivity Matrix for the Vertical Well Example	62
Table 4. 11 Input for Each Member for Stiffness Matrix Calculation.....	62
Table 4. 12 Connectivity Matrix for the Inclined Well Example	65
Table 4. 13 Generic Output for Stiffness Matrix Calculation for Each Member of the Inclined Well	65

Table 5. 1 Generic Output for Stiffness Matrix Calculation for Each Member of the Vertical Well	92
Table 5. 2 Formulas for Supporting Variables to Drill Ahead Process	98
Table 6. 1 Simulation Baseline Downhole Stick Slip Severity	139

List of Abbreviations

S/NO	Abbreviations	Full name
1	BHA	Bottom Hole Assembly
2	PID	Proportional Integral Derivative
3	WOB	Weight On Bit
4	RPM	Revolution Per Minute
5	ROP	Rate of Penetration
6	CCS	Concise Compressive Strength
7	MSE	Mechanical Specific Energy
8	MD	Measured Depth
9	RF	Ratio Factor
10	TVD	Total Vertical Depth
11	KOP	Kick-Off Point
12	DLS	Dog Leg Severity
13	ICP	Intermediate Closing Point
14	FEM	Fixed End Moment
15	DOC	Depth of Cut

Chapter 1 Introduction

1.1 Introduction to Drilling

Crude oil is made up of hydrocarbons, non-hydrocarbons, and other trace elements stored deep below the subsurface. The oil and gas industry is divided into 3 portions. The upstream, the midstream and the downstream are the 3 portions that categorize the operations in the oil and gas industry. Figure 1.1 below shows what each port of operations entails.

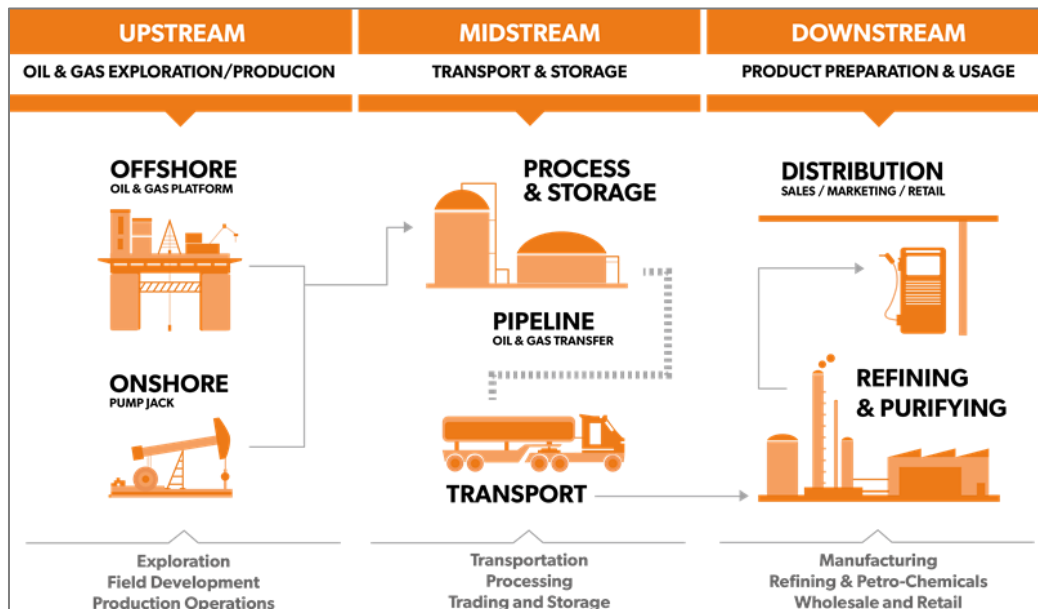


Figure 1. 1 Activities in the Upstream, Midstream, and Downstream Sector of the Oil and Gas Industry (Eland, 2021)

Drilling operations fall under the upstream sector. Drilling is a process whereby a hole is bored using a drill bit to create a well for oil and natural gas production (StudentEnergy, 2022). Figure 1.2 shows the different stages of the drilling process. The act of exploration for oil and gas is done by drilling a well with drilling tools such as a drill pipe attached to a Bottom Hole Assembly (BHA) in addition to various survey methods – geological, magnetic, gravitational, and seismographic. This BHA includes some specialized drilling tools for taking measurements while drilling, drill bit to cut through the rock, steering control, and vibration management. The drill string is made to follow a trajectory called a well path which is planned to target a particular oil-

rich zone (Okpозol, Peters, & Okologume, 2016). Drilling is the most sought and appropriate method to extract oil and gas from deep formations.

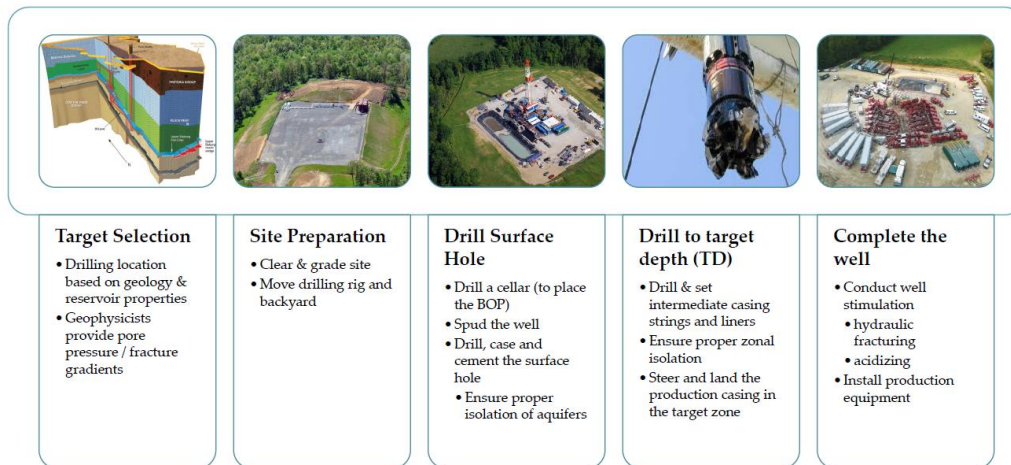


Figure 1. 2 Stages of the Drilling Process (Shor, 2019)

However, drilling is quite expensive with up to \$455,000 effective day rate – the daily cost of drilling an oil well, which includes the cost to run the rig, employees, and supplies (Hargrave, 2022). Specifically, the daily rate of drilling a well depends on the rig type, distance from shore, drilling depth, and water depth. Onshore drilling rates range from \$60,000 to \$310,000 per day while offshore drilling can cost between \$600,000 to \$800,000 per day (Hossain, 2015)

1.2 Brief Introduction to Drilling Systems

There are two categories of drilling systems: rotary methods and rotary percussive (Franca, 2011). This thesis focuses on the rotary method which is commonly used in the oil and gas industry. Rotary drilling utilizes high levels of torque supplied by a surface top drive motor to rotate a drill-bit attached to the end of a drill pipe to bore through the rock formation. Boring of wells is accomplished using a variety of rig types – land and offshore. Land rigs are sub-divided into mobile and conventional rigs. Offshore rigs include floating rigs (semi-submersible, drill ship) and bottom supported rigs such as platform, barge, and jack-up (DrillingManual, 2017).

Offshore wells are done by drilling using a drill string lowered (drill string consists of a drill-pipe, drill bit, and drill collar) via a conduit (riser) that extends from the drilling rig to the seafloor

(Sparks, 2007). Onshore drilling is similarly drilled using a drill string, but while offshore drilling involves extraction of oil from the seabed, onshore drilling encompasses the drilling operations into the Earth's subsurface from a land-based drilling platform. Systems of a drilling rig can be categorized into the: power system, well monitoring system, hoisting system, circulating system, rotating system, well control system, and monitoring system (offshore). The power system supplies the power to the entire drilling rig using AC or DC generators. The hoisting system oversees lowering or lifting the drill pipe onto borehole using masts and draw works. The rotating system provides torque to the drill string from the rotary table and top drive motor. The circulating system includes the mud pits, reservoirs, and mud pumps that provide cooling, lubrication, and rock cuttings disposal from the bore hole. Lastly, the well control and monitoring systems maintain operational limits in drilling such as the controlled release of well fluids, bleed pressure, chokes, and manifolds. In general terms, offshore drilling and onshore drilling operations are almost the same in function, but each process is made to solve the local condition of the well.

1.3 Problems During Drilling Processes and Operations

The drilling process involves drilling from the surface to the target depth. When the drill string needs to be retrieved, a tripping out process is applied, just hoisting up the entire drill string components stand by stand. For the next set of drilling to occur, the drill string is lowered or tripped into the wellbore till the current depth of the hole. At that point, drilling occurs again which rotating the bits while applying weight on the bit through the formation. There are potential stuck pipe problems when tripping out due to the drag that will be developed when the drill string rubs the wall of the hole. This drag adds to the weight of the drill string making it more difficult to pull the drill string. During drilling, the torque necessary to turn the drill string will increase as the drill string comes in contact with the wall of the wellbore make it more difficult to turn the drill string. This could lead to a twist-off. Twist-off is a disconnection of the pipes when excessive torque occurs or fatigue of the pipes.

Drilling operations lead to high costs during the development of oil and gas fields. Factors that lead to high costs include major disasters during the drilling operation such as a blowout – the uncontrolled release of oil or gas from a well. In addition to catastrophic failures, it is common to see drilling problems during operation – pack-offs, formation fracturing, pipe-sticking, loss of

circulation, hole deviation, pipe failures, borehole instability, and complications that arise from hole cleaning (Bradford, 2000). Most of these problems are highlighted in Figure 1.3.

Drilling operations are also affected by various types of vibrations – axial, lateral, and torsional. These vibrations induce problems such as bit-bounce, whirling, and stick-slip respectively. Vibrational problems cause damage to the BHA, result in inaccurate downhole readings, and lead to sub-optimal rates of penetration.

Difficulty in drilling operations can also be attributed to wellbore problems – borehole instability, formation damage, lost circulation, pipe sticking, kicks, hazardous gas, and shallow gas. Borehole instability occurs when an undesirable condition of an open hole interval does not maintain its gauge size, shape, and structural integrity. Formation damage is defined as the disruption of the reservoir (reduced production) triggered by wellbore fluids used during the entire drilling process. The permeability is reduced in the wellbore (skin) vicinity due to foreign-fluid invasion into the reservoir rock.

Hole cleaning is the drilling fluid's ability to transport and suspend drilled cuttings. Inadequate hole cleaning can lead to mud problems and contamination. Contamination, more commonly seen in water-based muds, causes a change in mud properties that lead to improper mud mixture.



Figure 1. 3 Common Drilling Problems (Pegasus Vertex, 2022)

Mud contamination can result from overtreatment of the mud system with additives or material entering the mud during drilling. Some of these problems arise due to the inherent complexity of

the environment/location of petroleum resources. They may also be a result of increased deviated hole drilling (eccentricity effect) and power requirements for adequate fluid circulation when removing drill cuttings. (Aryan, 2018)

1.4 Why Drilling Simulators are Needed.

Drilling simulation aids in the enhancement of drilling performance and productivity by simulating and predicting the problems encountered during a drilling operation effectively, which consequently improve personnel safety, optimum drilling performance, and productivity. Drilling simulation involves mimicking the behavior of drilling processes or systems. Therefore, the act of drilling simulation should be able to provide actionable information about drilling processes and systems without the physical action of sound construction (Harvey, 2018). Drilling simulations are effective ways to pre-emptively identify and locate potential disasters. Simulators also address the impacts of drilling phenomena like drill string dynamics. Simulators consider the fact that the drill string passes through various formations of different physical properties and is well immersed in the drilling fluid and remains in contact with the wellbore.

However, while new drilling simulations are being developed with state-of-the-art simulation technology, better hardware and software do not guarantee the successful application of a drilling simulator to improve drilling performance. Only the understanding of proper drilling operations, formation and equipment limitations can lead to the success seen in other industries.

1.5 Relating Drilling Simulators to Optimization

With the associated costs detailed in the previous sections about the economic impacts and expenses with drilling operations, optimization has become paramount and one of the leading drivers towards the development of drilling simulations. Drilling optimization mainly dictate the identification of optimum drilling parameters, processes, or equipment to achieve low vibration stable drill-string operation, effective well path trajectory, optimum directional steering recommendations, downhole tool reliability, and many more that may reduce the effective day rates of operation and increase productivity.

Drilling simulation is heavily bonded with the need to optimize drilling operations as evidenced by past and existing works being done today. (Herbig, et al., 2016) for instance, shows that

complex reaming operations can be optimized through post-well analysis using simulation and modeling techniques. The design of BHA reamers is optimized for lateral vibrations in (Najmi, et al., 2015). Optimizations have also been performed beyond the surface and down hole parameters to include personnel, project coordinators, operators, and analysts to assist in the set-up and management of a drilling project. (Hanley, Stuart, Bass, & Garcia, 2012)

1.6 Goal of Research

The goal of the research is the implementation of finite element method to drill string dynamics so that drilling operation parameters can be calculated through the finite element process. This process forms the basis for the development of a drilling simulator and consequently the trial of newer models on the simulator before field tests are done.

1.6.1 Research Questions

There are four questions that will be answered from this research.

- a. How to solve the governing equation of the finite element of 12 degree of freedom beam.
- b. How to relate the solved finite element model with drilling parameters to achieve both space and time-based simulation of drilling.
- c. How to develop a process to minimize mechanical specific energy using particle swarm optimization.
- d. Validate the finite element models, the drill ahead model, drilling parameter prediction and drilling vibration mitigation.

1.6.2 Outcomes and Impact of the Research

The outcomes of the research are estimation process of the outputs from the finite element method in a way that clearly relates to the drilling process. Here are those outputs:

- Stiffness coefficients for each element on a local and global scale. This leads to estimation of the global stiffness matrix for the entire drill string at an instance in time.
- Estimation of unrestrained stiffness matrix and the unrestrained displacements.
- Estimation process for the fixed end moments and the global end moments of the drill string

The impact of the research is that this thesis has set up a procedure to help mitigate stick slip. The same procedure can be followed to mitigate whirling in isolation or coupled with stick slip. The challenge in this is to fully model the behavior of the BHA as whirling occurs. A start point is to simulate the movement of the drill string from the perspective of the sensor placed on a position on the BHA.

It is a known fact that the error of the finite element model reduces as the order of the element increases. This thesis focused on linear nodal system, a two-node system. This means each element has only two nodes. This is potentially the reason why in Figure 6.8 to Figure 6.13 show the residuals having errors above 20 % even though the solution has less than 2 percent error. A higher order nodal system is needed. This thesis has laid the groundwork to build more nodes in each element of the drill string.

1.6.3 Outline of Thesis

Chapter 1 provides an overview of the thesis, introducing the background and motivation for studying drill string dynamics. It outlines the objectives and scope of the research, as well as the organization of the thesis. Chapter 2 presents a comprehensive literature review on drill string dynamics, covering various aspects such as drilling mechanics, wellbore stability, and vibration analysis. It discusses the existing theories, models, and methodologies in the field. Chapter 3 focuses on interpolation of azimuth for accurate simulation of movement of the drill string. Chapter 4 discusses the governing equations for the finite element modeling of a 2 node 3-dimensional system leading to the development of the interpolation functions for axial (loading and torsion) for X direction and transverse bending for Y and Z directions. Chapter 5 presents the use of the outputs of the finite element process to calculate normal force and friction factor. An introduction into the particle swarm optimization approach is done. Chapter 6 presents the computational results obtained from the drilling simulation. This chapter shows how the objective function for the optimized RPM is developed and also shows how reduction in stick slip can be incorporated into the objective function. Chapter 7 concludes the thesis by summarizing the key findings and contributions. It discusses the limitations of the research and suggests directions for future work, such as refining the increasing the number of nodes per element in the finite element model. Preliminary equations for higher order node system are shown.

Chapter 2 Literature Review

This chapter focuses on the literature review, starting with a discussion of previous works and models used in drilling simulations. A discussion on how the models is solved and their applications in optimizing drilling operations is provided. First, an overview of the existing drilling models in Figure 2.1.

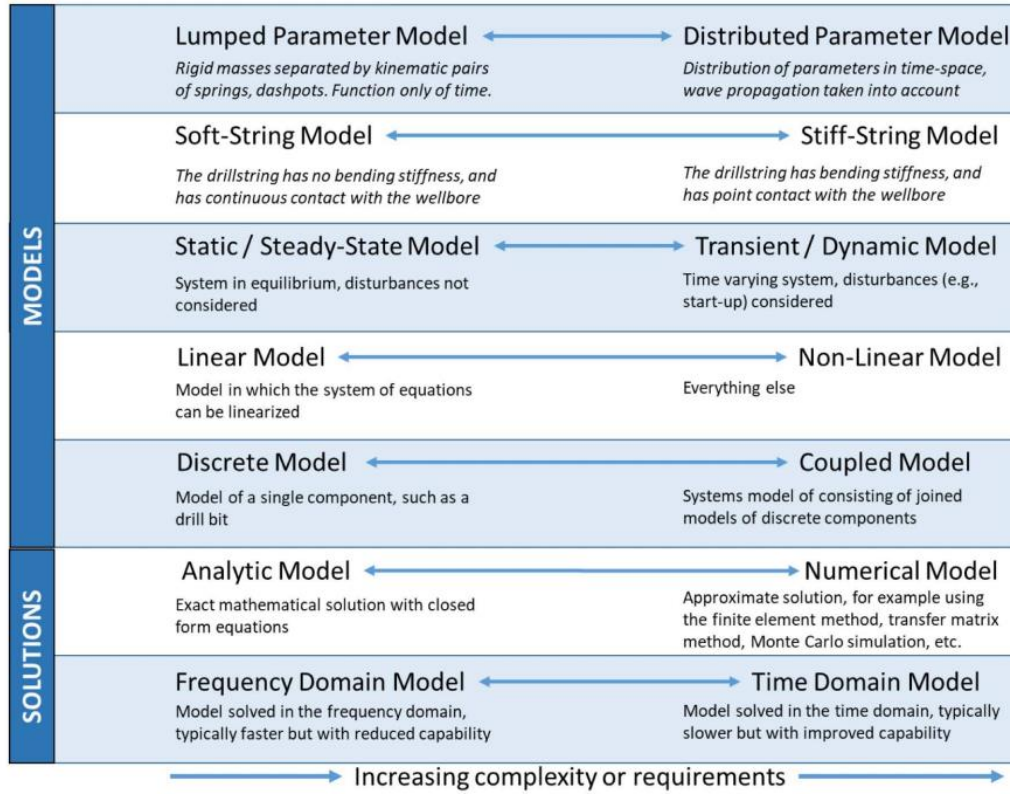


Figure 2. 1 A Summary of Models and Solutions for Drill String Dynamics (Pastusek, et al., 2019)

In general, each of these models have their uses and different ways the data used in them are sourced and sensed. Both soft string and stiff string models help in predicting the normal loads between the drill string and inner casing wall to help reduce wear on the casing (Samuel, Kumar, Gonzales, Marcou, & Rød, 2016). The source of data for those models are The BHA components data and the wellbore geometry data. The components data can be gotten before the drilling from the well plan data or in real time from surface measurement tools. The continuum from lumped parameter model (LPM) to distributed parameter model (DPM) is an example of a modeling dichotomy (see (Pastusek, et al., 2019)). Other characteristics are Linear to Non-Linear Models,

Static to Steady State to Transient Models; all of these models are useful in specific situations (for example, see (Aarsnes, Flø, Meglio, & Shor, 2018)).

2.1 Lumped Parameter Model

A lumped parameter model considers rigid masses separated by kinematic pairs of springs and dashpots. This model, which is the most commonly used in the analysis of drill string, drill pipe, and BHA, is a function only of time. Richardson et. al published a study on the self-excited torsional and axial vibrations of deep drilling systems using a discrete model and discrete state-dependent delay governing equations (Richardson, Gernay, & Detournay, 2007). In the 2-degrees-of-freedom lumped model shown in , the drilling system is consolidated into a series of spring and dashpot, allowing the drill bit to move parallel to the vertical direction and rotate around the axial direction.

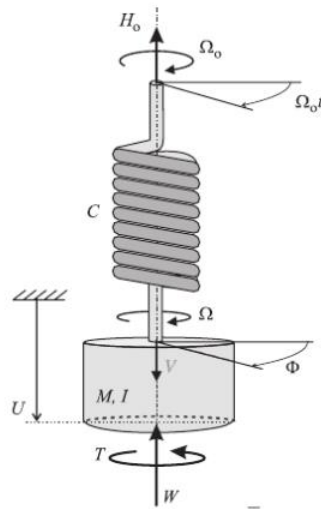


Figure 2. 2 Simplified Lumped Model of the Drilling System (Richardson, Gernay, & Detournay, 2007)

The cutting action of the drill bit and the friction due to the contact between the well bore and wear flat areas, are assumed to be the sole producers of the forces acting on the bit. The cutting forces are proportional to the height of the rock formation ahead of the cutter – whose rotation introduces a state-dependent delay in the governing equations (Depouhon & Detournay, 2015).

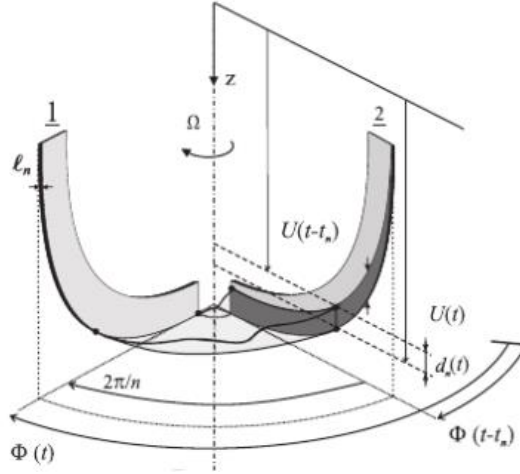


Figure 2. 3 Section of the Bottom-Hole Profile Located (Richardson, Germy, & Detournay, 2007)

Richardson et. al derived the following governing equations:

$$\ddot{u} \in n\psi \left(\tilde{u} - u - \alpha_o(\tilde{\phi} - \phi) + g(\dot{u}) \right) \quad \text{Equation 2. 1}$$

$$\ddot{\phi} + \phi \in n \left(\tilde{u} - u - \alpha_o(\tilde{\phi} - \phi) + \beta g(\dot{u}) \right) \quad \text{Equation 2. 2}$$

Where \ddot{u} and $\ddot{\phi}$ are the axial perturbations and angular displacement of the bit

$$\tilde{u} \text{ is the delayed argument } (\tilde{u} = u(t - t_n)) \quad \text{Equation 2. 3}$$

t_n is the delay or the time required for the bit to rotate an angle of $2\pi/n$

$$t_{n0} \text{ is the steady state delay } (t_{n0} = 2\pi/n\omega_0) \quad \text{Equation 2. 4}$$

ω_0 is the steady state rotation speed.

n is the number of blades.

β is the bit wear or bluntness.

α_o is the ratio between steady state axial and angular velocities.

The delay t_n is defined by,

$$\tilde{\phi} - \phi = \omega_0(t_n - t_{n0}) \quad \text{Equation 2. 5}$$

This 2-DOF lumped parameter model of the drilling system is used to analyze vibrational instabilities – stick slip and bit bouncing. The model is systems of equations are solved analytically and are key contributors towards optimizing a stable (reduced oscillation) directional drilling.

2.2 Soft and Stiff String Model

The first work done on drill string dynamics, particularly torque and drag, was published by Johancisk et. al in 1984. This has served as the foundation for successive works and research that has led to the development of soft and stiff string models to formulate drill string behavior.

The soft string model assumes that the drill string has no bending stiffness, and that it has continuous contact with the well bore (Menand, et al., 2006). In addition to the bending stiffness, this model also neglects tubulure stiffness and the effects of radial clearance.

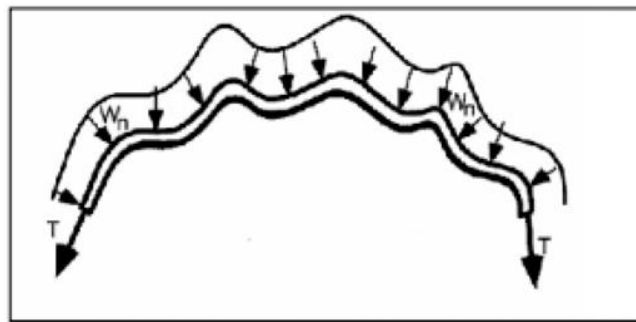


Figure 2. 4 Soft String Model Continuous Contact Phenomenon

In contrast, the stiff string model considers that the drill string has bending stiffness and that it has point contact with the well bore. In sections of higher well path curvature, there is correspondingly more contact points between the drill pipe and the bore wall, while straighter sections reduce wall contact forces (Menand, et al., 2006). In some cases, stiff string model assumption is preferred over soft string, especially for well path trajectories that have high tortuosity and dog leg severity, in order to accurately provide a realistic analysis of the loads and stresses acting on the drill string.

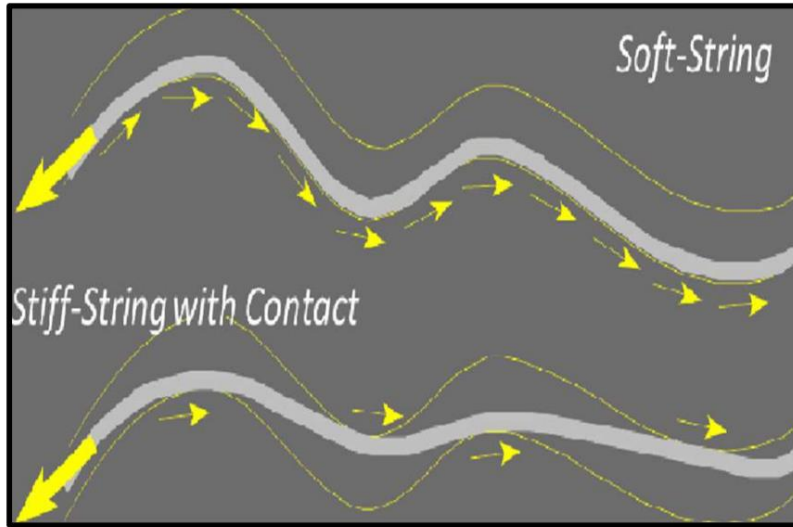


Figure 2. 5 Comparing Contact Points for Soft String and Stiff String Models (Sahal & Al-Zubaidi, 2021)

In 2021, Ohia et. al performed a comparative study of the soft string and stiff string models in torque and drag analysis. The comparison was made using a torque and drag drilling simulation software and conventional survey data, performed in both the conventional 90 to 100 ft intervals, and continuous 1 to 5ft intervals. They concluded that in order to use the stiff string torque and drag model on a highly deviated well, a high-resolution continuous survey must be used to capture the effects of doglegs and tortuosity in the well path.

The stiff string model provides not only a comprehensive analysis on drill string dynamics, but also a way to implement optimization in drilling. A stiff string casing and fluid displacement simulator was developed in 2019 to design and optimize cement jobs for various well bore configurations (Bogaerts, et al., 2019). Through the model and displacement simulator, they were able to optimize the placement of the centralizer subs and provide the best cement job design that forecasts possible challenges and contingencies to meet the design and well plan objectives.

2.3 Static and Transient Model

The static or steady state modeling of drilling systems is a model in which systems are assumed to be in equilibrium, and that the disturbances are not considered. This model was first introduced by (Gilbert, 1954) and (Mach, Proano, & Brown, 1979) who further popularized static modeling with the Nodal Analysis™ used in the and diagnosis of flow performance in a well bore for multi-phase

systems in steady-state conditions. This model combines constituents of the system to provide an estimation for production rates. The nature of the flow for drilling operations in practice is always in transient phase, therefore making the steady-state model inadequate to provide analysis on flow behavior that causes flow instability and mud/hole cleaning problems (Ashfahani, Sulistiyo, & Hapsari, 2020).

2.4 Linear and Non-Linear Model

A linear model is a model in which the systems of governing equations can be linearized. (Wang, 2022) published a paper on the simulation of well bore integrity during drilling wherein a linear Mohr-Coulomb criterion is used to define well bore instability. The governing equations of equilibrium temperature and pressures are linearized as:

$$T_e = Ap(r, t) \quad \text{Equation 2. 6}$$

$$p_e = T(r, t)/A \quad \text{Equation 2. 7}$$

Resulting in,

$$\frac{\bar{p}}{p_w} = \frac{K_o(\tau_2 r)}{sK_o(\tau_2 a)} - \frac{1}{1-\frac{c}{c_o}} \frac{c' T_w}{p_w} \frac{K_o(\tau_1 a)}{s \left[K_o(\tau_1 a) - \frac{\lambda \tau_1 K_1(\tau_1 a)}{h_w} \right]} \left[\frac{K_o(\tau_2 r)}{K_o(\tau_2 a)} - \frac{K_o(\tau_1 r)}{K_o(\tau_1 a)} \right] \quad \text{Equation 2. 8}$$

$$\frac{\bar{T}}{T_w - T_o} = \frac{K_o(\tau_1 r)}{s \left[K_o(\tau_1 a) - \frac{\lambda \tau_1 K_1(\tau_1 a)}{h_w} \right]} \quad \text{Equation 2. 9}$$

Where \bar{p} is the average equilibrium pressure.

\bar{T} is the average temperature.

K is the intrinsic reaction rate constant.

a is the volumetric thermal expansion.

λ is the thermal conductivity.

A is the specific area available for reaction.

r is the borehole radius.

The linear correlation developed by Wang in this model allows for the thermal-hydraulic equations to be solved analytically under the assumption that there is a constant bottom hole pressure and constant heat flux (Wang, 2022). The hydrate saturation effect on cohesion and well bore stability is shown in Figure 2.6.

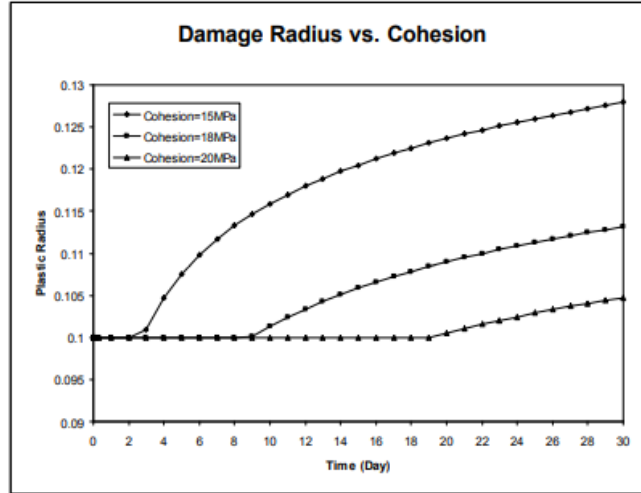


Figure 2. 6 Well bore stability based on hydrate saturation (Wang, 2022)

All models that do not utilize linearized systems of equations fall under non-linear models. (Reza & Alcocer, 1986) published a work on a computer simulation well drilling based on a non-dimensional non-linear mathematical model that utilizes Buckingham Pi theorem. The assumption made is that “the 3 sets of models depend on is the need to know how many dimensionless groups will constitute a complete set since dimensional analysis was in use.” The parameters include the ROP, rate of bit wear, WOB, RPM, fluid flow rate, bit and nozzle diameter, fluid properties, pressure, temperature, and heat transfer coefficient. The paper shows that the developed non-linear model yields realistic and accurate representation of deep well drilling processes and problems. The following non-linear equations were derived from (Reza & Alcocer, 1986).

The final form of the ROP is given by,

$$\frac{\dot{F}}{Nd} = 0.33 \left[\frac{Nd^2}{v} \right]^{0.43} \left[\frac{Nd^3}{Q} \right]^{-0.68} \left[\frac{Ed}{W} \right]^{-0.91} \left[\frac{pd}{W} \right]^{-0.15} \quad \text{Equation 2. 10}$$

The final form of the bit dulling rate equation is given by,

$$\frac{\dot{D}}{ND} = 0.001 \left[\frac{Q}{ND^3} \right]^{0.56} \left[\frac{W}{ED^2} \right]^{0.26} \left[\frac{D}{Q} \right]^{-0.03} \quad \text{Equation 2. 11}$$

The final form of bearing life equation is given by,

$$\frac{\dot{B}}{N} = 0.05 \left[\frac{thd}{WN} \right]^{0.51} \left[\frac{\nu}{Nd^2} \right]^{0.4} \left[\frac{Q}{Nd^3} \right]^{-0.5} \quad \text{Equation 2. 12}$$

Where \dot{F} is the rate of penetration (ft/min)

\dot{D} is the bit tooth dullness (fraction of original tooth)

\dot{B} is the bearing wear fraction of the total life.

N is the rotary speed (RPM)

d is the bearing diameter (in)

ν is the drilling fluid kinematic viscosity (cp)

Q is the volumetric flow rate (gal/min)

W is the WOB (lbs)

E is the rock hardness (psi)

p is the differential pressure (psi)

D is the bit diameter (in)

The oversimplification of linearized models implies that there is a need to assume that displacements are small and there are small contact points between the drill string and the wellbore (Wilson & Heisig, 2015). The nonlinear models are more realistic about the occurrence while drilling even though most events are difficult to model. The nonlinear models accommodate excitement from mud motors, bits, and also include velocity dependent Stribeck friction relation sometimes (Wilson & Heisig, 2015).

2.5 Discrete and Coupled Model

Discrete models focus on a particular aspect or component of the drilling system. Depouhon et. al performed a study on the stick slip instabilities in rotary drilling systems by using a discrete model of a drill string (Depouhon & Detournay, 2015). The paper concludes that the steady-state response of the discrete model drill string is stable for rotational speed greater than a given critical speed.

Coupled models consist of joined models of discrete components. Daireaux et. al developed a testing and validation of an adaptive drilling optimization system. The system is developed using a simulated environment and the adaptability is achieved by combining two independent processes – a physical model that updates an estimate of the bit-rock interaction in response to changes in drilling parameters, and a cuttings transport model that maintains the effects of the drilling parameters with respect to their safety constraints (Daireaux, et al., 2021). The model has been successfully used as an optimization program that provides set-point recommendations to the driller and as an integrated module in an automated drilling system.

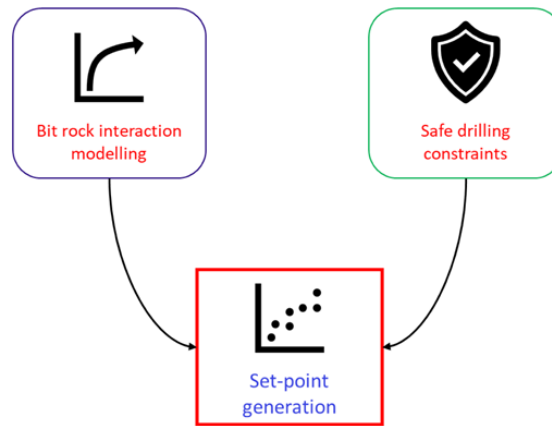


Figure 2. 7 Processes involved in the adaptive drilling optimization system (Daireaux, et al., 2021)



Figure 2. 8 Advisory mode interface (Daireaux, et al., 2021)

The models discussed in the previous sections are solved in two ways – analytical and numerical. The analytical method of solving the models involves using the derived governing equations and substituting all known values to calculate unknown parameters. The numerical approach involves using computer power and numerous numerical methods to iteratively solve unknown parameters. Each solution can either be in the time domain, which is typically slower but with improved capability (derivatives, ODE, PDE), or frequency domain which is comparatively faster but with reduced capabilities.

2.6 Gap in Knowledge

Solving finite element models for different topics in engineering are common but solving them to fit the drilling process is vaguely available. This thesis goes from the governing equation to develop a space and time-based solution to calculating displacements as forces and torques are applied on the drill string. The research goes further to show the procedure to optimize mechanical specific energy using particle swarm optimization after developing an optimized RPM objective function for mitigating stick slip mechanism while drilling.

2.7 Conclusion

The previous research on drilling simulation shows that many mathematical models have been developed to imitate drill-string behavior such as the DOF and the lumped-parameter model – which is the most used and straight forward model. Further models in literature include the distributed parameter model, soft and stiff string model, static/steady state model, transient/dynamic model, linear and non-linear model, discrete model, and coupled model. Models observed in literature are solved either analytically or numerically in both frequency and time domains. Optimization through the use of models and simulation in drilling proves to be significant in enhancing efficiency, safe drilling, and in arresting non-productive time (NPT) such as lost circulation, stuck pipe, hole cleaning, ROP, and measurement while drilling.

Chapter 3 Modeling Well Path Designing for Drilling Simulation

The well path sits at the core of the drilling process. The well path is the direction along the formation that the well is being drilled through. In terms of drilling simulation, the numbers that make up the well path are very important as it inputs into several models that define the drilling dynamics. Figure 3.1 below shows the inputs and outputs of a well path design system.

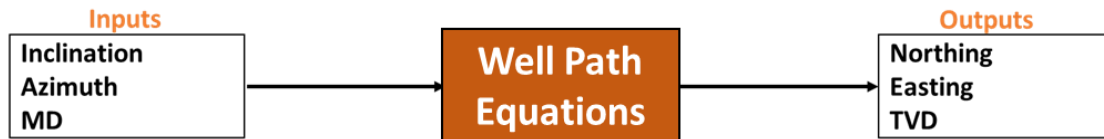


Figure 3. 1 Inputs and Outputs of a Well Path Equation

The inclination is the angle of vertical deviation from the vertical axis of the well path. The azimuth is the angle of horizontal deviation from the north of the well path. MD is the measured depth along the well path at every instant of measurement. With these 3 parameters, it is locating a certain point on the 3-coordinate system of the well path. In order to plot the well path on a 3-sided cartesian plane, the Northing, Easting and TVD are needed instead.

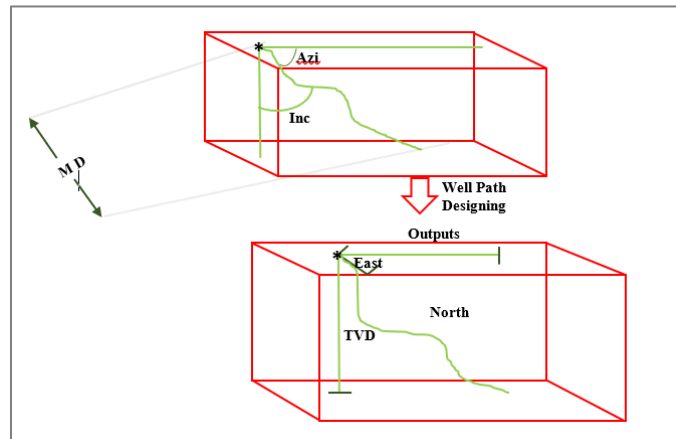


Figure 3. 2 Comparing Well Path Inputs and Outputs Schematically

From Figure 3.2, one can notice the visible difference in the measurements of Northing and Easting from inclination and azimuth. Well design modeling is the process of converting the inputs

(inclination, azimuth, and MD) to the outputs (Northing, Easting, and TVD). There are 6 methods modeling the well path:

1. **Tangential method** is the least accurate, it assumes a straight line well path taking into consideration the inclination and azimuth at upper survey station and lower station is not accounted.
2. **Balanced Tangential Method** takes into account the upper and lower survey station and approximates well path by two equal straight-line segments. The upper line segment is defined by inclination and azimuth at upper survey station and the respective values at lower survey station.
3. **Average Angle Method** assumes one straight line defined by averaging inclination and azimuth at both survey stations, intersects both upper and lower survey stations.
4. **Radius of Curvature Method** assumes that well path is not a straight line but a circular arc tangential to inclination and azimuth at each survey station.
5. **Minimum Curvature Method** is the most accurate, it further adds a Ratio Factor to smoothen the spherical arc formed by using radius of curvature method. This is the most practically used and accepted calculation method.
6. **Splines Method** are calculated based on conditions such as free end, set end, free inclination/set azimuth, and set inclination/free azimuth. The resulting trajectories are best for point-the-bit and push-the-bit systems due to their smooth continuous functions (Liu, Shor, & Park, 2019) (Sampaio, 2007).

3.1 Understanding the Minimum Curvature Method

As expected, the inputs are inclination, azimuth, and measured depth. The model also inputs Ratio Factor (RF) which is used to smoothen the spherical arc of the well path. Beta (β) is the dogleg angle which is the change in angle (direction) of the wellbore in a 3-dimensional space.

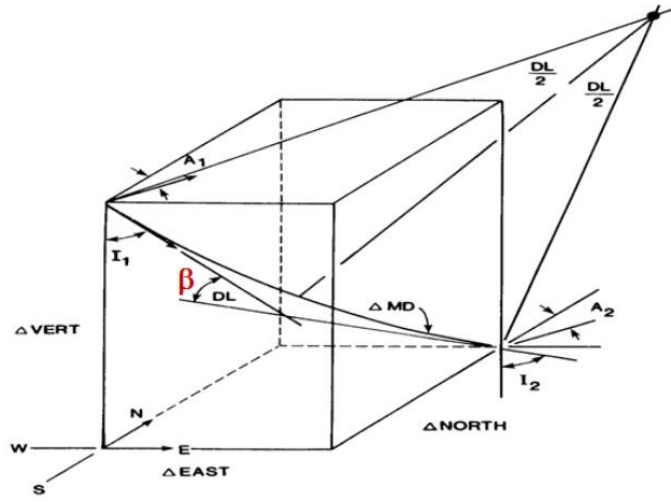


Figure 3. 3 Schematics for Minimum Curvature Method (Amorin & Broni-Bediako, 2010)

$\beta = DL \rightarrow$ Dogleg Angle, degrees

$I_1 =$ Inclination at survey point 1, degrees

$I_2 =$ Inclination at survey point 2, degrees

$A_1 =$ Azimuth at survey point 1, degrees

$A_2 =$ Azimuth at survey point 2, degrees

$\Delta Vert = TVD =$ Total Vertical Depth, ft

$\Delta East =$ Easting, ft

$\Delta North =$ Northing, ft

$MD =$ Measured Depth, ft

The minimum curvature calculation is implemented usually between two survey points.

The formulas that govern the minimum curvature method are as follows.

$$\Delta North = \frac{MD}{2} * [(\sin I_1 * \cos A_1) + (\sin I_2 * \cos A_2)] * RF \quad \text{Equation 3. 1}$$

$$\Delta East = \frac{MD}{2} * [(\sin I_1 * \sin A_1) + (\sin I_2 * \sin A_2)] * RF \quad \text{Equation 3. 2}$$

$$TVD = \frac{MD}{2} * [\cos I_1 + \cos I_2] * RF \quad \text{Equation 3. 3}$$

$$\beta = \cos^{-1}[\cos(I_2 - I_1) - (\sin(I_1) * \sin(I_2) * (1 - \cos(A_2 - A_1)))] \quad \text{Equation 3. 4}$$

$$RF = \frac{2}{\beta} \tan \frac{\beta}{2} \quad \text{Equation 3. 5}$$

The Northing and Easting calculated from this formula are the changes in North and changes in East to drill from survey point 1 to survey point 2. The corresponding change in vertical height, TVD, is also calculated. For drilling simulation purposes, this change is very important when simulating drill ahead of the bit. The forces that influence the direction of the drill string and the bit eventually reflect its impact in the change in Easting, Northing, and TVD which in a 3-D space could be upwards or downwards in 360 degrees direction.

3.2 Six Directions Considered for Well Path Design in a Drilling Simulator

For this research, 6 directions were used to determine the movement of the drill string. Normally in 2D, only changes in inclination is considered. The 3 directions being considered in that case are build-only, drop-only and straight (no inclination change). In 2D, azimuth is always kept constant. This is not feasible for reflecting the impact of the forces affecting the drilling string and the bit. Modeling the well path in 3D, if necessary, for accurate measurement of parameter changes while drilling. Hence the addition of 3 other directions, build and turn, drop and turn, and straight and turn. The turn refers to azimuth changes as the 2D movements occur. These six directions accommodate all possible movements of the drill string and the bit as the drilling operations occur.

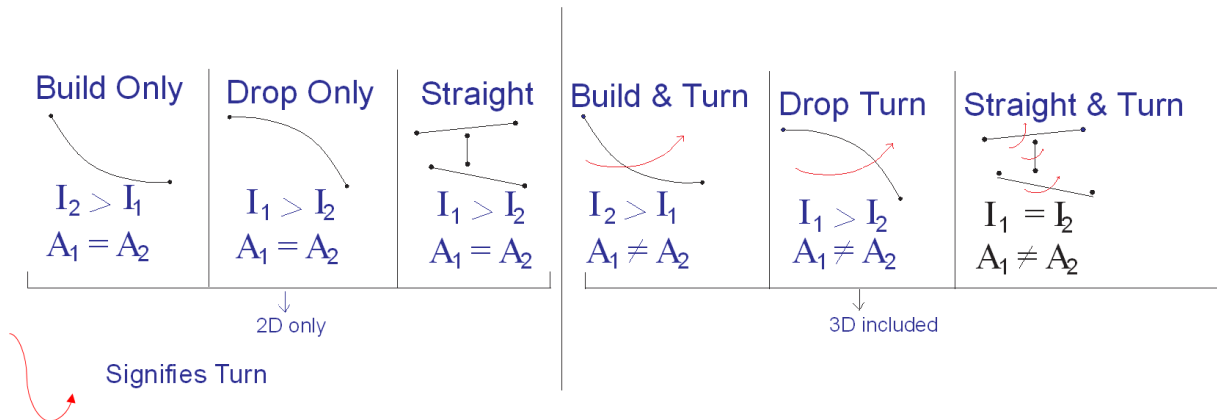


Figure 3. 4 The Six Directions of 3D Space Well Path

3.3 Calculating Course Length as Implemented in the Drilling Simulator

The way the course length is calculated is one of the defining factor for modeling the well path in the 3D space. First, a look at course length for 2D. In 2D, the course length is simply the arc length for build and drop and the length of the line for straight path. The formula below will always resolve course length calculation for 2D well path.

$$\text{arc length} = 2\pi r \left(\frac{\theta}{360} \right) \quad \text{Equation 3. 6}$$

$$\text{length of hypotenuse} = c = \sqrt{a^2 + b^2}, \text{ where } a \text{ and } b \text{ are the sides of the triangle}$$

Equation 3. 7

Depending on the type of well path, a combination of these two formulae is needed to calculate the total course length which is the measured depth for a 2D system. Here are the 3 types of well path from the perspective of 2D.

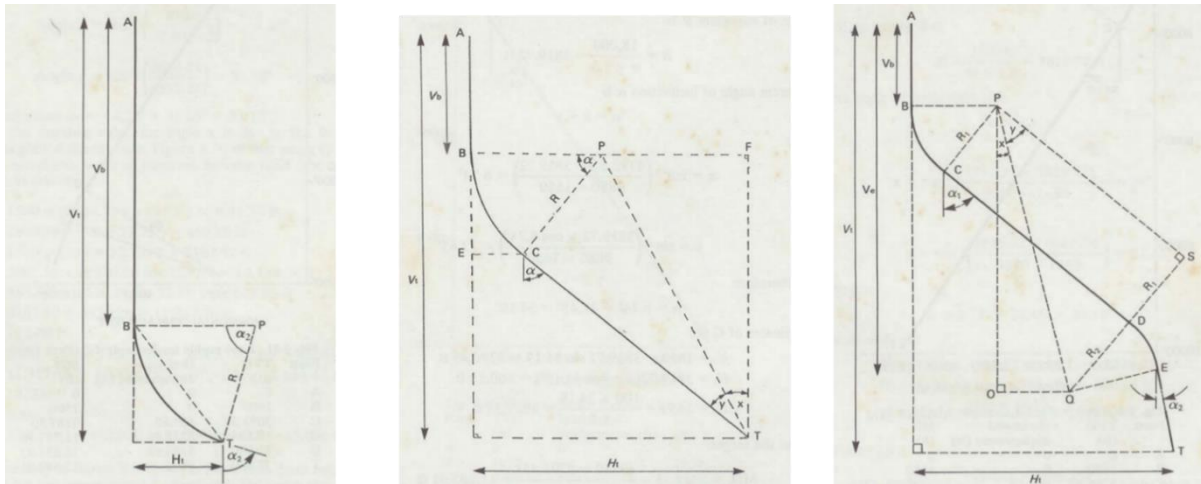


Figure 3. 5 Type I, II, & III Well Profiles for 2D Construction (Inglis, 2013)

For these 2D well types, the course length would be calculated depending on what the input is. The table below shows those inputs.

Table 3. 1 Inputs Needed to Calculate 2D Well Profile Types

S/N	Input Variables	Well Profiles		
		Type I: Build and Hold	Type II: Build, Hold and Drop	Type III: Deep Kick-Off and Build
1	Surface Coordinates	✓	✓	✓
2	Target Coordinates	✓	✓	✓
3	True Vertical Depth to Target	✓	✓	
4	True Vertical Depth to Kick-Off Point (KOP)	✓	✓	✓
5	True Vertical Depth to End of Drop-Off		✓	
6	Buildup Rate	✓	✓	✓
7	Drop-Off Rate		✓	
8	Final angle of inclination through target		✓	
9	Maximum angle of inclination			✓

However, 3D the course length is different because the path includes changes in azimuth. The arc length formula will not account for the changes in length of a curve as the path is turning at the same time. As shown in Figure 3.6, a change in direction from point 1 to point 2 can be likened to a 2D well path and the length of the path is the arc length of the circular path 0-1-2.

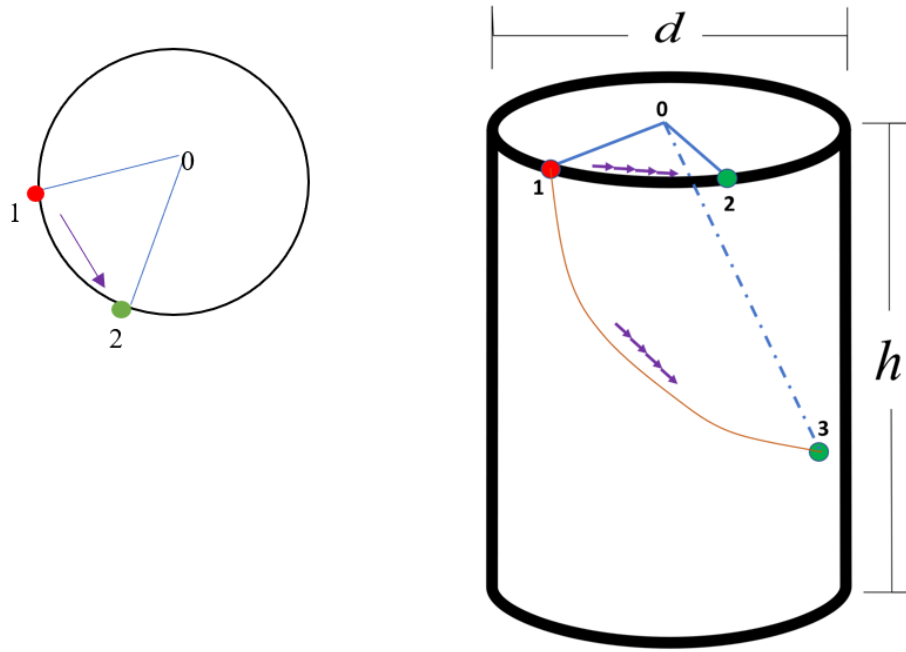


Figure 3. 6 Exemplifying Key Difference Between 2D and 3D Course Length

The path 0-1-3 is a 3D path which is like a build and a turn path. The length of an arc will not cover the full course length considering the turning it takes to go from point 1 to point 3. After much research and trials, the one angle that accounts for that course length is the dogleg angle, also known as beta in the minimum curvature method. To calculate the course length for those 3D well path curves in the drilling simulator, the formula below was used.

$$\text{Course Length for 3D Curves} = \frac{\text{Dogleg Angle}}{\text{Maximum Dogleg Severity } ^\circ/100\text{ft}} \quad \text{Equation 3. 8}$$

Dogleg severity DLS is the degree of curvature between two survey stations in the directional well path. A limit of maximum dogleg severity is used if based on pre-drilling planning, a desired DLS is required to avoid potential downhole tool damages. This already known concept of course length calculation is the bridge between 2D well trajectory calculations and 3D estimation.

3.4 Interpolating a Well Path

Usually when simulating a planned path, certain locations and their corresponding azimuth, inclination and measured depth are known. The key is to calculate the data in between those points

so they can all be inputted into the minimum curvature method. Interpolating the inclination between two known points is straight forward.

If $I_2 > I_1$ then the increments in between I_1 and I_2 in x steps are $\frac{I_2 - I_1}{x}$.

$$\text{Let } Incr = \frac{I_2 - I_1}{x}$$

Then increasing from I_1 to I_2 would become $I_1, I_1 + Incr, I_1 + 2 * Incr, \dots, I_1 + ((x - 1) * Incr), I_2$

The same principle works for the drop from I_2 to I_1

This interpolation process is a little different when dealing with azimuth change. The change in azimuth follows certain rules as implemented in this research.

1. Azimuth increases from 0° to 360° .
2. The change in azimuth follows the shortest distance between the two points being considered.
3. Depending on what the shortest distance is, the direction from point 1 to point 2 could be either incremental or decreasing even passing through 0° to 359° .

Here is an illustration of this change diagrammatically. Going forward α_1 is inclination at point 1 and α_2 is inclination at point 2

β_1 is azimuth at point 1 and β_2 is azimuth at point 2

Scenario 1: Forward Direction Moving from β_1 to β_2 :

$$\beta_1 = 30^\circ$$

$$\beta = 100^\circ$$

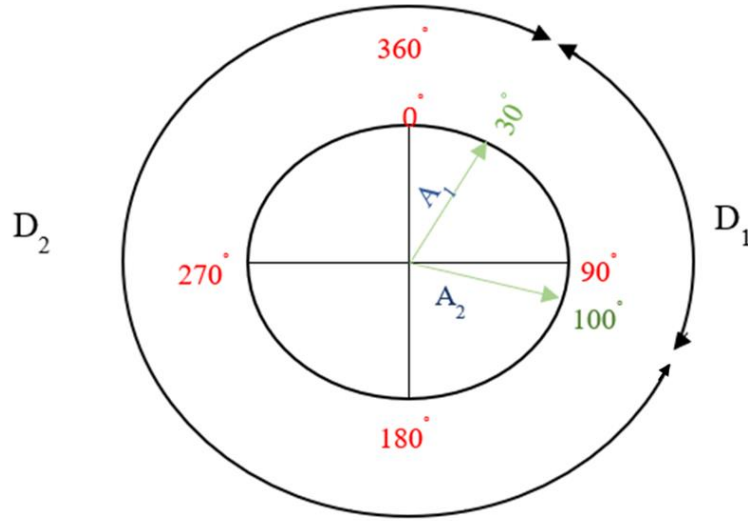


Figure 3. 7 Forward Direction Azimuth Scenario

$D1$ is the forward direction distance.

for moving from β_1 to β_2

$D2$ is the backward direction distance.

for moving from β_1 to β_2

$$D1 = (\beta_1 - \beta_2) = (30^\circ - 100^\circ)$$

$$D1 = 70^\circ$$

$$D2 = (\beta_1 - 0^\circ) + (360^\circ - \beta_2) = \beta_1 - \beta_2 + 360^\circ$$

$$D2 = 30 - 100 + 360$$

$$D2 = 290^\circ$$

The chooses direction is always the direction with lower distance.

In this scenario, $D1 < D2$

This means moving from β_1 to β_2 will require forward direction.

If n is the number of steps inputted to get from β_1 to β_2

Also, if increment is the step size, then increasing from β_1 to β_2 would be

$$\beta_1, \beta_1 + \text{increment}, \beta_1 + 2 * \text{increment}, \dots, \beta_1 + (n - 1) * \text{increment}, \beta_2$$

Scenario 2: Backward direction moving from β_1 to β_2 :

$$\beta_1 = 30^\circ$$

$$\beta_2 = 300^\circ$$

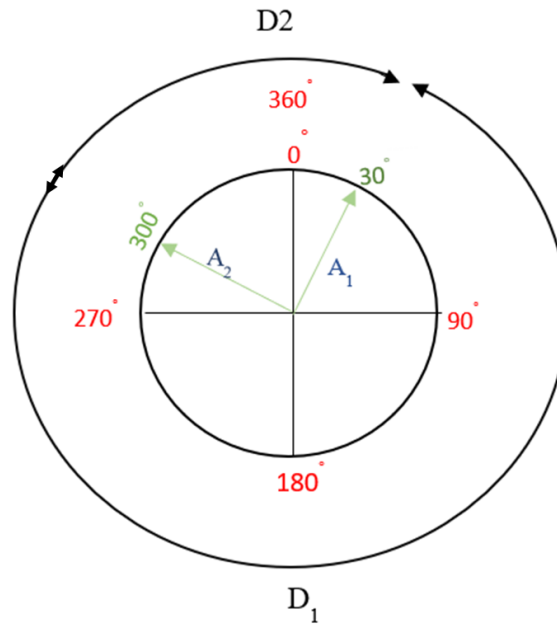


Figure 3. 8 Backward Direction Azimuth Scenario

$$D1 = |\beta_1 - \beta_2| = |30^\circ - 300^\circ|$$

$$D1 = 270^\circ$$

$$D2 = \beta_1 - \beta_2 + 360^\circ = 30 - 300 + 360^\circ$$

$$D2 = 90^\circ$$

Since $D2 < D1$, moving direction from β_1 to β_2 will require backward direction

Let y be the number of steps inputted to get from β_1 to β_2

Let x be the step size

then moving from β_1 to β_2 would be:

$$\beta_1, \beta_1 - x, \beta_1 + 2x, \dots, 360 - x, 360 - 2x, \dots, 360 - (y-1)x, \beta_2$$

3.5 Constructing Path for Multi-Lateral Well (MLW)

There are two main shapes for MLW, fishbone wells and roof wells. In both cases, the laterals are formed due to changes in the inclination or azimuth at different lateral lengths. Consider this schematic of a fishbone well:

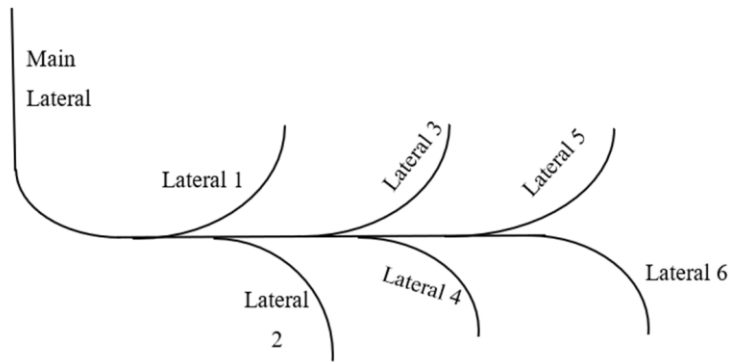


Figure 3. 9 Schematic for Fishbone Multi-Lateral

Zooming in on deviation into lateral 1 and 2

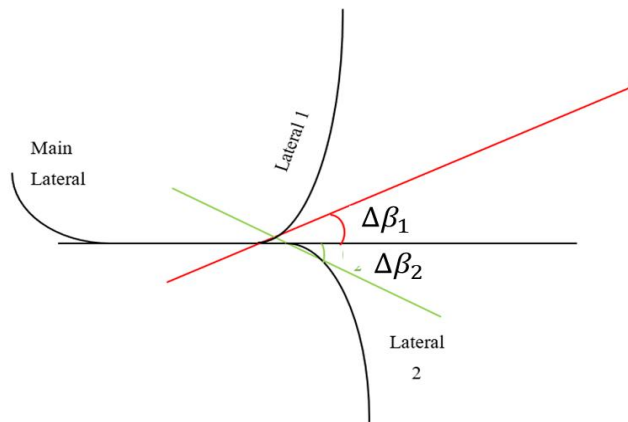


Figure 3. 10 Zooming in on First Two Lateral Deviation for Fishbone

In this case the inclination stays constant at 90° and then begins to change in azimuth

$\Delta\beta_1$ and $\Delta\beta_2$ are changes in azimuth on either side of the main lateral.

The joining process is to identify the measured depth where the deviation starts on the main lateral and calculate what change in azimuth is occurring. It could be a backward direction or a forward direction. The last data on the main lateral merges with the first data on the joining lateral. It is also possible that the inclination is increasing as well.

Consider this schematic for root-shaped multi-lateral as well.

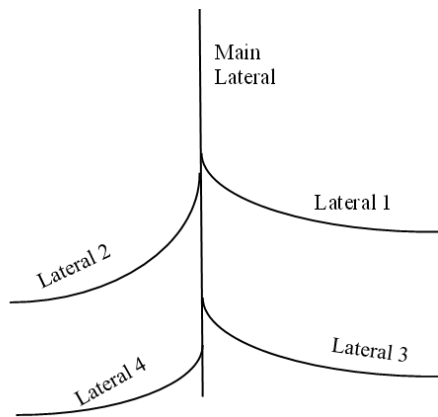


Figure 3. 11 Schematics for Root Shaped Multi-Lateral Well

The main lateral is kept at vertical 0° , the other laterals deviate from vertical as inclination changes. Taking a closer look at lateral 1 and 2:

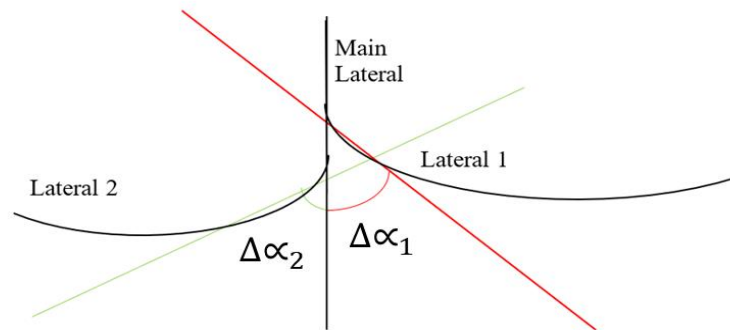


Figure 3. 12 Zooming in on the First Two Laterals for Root Multi-Lateral Wells

$\Delta\alpha_1$ and $\Delta\alpha_2$ are the deviation from vertical for lateral 1 and 2 on either side of the vertical.

The changes are both builds from the main lateral. This build is not restricted to 2D, there could be 3D change in direction as well.

An example will make the illustration better. Here is the generic form for a build only well.

Table 3. 2 Generic Form for a Build Only Well

INCLINATION	AZIMUTH	LENGTH	DESCRIPTION
α_1	β_1	0	Surface
α_1	β_1	KOP	Kick-off
α_2 (α_2 is usually 90°)	β_2	unknown	Intermediate closing point (ICP)
$\alpha_3 = \alpha_2$	$\beta_3 = \beta_2$	KOP+ Length	End of lateral

Consider a horizontal well which kicks off at 3000ft and builds to 90° , the lateral stretches for 1500ft while in 60° azimuth direction.

Let that well be the main lateral, the first deviated lateral begins 100ft into the horizontal section of the main lateral, and the other 3 lateral commence deviation 100ft apart targeting an addition 30° azimuth change to the right and left of the main lateral. There is a table of the path assuming the length of each deviating lateral is 500 ft.

Table 3. 3 Main Lateral Data

INCLINATION	AZIMUTH	LENGTH	DESCRIPTION
0	0	0	Surface
0	0	3000	Kick-off
90°	60°	unknown	Intermediate closing point (ICP)
90°	60°	+1500	End of lateral

Table 3. 4 Lateral 1 Data

INCLINATION	AZIMUTH	LENGTH	DESCRIPTI ON
90°	60°	0	Start
90°	60°	+1500ft	End

Table 3. 5 Lateral 2 Data

INCLINATION	AZIMUTH	LENGTH	DESCRIPTI ON
90°	60°	+100	Start
90°	30°	+500	End

Table 3. 6 Lateral 3 Data

INCLINATION	AZIMUTH	LENGTH	DESCRIPTI ON
90°	60°	+200	Start
90°	90°	+500	End

Table 3. 7 Lateral 4 Data

INCLINATION	AZIMUTH	LENGTH	DESCRIPTI ON
90°	60°	+300	Start
90°	30°	+500	End

Since inclination remains constant in this case, joining the azimuth then becomes the main task:

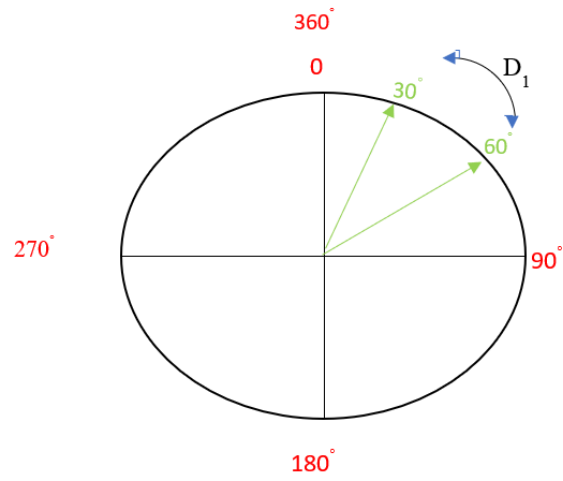


Figure 3.13 Deviation of Azimuth in Multi-Lateral Well

Change in direction for lateral 2 and 4

$$D_1 = |60^\circ - 30^\circ|$$

$$D_1 = 30^\circ$$

$$D_2 = 30^\circ - 60^\circ + 360^\circ$$

$$D_2 = 330^\circ$$

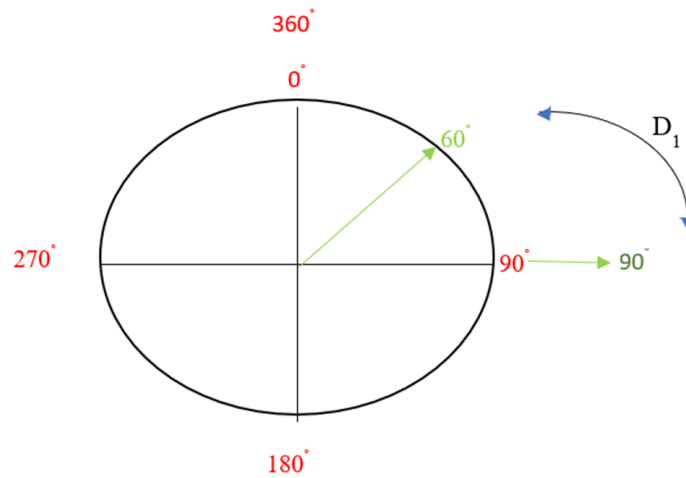


Figure 3.14 Reverse Azimuth Change in Multi-Lateral Wells

Change in direction for lateral 1 and 3.

$$D_1 = |60^\circ - 90^\circ|$$

$$D_1 = 30^\circ$$

$$D_2 = 60^\circ - 90^\circ + 360^\circ$$

$$D_2 = 330^\circ$$

Both changes are forward direction from the end of the main lateral to the beginning of each new lateral deviation from the main horizontal. The final well path for each lateral can be written independent of the other laterals. there is such a table for lateral 4:

Table 3. 8 Total Well Path for Lateral 4

INCLINATION	AZIMUTH	LENGTH	DESCRIPTION
0°	0°	3000	Kick off
90°	60°	unknown	Intermediate closing point (ICP)
90°	60°	+300	Start
.	.	.	.
.	.	.	.
.	.	.	.
90°	30°	+500	End

3.6 Practicing Well Path Design on Well 4

This practice will touch several things. First a description of the scenario. The scenario is about a multilateral well that starts off as a vertical well, builds a little bit, and then splits into three laterals. This is about well 4 that splits into well 4A, well 4B, and well 4C. Well 4 is a multilateral well drilled in the Niger-Delta region of Nigeria. Below is a summary table of the data for this practice.

Table 3. 9 Summary of Data for Well 4 and its Laterals

Well Name	Path Parameter	Start	Finish
Well 4	Measured Depth, ft	0	12290.03
	Inclination, degrees	0	60.94
	Azimuth, degrees	0	311.50
Well 4B	Measured Depth, ft	12356.86	14294.62
	Inclination, degrees	60.67	54.00
	Azimuth, degrees	316.71	313.00
Well 4A	Measured Depth, ft	11313.09	13858.27
	Inclination, degrees	60.52	60
	Azimuth, degrees	312.57	312
Well 4C	Measured Depth, ft	11356.04	14268.37
	Inclination, degrees	59.35	37.77
	Azimuth, degrees	311.88	301.62

The first test is to accurately interpolate inclination and azimuth data. Consider a trail of well B data from its deviation point in the main lateral well 4. The goal is to calculate all the in-between points.

Table 3. 10 Well 4B Data Summary Sheet

Measured Depth	Inclination	Azimuth
12356.86	60.67	316.71
12450.46	58.23	318.54
12602.66	58.44	319.76
12687.66	57.91	319.28

Assuming the two middle azimuths are not known then the interpolation process will be as follows

Table 3. 11 Unknown Azimuth in Well 4B Data

Measured Depth	Inclination	Azimuth
12356.86	60.67	316.71
12450.46	58.23	Unknown
12602.66	58.44	Unknown
12687.66	57.91	319.28

Between 316.71 to 319.28 is a forward direction azimuth change because

$$|316.71 - 319.28| < (316.71 - 319.28 + 360)$$

There are three steps required so $n = 3$

For a planned path simulation, the drilling simulator would have divided the path into equal paths. The azimuth becomes 316.71, 317.5667, 318.4234, 319.2801 Comparing this to the actual values. The actual values come from the measurement while drilling data when the well was actually drilled.

Table 3. 12 Error in Azimuth Calculation in Well 4B Data

Actual Azimuth for Well 4B	Calculated Azimuth for Well 4B	
316.71	316.71	
318.54	317.5667	Error=0.8567 absolute
319.76	318.4234	Error=1.3366 absolute
319.28	319.2801	

The error, this is the difference between the calculated azimuth and the actual azimuth.

$$(\Delta\theta = \theta_{calculated} - \theta_{actual})$$

The second test is the calculation of course length in a scenario of change in azimuth and change in inclination scenario.

Table 3. 13 Error in Measured Calculation in Well 4B Data

Measured Depth, ft	Inclination	Azimuth	DLS
12356.86	60.67	316.71	3.61
Unknown 1	58.23	318.54	3.05
Unknown 2	58.44	319.76	0.69
Unknown 3	57.91	319.28	0.77

$$\text{Dogleg Angle} = \cos^{-1}[\cos(I_2 - I_1) - (\sin(I_1) * \sin(I_2) * (1 - \cos(A_2 - A_1)))]$$

Equation 3. 9

$$\text{Unknown Change in Measured Depth} = \frac{\text{Dogleg Angle} * 100}{\text{DLS}}$$

Equation 3. 10

$\Delta MD1$

$$= \frac{100 * \cos^{-1}[\cos(58.23 - 60.67) - (\sin(60.67) * \sin(58.23) * (1 - \cos(316.71 - 318.54)))]}{3.05}$$

$$\Delta MD1 = 96.497 \text{ ft}$$

Therefore, Unknown 1 = 12356.86 + 96.497 = 12,453.357ft

Using the same principle, the other 2 unknowns can be found.

Table 3. 14 Error in Measured Depth Calculations for Well 4B

Actual Measured Depth ft	Calculated Measured Depth ft	
12356.86	12356.86	
12450.46	12453.357	Error=2.897 absolute
12602.66	12606.8927	Error=4.2327 absolute
12687.66	12693.7436	Error=6.0836 absolute

3.7 Conclusion

This chapter has reviewed how the well path is computed in the drilling simulator. The key equation of note is the 4 minimum curvature formula that converts inclination, azimuth, and measured depth into northing, easting, and TVD. **Interpolating inclination and azimuth is unique in procedures** as azimuth could go either forward direction changes or backward direction changes; the choice is based on the shortest distance between the start point and the end point in degrees. Course length changes are dependent on dogleg angle. The formulas used in 2D schematics of the well path will not work in the drilling simulator because changes in **azimuth are accounted for**. Hence 3D schematics are considered which accommodates azimuth changes. Error in azimuth changes calculations and course length calculations are minimal but do not take the direction away from the expected well path. Even though the Minimum Curvature Method (MCM) provides a method to interpolate azimuth, the real challenge is the computational implementation of the minimum curvature method, which could lead to a lot of errors. This thesis has implemented the minimum curvature method in 3D and has produced results of the azimuth that are closely aligned with the azimuth changes from the measurement while drilling data of the well. The calculations made in this chapter show a less than 2-degree error calculated, and this 2-degree differential may be due to noise in the recorded data.

Chapter 4 Drill String Displacement Estimation Using Finite Element Method

The goal of this chapter is to work from first principles on how to simulate the displacement calculations for a 3-dimensional structure, specifically the drill string. The parameter of focus is the displacement of the drill string during drill ahead process. The drill string is considered as a 3-dimensional linear set of elements with 6 degrees of freedom (DOF) at each node. The displacement vector w consists of 4 independent processes that make up the 12 DOF per element.

- **Axial Load:** This refers to the force applied directly at the axis of the element which in this case is the x direction.
- **Axial Torsion:** This refers to the twisting of the element in the axial direction due to torque applied leading to angular displacement.
- **Bending in XZ plane:** A load in y direction in one end will lead to rotation in the z direction or XZ plane.
- **Bending in the XY plane:** A load in the z direction will lead to rotation in the y direction or XY plane.

These 4 procedures occur simultaneously and independently leading to the 12 DOF per element. Here are the key assumptions for the finite element model.

1. Shear deformation is negligible
2. The beam is a linear element with 2 nodes

The overall equation for an element is as follows:

$$[K^e][U^e] = [F^e] = [f^e] + [Q^e] \quad (\text{Reddy, 2005}) \quad \text{Equation 4. 1}$$

$[K^e]$ is Element Stiffness Matrix

$[U^e]$ is Generalized Displacement Vector

$[F^e]$ is Generalized Force Vector

$[f^e]$ is Distributed Normal Force

$[Q^e]$ is Point Forces and Moments

The basic assumptions and limitations are:

- Linear relationship exists between applied load and the resulting displacement of the structure.
 - Making the principle of superposition valid (Reddy, 2005).

- Material of the structure must obey Hooke's Law.
 - Material must not be stressed beyond its elastic limit.
- Equations of equilibrium shall be developed using the geometry of the undeflected model.
 - Change in geometry caused by imposed loads is negligible compared to the original.

4.1 The Governing Equation and Stiffness Matrix for Bending in the XY and XZ Planes

The focus of this section will be bending in the XZ plane, and the results will be the same for the XY plane just with different moments of inertia which will be indicated later in this section. Figure 4.1 shows the schematics of how the unit load in Y direction causes rotation in the z direction.

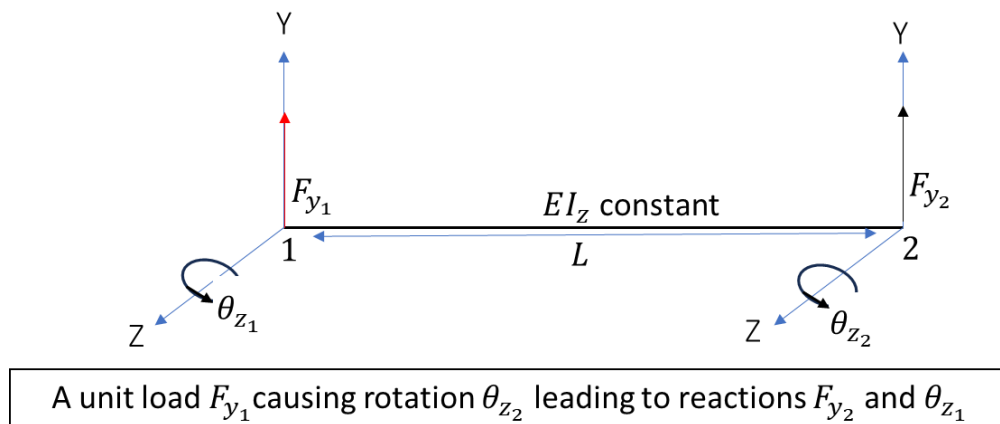


Figure 4. 1 Unit Loading in Y Direction

The dependent variable of focus is the displacement of the drill string as the drill ahead into the formation occurs. The equation that encapsulates this phenomenon is the Euler-Bernoulli classical beam theory. Suppose there is a beam with a neutral axis and when it bends, it bends in such a way that the deformed beam and the deformed neutral axis remains perpendicular to the edge of the beam.

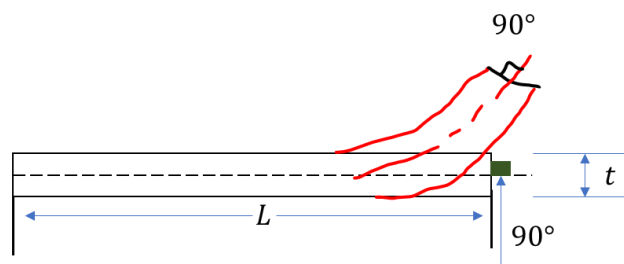


Figure 4. 2 The Bending of a Beam

For the Euler theory to exist the length of the beam, L , must be far greater than the thickness, t , of the beam. The governing equation is as follows.

$$\frac{d^2}{dy^2} \left(\frac{bd^2w}{dy^2} \right) = f(y) \quad (\text{Reddy, 2005}) \quad \text{Equation 4. 2}$$

This is the strong form, a 4th order ordinary differential equation. Where $f(y)$ is the distributed load (lb/ft) on the beam element.

$b = EI_z$; $E = \text{Young's Modulus, psi}$ and $I_z = \text{Moment of Inertia, in}^4$

w is the deflection of the beam, it is positive if it is going up and negative when it is coming down.

y is the variation of displacement along the length of the beam.

Consider a small element of a beam,

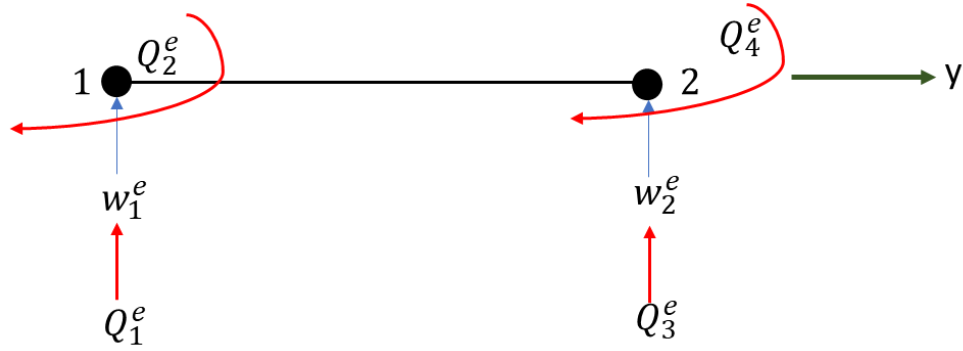


Figure 4. 3 Forces and Moments in a 2 Node Element

Q_1^e and Q_3^e are shear forces.

Q_2^e and Q_4^e are bending moments.

The sign convention is that bending moments are positive clockwise and negative anticlockwise. Shear forces are positive when going up and negative when coming down.

The weak formulation is:

$$\text{Error} = \int_0^L \left[\frac{d^2}{dy^2} \left(\frac{bd^2w}{dy^2} \right) - f(y) \right] dy \quad \text{Equation 4. 3}$$

This error will be zero if the solution to the governing equation were to be exact. If it is not exact, then Equation 4.2 will be the approximation of the solution. The next step is to multiply by a

weight function, $v(y)$ and equate to zero to achieve minimum potential energy, placing the system at equilibrium.

$$\int_0^L v \left[\frac{d^2}{dy^2} \left(\frac{bd^2w}{dy^2} \right) - f(y) \right] dy = 0 \quad \text{Equation 4. 4}$$

The next step is to integrate by parts which gives the following expression.

$$\int_0^L \left[-\frac{dv}{dy} \left[\frac{bd^2w}{dy^2} \right]' - vf \right] dy + \left[v \frac{d}{dy} \left(\frac{bd^2w}{dy^2} \right) \right]_0^L = 0 \quad \text{Equation 4. 5}$$

$\left[v \frac{d}{dy} \left(\frac{bd^2w}{dy^2} \right) \right]_0^L$ represents the first boundary condition term. To further weaken the differential, another integration is needed which gives the following.

$$\int_0^L \left[\frac{d^2v}{dy^2} \left[\frac{bd^2w}{dy^2} \right] - vf \right] dy + \left[v \frac{d}{dy} \left(\frac{bd^2w}{dy^2} \right) - \left(\frac{dv}{dy} \right) \left(\frac{bd^2w}{dy^2} \right) \right]_0^L = 0 \quad \text{Equation 4. 6}$$

$\left[-\left(\frac{dv}{dy} \right) \left(\frac{bd^2w}{dy^2} \right) \right]_0^L$ is another boundary condition term. Equation 4.5 is the weak form of the Euler Bernoulli equation which can be written as

$$\int_0^L \left[\frac{d^2v}{dy^2} \left[\frac{bd^2w}{dy^2} \right] - vf \right] dy + \left[\frac{v(bw'')' - v'(bw'')}{1} \right]_0^L = 0 \quad \text{Equation 4. 7}$$

The primary variables are obtained by replacing the weighting function with the unknown variables in the boundary terms. This means the primary variables are w and $-\frac{dw}{dy}$ which are generalized displacements while the generalized forces are $(bw'')'$ is shear force and (bw'') is moment. Note that the rotation displacement $\theta = \frac{dw}{dy}$.

Identifying the boundary conditions of the secondary variables:

$$(bw'')'|_{x=0} = Q_1^e \quad \text{Equation 4. 8}$$

$$(bw'')'|_{x=L} = Q_3^e \quad \text{Equation 4. 9}$$

$$-(bw'')|_{x=0} = Q_2^e \quad \text{Equation 4. 10}$$

$$-(bw'')|_{x=L} = Q_4^e \quad \text{Equation 4. 11}$$

Rewriting the weak form to get

$$\int_0^L \left[\frac{d^2 v}{dy^2} \left[\frac{bd^2 w}{dy^2} \right] \right] dy = \int_0^L f v dy + (v|_{y=0}) Q_1^e + ((-v'|_{y=0}) Q_2^e) + (v|_{y=L}) Q_3^e + ((-v'|_{y=L}) Q_4^e)$$

Equation 4. 12

This can help in determining the interpolation functions per element.

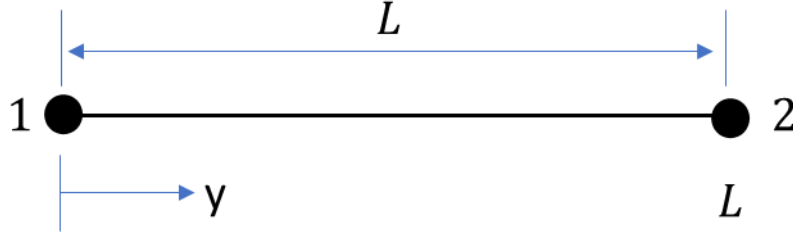


Figure 4. 4 The Boundaries of a Two Node Element

$$w^e|_y = \sum_{j=1}^4 u_j^e \phi_j^e(y) = u_1^e \phi_1^e(y) + u_2^e \phi_2^e(y) + u_3^e \phi_3^e(y) + u_4^e \phi_4^e(y) \quad \text{Equation 4. 13}$$

$$w|_{y=0} = w_1 = u_1^e \text{ meaning at } y = 0, \phi_1^e = 1 \quad \text{Equation 4. 14}$$

$$-w'|_{y=0} = \theta_1 = u_2^e \text{ meaning at } y = 0, (\phi_2^e)' = -1 \quad \text{Equation 4. 15}$$

$$w|_{y=L} = w_2 = u_3^e \text{ meaning at } y = L, \phi_3^e = 1 \quad \text{Equation 4. 16}$$

$$-w'|_{y=L} = \theta_2 = u_4^e \text{ meaning at } y = L, (\phi_4^e)' = -1 \quad \text{Equation 4. 17}$$

The aim is to develop $\phi_1^e(y)$, $\phi_2^e(y)$, $\phi_3^e(y)$, and $\phi_4^e(y)$ which are the interpolation functions. Here are the boundary conditions.

Table 4. 1 Boundary Conditions Table for 2 Node Element

	ϕ_1^e	$(\phi_1^e)'$	ϕ_2^e	$(\phi_2^e)'$	ϕ_3^e	$(\phi_3^e)'$	ϕ_4^e	$(\phi_4^e)'$
$y = 0$	1	0	0	-1	0	0	0	0
$y = L$	0	0	0	0	1	0	0	-1

Each function will have 4 constants since there are 4 degrees of freedom.

$$\phi_1^e(y) = a + by + cy^2 + dy^3 \quad \text{Equation 4. 18}$$

$$\phi_2^e(y) = e + fy + gy^2 + hy^3 \quad \text{Equation 4. 19}$$

$$\phi_3^e(y) = m + ny + py^2 + qy^3 \quad \text{Equation 4. 20}$$

$$\phi_4^e(y) = r + ly + Vy^2 + Ty^3 \quad \text{Equation 4. 21}$$

Based on the boundary conditions Table 4.1, here are the value of the constants.

Table 4. 2 Expressions of Interpolation Functions for Linear 2 Node Beam

Interpolation Function	Constants	Expression per Constant
$\phi_1^e(y)$	a	1
	b	0
	c	$-\frac{3}{L^2}$
	d	$\frac{2}{L^3}$
$\phi_2^e(y)$	e	0
	f	-1
	g	$\frac{2}{L}$
	h	$-\frac{1}{L^2}$
$\phi_3^e(y)$	m	0
	n	0
	p	$\frac{3}{L^2}$
	q	$-\frac{2}{L^3}$
$\phi_4^e(y)$	r	0
	l	0
	V	$\frac{1}{L}$
	T	$-\frac{1}{L^2}$

Here are the final full expressions of the interpolation functions.

$$\phi_1^e(y) = 1 - \frac{3}{L^2}y^2 + \frac{2}{L^3}y^3 \quad \text{Equation 4. 22}$$

$$\phi_2^e(y) = -y + \frac{2}{L}y^2 - \frac{1}{L^2}y^3 \quad \text{Equation 4. 23}$$

$$\phi_3^e(y) = \frac{3}{L^2}y^2 - \frac{2}{L^3}y^3 \quad \text{Equation 4. 24}$$

$$\phi_4^e(y) = \frac{1}{L}y^2 - \frac{1}{L^2}y^3 \quad \text{Equation 4. 25}$$

The figures below show the progression from node 1 to node 2 for each of the interpolation functions.

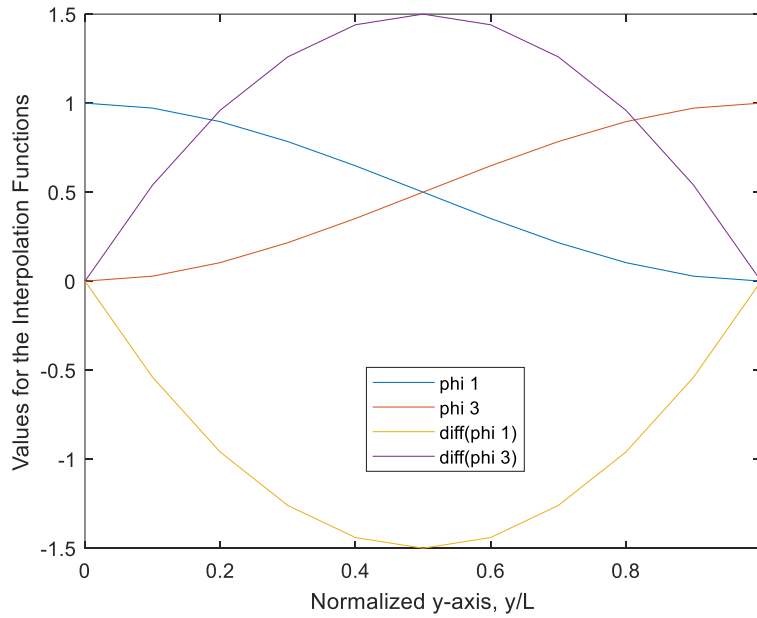


Figure 4. 5 Variation of Translation Interpolation Functions for 2 Node Element

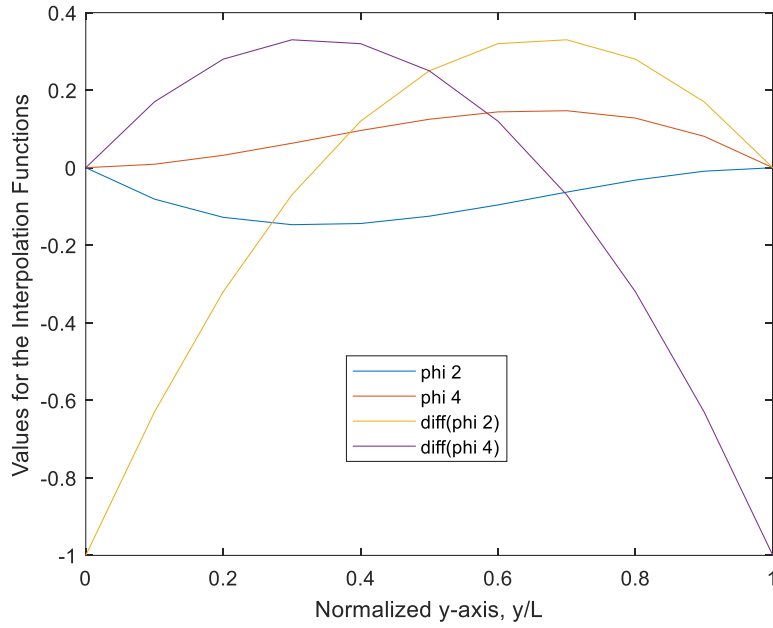


Figure 4. 6 Variation of Rotation Interpolation Functions for 2 Node Element

Recall, this is a two-node element, with each side having 2 degrees of freedom.

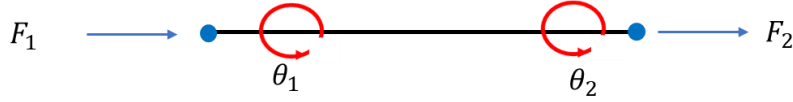


Figure 4. 7 4 DOFs in Beam Element

This means the stiffness matrix is a 4 by 4 matrix.

$$K = [4 \times 4] \quad \text{Equation 4. 26}$$

Based on the left-hand side of Equation 4.12,

$$K_{ij}^e = \int_0^L b \left[\frac{d^2 \phi_i^e}{dy^2} \left[\frac{d^2 \phi_j^e}{dy^2} \right] \right] dy \quad \text{Equation 4. 27}$$

K matrix is bilinear in ϕ_i^e and ϕ_j^e and symmetric in ϕ_i^e and ϕ_j^e . In an overall sense in the Y axis,

$$K = \begin{bmatrix} K_{11}^e & K_{12}^e & K_{13}^e & K_{14}^e \\ K_{21}^e & K_{22}^e & K_{23}^e & K_{24}^e \\ K_{31}^e & K_{32}^e & K_{33}^e & K_{34}^e \\ K_{41}^e & K_{42}^e & K_{43}^e & K_{44}^e \end{bmatrix} \quad \text{Equation 4. 28}$$

The equations for \emptyset_i^e and \emptyset_j^e are gotten from the interpolation functions in Equation 4.22 to Equation 4.25. For example, K_{34}^e is calculated thus.

$$K_{34}^e = \int_0^L b \left[\frac{d^2 \emptyset_3^e}{dy^2} \left[\frac{d^2 \emptyset_4^e}{dy^2} \right] \right] dy \quad \text{Equation 4. 29}$$

$$K_{34}^e = \int_0^L b \left[\frac{d^2 \left(\frac{3}{L^2} y^2 - \frac{2}{L^3} y^3 \right)}{dy^2} \left[\frac{d^2 \left(\frac{1}{L} y^2 - \frac{1}{L^2} y^3 \right)}{dy^2} \right] \right] dy \quad \text{Equation 4. 30}$$

$$K_{34}^e = \frac{6b}{L^2} = \frac{6EI_z}{L^2} \quad \text{Equation 4. 31}$$

Here are the second differentials of the interpolation functions.

$$\frac{d^2 \emptyset_1^e}{dy^2} = \frac{-6}{L^2} + \frac{12y}{L^3} \quad \text{Equation 4. 32}$$

$$\frac{d^2 \emptyset_2^e}{dy^2} = \frac{4}{L} - \frac{6y}{L^2} \quad \text{Equation 4. 33}$$

$$\frac{d^2 \emptyset_3^e}{dy^2} = \frac{6}{L^2} - \frac{12y}{L^3} \quad \text{Equation 4. 34}$$

$$\frac{d^2 \emptyset_4^e}{dy^2} = \frac{2}{L} - \frac{6y}{L^2} \quad \text{Equation 4. 35}$$

The full stiffness matrix for the y direction loading is.

$$K_y = \begin{bmatrix} \frac{12EI_z}{L^3} & \frac{-6EI_z}{L^2} & \frac{-12EI_z}{L^3} & \frac{-6EI_z}{L^2} \\ \frac{-6EI_z}{L^2} & \frac{4EI_z}{L} & \frac{6EI_z}{L^2} & \frac{2EI_z}{L} \\ \frac{-12EI_z}{L^3} & \frac{6EI_z}{L^2} & \frac{12EI_z}{L^3} & \frac{6EI_z}{L^2} \\ \frac{-6EI_z}{L^2} & \frac{2EI_z}{L} & \frac{6EI_z}{L^2} & \frac{4EI_z}{L} \end{bmatrix} \quad \text{Equation 4. 36}$$

Similarly, the Z direction stiffness matrix can be computed.

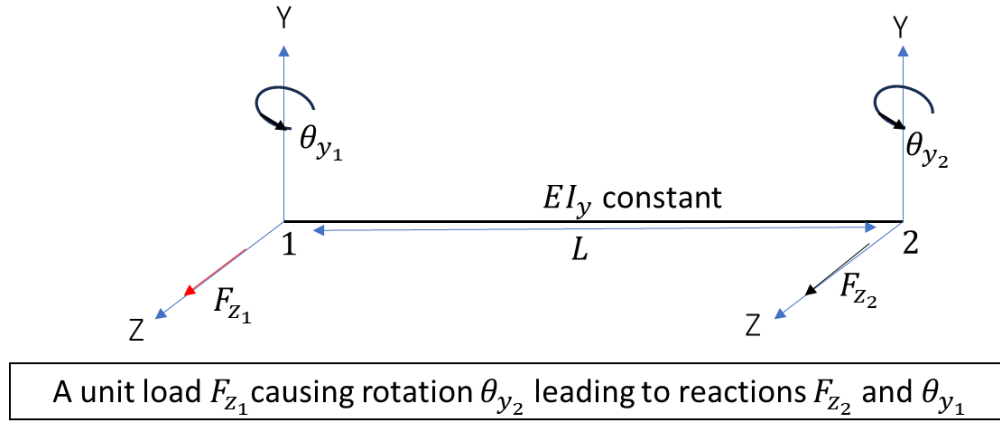


Figure 4. 8 Unit Loading in Z Direction

Based on similar principles as the Y direction, the Z direction stiffness matrix is

$$K_z = \begin{bmatrix} \frac{12EI_y}{L^3} & \frac{-6EI_y}{L^2} & \frac{-12EI_y}{L^3} & \frac{-6EI_y}{L^2} \\ \frac{-6EI_y}{L^2} & \frac{4EI_y}{L} & \frac{6EI_y}{L^2} & \frac{2EI_y}{L} \\ \frac{-12EI_y}{L^3} & \frac{6EI_y}{L^2} & \frac{12EI_y}{L^3} & \frac{6EI_y}{L^2} \\ \frac{-6EI_y}{L^2} & \frac{2EI_y}{L} & \frac{6EI_y}{L^2} & \frac{4EI_y}{L} \end{bmatrix} \quad \text{Equation 4. 37}$$

4.2 The Governing Equation and Stiffness Matrix for Axial Loading

Consider a beam which is axially loaded as shown in Figure 4.9



Figure 4. 9 Axial Loading in x Direction

Here is the governing equation.

$$-\frac{d}{dx} \left[EA \frac{du}{dx} \right] = q(x) \quad (\text{Reddy, 2005}) \quad \text{Equation 4. 38}$$

Assuming constant Young's Modulus, E. u is the displacement in x direction. $q(x)$ is the point axial load of the system.

The weak formulation is:

$$Error = \int_0^L \left[-\frac{d}{dx} \left[EA \frac{du}{dx} \right] - q(x) \right] dx \quad \text{Equation 4. 39}$$

This error will be zero if the solution to the governing equation were to be exact. If it is not exact, then Equation 4.39 will be the approximation of the solution. The next step is to multiply by a weight function, $v(x)$ and equate to zero to achieve minimum potential energy which places the system in equilibrium,

$$\int_0^L v \left[-\frac{d}{dx} \left[EA \frac{du}{dx} \right] - q(x) \right] dx = 0 \quad \text{Equation 4. 40}$$

The next step is to integrate by parts which gives the following expression.

$$\int_0^L \left[\frac{dv}{dx} EA \left[\frac{du}{dx} \right] - vq \right] dx + \left[vEA \left[\frac{du}{dx} \right] \right]_0^L = 0 \quad \text{Equation 4. 41}$$

$\left[EA \left[\frac{du}{dx} \right] \right]_0^L$ represents the boundary condition term. The primary variable in this case is $u|_{x=0}$ and $u|_{x=L}$. Rearranging Equation 4.41 to obtain

$$\int_0^L \left[EA \frac{dv}{dx} \left[\frac{du}{dx} \right] \right] dx = \int_0^L vq - \left[vEA \left[\frac{du}{dx} \right] \right]_0^L \quad \text{Equation 4. 42}$$

This can help in determining the interpolation functions per element.

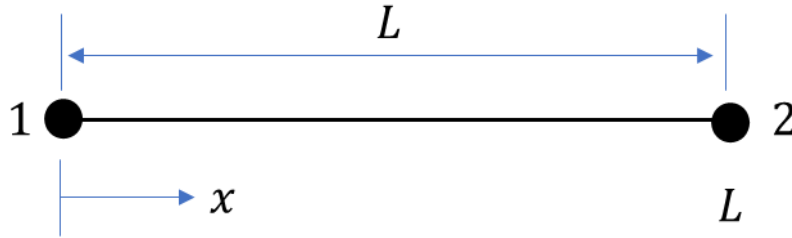


Figure 4. 10 Axial Boundaries of a Two Node Element

$$u^e|_x = \sum_{j=1}^2 u_j^e \phi_j^e(x) = u_1^e \phi_1^e(x) + u_2^e \phi_2^e(x) \quad \text{Equation 4. 43}$$

$$u|_{x=0} = u_1^e \text{ meaning at } x = 0, \phi_1^e = 1 \quad \text{Equation 4. 44}$$

$$u|_{x=L} = u_2^e \text{ meaning at } x = L, \phi_2^e = 1 \quad \text{Equation 4. 45}$$

The aim is to develop $\phi_1^e(x)$ and $\phi_2^e(x)$ which are the interpolation functions. Here are the boundary conditions.

Table 4. 3 Axial Loading Boundary Conditions Table for 2 Node Element

	ϕ_1^e	ϕ_2^e
$x = 0$	1	0
$x = L$	0	1

Each function will have 2 constants since there are 2 degrees of freedom.

$$\phi_1^e(x) = a + bx \quad \text{Equation 4. 46}$$

$$\phi_2^e(x) = c + dx \quad \text{Equation 4. 47}$$

Based on the boundary conditions in Table 4.3, here are the value of the constants.

Table 4. 4 Axial Loading Expressions of Interpolation Functions for Linear 2 Node Beam

Interpolation Function	Constants	Expression per Constant
$\phi_1^e(x)$	a	1
	b	$-\frac{1}{L}$
$\phi_2^e(x)$	c	0
	d	$\frac{1}{L}$

Here are the final full expressions of the interpolation functions.

$$\phi_1^e(x) = 1 - \frac{x}{L} \quad \text{Equation 4. 48}$$

$$\phi_2^e(x) = \frac{x}{L} \quad \text{Equation 4. 49}$$

Recall, this is a two-node element, with each side having 1 degree of freedom.

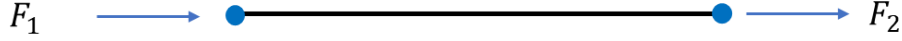


Figure 4. 11 Two DOFs in Axial Loaded Beam Element

This means the stiffness matrix is a 2 by 2 matrix.

$$K = [2 \times 2] \quad \text{Equation 4. 50}$$

Based on the left-hand side of Equation 4.42

$$K_{ij}^e = \int_0^L \left[EA \frac{d\phi_i^e}{dx} \left[\frac{d\phi_j^e}{dx} \right] \right] dx \quad \text{Equation 4. 51}$$

K matrix is bilinear in ϕ_i^e and ϕ_j^e and symmetric in ϕ_i^e and ϕ_j^e . In an overall sense in the x axis,

$$K_{x_{Load}} = \begin{bmatrix} K_{11}^e & K_{12}^e \\ K_{21}^e & K_{22}^e \end{bmatrix} \quad \text{Equation 4. 52}$$

The equations for ϕ_i^e and ϕ_j^e are gotten from the interpolation functions in Equation 4.48 and Equation 4.49. For example, K_{21}^e is calculated thus.

$$K_{21}^e = \int_0^L EA \left[\frac{d\phi_2^e}{dx} \left[\frac{d\phi_1^e}{dx} \right] \right] dx \quad \text{Equation 4. 53}$$

$$K_{21}^e = \int_0^L EA \left[\frac{d\left(\frac{x}{L}\right)}{dx} \left[\frac{d\left(1-\frac{x}{L}\right)}{dx} \right] \right] dx \quad \text{Equation 4. 54}$$

$$K_{21}^e = \frac{-EA}{L} \quad \text{Equation 4. 55}$$

The full stiffness matrix for the x direction loading is

$$K_{x_{Load}} = \begin{bmatrix} \frac{EA}{L} & \frac{-EA}{L} \\ \frac{-EA}{L} & \frac{EA}{L} \end{bmatrix} \quad \text{Equation 4. 56}$$

4.3 The Governing Equation and Stiffness Matrix for Axial Torsion

Consider a homogeneous elastic beam which is axially spun due to Moment M_1 as shown in Figure 4.12.



Figure 4. 12 Axial Torsion Phenomenon

Here is the governing equation.

$$-\frac{d}{dx} \left[GJ \frac{d\theta}{dx} \right] = M(x) \quad (\text{Reddy, 2005}) \quad \text{Equation 4. 57}$$

G = Shear Modulus, psi

J = Polar Moment of Inertia, inches⁴. θ = Twist angle

Assuming constant Shear Modulus, G . u is the displacement in x direction. $M(x)$ is the point axial torsion exerted on the system.

The weak formulation is:

$$\text{Error} = \int_0^L \left[-\frac{d}{dx} \left[GJ \frac{d\theta}{dx} \right] - M(x) \right] dx \quad \text{Equation 4. 58}$$

As seen in earlier sections, next step is to multiply by a weight function, $v(x)$ and equate to zero to achieve minimum potential energy which places the system in equilibrium,

$$\int_0^L v \left[-\frac{d}{dx} \left[GJ \frac{d\theta}{dx} \right] - M(x) \right] dx = 0 \quad \text{Equation 4. 59}$$

The next step is to integrate by parts which gives the following expression.

$$\int_0^L \left[\frac{dv}{dx} GJ \left[\frac{d\theta}{dx} \right] - vM \right] dx + \left[vGJ \left[\frac{d\theta}{dx} \right] \right]_0^L = 0 \quad \text{Equation 4. 60}$$

$\left[GJ \left[\frac{d\theta}{dx} \right] \right]_0^L$ represents the boundary condition term. The primary variable in this case is $\theta|_{x=0}$ and

$\theta|_{x=L}$. Rearranging Equation 4.60 to obtain.

$$\int_0^L \left[GJ \frac{dv}{dx} \left[\frac{d\theta}{dx} \right] \right] dx = \int_0^L vM - \left[vGJ \left[\frac{d\theta}{dx} \right] \right]_0^L \quad \text{Equation 4. 61}$$

This can help in determining the interpolation functions per element referring to Figure 4.13.

$$\theta^e|_x = \sum_{j=1}^2 \theta_j^e \phi_j^e(x_M) = \theta_1^e \phi_1^e(x_M) + \theta_2^e \phi_2^e(x_M) \quad \text{Equation 4. 62}$$

$$\theta|_{x=0} = \theta_1^e \text{ meaning at } x = 0, \phi_1^e = 1 \quad \text{Equation 4. 63}$$

$$\theta|_{x=L} = \theta_2^e \text{ meaning at } x = L, \phi_2^e = 1 \quad \text{Equation 4. 64}$$

Developing expressions for $\phi_1^e(x)$ and $\phi_2^e(x)$ is the goal. Here are the boundary conditions.

Table 4. 5 Axial Torsion Boundary Conditions Table for 2 Node Element

	ϕ_1^e	ϕ_2^e
$x = 0$	1	0
$x = L$	0	1

Just like the axial loading case, each function will have 2 constants since there are 2 degrees of freedom.

$$\phi_1^e(x_M) = a + bx \quad \text{Equation 4. 65}$$

$$\phi_2^e(x_M) = c + dx \quad \text{Equation 4. 66}$$

Based on the boundary conditions in Table 4.5, here are the value of the constants.

Table 4. 6 Axial Torsion Expressions of Interpolation Functions for Linear 2 Node Beam

Interpolation Function	Constants	Expression per Constant
$\phi_1^e(x_M)$	a	1
	b	$-\frac{1}{L}$
$\phi_2^e(x_M)$	c	0
	d	$\frac{1}{L}$

Here are the final full expressions of the interpolation functions.

$$\phi_1^e(x_M) = 1 - \frac{x}{L} \quad \text{Equation 4. 67}$$

$$\phi_2^e(x_M) = \frac{x}{L} \quad \text{Equation 4. 68}$$

Recall, this is a two-node element, with each side having 1 degree of freedom.

This means the stiffness matrix for torsion as well is a 2 by 2 matrix.

$$K = [2 \times 2] \quad \text{Equation 4. 69}$$

Based on the left-hand side of Equation 4.61

$$K_{ij}^e = \int_0^L \left[GJ \frac{d\phi_i^e}{dx} \left[\frac{d\phi_j^e}{dx} \right] \right] dx \quad \text{Equation 4. 70}$$

K matrix is bilinear in ϕ_i^e and ϕ_j^e and symmetric in ϕ_i^e and ϕ_j^e . In an overall sense in the x axis,

$$K_{x_{Moment}} = \begin{bmatrix} K_{11}^e & K_{12}^e \\ K_{21}^e & K_{22}^e \end{bmatrix} \quad \text{Equation 4. 71}$$

The equations for ϕ_i^e and ϕ_j^e are gotten from the interpolation functions in Equation 4.67 and Equation 4.68. For example, K_{12}^e is calculated thus.

$$K_{12}^e = \int_0^L GJ \left[\frac{d\phi_1^e}{dx} \left[\frac{d\phi_2^e}{dx} \right] \right] dx \quad \text{Equation 4. 72}$$

$$K_{12}^e = \int_0^L GJ \left[\frac{d\left(1-\frac{x}{L}\right)}{dx} \left[\frac{d\left(\frac{x}{L}\right)}{dx} \right] \right] dx \quad \text{Equation 4. 73}$$

$$K_{12}^e = -\frac{GJ}{L} \quad \text{Equation 4. 74}$$

The full stiffness matrix for the x direction loading is

$$K_{x_{Torsion}} = \begin{bmatrix} \frac{GJ}{L} & -\frac{GJ}{L} \\ -\frac{GJ}{L} & \frac{GJ}{L} \end{bmatrix} \quad \text{Equation 4. 75}$$

Figure 4.13 shows the variations in interpolation function.

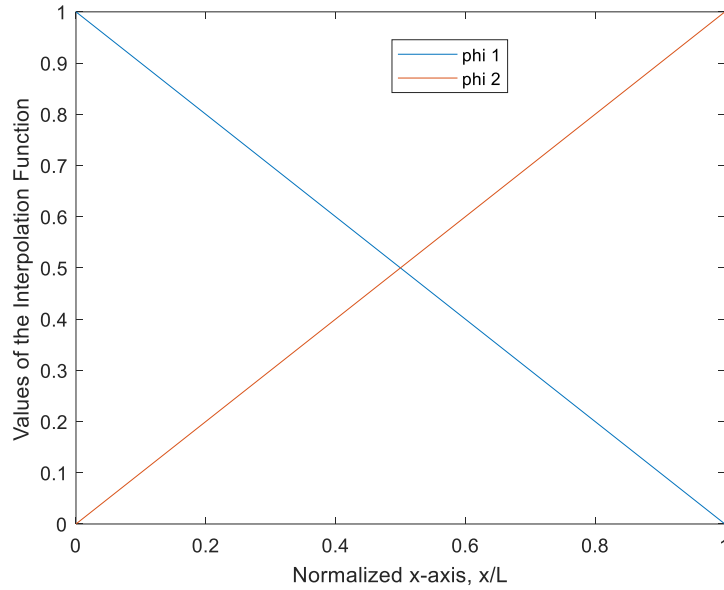


Figure 4. 13 Variations in Interpolation Functions for Axial Loads and Torsion in x Direction

4.4 Full Element Stiffness Matrix of 3D Beams

The drill string is considered a 3-dimensional beam. Since while drilling, the drill bit changes direction from the original axes system, then the original reference of the drill string can be referred to as the global axes system, as shown in the figure below.

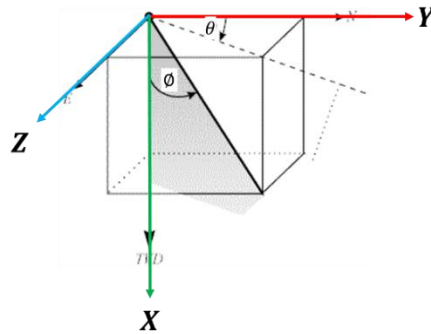


Figure 4. 14 Global Axes System of the Drill String

The x -axis is downwards, indicating that the member is in the x -axis direction. ϕ and θ are inclination and azimuth, respectively. Y can be referred to as Northing, Z as Easting and X as TVD (total vertical depth) axis. For 3 dimensional structures, there are 12 degrees of freedom. This is because the j^{th} end and the k^{th} end have X , Y , and Z coordinates each. The axial

deformation is not ignored, so there are X, Y, and Z displacements and rotations. The labelling starts from j to k .

The figure below shows the position of the displacements on one member of the drill string, assuming the member is placed upright in the global reference system position.

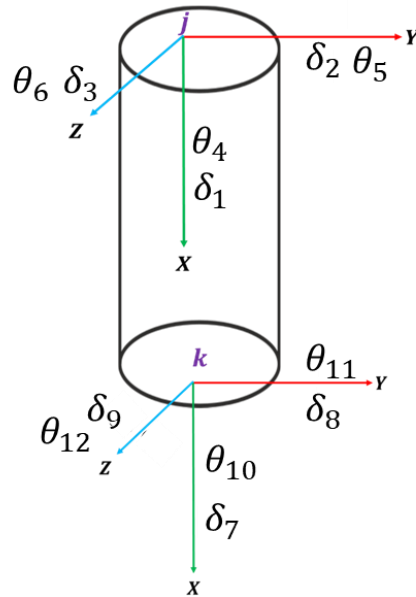


Figure 4. 15 Global Reference Labelling of Drill String

Based on the four independent occurrences, here is how they reflect on the global labelling.

Table 4. 7 Displacement Labelling for 4 Independent Processes of 3D Beams

Process	Relevant Degree of Freedom Labels											
	j^{th} end						k^{th} end					
	Translation			Rotation			Translation			Rotation		
	x	y	z	x	y	z	x	y	z	x	y	z
Axial Loading	δ_1						δ_7					
Axial Torsion				θ_4						θ_{10}		
Bending in XZ		δ_2				θ_6		δ_8				θ_{12}
Bending in XY			δ_3		θ_5				δ_9		θ_{11}	

Since these processes are independent and yet simultaneous, other processes are placed as zero when they occur. Following the fact that there are 12 degrees of freedom, the stiffness matrix will be a 12 by 12 matrix with a number as shown in the table below.

Table 4. 8 Process Per Row of 12 by 12 Stiffness Matrix for Drill String

Process	Relevant Degree of Freedom Labels											
	$j^{th} \text{ end}$						$k^{th} \text{ end}$					
	Translation			Rotation			Translation			Rotation		
	x	y	z	x	y	z	x	y	z	x	y	z
Axial Loading	K_{11}	K_{12}	K_{13}	K_{14}	K_{15}	K_{16}	K_{17}	K_{18}	K_{19}	$K_{1,10}$	$K_{1,11}$	$K_{1,12}$
Bending in XZ	K_{21}	K_{22}	K_{23}	K_{24}	K_{25}	K_{26}	K_{27}	K_{28}	K_{29}	$K_{2,10}$	$K_{2,11}$	$K_{2,12}$
Bending in XY	K_{31}	K_{32}	K_{33}	K_{34}	K_{35}	K_{36}	K_{37}	K_{38}	K_{39}	$K_{3,10}$	$K_{3,11}$	$K_{3,12}$
Axial Torsion	K_{41}	K_{42}	K_{43}	K_{44}	K_{45}	K_{46}	K_{47}	K_{48}	K_{49}	$K_{4,10}$	$K_{4,11}$	$K_{4,12}$
Bending in XY	K_{51}	K_{52}	K_{53}	K_{54}	K_{55}	K_{56}	K_{57}	K_{58}	K_{59}	$K_{5,10}$	$K_{5,11}$	$K_{5,12}$
Bending in XZ	K_{61}	K_{62}	K_{63}	K_{64}	K_{65}	K_{66}	K_{67}	K_{68}	K_{69}	$K_{6,10}$	$K_{6,11}$	$K_{6,12}$
Axial Loading	K_{71}	K_{72}	K_{73}	K_{74}	K_{75}	K_{76}	K_{77}	K_{78}	K_{79}	$K_{7,10}$	$K_{7,11}$	$K_{7,12}$
Bending in XZ	K_{81}	K_{82}	K_{83}	K_{84}	K_{85}	K_{86}	K_{87}	K_{88}	K_{89}	$K_{8,10}$	$K_{8,11}$	$K_{8,12}$
Bending in XY	K_{91}	K_{92}	K_{93}	K_{94}	K_{95}	K_{96}	K_{97}	K_{98}	K_{99}	$K_{9,10}$	$K_{9,11}$	$K_{9,12}$
Axial Torsion	$K_{10,1}$	$K_{10,2}$	$K_{10,3}$	$K_{10,4}$	$K_{10,5}$	$K_{10,6}$	$K_{10,7}$	$K_{10,8}$	$K_{10,9}$	$K_{10,10}$	$K_{10,11}$	$K_{10,12}$
Bending in XY	$K_{11,1}$	$K_{11,2}$	$K_{11,3}$	$K_{11,4}$	$K_{11,5}$	$K_{11,6}$	$K_{11,7}$	$K_{11,8}$	$K_{11,9}$	$K_{11,10}$	$K_{11,11}$	$K_{11,12}$
Bending in XZ	$K_{12,1}$	$K_{12,2}$	$K_{12,3}$	$K_{12,4}$	$K_{12,5}$	$K_{12,6}$	$K_{12,7}$	$K_{12,8}$	$K_{12,9}$	$K_{12,10}$	$K_{12,11}$	$K_{12,12}$

According to equations Equation 4.36, Equation 4.37, Equation 4.52, and Equation 4.75, and their respective processes shown in Table 4.8, it can be inferred the following equations are true.

$$K_{xLoad} = \begin{bmatrix} \frac{EA}{L} & \frac{-EA}{L} \\ \frac{-EA}{L} & \frac{EA}{L} \end{bmatrix} = \begin{bmatrix} K_{11}^e & K_{17}^e \\ K_{71}^e & K_{77}^e \end{bmatrix} \quad \text{Equation 4. 76}$$

$$K_{xTorsion} = \begin{bmatrix} \frac{GJ}{L} & \frac{-GJ}{L} \\ \frac{-GJ}{L} & \frac{GJ}{L} \end{bmatrix} = \begin{bmatrix} K_{44}^e & K_{4,10}^e \\ K_{10,4}^e & K_{10,10}^e \end{bmatrix} \quad \text{Equation 4. 77}$$

$$K_y = \begin{bmatrix} \frac{12EI_z}{L^3} & \frac{-6EI_z}{L^2} & \frac{-12EI_z}{L^3} & \frac{-6EI_z}{L^2} \\ \frac{-6EI_z}{L^2} & \frac{4EI_z}{L} & \frac{6EI_z}{L^2} & \frac{2EI_z}{L} \\ \frac{-12EI_z}{L^3} & \frac{6EI_z}{L^2} & \frac{12EI_z}{L^3} & \frac{6EI_z}{L^2} \\ \frac{-6EI_z}{L^2} & \frac{2EI_z}{L} & \frac{6EI_z}{L^2} & \frac{4EI_z}{L} \end{bmatrix} = \begin{bmatrix} K_{22}^e & K_{26}^e & K_{28}^e & K_{2,12}^e \\ K_{62}^e & K_{66}^e & K_{68}^e & K_{6,12}^e \\ K_{82}^e & K_{86}^e & K_{88}^e & K_{8,12}^e \\ K_{12,2}^e & K_{12,6}^e & K_{12,8}^e & K_{12,12}^e \end{bmatrix} \quad \text{Equation 4. 78}$$

$$K_z = \begin{bmatrix} \frac{12EI_y}{L^3} & \frac{-6EI_y}{L^2} & \frac{-12EI_y}{L^3} & \frac{-6EI_y}{L^2} \\ \frac{-6EI_y}{L^2} & \frac{4EI_y}{L} & \frac{6EI_y}{L^2} & \frac{2EI_y}{L} \\ \frac{-12EI_y}{L^3} & \frac{6EI_y}{L^2} & \frac{12EI_y}{L^3} & \frac{6EI_y}{L^2} \\ \frac{-6EI_y}{L^2} & \frac{2EI_y}{L} & \frac{6EI_y}{L^2} & \frac{4EI_y}{L} \end{bmatrix} = \begin{bmatrix} K_{33}^e & K_{35}^e & K_{39}^e & K_{3,11}^e \\ K_{53}^e & K_{55}^e & K_{59}^e & K_{5,11}^e \\ K_{93}^e & K_{95}^e & K_{99}^e & K_{9,11}^e \\ K_{11,3}^e & K_{11,5}^e & K_{11,9}^e & K_{11,11}^e \end{bmatrix} \quad \text{Equation 4. 79}$$

Therefore, the full stiffness matrix will be as stated below:

Table 4. 9 Expressions of Stiffness in 3 D 12 by 12 Matrix

Process	Relevant Degree of Freedom Labels											
	$j^{th} \text{ end}$						$k^{th} \text{ end}$					
	Translation			Rotation			Translation			Rotation		
	x	y	z	x	y	z	x	y	z	x	y	z
Axial Loading	$\frac{EA}{L}$	0	0	0	0	0	$-\frac{EA}{L}$	0	0	0	0	0
Bending in XZ	0	$\frac{12EI_z}{L^3}$	0	0	0	$\frac{-6EI_z}{L^2}$	0	$\frac{-12EI_z}{L^3}$	0	0	0	$\frac{-6EI_z}{L^2}$
Bending in XY	0	0	$\frac{12EI_y}{L^3}$	0	$\frac{-6EI_y}{L^2}$	0	0	0	$\frac{-12EI_y}{L^3}$	0	$\frac{-6EI_y}{L^2}$	0
Axial Torsion	0	0	0	$\frac{GJ}{L}$	0	0	0	0	0	$-\frac{GJ}{L}$	0	0
Bending in XY	0	0	$\frac{-6EI_y}{L^2}$	0	$\frac{4EI_y}{L}$	0	0	0	$\frac{6EI_y}{L^2}$	0	$\frac{2EI_y}{L}$	0
Bending in XZ	0	$\frac{-6EI_z}{L^2}$	0	0	0	$\frac{4EI_z}{L}$	0	$\frac{6EI_z}{L^2}$	0	0	0	$\frac{2EI_z}{L}$
Axial Loading	$-\frac{EA}{L}$	0	0	0	0	0	$\frac{EA}{L}$	0	0	0	0	0
Bending in XZ	0	$\frac{-12EI_z}{L^3}$	0	0	0	$\frac{6EI_z}{L^2}$	0	$\frac{12EI_z}{L^3}$	0	0	0	$\frac{6EI_z}{L^2}$
Bending in XY	0	0	$\frac{-12EI_y}{L^3}$	0	$\frac{6EI_y}{L^2}$	0	0	0	$\frac{12EI_y}{L^3}$	0	$\frac{6EI_y}{L^2}$	0
Axial Torsion	0	0	0	$-\frac{GJ}{L}$	0	0	0	0	0	$\frac{GJ}{L}$	0	0
Bending in XY	0	0	$\frac{-6EI_y}{L^2}$	0	$\frac{2EI_y}{L}$	0	0	0	$\frac{6EI_y}{L^2}$	0	$\frac{4EI_y}{L}$	0
Bending in XZ	0	$\frac{-6EI_z}{L^2}$	0	0	0	$\frac{2EI_z}{L}$	0	$\frac{6EI_z}{L^2}$	0	0	0	$\frac{4EI_z}{L}$

For steel, here are the values of the constants:

$E = \text{Young's Modulus} = 30,000 \text{ psi}$

$$A = \text{Cross – Sectional Area} = \pi * \frac{OD^2 - ID^2}{4}, \text{in}^2 \quad \text{Equation 4. 80}$$

$$I = \text{Cross – Sectional Moment of Inertia} = \frac{\pi(OD^4 - ID^4)}{64}, \text{in}^4 \quad \text{Equation 4. 81}$$

$L = \text{Length of Element, ft}$

$G = \text{Shear Modulus} = 11,501,513.4 \text{ psi}$

$$J = \text{Polar Moment of Inertia} = \frac{\pi(OD^4 - ID^4)}{2}, \text{inches}^4. \quad \text{Equation 4. 82}$$

4.5 Global and Local Members of the Drill String

The drill string has a non orthogonal axis system due to the fact that the when the drilling operations occur, the drill bit keeps changing direction therefore changing the axis of the drill string. The stiffness matrix of 12 by 12 matrix remains the same but it has to be transformed to the reference axis system. The reference axis is called “the global axis” while the current axis of the bit is called “the local axis.” The figure below shows the combined global and local axis in a well path.

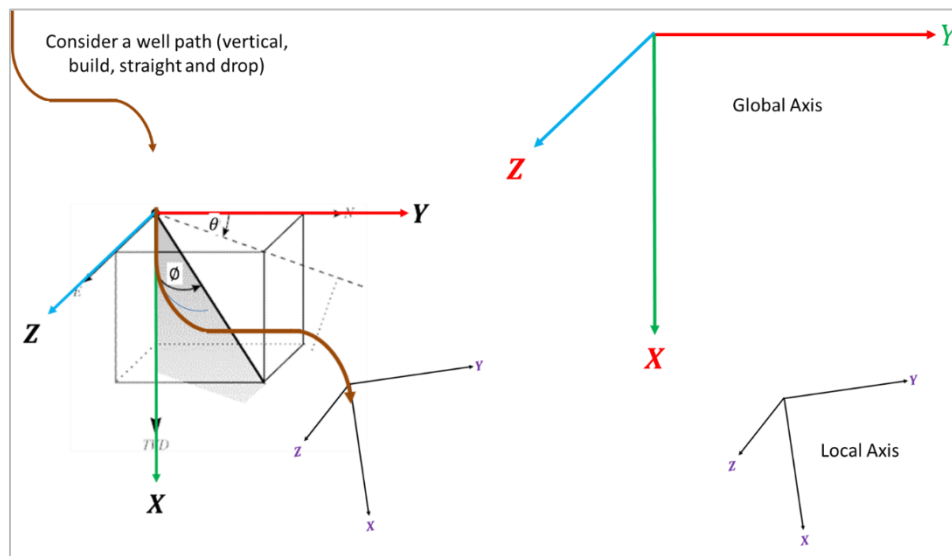


Figure 4. 16 Global and Local Axis System in Drill String

structure of a sample drill string. Of the 11 members, 3 of them are restrained when the condition is rotary drilling and sliding. The 3 restrained members are stabilizers. The displacements in the radial direction are placed as zero. This are the fixed ends of this drill string. Since the rotary table is not a member, the fixed ends at the top are not inputted.

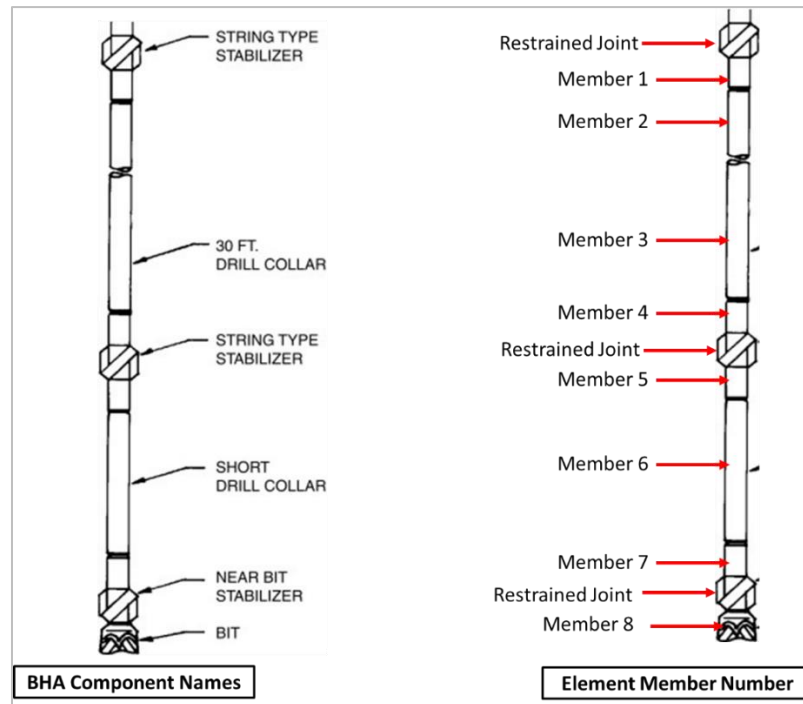


Figure 4. 18 Assigning Member Nomenclature for Vertical Well (Xiaozhen, 2013)

To identify the number of degrees of freedom, labelling the restrained and unrestrained displacements is key. In this case, the drill string is in vertical position which is pretty much the global axis of the drill string. Subsequent examples will show when the local axis deviates from the global axis. The first step is to label global axis. Here are the rules:

- Start with xyz translation at j^{th} end
- Then label xyz rotation at j^{th} end
- Next is to label xyz translation at k^{th} end
- Finally label xyz rotation at k^{th} end

It is important to note that not all the axis of a restrained joint will be unreleased. Sometimes, one axis might be unrestrained. In the stabilizer joints for instance, the global x-axis is unrestrained even though the Y and Z axis are restrained. At some other instance it could be just the rotation

displacement that is restrained just like in the case of “sliding, tripping in, and tripping out,” only the rotation on the global x-axis is restrained, the translation displacement is unrestrained. In this example of drill string in a vertical well, there are 54 degrees of freedom which includes 42 unrestrained degrees of freedom and 12 restrained degrees of freedom.

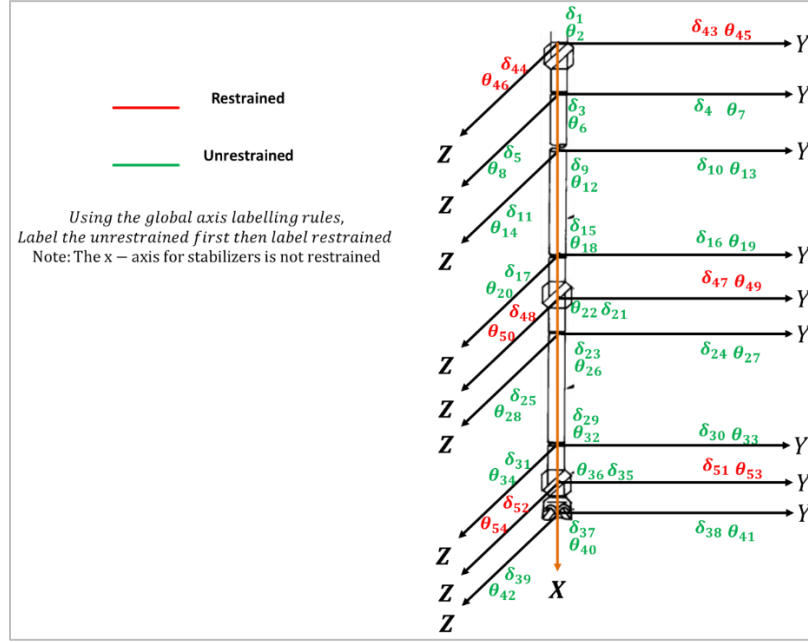


Figure 4. 19 Labelled Drill String with Unrestrained DOF Shown

Here is the table of members and their respective global labels. The labels on the j^{th} end is written first then the labels on the k^{th} end are written. The labels are written according to the rules of global axis labelling. Only the global numbers are written.

It is important to note that the labels of the k^{th} end of one member becomes the labels of the j^{th} end of the next member. This makes it easier to run the computation of the labelling especially as the number of drilling component gets larger.

Table 4. 10 Connectivity Matrix for the Vertical Well Example

Member Number	Degree of Freedom Labels											
	j^{th} end						k^{th} end					
	Translation			Rotation			Translation			Rotation		
	x	y	z	x	y	z	x	y	z	x	y	z
1	1	43	44	2	45	46	3	4	5	6	7	8
2	3	4	5	6	7	8	9	10	11	12	13	14
3	9	10	11	12	13	14	15	16	17	18	19	20
4	15	16	17	18	19	20	21	47	48	22	49	50
5	21	47	48	22	49	50	23	24	25	26	27	28
6	23	24	25	26	27	28	29	30	31	32	33	34
7	29	30	31	32	33	34	35	51	52	36	53	54
8	35	51	52	36	53	54	37	38	39	40	41	42

4.5.1.1 Calculating Stiffness Matrix for Each Member of the Drill String

The entire component of the drill string is in 3 dimensions so their individual stiffness matrix will be a 12 by 12 matrix made up of stiffness coefficients.

Table 4. 11 Input for Each Member for Stiffness Matrix Calculation

Member Number	L , ft	OD , in	ID , in
1	15	8.725	3
2	20	8.725	3
3	30	8.725	3
4	15	8.725	3
5	15	8.725	3
6	30	8.725	3
7	15	8.725	3
8	3	11	0.3

This example is for a scenario where the drill string is in same coordinates in local axis and global axis. Moving on in this example, the next step is to write the global stiffness matrix for the complete structure. The principle is to write the unrestrained degree of freedom first before writing the unrestrained degree of freedom in the matrix. Recall that displacements 1 to 42 are unrestrained while displacements 43 to 54 are restrained degree of freedom. The figure below shows exactly how the global stiffness matrix for this entire structure of this example is arranged.

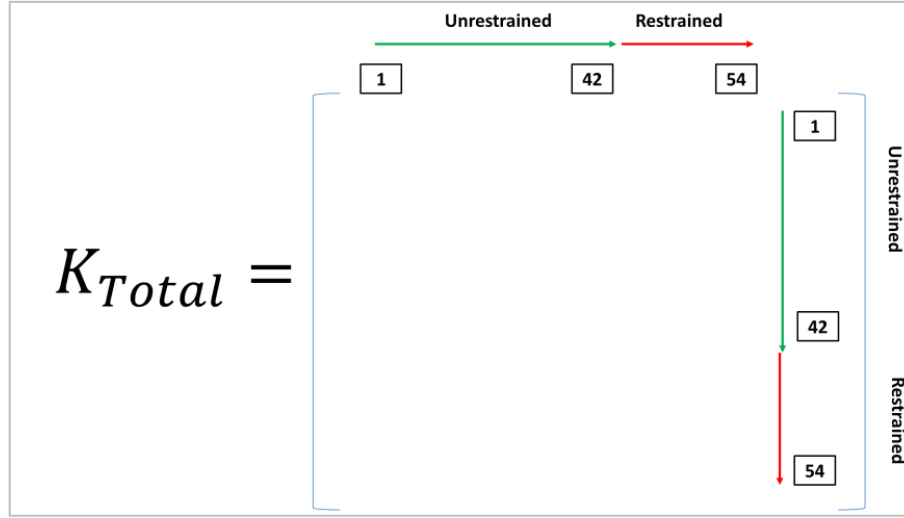


Figure 4. 20 Structural Description of Global Stiffness Matrix

The total global stiffness matrix can be divided into 4 quadrants of a cross partition matrix as follows.

1. A group of stiffness coefficients with the impact location at the unrestrained degree of freedom and reaction at the unrestrained degree of freedom points K_{uu}
2. A group of stiffness coefficients where the impact location is the unrestrained degree of freedom but the reaction occurs at the restrained degree of freedom points, K_{ur}
3. A group of stiffness coefficients having their impact location at the restrained degree of freedom and the reaction location at the unrestrained degree of freedom points K_{ru}
4. A group of stiffness coefficients made up of impact location at the restrained degree of freedom and reaction location at the restrained degree of freedom points K_{rr}

Here is the location of each of these four stiffness matrices.

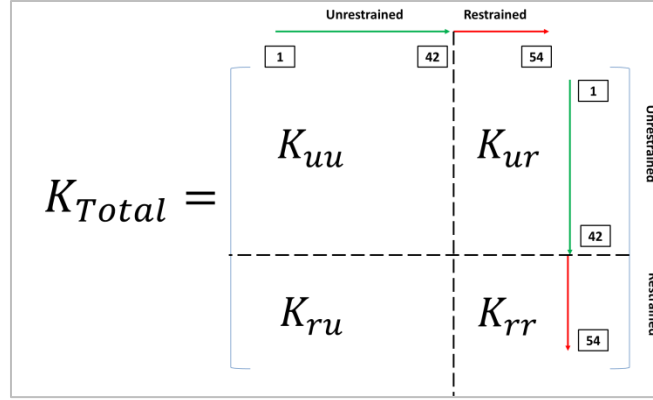


Figure 4. 21 The Four Quadrants of the Global Stiffness Matrix for the Complete Structure

4.5.2 Switching from Bit Axis to Global Axis Using the Transformation Matrix

Another example will be considered with just two members in order to have enough room show the global stiffness matrix for the entire structure. These simple equations can tell the number of degree of freedom expected.

$$\text{Number of Degree of Freedom} = \text{Number of Members} + 1$$

Equation 4. 83

The other addition to this new example is that the drill string is at 30° inclination and 20° azimuth.

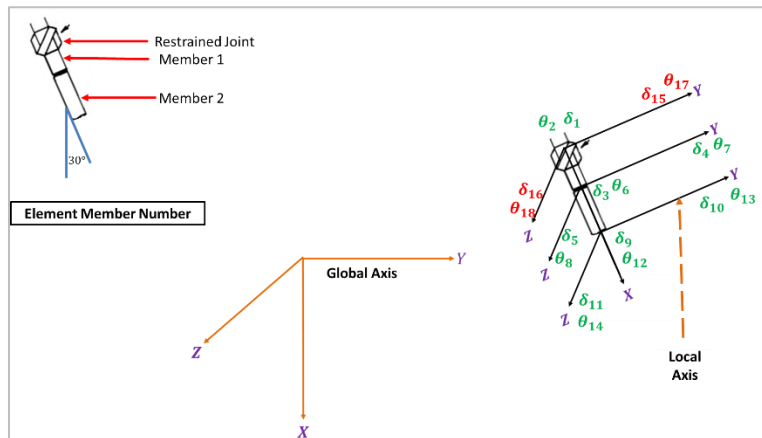


Figure 4. 22 Inclined Members of the Drill String

Here is the connectivity matrix for this assembly of members.

Table 4. 12 Connectivity Matrix for the Inclined Well Example

Member Number	Global Degree of Freedom Labels											
	j^{th} end						k^{th} end					
	Translation			Rotation			Translation			Rotation		
	x	y	z	x	y	z	x	y	z	x	y	z
1	1	15	16	2	17	18	3	4	5	6	7	8
2	3	4	5	6	7	8	9	10	11	12	13	14

The calculation of stiffness matrix for each member is still the same as shown below.

Table 4. 13 Generic Output for Stiffness Matrix Calculation for Each Member of the Inclined Well

Member Number	L, ft	OD, in	ID, in	A, in^2	I, in^4	J, in^4	$\frac{EA}{L}, lb/ft$	$\frac{12EI}{L^3}, lb * in^2/ft^3$	$\frac{6EI}{L^2}, lb * in^2/ft^2$	$\frac{4EI}{L}, lb * in^2/ft$	$\frac{2EI}{L}, lb * in^2/ft$	$\frac{GJ}{L}, lb * in^2/ft$
1	15	8.725	3	52.720	280.491	8975.704	105440	29919	224393	33658920	1121964	6882278655.36
2	20	8.725	3	52.720	280.491	8975.704	79080	12622	126221	1682946	841473	5161708991.52

Since the two members are inclined, the stiffness matrix for each member is the local stiffness matrix for that member. This means, the local stiffness matrix has to be converted to the global stiffness matrix. The calculation of the local stiffness matrix is the same 12 by 12 matrix as before. The procedure is the same.

$$K_1 = \begin{bmatrix} \begin{matrix} j \\ \text{Translation} \\ 1 & 15 & 16 \\ x & y & z \\ 105440 & 0 & 0 \\ 0 & 29919 & 0 \\ 0 & 0 & 29919 \\ 0 & 0 & 0 \\ 0 & 0 & -224393 \\ 0 & 224393 & 0 \\ -105440 & 0 & 0 \\ 0 & -29919 & 0 \\ 0 & 0 & -29919 \\ 0 & 0 & 0 \\ 0 & 0 & -224393 \\ 0 & 224393 & 0 \end{matrix} & \begin{matrix} j \\ \text{Rotation} \\ 2 & 17 & 18 \\ x & y & z \\ 0 & 0 & 0 \\ 0 & 0 & 224393 \\ -224393 & 0 & 0 \\ 0 & 0 & 0 \\ 33658920 & 0 & 0 \\ 0 & 0 & 0 \\ 0 & -224393 & 0 \\ 224393 & 0 & 0 \\ 0 & 0 & 0 \\ 1121964 & 0 & 0 \end{matrix} & \begin{matrix} k \\ \text{Translation} \\ 3 & 4 & 5 \\ x & y & z \\ -105440 & 0 & 0 \\ -29919 & 0 & 0 \\ 0 & -29919 & 0 \\ 0 & 0 & 224393 \\ -224393 & 0 & 0 \\ 0 & 0 & 0 \\ 29919 & 0 & 0 \\ 0 & 29919 & 0 \\ 0 & 0 & 224393 \\ 0 & 0 & 0 \end{matrix} & \begin{matrix} k \\ \text{Rotation} \\ 6 & 7 & 8 \\ x & y & z \\ 0 & 0 & 0 \\ 0 & 0 & 224393 \\ -224393 & 0 & 0 \\ 0 & 0 & 0 \\ 1121964 & 0 & 0 \\ 0 & 0 & 1121964 \\ 0 & 0 & 0 \\ -224393 & 0 & 0 \\ 33658920 & 0 & 0 \end{matrix} & \begin{matrix} \leftarrow DOF \\ \downarrow \\ x \\ y \\ z \\ x \\ y \\ z \\ x \\ y \\ z \\ x \\ y \\ z \end{matrix} \end{bmatrix}$$

In the same manner, the stiffness matrix for the second member is calculated.

$$K_2 = \begin{bmatrix} \begin{matrix} & \begin{matrix} j \\ \text{Translation} \end{matrix} & & \begin{matrix} j \\ \text{Rotation} \end{matrix} & & \begin{matrix} k \\ \text{Translation} \end{matrix} & & \begin{matrix} k \\ \text{Rotation} \end{matrix} \\ \begin{matrix} 3 \\ x \\ 79080 \\ 0 \\ 0 \\ 0 \\ 0 \\ 0 \\ 0 \\ 0 \\ 0 \\ 0 \\ 0 \\ 0 \\ 0 \end{matrix} & \begin{matrix} 4 \\ y \\ 0 \\ 12622 \\ 0 \\ 0 \\ 126221 \\ -12622 \\ 0 \\ 0 \\ 0 \\ 126221 \\ 0 \\ 126221 \end{matrix} & \begin{matrix} 5 \\ z \\ 0 \\ 0 \\ 12622 \\ 0 \\ 0 \\ 0 \\ -126221 \\ 0 \\ -126221 \\ 0 \\ 0 \\ 0 \end{matrix} & \begin{matrix} 6 \\ x \\ 0 \\ 0 \\ 0 \\ 5161708991.52 \\ 0 \\ 0 \\ 0 \\ 0 \\ 0 \\ 0 \\ 841473 \\ 0 \end{matrix} & \begin{matrix} 7 \\ y \\ 0 \\ 0 \\ 0 \\ 0 \\ 0 \\ 1682946 \\ 0 \\ 126221 \\ 0 \\ 0 \\ 0 \\ 0 \end{matrix} & \begin{matrix} 8 \\ z \\ 0 \\ 126221 \\ 0 \\ 0 \\ 1682946 \\ 0 \\ 0 \\ 0 \\ 0 \\ 0 \\ 0 \\ 0 \end{matrix} & \begin{matrix} 9 \\ x \\ -79080 \\ 0 \\ 0 \\ 0 \\ 0 \\ 0 \\ 79080 \\ 0 \\ 0 \\ 0 \\ 0 \\ 0 \end{matrix} & \begin{matrix} 10 \\ y \\ 0 \\ -12622 \\ 0 \\ 0 \\ -126221 \\ 12622 \\ 0 \\ 0 \\ 12622 \\ 0 \\ -126221 \end{matrix} & \begin{matrix} 11 \\ z \\ 0 \\ 0 \\ -12622 \\ 0 \\ 0 \\ 0 \\ 0 \\ 12622 \\ 0 \\ 0 \\ 126221 \end{matrix} & \begin{matrix} 12 \\ x \\ 0 \\ 0 \\ 0 \\ -5161708991.52 \\ 0 \\ 0 \\ 0 \\ 0 \\ 5161708991.52 \\ 0 \\ 1682946 \end{matrix} & \begin{matrix} 13 \\ y \\ 0 \\ 0 \\ 0 \\ 0 \\ 841473 \\ 0 \\ 0 \\ 126221 \\ 0 \\ 0 \\ 0 \end{matrix} & \begin{matrix} 14 \\ z \\ 0 \\ 126221 \\ 0 \\ 0 \\ 0 \\ 0 \\ -126221 \\ 0 \\ 0 \\ 0 \\ 1682946 \end{matrix} & \begin{matrix} \leftarrow \\ \downarrow \\ x \\ y \\ z \\ x \\ y \\ z \\ x \\ y \\ z \\ x \\ y \\ z \end{matrix} & \begin{matrix} DOF \\ 3 \\ 4 \\ 5 \\ 6 \\ 7 \\ 8 \\ 9 \\ 10 \\ 11 \\ 12 \\ 13 \\ 14 \end{matrix} \end{bmatrix}$$

Now a transformation matrix is needed to transform the local stiffness matrix to its corresponding global matrix using the following formula.

$$[\overline{K}_i] = [T_i^T][K_i][T] \quad (\text{Reddy, 2005}) \quad \text{Equation 4. 84}$$

Where $[\overline{K}_i] = \text{Global Stiffness Matrix for Each Member}$

$$[T] = \begin{bmatrix} \begin{matrix} \cos \alpha & \sin \alpha \cos \beta & \sin \alpha \sin \beta \\ -\sin \alpha & \cos \alpha \cos \beta & \cos \alpha \sin \beta \\ 0 & -\sin \beta & \cos \beta \end{matrix} & \begin{matrix} 0 \\ 0 \\ 0 \end{matrix} & \begin{matrix} \cos \alpha & \sin \alpha \cos \beta & \sin \alpha \sin \beta \\ -\sin \alpha & \cos \alpha \cos \beta & \cos \alpha \sin \beta \\ 0 & -\sin \beta & \cos \beta \end{matrix} & \begin{matrix} 0 \\ 0 \\ 0 \end{matrix} & \begin{matrix} \cos \alpha & \sin \alpha \cos \beta & \sin \alpha \sin \beta \\ -\sin \alpha & \cos \alpha \cos \beta & \cos \alpha \sin \beta \\ 0 & -\sin \beta & \cos \beta \end{matrix} & \begin{matrix} 0 \\ 0 \\ 0 \end{matrix} & \begin{matrix} \cos \alpha & \sin \alpha \cos \beta & \sin \alpha \sin \beta \\ -\sin \alpha & \cos \alpha \cos \beta & \cos \alpha \sin \beta \\ 0 & -\sin \beta & \cos \beta \end{matrix} & \begin{matrix} 0 \\ 0 \\ 0 \end{matrix} \end{bmatrix} \quad \text{Equation 4. 85}$$

The transpose of this will become,

$$[T^T] = \begin{bmatrix} \begin{matrix} \cos \alpha & -\sin \alpha & 0 \\ \sin \alpha \cos \beta & \cos \alpha \cos \beta & -\sin \beta \\ \sin \alpha \sin \beta & \cos \alpha \sin \beta & \cos \beta \end{matrix} & \begin{matrix} 0 \\ 0 \\ 0 \end{matrix} & \begin{matrix} \cos \alpha & -\sin \alpha & 0 \\ \sin \alpha \cos \beta & \cos \alpha \cos \beta & -\sin \beta \\ \sin \alpha \sin \beta & \cos \alpha \sin \beta & \cos \beta \end{matrix} & \begin{matrix} 0 \\ 0 \\ 0 \end{matrix} & \begin{matrix} \cos \alpha & -\sin \alpha & 0 \\ \sin \alpha \cos \beta & \cos \alpha \cos \beta & -\sin \beta \\ \sin \alpha \sin \beta & \cos \alpha \sin \beta & \cos \beta \end{matrix} & \begin{matrix} 0 \\ 0 \\ 0 \end{matrix} & \begin{matrix} \cos \alpha & -\sin \alpha & 0 \\ \sin \alpha \cos \beta & \cos \alpha \cos \beta & -\sin \beta \\ \sin \alpha \sin \beta & \cos \alpha \sin \beta & \cos \beta \end{matrix} & \begin{matrix} 0 \\ 0 \\ 0 \end{matrix} \end{bmatrix} \quad \text{Equation 4. 86}$$

Where $\alpha = \text{Inclination is } 30^\circ$ and $\beta = \text{azimuth is } 20^\circ$

$$\begin{aligned}
& [T^T] \\
& = \begin{bmatrix} \cos 30 & -\sin 30 & 0 & & & & & & \\ \sin 30 \cos 20 & \cos 30 \cos 20 & -\sin 20 & 0 & & 0 & & 0 & \\ \sin 30 \sin 20 & \cos 30 \sin 20 & \cos 20 & & & & & & \\ & 0 & & \cos 30 & -\sin 30 & 0 & & & \\ & & & \sin 30 \cos 20 & \cos 30 \cos 20 & -\sin 20 & 0 & & \\ & & & \sin 30 \sin 20 & \cos 30 \sin 20 & \cos 20 & & & \\ & & & & & & \cos 30 & -\sin 30 & 0 \\ & & & & & & \sin 30 \cos 20 & \cos 30 \cos 20 & -\sin 20 \\ & & & & & & \sin 30 \sin 20 & \cos 30 \sin 20 & \cos 20 \end{bmatrix}
\end{aligned}$$

$$\begin{aligned}
& [T] \\
& = \begin{bmatrix} \cos 30 & \sin 30 \cos 20 & \sin 30 \cos 20 & & & & & & \\ -\sin 30 & \cos 30 \cos 20 & \cos 30 \sin 20 & 0 & & 0 & & 0 & \\ 0 & -\sin 20 & \cos 20 & & & & & & \\ & 0 & & \cos 30 & \sin 30 \cos 20 & \sin 30 \cos 20 & & & \\ & & & -\sin 30 & \cos 30 \cos 20 & \cos 30 \sin 20 & 0 & & \\ & & & 0 & -\sin 20 & \cos 20 & & & \\ & & & & & & \cos 30 & \sin 30 \cos 20 & \sin 30 \cos 20 \\ & & & & & & -\sin 30 & \cos 30 \cos 20 & \cos 30 \sin 20 \\ & & & & & & 0 & -\sin 20 & \cos 20 \end{bmatrix}
\end{aligned}$$

$$\begin{aligned}
& [T^T] \\
& = \begin{bmatrix} 0.8660 & -0.5000 & 0 & & & & & & \\ 0.4698 & 0.8138 & 0.3420 & 0 & & 0 & & 0 & \\ 0.1710 & 0.2962 & 0.9400 & & & & & & \\ & 0 & & 0.8660 & -0.5000 & 0 & & & \\ & & & 0.4698 & 0.8138 & 0.3420 & 0 & & \\ & & & 0.1710 & 0.2962 & 0.9400 & & & \\ & & & & & & 0.8660 & -0.5000 & 0 \\ & & & & & & 0.4698 & 0.8138 & 0.3420 \\ & & & & & & 0.1710 & 0.2962 & 0.9400 \\ & & & & & & & 0.8660 & -0.5000 & 0 \\ & & & & & & & 0.4698 & 0.8138 & 0.3420 \\ & & & & & & & 0.1710 & 0.2962 & 0.9400 \end{bmatrix}
\end{aligned}$$

$$\begin{aligned}
& [T] \\
& = \begin{bmatrix} 0.8660 & 0.4698 & 0.1710 & & & & & & \\ -0.5000 & 0.8138 & 0.2692 & 0 & & 0 & & 0 & \\ 0 & 0.3420 & 0.9400 & & & & & & \\ & 0 & & 0.8660 & 0.4698 & 0.1710 & & & \\ & & & -0.5000 & 0.8138 & 0.2692 & 0 & & \\ & & & 0 & 0.3420 & 0.9400 & & & \\ & & & & & & 0.8660 & 0.4698 & 0.1710 \\ & & & & & & -0.5000 & 0.8138 & 0.2692 \\ & & & & & & 0 & 0.3420 & 0.9400 \\ & & & & & & & 0.8660 & 0.4698 & 0.1710 \\ & & & & & & & -0.5000 & 0.8138 & 0.2692 \\ & & & & & & & 0 & 0.3420 & 0.9400 \end{bmatrix}
\end{aligned}$$

$$[k] = [T^T]_i / [k_{1global}] / [T]$$

Equation 4. 87

4.6 Formulas Leading to the Force and Moment Calculations

A continuation of the previous example shows a cross partition as shown below.

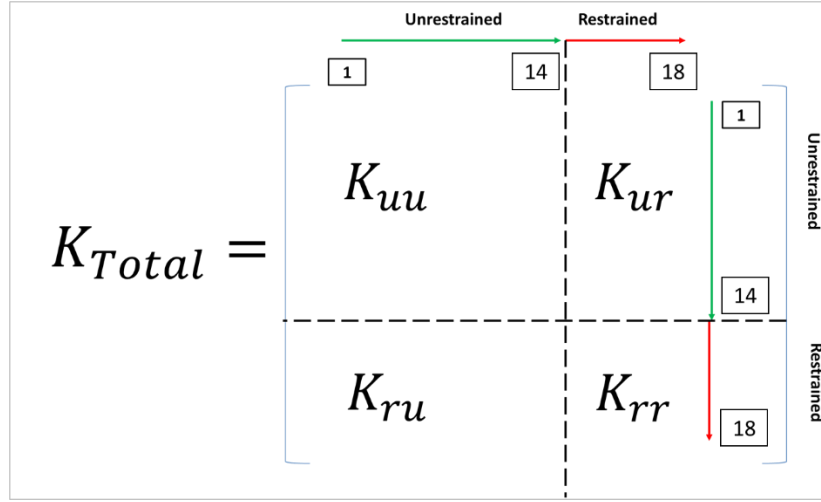


Figure 4. 23 Categorizing Total K into Unrestrained and Restrained DOF

The zone of interest is the matrix where the unrestrained load impacted the unrestrained joint, which is K_{uu} . This can lead to calculating the displacements at the unrestrained joints using Equation 4.88 which can be inferred from Equation 4.1.

$$[K_{uu}][\Delta u] = [J_L]_u \quad \text{Equation 4. 88}$$

Where $[\Delta u]$ is the unrestrained displacements at the unrestrained joints and $[J_L]_u$ is the joint load at the unrestrained degree of freedom.

$$[\Delta u] = [K_{uu}^{-1}][J_L]_u \quad \text{Equation 4. 89}$$

All the restrained displacements are zero. Next is to calculate moments and forces of the individual members before merging them into one final global moments and forces. The right-hand side of Equation 4.1 can be interpreted to calculate the forces and moments for each member as shown in Equation 4.90.

$$[\overline{M}]_i = [\overline{K}_i][\bar{\delta}]_i + [\overline{FEM}]_i \quad \text{Equation 4. 90}$$

Where $[\overline{M}]_i$ is the global moment and forces for each member. $[\overline{K}_i]$ is the global stiffness matrix for each member. $[\bar{\delta}]_i$ are the global displacements for each member which includes restrained

displacements (zero in value) and the unrestrained displacements, $[\Delta u]$. $[\overline{FEM}]_I$ are the fixed end moments for each member, which in value are a reserve sign of the joint load, meaning

$$[\overline{FEM}]_I = -[J_L]_u \quad (\text{Reddy, 2005}) \quad \text{Equation 4. 91}$$

4.6.1 Fixed End Moments of the Drill String

There are generic formulas to calculating the fixed end moments of any structure. Each member of the drill string will have its approximate gravity forces depending on which position it is on the drill string and the position of the drill string in the well plan. One important fact is that each member has to be first treated as a fixed end and when the forces and moments at each end is calculated, it can then be resolved into its 3-dimensional components.

Going back to the inclined example, the approximate gravitational force can be assumed to be the forces in play. The figure below shows the process in generating the fixed end moments and the joint loads.

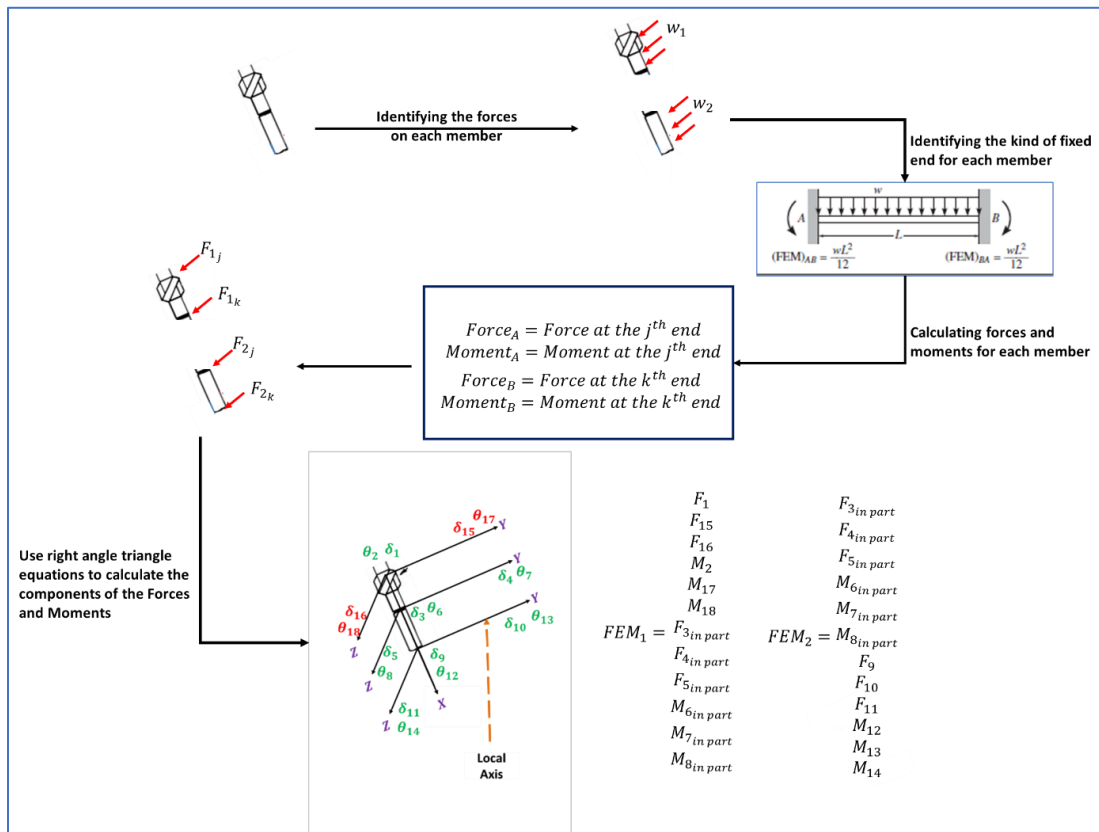


Figure 4. 24 Process of Obtaining Fixed End Moments of the Drill String

4.6.2 Calculating Joint Load of the Drill String

The fixed end moment calculated is based on the local axis of each member. Therefore, it has to be transformed to the global axis before the joint load can be calculated. The joint load is the reverse sign of the global fixed end moment. Based on Equation 4.87, the local fixed end moment can be related to the global fixed end moment.

$$[\overline{FEM}]_i = [T]_i^T [FEM]_i \quad \text{Equation 4. 92}$$

For the inclined wellbore example, the formula becomes:

$$[\overline{FEM}]_1 = \begin{bmatrix} \cos \alpha & -\sin \alpha & 0 & 0 & 0 & 0 \\ \sin \alpha \cos \beta & \cos \alpha \cos \beta & -\sin \beta & 0 & 0 & 0 \\ \sin \alpha \sin \beta & \cos \alpha \sin \beta & \cos \beta & 0 & 0 & 0 \\ 0 & \cos \alpha & -\sin \alpha & 0 & 0 & 0 \\ 0 & \sin \alpha \cos \beta & \cos \alpha \cos \beta & -\sin \beta & 0 & 0 \\ 0 & \sin \alpha \sin \beta & \cos \alpha \sin \beta & \cos \beta & 0 & 0 \end{bmatrix} \begin{bmatrix} F_1 \\ F_{15} \\ F_{16} \\ M_2 \\ M_{17} \\ M_{18} \\ F_{3in\ part} \\ F_{4in\ part} \\ F_{5in\ part} \\ M_{6in\ part} \\ M_{7in\ part} \\ M_{8in\ part} \end{bmatrix} \quad \text{Equation 4. 93}$$

$$[\overline{FEM}]_2 = \begin{bmatrix} \cos \alpha & -\sin \alpha & 0 & 0 & 0 & 0 \\ \sin \alpha \cos \beta & \cos \alpha \cos \beta & -\sin \beta & 0 & 0 & 0 \\ \sin \alpha \sin \beta & \cos \alpha \sin \beta & \cos \beta & 0 & 0 & 0 \\ 0 & \cos \alpha & -\sin \alpha & 0 & 0 & 0 \\ 0 & \sin \alpha \cos \beta & \cos \alpha \cos \beta & -\sin \beta & 0 & 0 \\ 0 & \sin \alpha \sin \beta & \cos \alpha \sin \beta & \cos \beta & 0 & 0 \end{bmatrix} \begin{bmatrix} F_{3in\ part} \\ F_{4in\ part} \\ F_{5in\ part} \\ M_{6in\ part} \\ M_{7in\ part} \\ M_{8in\ part} \\ F_9 \\ F_{10} \\ F_{11} \\ M_{12} \\ M_{13} \\ M_{14} \end{bmatrix} \quad \text{Equation 4. 94}$$

The joint load is then the reverse sign of the global fixed end moment.

$$JL_1 = \begin{bmatrix} -\bar{F}_1 \\ -\bar{F}_{15} \\ -\bar{F}_{16} \\ -\bar{M}_2 \\ -\bar{M}_{17} \\ -\bar{M}_{18} \\ -\bar{F}_{3in\ part} \\ -\bar{F}_{4in\ part} \\ -\bar{F}_{5in\ part} \\ -\bar{M}_{6in\ part} \\ -\bar{M}_{7in\ part} \\ -\bar{M}_{8in\ part} \end{bmatrix} \quad JL_2 = \begin{bmatrix} -\bar{F}_{3in\ part} \\ -\bar{F}_{4in\ part} \\ -\bar{F}_{5in\ part} \\ -\bar{M}_{6in\ part} \\ -\bar{M}_{7in\ part} \\ -\bar{M}_{8in\ part} \\ -\bar{F}_9 \\ -\bar{F}_{10} \\ -\bar{F}_{11} \\ -\bar{M}_{12} \\ -\bar{M}_{13} \\ -\bar{M}_{14} \end{bmatrix} \quad \text{Equation 4. 95}$$

4.7 Conclusion

The interpolation functions for axial loading, axial torsion, bending in XY and bending in XZ planes were derived and for the two-node element, there was a quadratic path for the functions for all bending in Y and Z while a linear path for the change in loading and torsion from node 1 to node 2. Important rules to note are the following:

- Displacements at restrained degree of freedom are zero.
- Fixed end moments at restrained degree of freedom are zero.
- Joint loads are same magnitude but a reverse sign when compared to global fixed end moments.

In summary, it is the joint load at some degree of freedom that triggers the displacement across the unrestrained degrees of freedom in the entire structure. The end moments calculated based on the displacement are the resultant forces and moments across the entire structure due to the load applied.

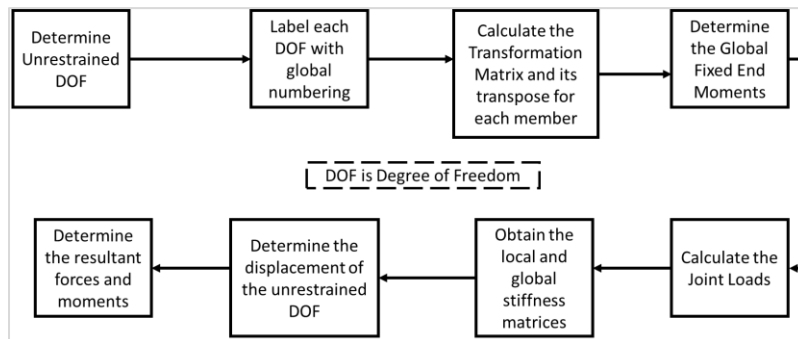


Figure 4. 25 Process for Finite Element Drill String Dynamics Process

Chapter 5 Optimizing the Finite Element Drilling Simulation

The goal of the optimization is to minimize the mechanical specific energy for the drill ahead process. Some factors have to be established about the finite element displacement estimation in order to fully cover the drilling process.

5.1 The Drilling Dynamics

During each run of the drill string, the bit cuts the rock and moves ahead into the wellbore hole at certain speed and acceleration. The formation would form resistance to the flow as the drill string touches the wall of the wellbore. The finite element dynamics equation is as follows.

$$[M^e][\ddot{U}^e] + [C^e][\dot{U}^e] + [K^e][U^e] = [F^e] = [f^e] + [Q^e] \quad \text{Equation 5. 1}$$

$[M^e]$ is the Mass Matrix per element.

$[\ddot{U}^e]$ is the vector of accelerations.

$[C^e]$ is the damping matrix per element.

$[\dot{U}]$ is the vector of velocities.

$[K^e]$, $[U^e]$, $[F^e]$, $[f^e]$ and $[Q^e]$ have been described in Equation 4.1.

5.1.1 Estimating the Mass Matrix and The Damping Matrix

The mass matrix and the damping matrix will be assembled just the way the stiffness matrix was assembled in the previous chapter. For axial loading and axial torsion, the mass matrix is the same while for bending in XY and XZ plane, the mass matrix is the same.

For axial displacements,

$$M_{ij}^e = \int_0^L \rho A \phi_i^e \phi_j^e dx \quad (\text{Reddy, 2005}) \quad \text{Equation 5. 2}$$

ϕ_i^e and ϕ_j^e have been derived in Equation 4.48 and Equation 4.49.

$$[M_{12}^e]_{Load} = \int_0^L \rho A \left(1 - \frac{x}{L}\right) \left(\frac{x}{L}\right) dx = \frac{\rho AL}{6} \quad \text{Equation 5. 3}$$

This method is used to calculate the other expressions in the full matrix. Therefore,

$$[M_x^e]_{Load} = \begin{bmatrix} \frac{\rho AL}{3} & \frac{\rho AL}{6} \\ \frac{\rho AL}{6} & \frac{\rho AL}{3} \end{bmatrix} \quad \text{Equation 5. 4}$$

$$[M_x^e]_{Torsion} = \begin{bmatrix} \frac{\rho AL}{3} & \frac{\rho AL}{6} \\ \frac{\rho AL}{6} & \frac{\rho AL}{3} \end{bmatrix} \quad \text{Equation 5. 5}$$

For transverse displacements,

$$[M_{ij}^e]_y = \int_0^L \left(\rho A \phi_i^e \phi_j^e + \rho I_z \frac{d\phi_i^e}{dy} \frac{d\phi_j^e}{dy} \right) dy \quad (\text{Reddy, 2005}) \quad \text{Equation 5. 6}$$

$$[M_{ij}^e]_z = \int_0^L \left(\rho A \phi_i^e \phi_j^e + \rho I_y \frac{d\phi_i^e}{dz} \frac{d\phi_j^e}{dz} \right) dz \quad \text{Equation 5. 7}$$

There are 4 constants which can be found in Equation 4.22 to Equation 4.25. Based on this,

$$[M_{34}^e]_y = \int_0^L \left(\rho A \phi_3^e \phi_4^e + \rho I_z \frac{d\phi_3^e}{dy} \frac{d\phi_4^e}{dy} \right) dy \quad \text{Equation 5. 8}$$

$$[M_{34}^e]_y = \int_0^L \left(\rho A \left(\frac{3}{L^2} y^2 - \frac{2}{L^3} y^3 \right) \left(\frac{1}{L} y^2 - \frac{1}{L^2} y^3 \right) + \rho I_z \frac{d\left(\frac{3}{L^2} y^2 - \frac{2}{L^3} y^3\right)}{dy} \frac{d\left(\frac{1}{L} y^2 - \frac{1}{L^2} y^3\right)}{dy} \right) dy \quad \text{Equation 5. 9}$$

$$[M_{34}^e]_y = \frac{11\rho AL^2 + 21\rho I_z}{210} \quad \text{Equation 5. 10}$$

In the same manner, for bending in XY,

$$[M_{34}^e]_z = \frac{11\rho AL^2 + 21\rho I_y}{210} \quad \text{Equation 5. 11}$$

Using the same principle, the Mass Matrix for the XZ plane is

$$M_y^e = \begin{bmatrix} \frac{13\rho AL^2 + 42\rho I_z}{35L} & \frac{-11\rho AL^2 - 21\rho I_z}{210} & \frac{9\rho AL^2 - 84\rho I_z}{70L} & \frac{13\rho AL^2 - 42\rho I_z}{420} \\ \frac{-11\rho AL^2 - 21\rho I_z}{210} & \frac{\rho AL^3 + 14\rho L I_z}{105} & \frac{-13\rho AL^2 + 42\rho I_z}{420} & \frac{-3\rho AL^3 - 14\rho I_z}{420} \\ \frac{9\rho AL^2 - 84\rho I_z}{70L} & \frac{-13\rho AL^2 + 42\rho I_z}{420} & \frac{13\rho AL^2 + 42\rho I_z}{35L} & \frac{11\rho AL^2 + 21\rho I_z}{210} \\ \frac{13\rho AL^2 - 42\rho I_z}{420} & \frac{-3\rho AL^3 - 14\rho I_z}{420} & \frac{11\rho AL^2 + 21\rho I_z}{210} & \frac{\rho AL^3 + 14\rho L I_y}{105} \end{bmatrix} \quad \text{Equation 5. 12}$$

Consequently,

$$M_z^e = \begin{bmatrix} \frac{13\rho AL^2 + 42\rho I_y}{35L} & \frac{-11\rho AL^2 - 21\rho I_y}{210} & \frac{9\rho AL^2 - 84\rho I_y}{70L} & \frac{13\rho AL^2 - 42\rho I_y}{420} \\ \frac{-11\rho AL^2 - 21\rho I_y}{210} & \frac{\rho AL^3 + 14\rho LI_y}{\rho AL^3 + 14\rho LI_y} & \frac{-13\rho AL^2 + 42\rho I_y}{420} & \frac{-3\rho AL^3 - 14\rho I_y}{420} \\ \frac{9\rho AL^2 - 84\rho I_y}{70L} & \frac{-13\rho AL^2 + 42\rho I_y}{420} & \frac{13\rho AL^2 + 42\rho I_y}{35L} & \frac{11\rho AL^2 + 21\rho I_y}{210} \\ \frac{13\rho AL^2 - 42\rho I_y}{420} & \frac{-3\rho AL^3 - 14\rho I_y}{420} & \frac{11\rho AL^2 + 21\rho I_y}{210} & \frac{\rho AL^3 + 14\rho LI_y}{105} \end{bmatrix} \quad \text{Equation 5. 13}$$

The complete Mass Matrix combines the axial loading, axial torsion, and all transverse Mass Matrices.

$$M^e = \begin{bmatrix} \frac{\rho AL}{3} & 0 & 0 & 0 & 0 & 0 & \frac{\rho AL}{6} & 0 & 0 & 0 & 0 & 0 \\ 0 & \frac{13\rho AL^2 + 42\rho I_z}{35L} & 0 & 0 & 0 & \frac{-11\rho AL^2 - 21\rho I_z}{210} & 0 & \frac{9\rho AL^2 - 84\rho I_z}{70L} & 0 & 0 & 0 & \frac{13\rho AL^2 - 42\rho I_z}{420} \\ 0 & 0 & \frac{13\rho AL^2 + 42\rho I_y}{35L} & 0 & \frac{-11\rho AL^2 - 21\rho I_y}{210} & 0 & 0 & 0 & \frac{9\rho AL^2 - 84\rho I_y}{70L} & 0 & \frac{13\rho AL^2 - 42\rho I_y}{420} & 0 \\ 0 & 0 & 0 & \frac{\rho AL}{3} & 0 & 0 & 0 & 0 & 0 & \frac{\rho AL}{6} & 0 & 0 \\ 0 & 0 & \frac{-11\rho AL^2 - 21\rho I_y}{210} & 0 & \frac{\rho AL^3 + 14\rho LI_y}{105} & 0 & 0 & 0 & \frac{-13\rho AL^2 + 42\rho I_y}{420} & 0 & \frac{-3\rho AL^3 - 14\rho I_y}{420} & 0 \\ 0 & \frac{-11\rho AL^2 - 21\rho I_z}{210} & 0 & 0 & 0 & \frac{\rho AL^3 + 14\rho LI_z}{105} & 0 & \frac{-13\rho AL^2 + 42\rho I_z}{420} & 0 & 0 & 0 & \frac{-3\rho AL^3 - 14\rho I_z}{420} \\ 0 & \frac{\rho AL}{6} & 0 & 0 & 0 & 0 & \frac{\rho AL}{3} & 0 & 0 & 0 & 0 & 0 \\ 0 & \frac{9\rho AL^2 - 84\rho I_z}{70L} & 0 & 0 & 0 & \frac{-13\rho AL^2 + 42\rho I_z}{420} & 0 & \frac{13\rho AL^2 + 42\rho I_z}{35L} & 0 & 0 & 0 & \frac{11\rho AL^2 + 21\rho I_z}{210} \\ 0 & 0 & \frac{9\rho AL^2 - 84\rho I_y}{70L} & 0 & \frac{-13\rho AL^2 + 42\rho I_y}{420} & 0 & 0 & 0 & \frac{13\rho AL^2 + 42\rho I_y}{35L} & 0 & \frac{11\rho AL^2 + 21\rho I_y}{210} & 0 \\ 0 & 0 & 0 & \frac{\rho AL}{6} & 0 & 0 & 0 & 0 & 0 & \frac{\rho AL}{3} & 0 & 0 \\ 0 & 0 & \frac{13\rho AL^2 - 42\rho I_y}{420} & 0 & \frac{-3\rho AL^3 - 14\rho I_y}{420} & 0 & 0 & 0 & \frac{11\rho AL^2 + 21\rho I_y}{210} & 0 & \frac{\rho AL^3 + 14\rho LI_y}{105} & 0 \\ 0 & \frac{13\rho AL^2 - 42\rho I_z}{420} & 0 & 0 & 0 & \frac{-3\rho AL^3 - 14\rho I_z}{420} & 0 & \frac{11\rho AL^2 + 21\rho I_z}{210} & 0 & 0 & 0 & \frac{\rho AL^3 + 14\rho LI_z}{105} \end{bmatrix}$$

Equation 5. 14

This thesis aligns with Rayleigh damping assumes a linear combination of the mass matrix and the stiffness matrix (Reddy, 2005). $[C^e] = c_1[M^e] + c_2[K^e]$ Equation 5. 15

For homogeneous systems,

$$\det([K^e] - \omega^2[M^e]) = 0 \quad (\text{Katsikadelis, 2020}) \quad \text{Equation 5. 16}$$

ω is the natural frequency of the system. Based on Rayleigh damping conditions,

$$\frac{1}{2} \begin{bmatrix} \frac{1}{\omega_n} & \omega_n \\ \frac{1}{\omega_m} & \omega_m \end{bmatrix} \begin{bmatrix} c_1 \\ c_2 \end{bmatrix} = \begin{bmatrix} \varepsilon_n \\ \varepsilon_m \end{bmatrix} \quad (\text{Katsikadelis, 2020}) \quad \text{Equation 5. 17}$$

$\begin{bmatrix} \varepsilon_n \\ \varepsilon_m \end{bmatrix}$ are the damping ratio of the system which range from 0 to 0.8 (Katsikadelis, 2020). Therefore,

$$\begin{bmatrix} c_1 \\ c_2 \end{bmatrix} = 2 \begin{bmatrix} \frac{1}{\omega_n} & \omega_n \\ \frac{1}{\omega_n} & \omega_m \end{bmatrix}^{-1} \begin{bmatrix} \varepsilon_n \\ \varepsilon_m \end{bmatrix} \quad \text{Equation 5. 18}$$

The damping ratio can also be estimated as an addition of internal damping and external damping if all the formation information is known.

5.1.2 The Time Dependent Governing Solutions for Y and Z Direction

A combination of the drilling dynamics equations and the space equations in chapter 4 give the time dependent governing equations. The benefit of solving the time dependent displacement is that it gives the ability to calculate accelerations of each direction which in the field is being measured by accelerometers downhole. The calculated accelerometers are closely aligned with the field readings, then forecasting for drilling problems downhole will be feasible.

A combination of Equation 4.1 and Equation 5.1 for the y direction gives the following.

$$[M^e][\ddot{U}^e] + [C^e][\dot{U}^e] + [K^e][U^e] = \frac{d^2}{dy^2} \left(\frac{bd^2w}{dy^2} \right) \quad \text{Equation 5. 19}$$

Let $[M^e]$, $[C^e]$, and $[K^e]$ be constants M, C and K. Equation 5.19 can be rewritten as:

$$M \frac{d^2w}{dt^2} + C \frac{dw}{dt} + Kw = EI \frac{d^4w}{dy^4} \quad \text{Equation 5. 20}$$

Assuming no movement at initiation of the simulation, the initial value of the system would be:

$$w|_{(y,0)} = \left[\frac{dw}{dt} \right]_{(y,0)} = 0 \quad \text{Equation 5. 21}$$

Here is the general state of each element for the y direction.

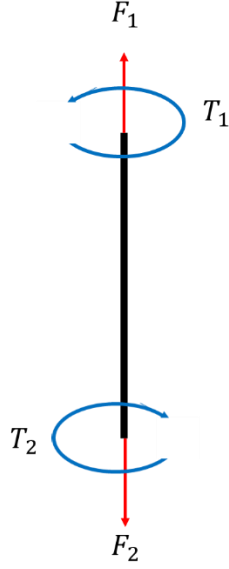


Figure 5. 1 Forces and Moment in Y and Z Direction

Rewriting the boundary conditions stated in Equation 4.8 to Equation 4.11, the following expressions are obtained.

$$\left[\frac{d^2 w}{dy^2} \right]_{(0,t)} = \frac{-T_1}{EI} \quad \text{Equation 5. 22}$$

$$\left[\frac{d^2 w}{dy^2} \right]_{(L,t)} = \frac{-T_2}{EI} \quad \text{Equation 5. 23}$$

$$\left[\frac{d^3 w}{dy^3} \right]_{(0,t)} = \frac{F_1}{EI} \quad \text{Equation 5. 24}$$

$$\left[\frac{d^3 w}{dy^3} \right]_{(L,t)} = \frac{F_2}{EI} \quad \text{Equation 5. 25}$$

Applying Laplace Transform to Equation 5.20

$$Ms^2 \bar{w} + Cs \bar{w} + K \bar{w} = EI \frac{d^4 \bar{w}}{dy^4} \quad \text{Equation 5. 26}$$

Simplifying gives

$$\frac{d^4 \bar{w}}{dy^4} - \left(\frac{Ms^2 + Cs + K}{EI} \right) \bar{w} = 0 \quad \text{Equation 5. 27}$$

$$\text{Let } \aleph = \sqrt{\left(\frac{Ms^2 + Cs + K}{EI}\right)} \quad \text{Equation 5. 28}$$

The characteristic equation of Equation 5.27 is

$$r^4 - \aleph^2 = 0 \quad \text{Equation 5. 29}$$

$$\text{Therefore, } r = \begin{matrix} + \\ - \end{matrix} \sqrt{\aleph} \quad \text{Equation 5. 30}$$

Based on differential characteristics

$$\bar{w}|_{(y,s)} = c_1 \cosh(y\sqrt{\aleph}) + c_2 \sinh(y\sqrt{\aleph}) + c_3 \cos(y\sqrt{\aleph}) + c_4 \sin(y\sqrt{\aleph}) \quad \text{Equation 5. 31}$$

Taking Laplace Transform of all boundary conditions.

$$\left[\frac{d^2 \bar{w}}{dy^2}\right]_{(0,s)} = \frac{-T_1}{EI} \left(\frac{1}{s}\right) \quad \text{Equation 5. 32}$$

$$\left[\frac{d^2 \bar{w}}{dy^2}\right]_{(L,s)} = \frac{-T_2}{EI} \left(\frac{1}{s}\right) \quad \text{Equation 5. 33}$$

$$\left[\frac{d^3 \bar{w}}{dy^3}\right]_{(0,s)} = \frac{F_1}{EI} \left(\frac{1}{s}\right) \quad \text{Equation 5. 34}$$

$$\left[\frac{d^3 \bar{w}}{dy^3}\right]_{(L,s)} = \frac{F_2}{EI} \left(\frac{1}{s}\right) \quad \text{Equation 5. 35}$$

Effecting Equation 5.32 gives the following expression.

$$\left[\frac{d^2 \bar{w}}{dy^2}\right]_{(0,s)} = \aleph(c_1 - c_3) = \frac{-T_1}{EI} \left(\frac{1}{s}\right) \quad \text{Equation 5. 36}$$

Effecting Equation 5.33 gives the following expression.

$$\left[\frac{d^2 \bar{w}}{dy^2}\right]_{(L,s)} = \aleph[c_1 \cosh(L\sqrt{\aleph}) + c_2 \sinh(L\sqrt{\aleph}) - c_3 \cos(L\sqrt{\aleph}) - c_4 \sin(L\sqrt{\aleph})] = \frac{-T_2}{EI} \left(\frac{1}{s}\right) \quad \text{Equation 5. 37}$$

Effecting Equation 5.34 gives the following expression.

$$\left[\frac{d^3 \bar{w}}{dy^3}\right]_{(0,s)} = \aleph\sqrt{\aleph}(c_2 - c_4) = \frac{F_1}{EI} \left(\frac{1}{s}\right) \quad \text{Equation 5. 38}$$

Effecting Equation 5.35 gives the following expression.

$$\left[\frac{d^3 \bar{w}}{dy^3} \right]_{(L,s)} = \aleph \sqrt{\aleph} [c_1 \sinh(L\sqrt{\aleph}) + c_2 \cosh(L\sqrt{\aleph}) + c_3 \sin(L\sqrt{\aleph}) - c_4 \cos(L\sqrt{\aleph})] = \frac{F_2}{EI} \left(\frac{1}{s} \right)$$

Equation 5. 39

For shorter notation, let the following be set as

$$\beth = L\sqrt{\aleph} \quad \text{Equation 5. 40}$$

$$k_1 = \frac{-T_1}{\aleph EI} \left(\frac{1}{s} \right) \quad \text{Equation 5. 41}$$

$$k_2 = \frac{-T_2}{\aleph EI} \left(\frac{1}{s} \right) \quad \text{Equation 5.42}$$

$$k_3 = \frac{F_1}{\aleph \sqrt{\aleph} EI} \left(\frac{1}{s} \right) \quad \text{Equation 5. 42}$$

$$k_4 = \frac{F_2}{\aleph \sqrt{\aleph} EI} \left(\frac{1}{s} \right) \quad \text{Equation 5. 43}$$

Substitute Equation 5.41 into Equation 5.36 and rearranging to get the expression below.

$$c_3 = c_1 - k_1 \quad \text{Equation 5. 44}$$

Substitute Equation 5.43 and Equation 5.38 and rearranging to get the expression below.

$$c_4 = c_2 - k_3 \quad \text{Equation 5. 45}$$

Substitute Equation 5.40, Equation 5.42, Equation 5.45, and Equation 5.46 into Equation 5.37 and Equation 5.38 and rearranging to get the expression below.

$$[\cosh(\beth) - \cos(\beth)]c_1 + [\sinh(\beth) - \sin(\beth)]c_2 = k_2 - k_1 \cos(\beth) - k_3 \sin(\beth)$$

Equation 5. 46

Substitute Equation 5.40, Equation 5.41, Equation 5.44, and Equation 5.46 into Equation 5.39 and Equation 5.38 and rearranging to get the expression below.

$$[\sinh(\beth) + \sin(\beth)]c_1 + [\cosh(\beth) - \cos(\beth)]c_2 = k_4 + k_1 \sin(\beth) - k_3 \cos(\beth)$$

Equation 5. 47

$$\text{Let } k_2 - k_1 \cos(\beth) - k_3 \sin(\beth) = \Psi$$

Equation 5. 48

$$\text{Let } k_4 + k_1 \sin(\vartheta) - k_3 \cos(\vartheta) = \varsigma \quad \text{Equation 5. 49}$$

Substituting Equation 5.49 and Equation 5.50 into Equation 5.47 and Equation 5.48 to obtain:

$$[\cosh(\vartheta) - \cos(\vartheta)]c_1 + [\sinh(\vartheta) - \sin(\vartheta)]c_2 = \Psi \quad \text{Equation 5. 50}$$

$$[\sinh(\vartheta) + \sin(\vartheta)]c_1 + [\cosh(\vartheta) - \cos(\vartheta)]c_2 = \varsigma \quad \text{Equation 5. 51}$$

Solving for the two constants to obtain

$$c_1 = \frac{\begin{vmatrix} \Psi & \sinh(\vartheta) - \sin(\vartheta) \\ \varsigma & \cosh(\vartheta) - \cos(\vartheta) \end{vmatrix}}{\begin{vmatrix} \cosh(\vartheta) - \cos(\vartheta) & \sinh(\vartheta) - \sin(\vartheta) \\ \sinh(\vartheta) + \sin(\vartheta) & \cosh(\vartheta) - \cos(\vartheta) \end{vmatrix}} = \frac{\Psi(\cosh(\vartheta) - \cos(\vartheta)) - \varsigma(\sinh(\vartheta) - \sin(\vartheta))}{2(1 - \cos(\vartheta)\cosh(\vartheta))} \quad \text{Equation 5. 52}$$

$$c_2 = \frac{\begin{vmatrix} \cosh(\vartheta) - \cos(\vartheta) & \Psi \\ \sinh(\vartheta) + \sin(\vartheta) & \varsigma \end{vmatrix}}{\begin{vmatrix} \cosh(\vartheta) - \cos(\vartheta) & \sinh(\vartheta) - \sin(\vartheta) \\ \sinh(\vartheta) + \sin(\vartheta) & \cosh(\vartheta) - \cos(\vartheta) \end{vmatrix}} = \frac{\varsigma(\cosh(\vartheta) - \cos(\vartheta)) - \Psi(\sinh(\vartheta) + \sin(\vartheta))}{2(1 - \cos(\vartheta)\cosh(\vartheta))} \quad \text{Equation 5. 53}$$

c_3 and c_4 can be calculated by substituting c_1 and c_2 in equations Equation 5.45 and Equation 5.46 respectively. To calculate $\bar{w}|_{(y,t)}$, it is necessary to find the inverse Laplace Transform of $\bar{w}|_{(y,s)}$ in Equation 5.31

$$f(t) = \frac{e^{at}}{t} \left[\frac{1}{2} F(a) + \operatorname{Re} \sum_{k=1}^n F \left(a + \frac{jk\pi}{t} \right) (-1)^k \right] \quad (\text{Hassanzadeh \& Pooladi-Darvish, 2007})$$

$$\quad \text{Equation 5. 54}$$

$$j = \sqrt{-1} \quad \text{Equation 5. 55}$$

$a = \text{best between 4 and 5}$ (Hassanzadeh & Pooladi-Darvish, 2007)

$a = \text{constant in Fourier Series}$

$F = \text{Laplace Domain Function}$

$$\text{In this case, } F = \bar{w}|_{(y,s)} \quad \text{Equation 5. 56}$$

Here is a test of the result and more detailed results will be shown in chapter 6.

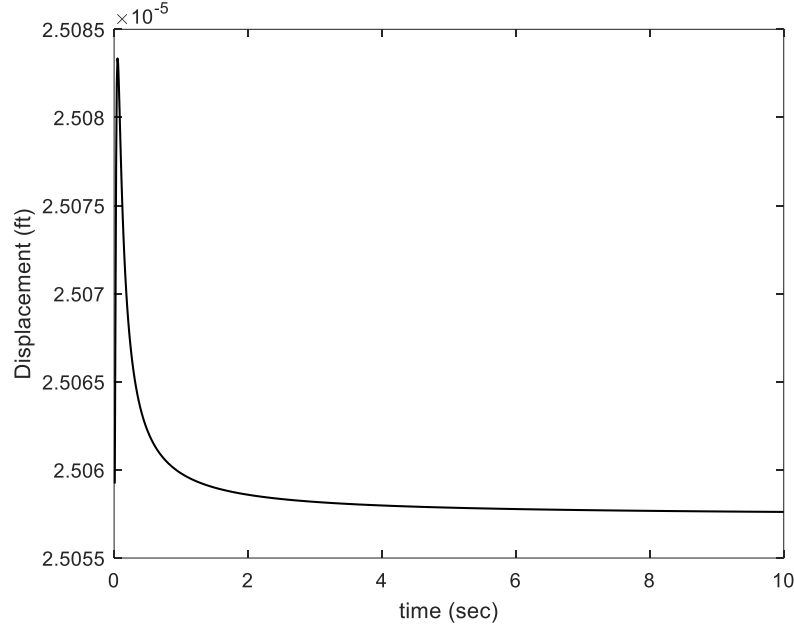


Figure 5. 2 Convergence of Displacement in Y or Z Direction

5.1.3 The Time Dependent Governing Solutions for X Direction (Axial and Torsion)

A combination of Equation 4.38 and Equation 5.1 for the axial loading in x direction gives the following.

$$[M^e][\ddot{U}^e] + [C^e][\dot{U}^e] + [K^e][U^e] = -EA \frac{d^2 w}{dx^2} \quad \text{Equation 5. 57}$$

Assuming no movement at initiation of the simulation, the initial value of the system would be:

$$w|_{(x,0)} = \left[\frac{dw}{dt} \right]_{(x,0)} = 0 \quad \text{Equation 5. 58}$$

Here is the schematic of the forces.



Figure 5. 3 Forces of Axial Loading in X Direction

Based on the boundary conditions gotten from Equation 4.41

$$\left[\frac{dw}{dx} \right]_{(x,0)} = \frac{F_1}{EA} \quad \text{Equation 5. 59}$$

$$\left[\frac{dw}{dx} \right]_{(x,L)} = \frac{F_2}{EA} \quad \text{Equation 5. 60}$$

Applying Laplace Transform

$$Ms^2\bar{w} + Cs\bar{w} + K\bar{w} = -EA \frac{d^2\bar{w}}{dx^2} \quad \text{Equation 5. 61}$$

$$\frac{d^2\bar{w}}{dx^2} + \left(\frac{Ms^2 + Cs + K}{EA} \right) \bar{w} = 0 \quad \text{Equation 5. 62}$$

$$\text{Let } \aleph = \sqrt{\left(\frac{Ms^2 + Cs + K}{EA} \right)} \quad \text{Equation 5. 63}$$

Here is the characteristic equation.

$$r^2 - \aleph^2 = 0 \quad \text{Equation 5. 64}$$

$$r = \pm \aleph \quad \text{Equation 5. 65}$$

$$\bar{w}(x, s) = c_1 e^{\aleph x} + c_2 e^{-\aleph x} \quad \text{Equation 5. 66}$$

$$\frac{d\bar{w}}{dx} = c_1 \aleph e^{\aleph x} - c_2 \aleph e^{-\aleph x} \quad \text{Equation 5. 67}$$

Applying Laplace Transform to the Boundary Conditions

$$\left[\frac{d\bar{w}}{dx} \right]_{(x=0)} = \aleph(c_1 - c_2) = \frac{F_1}{EA} \left(\frac{1}{s} \right) \quad \text{Equation 5. 68}$$

$$\left[\frac{d\bar{w}}{dx} \right]_{(x=L)} = \aleph(c_1 e^{\aleph L} - c_2 e^{-\aleph L}) = \frac{F_2}{EA} \left(\frac{1}{s} \right) \quad \text{Equation 5. 69}$$

$$\text{Let } k_1 = \frac{F_1}{EA\aleph} \quad \text{Equation 5. 70}$$

$$\text{Let } k_2 = \frac{F_2}{EA\aleph} \quad \text{Equation 5. 71}$$

Substitute Equation 5.71 and Equation 5.72 in Equation 5.69 and Equation 5.70

$$c_1 - c_2 = k_1 \quad \text{Equation 5. 72}$$

$$c_1 e^{\aleph L} - c_2 e^{-\aleph L} = k_2 \quad \text{Equation 5. 73}$$

Therefore

$$c_1 = \frac{\begin{vmatrix} k_1 & -1 \\ k_2 & -e^{-\aleph L} \end{vmatrix}}{\begin{vmatrix} 1 & -1 \\ e^{\aleph L} & -e^{-\aleph L} \end{vmatrix}} = \frac{-k_1 e^{-\aleph L} + k_2}{-e^{-\aleph L} + e^{\aleph L}} \quad \text{Equation 5. 74}$$

$$c_2 = \frac{\begin{vmatrix} 1 & k_1 \\ e^{\aleph L} & k_2 \end{vmatrix}}{\begin{vmatrix} 1 & -1 \\ e^{\aleph L} & -e^{-\aleph L} \end{vmatrix}} = \frac{k_2 - k_1 e^{\aleph L}}{-e^{-\aleph L} + e^{\aleph L}} \quad \text{Equation 5. 75}$$

Equation 5.55 is used for inverse Laplace Transform. Here is the convergence curve for a test.

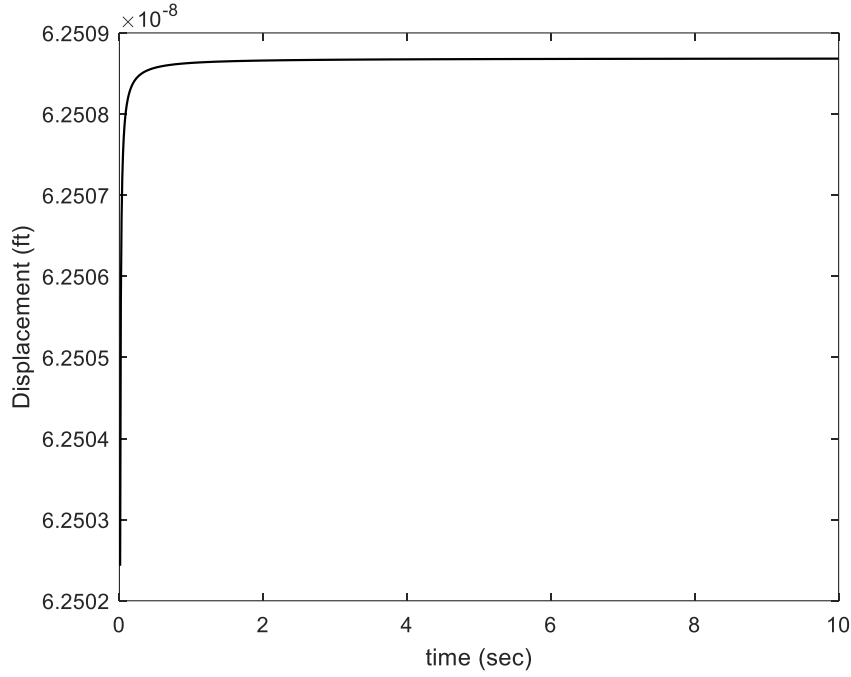


Figure 5. 4 Convergence of Displacement in X Direction

The axial loading behavior is like the axial torsion behavior.

5.1.4 Validation of the Finite Element Process

The validation process for the finite element models is built within the global numbering. If the fixed ends were not placed as zero because of the restriction of displacement, the validation is done by the equation below.

$$[K_{ru}] * [\Delta u] - [J_L]_r = [R_r] \quad \text{Equation 5. 76}$$

K_{ru} is a group of stiffness coefficients having their impact location at the restrained degree of freedom and the reaction location at the unrestrained degree of freedom points.

- Δu is the unrestrained displacements.
- $-[J_L]_r$ are the joint loads at the restrained fixed end moments.
- R_r are the forces and moments for the restrained degrees of freedom.

R_r can be extracted from the global total end forces and moments calculated.

5.2 Torque Calculations

Torque and drag calculations are very critical in the planning of a well and selection of the bottomhole assembly. The torque calculations are necessary to avoid twist-off and other damages that can occur due to buckling of the parts of the drill string. The drag calculations are also necessary when considering fatigue of the drill string and planning to avoid stuck pipe events. This chapter will discuss how the drilling simulator can be designed using finite element method and accurately predict the friction factor while drilling.

While transferring torque to the bit, power is lost due to friction, and this can be calculated. This calculation is very dependent on the geometry of the wellbore. If the power lost is too high, it can increase the rate of fatigue of downhole tools. Excessive torque is not the plan and there is a need to plan the trajectory in such a way to reduce excessive torque.

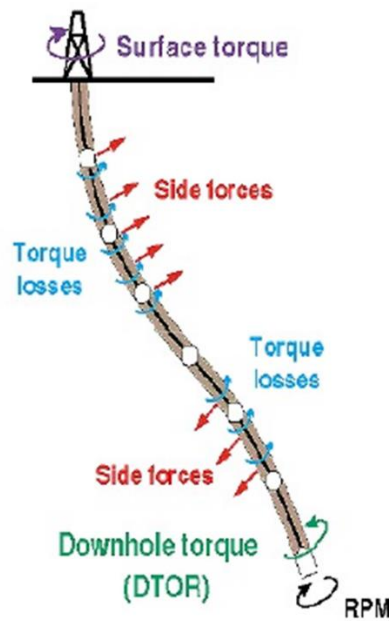


Figure 5. 5 The Concept of Torque Losses Downhole (Beeh, 2017)

From the figure above, it can be clearly seen that the revolution per minute speed (rpm) goes in the direction of the intended surface torque but the due to torque losses (which are the forces required to turn the drill string), the downhole will be different from the surface torque. The basic formula for torque losses is as follows.

$$Torque = F_n r \mu$$

Equation 5. 77

When tripping, Torque is assumed zero.

$F_n = \text{normal force, lb}$

$r = \text{radius of drill string component, ft}$

$\mu = \text{Friction Factor}$

$An = \text{Angular speed, in/sec}$

$V = \text{Resultant Speed, in/sec}$

$V = \sqrt{T^2 - An^2}$, T is Trip Speed and when no tripping occurs, $An = V$

When tripping, Torque is approximately 0 but if you want the exact values, then the ration of $\frac{An}{V}$ would be important factors.

When rotating, $An = V$

Therefore,

$$\text{Torque} = F_n r \mu \left(\frac{An}{V} \right) \quad \text{Equation 5. 78}$$

It is the sum of all these torque created downhole that makes up surface torque. Another way to explain it is when surface torque is applied in a certain direction, torque in the opposite direction is created in the drill string components downhole. The torque created downhole is the amount of resistant force needed to turn the drill string component due to the contact between the components and the wellbore.

5.2 Drag Calculations

Drag is measured in string weight and it is the gain in string weight when the drill string is being pulled out of the hole and the decrease in string weight when the drill string is lowered into the wellbore.

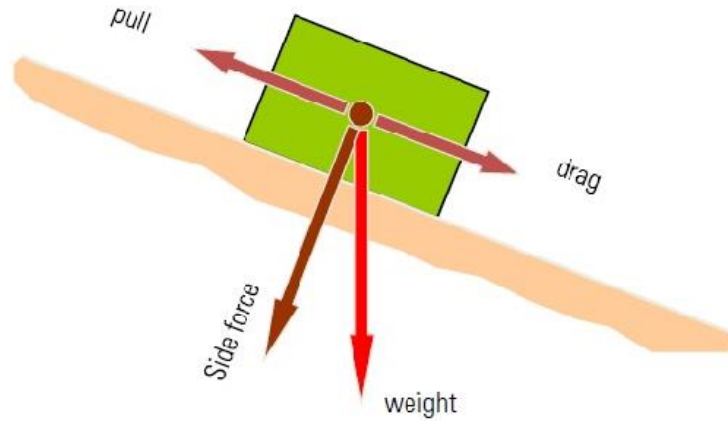


Figure 5. 6 Understanding the Concept of Drag (Beeh, 2017)

The tripping weight is different because the drag adds to the weight of the drill string and makes it more difficult to pull. This is the reason why excessive unplanned drag is dangerous to the life span of downhole tools. Here is the general formula for calculating drag.

$$\text{Drag Force} = F_n \mu \frac{|T|}{|V|} \quad \text{Equation 5. 79}$$

F_n = normal force, lb

μ = Friction Factor

T = Trip Speed, $\frac{\text{in}}{\text{sec}}$

V = Resultant Speed, in/sec

D = Diameter, inch

$$An = \text{Angular speed, } \frac{\text{in}}{\text{sec}} = D * 3.14 * \frac{\text{rpm}}{60} \quad \text{Equation 5. 80}$$

When drilling, Drag force is approximately 0 but when the exact values are to be calculated, then the ration of $\frac{|T|}{|V|}$ becomes important. However, when there is no drilling, this becomes the drag force. When the hook load at the surface increases beyond the anticipated string weight, it is certainly because of the inclusion of drag forces downhole especially during pull up. During sliding

mode of drilling, drag can also occur as the vertical portion of the drill string is approximately not rotating during sliding. The general concept is shown in the figure below.

Drilling Type	Torque	Drag
Sliding	Low	High
Rotating	High	Low

Figure 5. 7 Magnitude of Torque and Drag Based on Drilling Type

5.3 Needed Output from Finite Element Method

The normal force is the net force normal to the point of contact between components of the drill string and the borehole wall. It is dependent on the tension extensions on either side of each member in a drill string and the compressions between gravitational force and the wall of the hole as shown below.

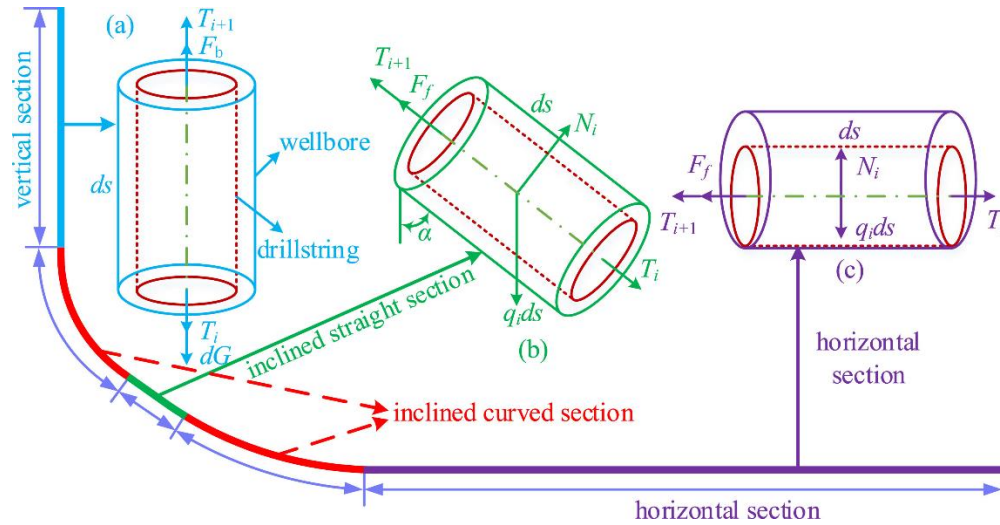


Figure 5. 8 Interactions Between Gravitational Pull and Tension Stretch in the Drill String (Liu, Ma, Chen, & Yang, 2018)

In cases a, b, c, the common forces of note are the T_{i+1} and T_i which are the axial forces at either ends of the drill string. In case (a), a vertical wellbore, the gravitational pull acts in the same direction with the downward facing axial force while for case (b), the gravitation pull acts vertically downwards whilst the axial forces are in angles depending on the inclination and azimuth of the drill string. For case (c), the axial forces are horizontal while the gravitational pull are perpendicular to the axial forces. The azimuth changes mean the straight path on a 2D view might

be curved on 3D view. This is where the importance of 3D modeling of the well path comes to play.

Here is the formula for the normal force.

$$F_n = \sqrt{[(F_t \Delta\beta \sin \bar{\alpha})^2 + (F_t \Delta\alpha + \omega \sin \bar{\alpha})^2]} \quad \text{Equation 5. 81}$$

F_n = Resultant normal force, lb

F_t = Axial tension on lower end of element, lb

$\bar{\alpha}$ = Average inclination angle, degrees °

$\Delta\alpha$ = Change in inclination angle, radians (1 deg = 0.0174 radians)

$\Delta\beta$ = Change in azimuth, radians

ω = Buoyed weight of element, lb

It is paramount to state that the F_t is equivalent to the axial force of each member of the drill string.

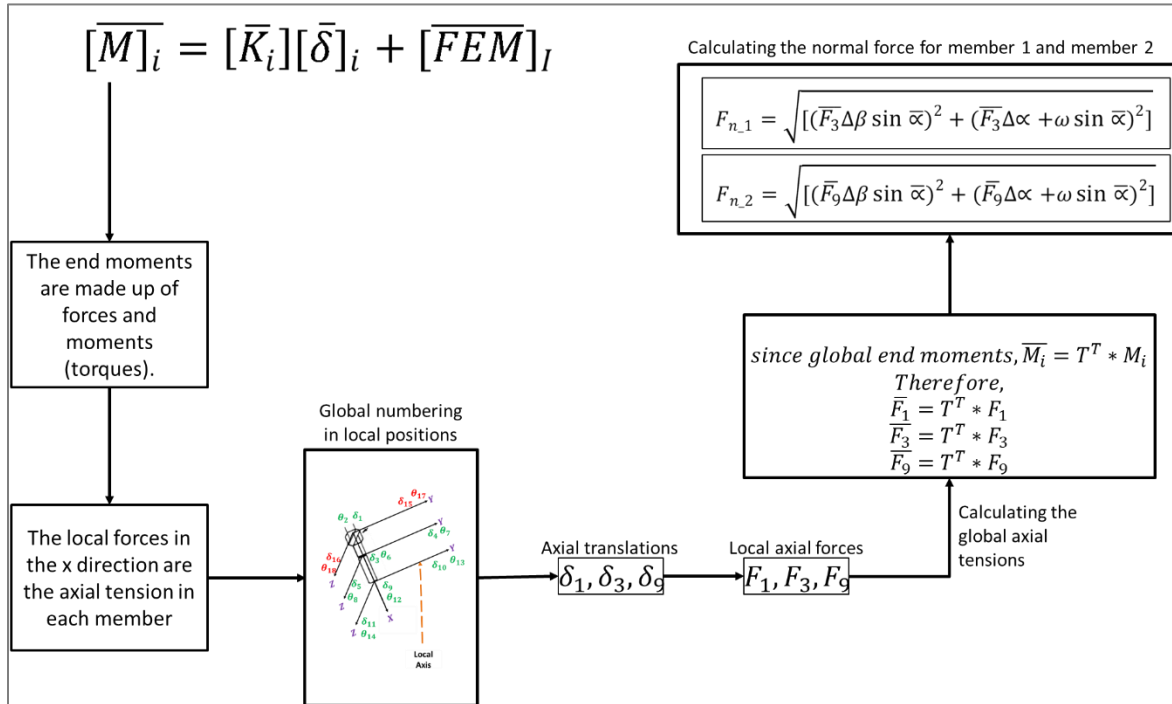


Figure 5. 9 Steps for Calculating Normal Force from Outputs of Finite Element Method

A common point being made is that it is only the global values of parameters in the finite element method that can be used in external equations. The reason is because each global value in the finite element method is a resultant of all factors affecting each member of the entire structure. Therefore, it is important that only global values are used to interact between members and external factors. This is why the transformation matrix is key to accurate computation all the time.

5.4 Coefficient of Friction Estimation

For motion of the drill string to occur, the surface torque applied has to overcome a force to ensure the drill string is set in rotation and drilling the hole. The resisting forces are caused by the contacts between the drill string and the wellbore walls and also the mud cakes on the wall of the borehole. A high friction coefficient means there will high resistance to initial motion of the drill string. The resistance continues even after the initial resistance to motion. The friction coefficient will depend on the type of drilling fluid in use and whether the hole is cased or not. Here is the formula for friction coefficient.

$$\mu = \frac{\text{Drag Force}}{F_n} * \frac{|V|}{|T|} \quad \text{Equation 5. 82}$$

The parameters are as defined previously. The friction coefficient will be lesser obviously in cased hole as the resistance to flow will be lower except other factors change.

	Water based mud		Oil based mud		Synthetic OBM	
	Min	Max	Min	Max	Min	Max
Cased hole	0.18	0.25	0.15	0.20	0.15	0.20
Open hole	0.30	0.35	0.22	0.25	0.22	0.25

Figure 5. 10 Friction Coefficient Values in Cased and Open Holes (SoftDrill NL, 2023)

An alternative calculation for friction coefficient is from torque calculations and this is the linkage to the finite element method.

$$\mu = \frac{\text{Torque}}{F_n r} * \frac{V}{A_n} \quad \text{Equation 5. 83}$$

While drilling, $\frac{V}{A_n} = 1$

Therefore,

$$\mu = \frac{\text{Torque}}{F_n r} \quad \text{Equation 5. 84}$$

Note that before the drilling starts, the friction coefficient is static friction and after the drilling commences, the friction coefficient is dynamic friction. Static friction is the representation of the amount of force needed to get the drill string to start rotating and moving downwards. After that maximum force was reached. The friction drops two dynamic friction which is the force needed to rotate and move the drill string down the hole. The friction is closely related to the Torque because Torque is the force required to turn the drill string a certain distance.

This *Torque* is the axial torque per member of the 3D drill string structure.

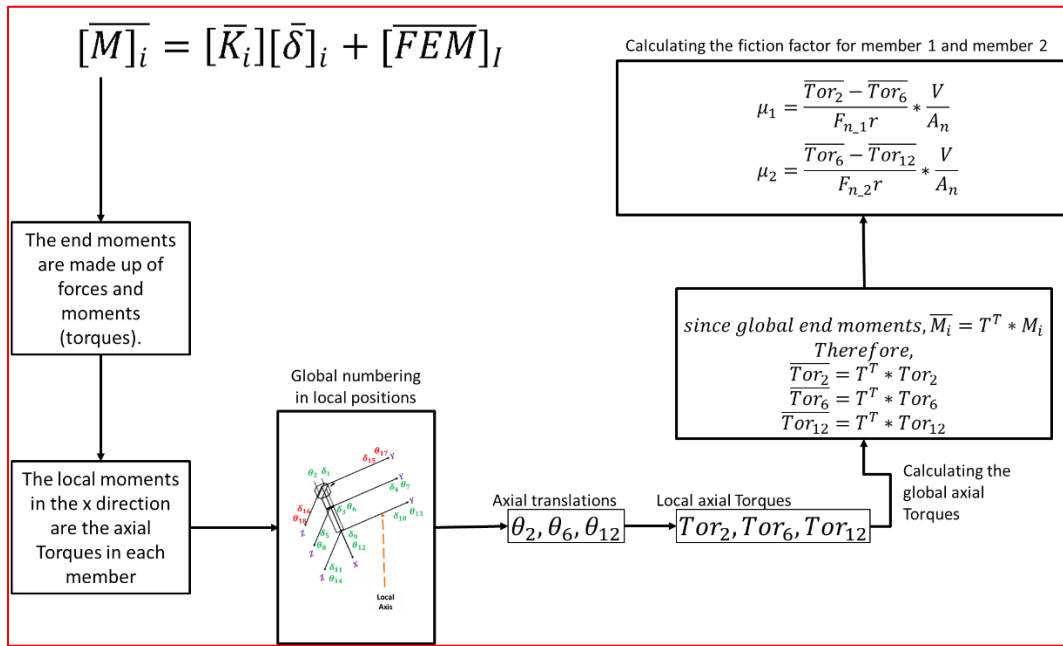


Figure 5. 11 Steps for Calculating Friction Factor from Outputs of Finite Element Method

It is better to use the torque output from the finite element to calculate the friction factor because the drag force formula for friction factor calculation is dependent on drag force which is calculated based on outputs from the finite element. The torque formula takes its inputs directly from the finite element outputs.

5.4.1 Graphical Representation of Coefficient of Friction While Drilling

The real importance of friction coefficient is how it helps map out risk zones based on hook load and torque readings at the surface. Here is an example of how the plot could look like.

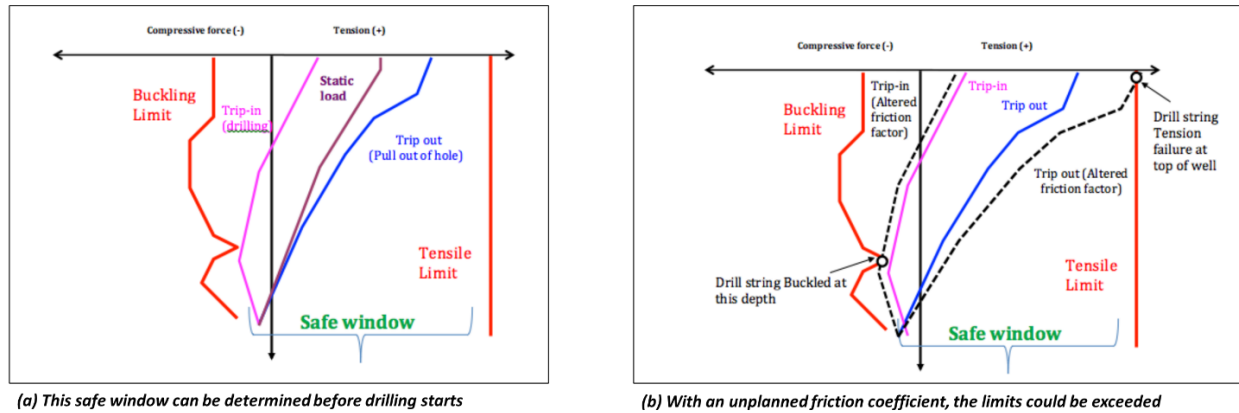


Figure 5. 12 Bucking and Tensile Limit Safety Windows (Brekke, 2016)

The friction coefficients are planned to be within the safe zone. The friction is planned by using the bottom hole assembly and the well part to run some pre-drilling analysis to see what potential buckling and tensile limit could be exceeded. Each friction coefficient from 0.1 – 0.4 would be tested in the formulas to see if they exceed the buckling and tensile limit of the bottom hole assembly. Based on that, a friction factor which is safe for the drilling process based on the bottom hole assembly and the well part set will be chosen and assumed to be the safe zone for drilling. This now means that during the drilling, if the back calculated friction coefficient exceeds the boundary friction coefficient, then there is bound to be potential problem if the bottom hole pressure and well part were combined. This means the bottom hole assembly chosen will be such that the expected friction coefficient keeps the operations within the safe window. If the friction factor is altered, then there would be the risk of buckling the drill string and extending beyond the tensile limit of the drill string which could lead to damage of downhole tools. The plot shape is known because pre-drilling planning would allow the drilling team to plot or find out what friction factors are safe for drilling. The next question is why is the plot taking such converging shape at the bottom and diverging at the top? This can be answered in the table below showing an attempt to bring a structure into the plot.

Table 5. 1 Generic Output for Stiffness Matrix Calculation for Each Member of the Vertical Well

	Axial Load of Drill String								
	Slack Off Weight				Static Load	Pull Up Weight			
Friction Coefficient	0.4	0.3	0.2	0.1	Assume no drill string contact with the hole	0.1	0.2	0.3	0.4
Increment	The slack off weight which occurs as the drilling occurs or the drill string being lowered into the hole, increases as the friction coefficient increases from 0.1 to 0.4.				The static load is the buoyed weight of the drill string based on the combined components of the selected bottomhole assembly. The assumption is no movement ($\mu = 0$).	The pull up weight which occurs as the drill string is being pulled up the hole increases as the friction coefficient increases from 0.1 to 0.4.			
Formula	<i>Static Load – Drag Force</i>				$(BF) \sum (W * L)$	<i>Static Load + Drag Force</i>			

BF is bouyancy factor, *W* is weight per foot of each component, *L* is lenght of each component

The figure below shows the structure of the plot showing the buckling and tensile limit.

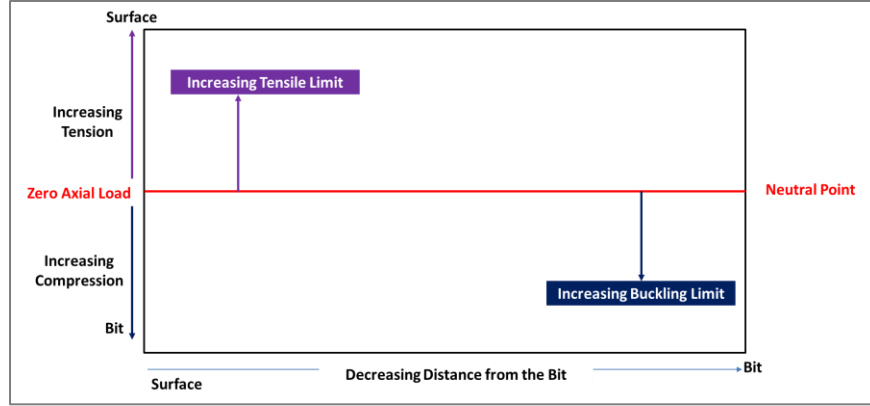


Figure 5. 13 Structure of the Buckling Tensile Plot

The neutral point occurs at the point of zero axial load which means zero x direction force. The figure below shows how the finite element helps identify the neutral point.

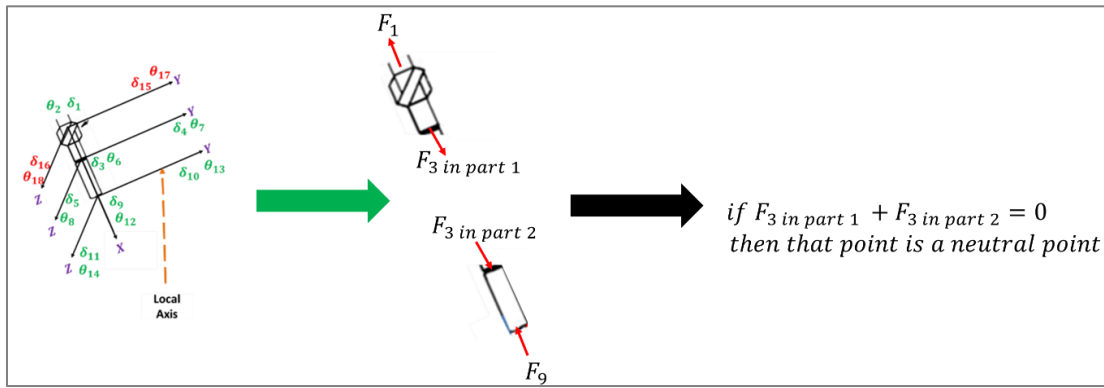


Figure 5. 14 Obtaining Neutral Point from Axial Forces

The easiest way to plot the buckling graph is to work with the unit of tension. Anytime the tension forces are identified in the axial direction, it will be added to the cumulative forces on the buckling tensile graph. If compression forces are identified, they will be subtracted from the cumulative forces. The point of zero forces is the neutral point. The buckling reading starts counting to the left of the neutral point. The tensile limit starts counting to the right of the neutral point. If more than one neutral point is identified at an instance, the neutral point nearer to the bit would be used as the point of origin for the graph.

5.5 Drill Ahead Modeling Based on Finite Element

This is the most exciting part of this work. Drilling ahead modeling is the crux of new technologies in drilling operations. An accurate drill ahead model allows the testing of new ideas and validation

of principles ahead of field testing. It is cheaper to make mistakes in a simulator than in real life. The benefits really depend on the accuracy of the model. The finite element model being discussed in the previous chapter makes it straightforward to compute the drill ahead model.

5.5.1 Important Parameters for Drill Ahead Modeling

Here are five parameters that determine how the bit and the entire drill string move.

- The inclination at the bit
- The three component forces at the bit
- Measured depth at the bit.
- Resultant side force
- The azimuth at the bit

From the finite element side, the figure below shows the scenario that always happens for each loop of simulation.



Figure 5. 15 The 3 Key Steps of The Finite Element Implementation on Drill String

In terms of drilling, the joint loads are the gravity forces, and the 3D resultant forces at the nodes of each member from the previous loop of simulation. The displacements are the rotations and translations at each unrestrained node. In other words, the joint loads prompt the displacement which then set the entire structure on a set of resultant forces and moments. The diagram below shows the forces that influence drilling ahead.

Consider two points in the well path, point 1 and point 2.

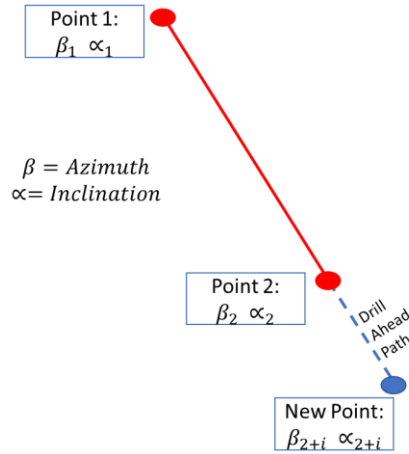


Figure 5. 16 Initial Schematic of Drill Ahead Path

If the buildup rate (BUR) and turn rate (TUR) remain the same, then,

$$TUR = \frac{\beta_2 - \beta_1}{CL}, CL = \text{course length} \quad \text{Equation 5. 85}$$

$$BUR = \frac{\alpha_2 - \alpha_1}{CL}$$

Equation 5. 86

$$\beta_{2+i} = TUR + \beta_2 \quad \text{Equation 5. 87}$$

$$\alpha_{2+i} = BUR + \alpha_2 \quad \text{Equation 5. 88}$$

However, these rates might not be the same as the resultant forces at point 1 and point 2 might not lead to a corresponding equal BUR nor TUR in the next position.

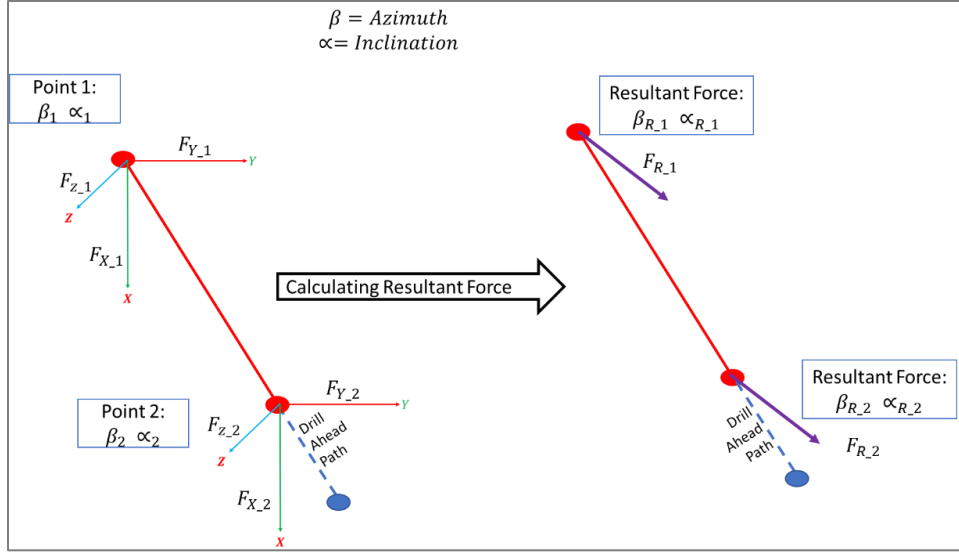


Figure 5. 17 Schematics for Resultant Force for Drill Ahead Modelling

If the inclination and the azimuth are the same for both resultant forces, then the buildup rate and the turn rate will remain constant. However, if these angles are different, the ratio will alter the buildup rate and turn rate in the equations below.

First, a look at how the resultant force is calculated.

$$F_{R1} = \sqrt{F_{X1}^2 + F_{Y1}^2 + F_{Z1}^2} \quad \text{Equation 5. 89}$$

$$\alpha_{R1} = \cos^{-1} \left(\frac{F_{Y1}}{F_{R1}} \right) \quad \text{Equation 5. 90}$$

$$\beta_{R1} = \sin^{-1} \left(\frac{F_{X1}}{F_{R1}} \right) \quad \text{Equation 5. 91}$$

Similarly,

$$F_{R2} = \sqrt{F_{X2}^2 + F_{Y2}^2 + F_{Z2}^2} \quad \text{Equation 5. 92}$$

$$\alpha_{R2} = \cos^{-1} \left(\frac{F_{Y2}}{F_{R2}} \right) \quad \text{Equation 5. 93}$$

$$\beta_{R_2} = \sin^{-1} \left(\frac{F_{X_2}}{F_{R_2}} \right) \quad \text{Equation 5. 94}$$

For the new points, there will be a desired build rate and desired turn rate which will be used to calculate the expected inclination and azimuth.

$$TUR_{desired} = \frac{\beta_{desired} - \beta_2}{CL} \quad \text{Equation 5. 95}$$

$$BUR_{desired} = \frac{\alpha_{desired} - \alpha_2}{CL} \quad \text{Equation 5. 96}$$

Since the resultant forces might not be the same, the eventual next inclination and next azimuth may not be the same with the desired inclination and azimuth.

$$\beta_{2+i} = \left(\frac{\beta_{R_2}}{\beta_{R_1}} * TUR_{desired} \right) + \beta_2 \quad \text{Equation 5. 97}$$

$$\alpha_{2+i} = \left(\frac{\alpha_{R_2}}{\alpha_{R_1}} * BUR_{desired} \right) + \alpha_2 \quad \text{Equation 5. 98}$$

This means anytime the inclination ratio or the azimuth ratio is 1, then the increase in inclination and azimuth will just follow the desired buildup rate and the desired turn rate respectively.

5.5.2 Supporting Variables for the Drill Ahead Process

The basis of the supporting variables ties back to outputs of the finite element process. The most important output is the displacement as time ticks. The displacement is a couple of transverse displacements and the axial displacements as shown in Equation 5.31 and Equation 5.67 respectively. The parameters that matter are the rate of penetration, the weight on bit, and the side forces. The table below shows the formula for these variables in the assembly of elements in the finite element process. It is crucial to note that the displacement expression for transverse motion is different from that of axial motion. They coexist in the full matrix, but their formulations are different. Differentiation with respect to x is used as a generic term in the table.

Table 5. 2 Formulas for Supporting Variables to Drill Ahead Process

Variable Name	Formula	Position
Translation Displacement, ft	$[w]_{(x,t)}$	In x, y and z directions
Rotation Displacement, degrees	$\frac{dw}{dx}$	In x, y and z directions
Velocity, $\frac{ft}{sec}$	$\frac{dw}{dt}$	In x, y and z directions
Acceleration, $\frac{ft^2}{sec}$	$\frac{d^2w}{dt^2}$	In x, y and z directions
Torque, $lb\ ft$	$EI \frac{d^2w}{dy^2}$ for y and z $GJ \frac{d^2w}{dx^2}$ for x	In x, y and z directions
Force, lb	$EI \frac{d^3w}{dy^3}$ for y and z $GJ \frac{d^3w}{dx^3}$ for x	In x, y and z directions
RPM, rpm	$\left(\frac{1}{2\pi}\right) \frac{dw}{dx}$	In x, y and z directions

5.6 Validation Process for the Drilling Simulation

The drilling simulation is a set of physics-based models that predict the parameter variation as drilling occurs from one point in a wellbore to the next. The input to the system will be parameters that can be changed by human intervention. The value to be inputted will be weight on bit (WOB), lb. The WOB influences the Hookload. The Hookload is measured at the surface and transmitted to the producer in real time. The formula for its calculation is stated below.

$$[Hookload]_{Calculated} = [WOB]_{inputed} + \sum GJ \frac{d^3w}{dx^3} \quad \text{Equation 5. 99}$$

It is necessary to validate the results of the drilling simulation. One credible validation process is to compare results with field data. The downhole data gives an accurate measurement of the dynamics occurring during drilling operations. Two variables of interest are the accelerations and the confined compressive strength (CCS) of the formation.

5.6.1 CCS Validation

CCS is a property of the formation, and the actual values can be gotten from log readings. Rock strength is essential in the drilling process. Confined Compressive Strength (CCS) is a geo-mechanical rock property that indicates the rock strength when confined to some medium (Fabain, 1994). Since UCS is widely used, the classification of rock formations based on UCS is readily available. Moreover, the estimation of rock strength classification is based on UCS. CCS then will be related to UCS using the equation proposed by Caicedo et al., 2005 (Caicedo, Calhoun, & Ewy, 2005).

$$CCS = UCS + DP + \left(2 * DP * \frac{\sin(Fa)}{1 - \sin(Fa)} \right) \quad \text{Equation 5. 100}$$

Where UCS is the rock unconfined compressive strength (psi). DP is the differential pressure or confining stress (psi). Fa is the rock internal angle of friction (degrees).

For the finite element process, the CCS is calculated. The formulas used to calculate the CCS have to be solely from the simulation for the testing process to be accurate. Here is the formula.

$$CCS = (eff * WOB) \left[\frac{13.33 * \mu_B * N}{D_B * ROP} + \frac{1}{A_B} \right] \quad (Calhoun, Caicedo, \& Ewy, 2008) \quad \text{Equation 5. 101}$$

All the input variables are gotten from downhole x direction.

$ROP = \text{Downhole rate of penetration} \left(\frac{ft}{hr} \right)$. This is velocity in x direction of last node;

$\mu_B = \text{bit specific coefficient of sliding friction}$

$D_B = \text{Bit Diameter (inches)}$;

$CCS = \text{Confined Compressive Strength (psi)}$;

$eff = \text{Mechanical Efficiency (\%)}$

$A_B = \text{Borehole Area (in}^2\text{)}$

$WOB = \text{Weight on Bit (lbs)}$.

$N = \text{Revolution per minute at the bit (rpm)}$. This is RPM of last node

The formula for some variables is as follows:

$$\mu_B = 36 * \frac{TOB}{D_B * WOB} \quad \text{Equation 5. 102}$$

TOB is Torque on Bit.

$$A_B = \pi * \frac{D_B^2}{4} \quad \text{Equation 5. 103}$$

$$N = \frac{\theta_{downhole}}{2 * \pi}, \text{ where } \theta_{downhole} \text{ is the rotational displacement of the last node.}$$

$$eff = \left(1 - \left(\frac{\left| \frac{\beta_{2+i} - \beta_{desired}}{\beta_{desired}} \right| + \left| \frac{\alpha_{2+i} - \alpha_{desired}}{\alpha_{desired}} \right|}{2} \right) \right) * 100 \quad \text{Equation 5. 104}$$

The above equation is derived from the error from the inclination and the azimuth.

$$\text{Azimuth Error} = \frac{\beta_{2+i} - \beta_{desired}}{\beta_{desired}} \quad \text{Equation 5. 105}$$

$$\text{Inclination Error} = \frac{\alpha_{2+i} - \alpha_{desired}}{\alpha_{desired}} \quad \text{Equation 5. 106}$$

The efficiency is gotten from the average accuracy on the inclination and on azimuth.

$$\text{Therefore, Average Error} = \frac{\left| \frac{\beta_{2+i} - \beta_{desired}}{\beta_{desired}} \right| + \left| \frac{\alpha_{2+i} - \alpha_{desired}}{\alpha_{desired}} \right|}{2} \quad \text{Equation 5. 107}$$

$$\text{Accuracy} = 1 - \left(\frac{\left| \frac{\beta_{2+i} - \beta_{desired}}{\beta_{desired}} \right| + \left| \frac{\alpha_{2+i} - \alpha_{desired}}{\alpha_{desired}} \right|}{2} \right) \quad \text{Equation 5. 108}$$

$$\text{On a Percentage} = \left(1 - \left(\frac{\left| \frac{\beta_{2+i} - \beta_{desired}}{\beta_{desired}} \right| + \left| \frac{\alpha_{2+i} - \alpha_{desired}}{\alpha_{desired}} \right|}{2} \right) \right) * 100 \quad \text{Equation 5. 109}$$

5.6.2 Acceleration Validation

As for the accelerations in x, y and z directions, their values are useful in informing more details about the kind of vibration occurring downhole. The expression for acceleration is stated in Table 5.2. Let the accelerations measured by the measurement while drilling (MWD) tool be Acc_x , Acc_y , and Acc_z .

$$\text{Pure lateral vibration is } a_{lateral} = \sqrt{(Acc_z^2 + Acc_y^2)} \quad \text{Equation 5. 110}$$

$$\text{Pure axial vibration is } A_{acc_x} = Acc_x \quad \text{Equation 5. 111}$$

Plots showing comparison between accelerations gotten from the finite element process and accelerations from the MWD tool would boost confidence on the reliability of the drilling simulation results generated.

With the value of the acceleration known, issues concerning vibration can be forecasted. The outputs from the finite element method can act as the measurement tool downhole and measure accelerations in 3 dimensions and the severity of stick slip and lateral vibrations can be known. Forecasting beyond the bit is possible as the drill ahead modeling takes place with calculation of next inclination and the next azimuth creates the pseudo well path for further drilling. If the formation CCS profile is already known, then the results from the simulation can be very close to the expected results.

5.7 Optimization to Reduce Energy Loss

The expectation is that the energy produced by the rotation and translational movements of the drill string will lead to drilling the borehole effectively thereby maximizing the energy to break through the confined compressive strength (CCS) of the rock. However, energy is lost due to frictional and excessive vibration of the drill string. This energy loss adds to the mechanical specific energy (MSE) needed to drill. It is therefore necessary to introduce an optimization process that will show optimized parameters for minimizing the MSE.

$$MSE = \frac{480 * Torque * RPM}{D_B^2 * ROP} + \frac{4 * WOB}{\pi * D_B^2} \quad \text{Equation 5. 112}$$

The objective function is to minimize MSE. This would mean calculating optimum values when the derivative of MSE with respect to x is equal to zero.

$$\text{At minimum MSE, } \frac{dMSE}{dx} = 0 \quad \text{Equation 5. 113}$$

Modern stochastic optimization algorithm is the optimization chosen because it has high local optima avoidance, and gradient free mechanism. Particle swarm optimization is the type of stochastic algorithm to be used. Here are the algorithms.

$$\overrightarrow{X_i^{t+1}} = \overrightarrow{X_i^t} + \overrightarrow{V_i^{t+1}} \quad \text{Equation 5. 114}$$

$$\overrightarrow{V_i^{t+1}} = w\overrightarrow{V_i^t} + c_1r_1(\overrightarrow{P_i^t} - \overrightarrow{X_i^t}) + c_2r_2(\overrightarrow{G_i^t} - \overrightarrow{X_i^t}) \quad \text{Equation 5. 115}$$

V_i^t is the inertia term or velocity of the particle.

$(\overrightarrow{P_i^t} - \overrightarrow{X_i^t})$ is the cognitive component or the personal best of the particle.

$(\overrightarrow{G_i^t} - \overrightarrow{X_i^t})$ is the global best or social component of the particle in each run of the optimization program. The particle will be the $MSE_{Objective}$ calculated for each drilling simulation run. The results will be shown in the next chapter.

5.8 Conclusion

When the drill string is in contact with the wall of the wellbore, there is bound to be drag during pull or slacking and torque during drilling. The finite element process is able to output important variables like **tension on each node of every element** in the entire structure which leads to the calculation of normal force while calculation of friction coefficient depends on the global torque difference between nodes of each member. The **buckling and tensile limit** can be set in a friction coefficient plot. The resultant force at the bit and before the bit is key to calculating **the next inclination and the next azimuth** in the drill ahead model. Particle Swarm Optimization is used to minimize the MSE of each run of the drilling process.

Chapter 6 Computational Results of Drill String Dynamics

The data used for this computational analysis is from a horizontal well drilled in Europe.

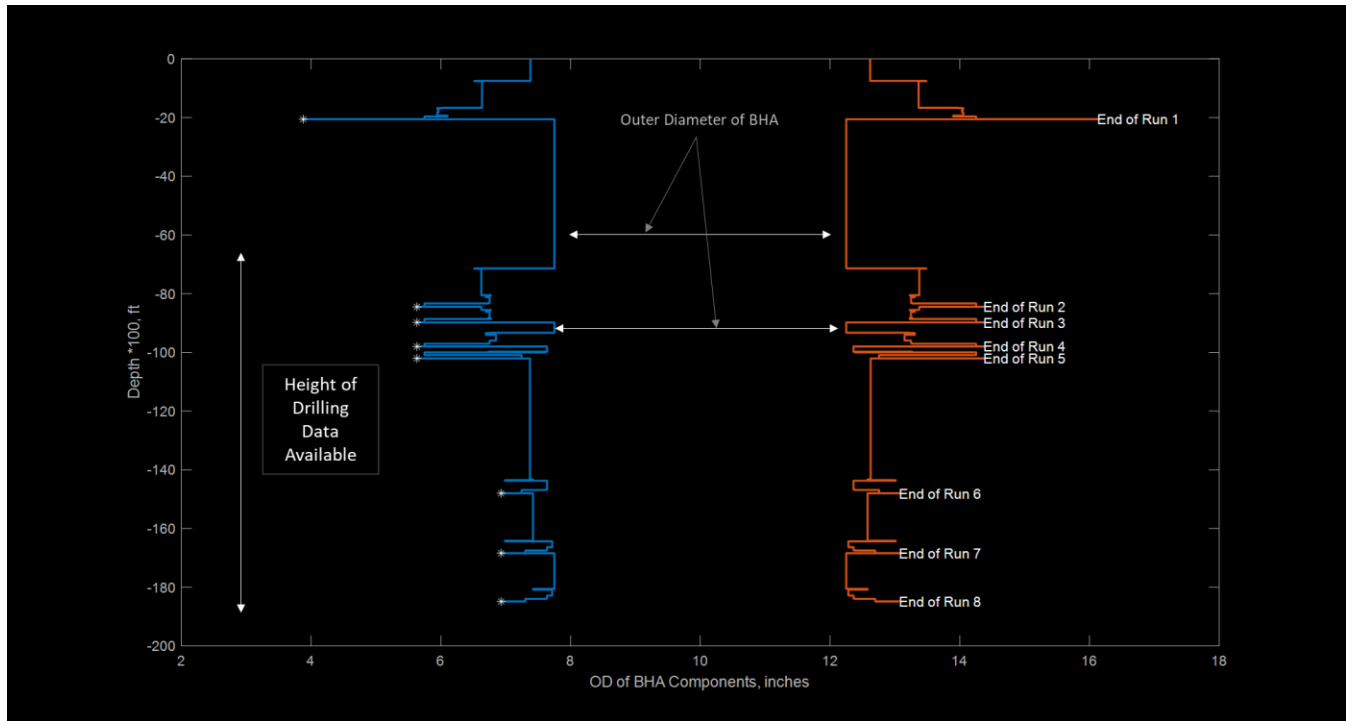


Figure 6. 1 Diameter of BHA Used for Test Data

The data used was for a well drilled to just over 18534.38 feet, however, the drilling data provided starts drilling at 6624.5 feet as shown in the bit depth graph. Figure 6.2 shows several peaks in the bit depth data indicative of trip in and trip out actions. Here are some key preprocessing steps.

- Remove null values (usually -999.25).
- To achieve drilling data only, only select data where bit depth equals measured depth which ignores tripping in the bit depth data as shown in Figure 6.3.
- Create Bottom Hole Assembly, BHA, Balance Sheet which sums up all drilling runs to only include the parts of the BHAs used that was drilled through the formation. Figure 6.4 shows the height of drilling data available meaning the investigation studies data where the drilling in view started at about 6624.5 ft.

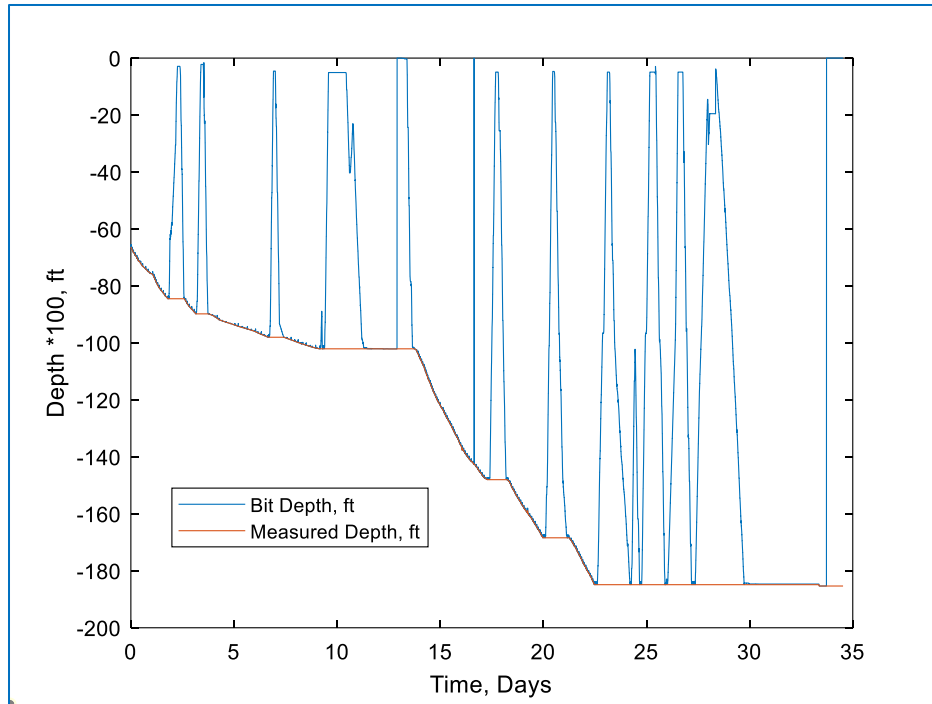


Figure 6. 2 Bit Depth vs Measured Depth of Sample Data

The filtering to achieve drilling only data is to find data where $Bit\ Depth \leq Measured\ Depth$.

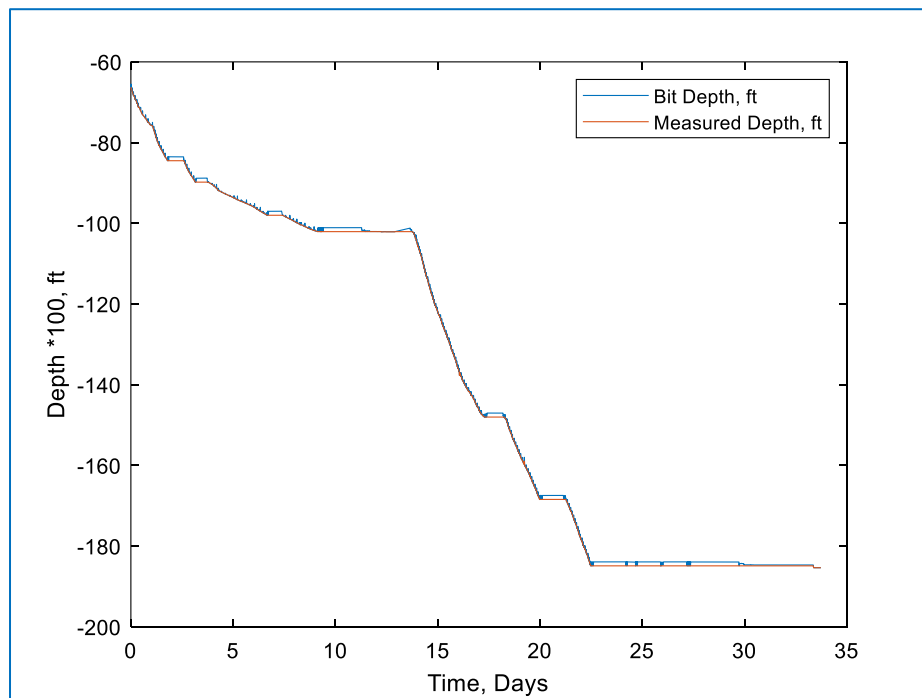


Figure 6. 3 Drilling Data for Bit Depth vs Measured Depth

A total of 5 validation processes and 1 test is done to validate the models and tests the benefits of the analyzing drilling operations in using the finite element method.

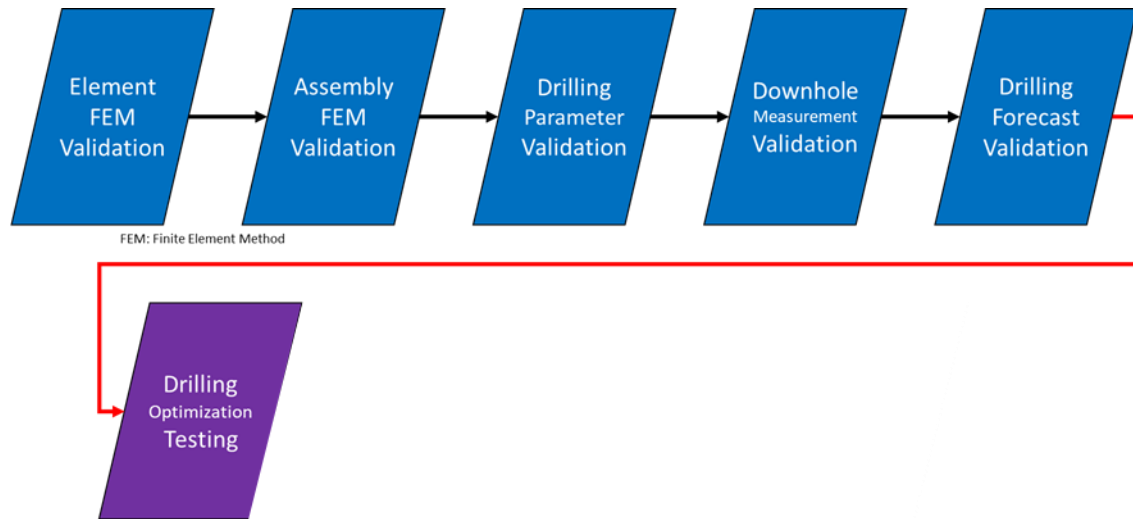


Figure 6. 4 Series of Validation and Testing for the FEM Based Drilling Simulation

6.1 Transverse Element FEM Validation

Consider one string of heavy weight drill pipe, with 4 feet of its length in investigation having 3.25 inches inner diameter and 5 inches outer diameter as shown in Figure 6.3.

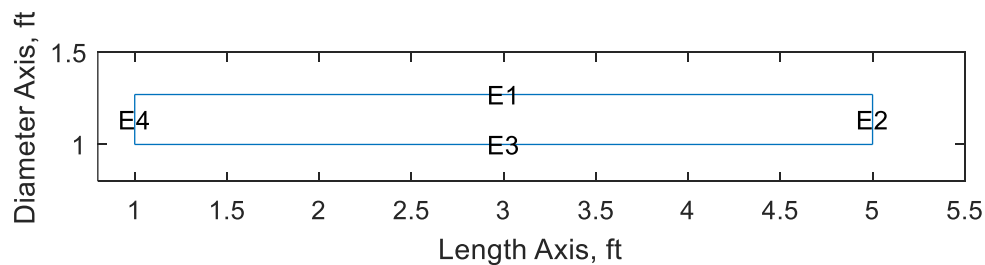


Figure 6. 5 Four Feet Beam Element

Assuming the pipe takes the form of a cantilever beam with a uniformly distributed load. Here is the formula to calculate the boundary conditions.

Inner Diameter of Pipe, ID = 3.25 inches

Outer Diameter of Pipe, OD = 5 inches

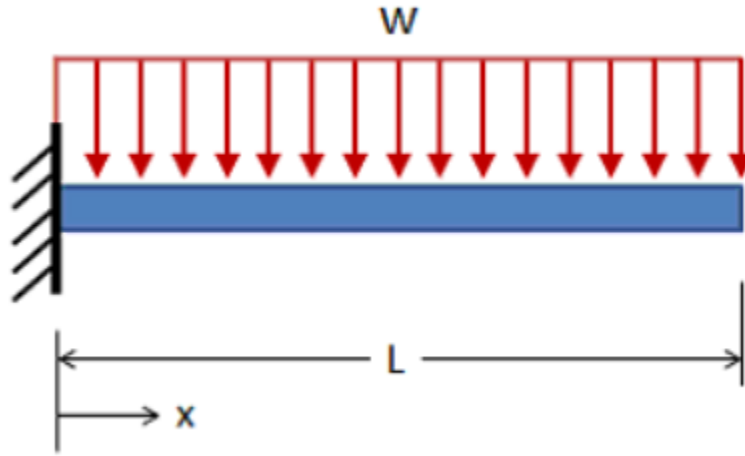


Figure 6. 6 Cantilever with Uniformly Distributed Load (Budynas-Nisbett, 2011)

From the deflection tables:

$$\delta = \frac{-wx^2((6L^2 - 4Lx + x^2))}{24EI} \quad (\text{Budynas-Nisbett, 2011}) \quad \text{Equation 6. 1}$$

$$\theta = \frac{-wx((3L^2 - 3Lx + x^2))}{6EI} \quad (\text{Budynas-Nisbett, 2011}) \quad \text{Equation 6. 2}$$

$$\text{Weight per foot} = w = 2.66(OD^2 - ID^2) = 42.56 \text{ lb/ft} \quad \text{Equation 6. 3}$$

Based on Equation 6.1, at $y = 0$, translation, $u = 0 \text{ ft}$ and rotation, $\frac{du}{dy} = 0 \text{ degrees}$

At $y = L$, translation, $u = -5.3791 \text{ ft}$ and rotation, $\frac{du}{dy} = -0.2391 \text{ degrees}$

Here are other inputs into the one element beam.

$E = \text{Young's Modulus} = 30,000 \text{ psi}$

$\text{Density of Pipe, } \rho = 503 \frac{\text{lb}}{\text{cu ft}}$

Discretized to 100 divisions, the plots of the exact solution versus the approximation used shows a perfect match.

The initiation and termination points in

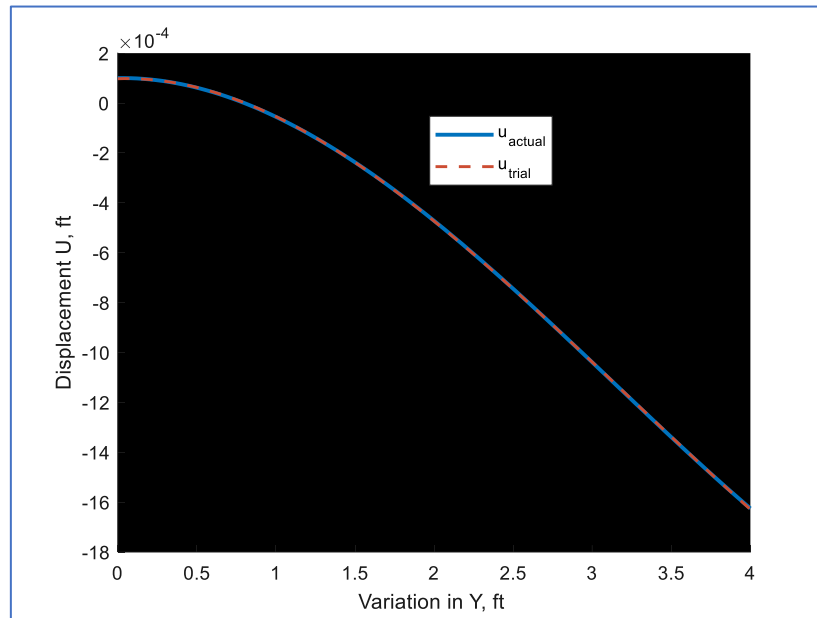


Figure 6. 7 Comparing the Actual and Trial Solutions for the Transverse Displacements

The derivative of the displacement function also tallies with the derivative of the actual solution.

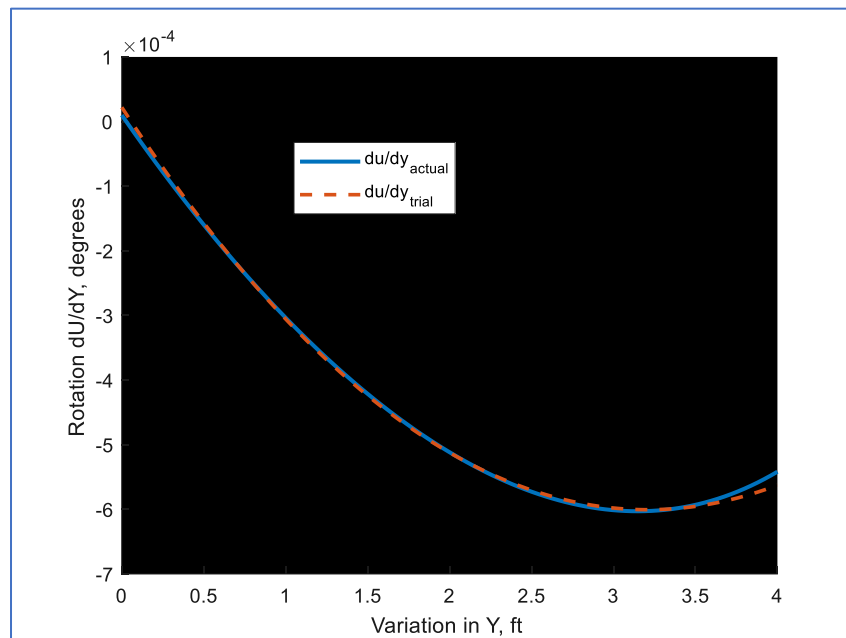


Figure 6. 8 Comparing the Actual and Trial Derivatives of the Transverse Displacements

The residual, which represents how far off from the governing differential equation is the trial solution, ranges between -20 ft and 60 ft. An ideal situation would be to have residuals below 1 ft intervals. On the other hand, the error between the trial solution and the actual solution is an average percentage error of 1.5048 percent. Figure 6.9 shows the overview of the error and the residual throughout the domain of the beam element.

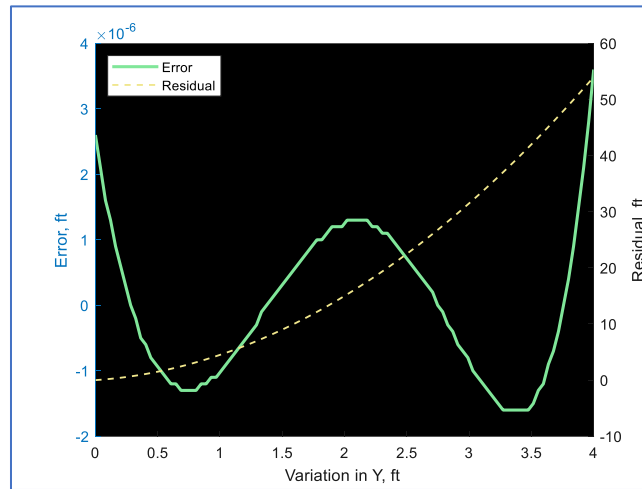


Figure 6. 9 Residual of the Transverse Governing Equation

In order to reduce the residual errors, more or less divisions of the element are tried and here are the results. Here is the result for 500 divisions of the domain of the element.

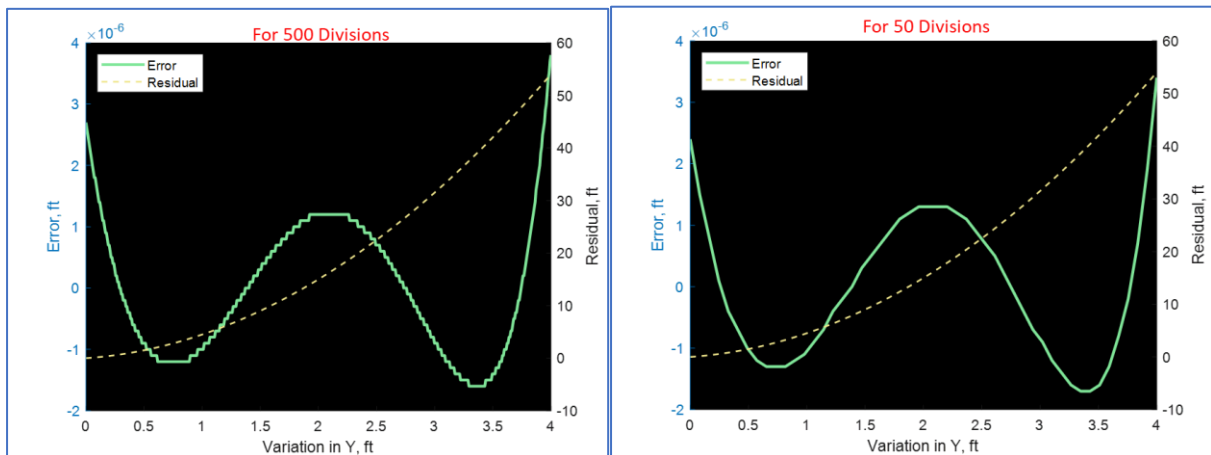


Figure 6. 10 Residuals for 500 and 50 Divisions of the 4ft Beam Domain

6.2 Axial Element FEM Validation

Consider a beam fixed at one end with a tensile load, P , on the other end. Assuming constant cross section, and a homogeneous material with constant young's modulus.

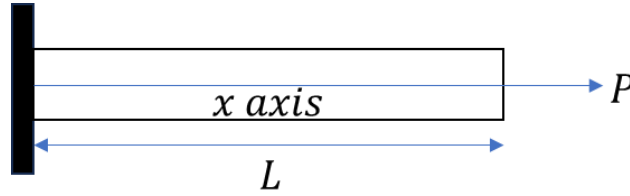


Figure 6. 11 Axial Load on a Fixed Beam

$$\text{Stress} = \frac{P}{\text{Cross Section Area}} \quad (\text{Morley, 1961}) \quad \text{Equation 6. 4}$$

$$\text{Strain} = \frac{\text{deflection, } \delta}{L} \quad (\text{Morley, 1961}) \quad \text{Equation 6. 5}$$

$$\text{According to Hooke's Law, Stress} = E * \text{Strain} \quad \text{Equation 6. 6}$$

This assumption leads to an expression for the deflection.

$$\delta = \frac{PL}{EA} \quad \text{Equation 6. 7}$$

Equation 6.7 is used to calculate the boundary conditions. Since the governing equation for the axial loading is a second order ODE, therefore, only two boundary conditions are needed. If $P = 10 \text{ klb} = 10,000 \text{ lb}$ for $L = 4 \text{ ft}$, $ID = 3.25 \text{ inches}$ and $OD = 5 \text{ inches}$

at $x = 0$, translation, $u = 0 \text{ ft}$

At $x = L$, translation, $u = 0.161 \text{ ft}$

Here are the results.

It can be clearly seen in Figure 6.10 and Figure 6.11 that the residuals have a higher margin for the 50 divisions showing that the results become better as the element is broken into more divisions. The solutions come with an equation for each case which can then be used to calculate the corresponding force, moment, and other important space dependent variables throughout the length of the element.

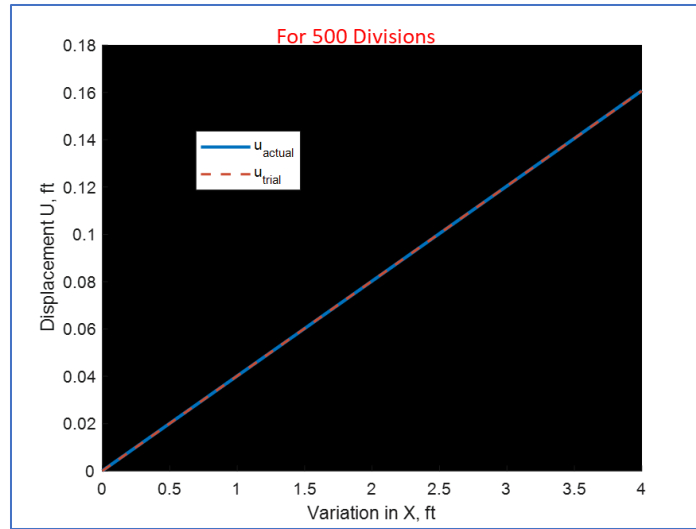


Figure 6. 12 Displacement Graph for Axial Loading

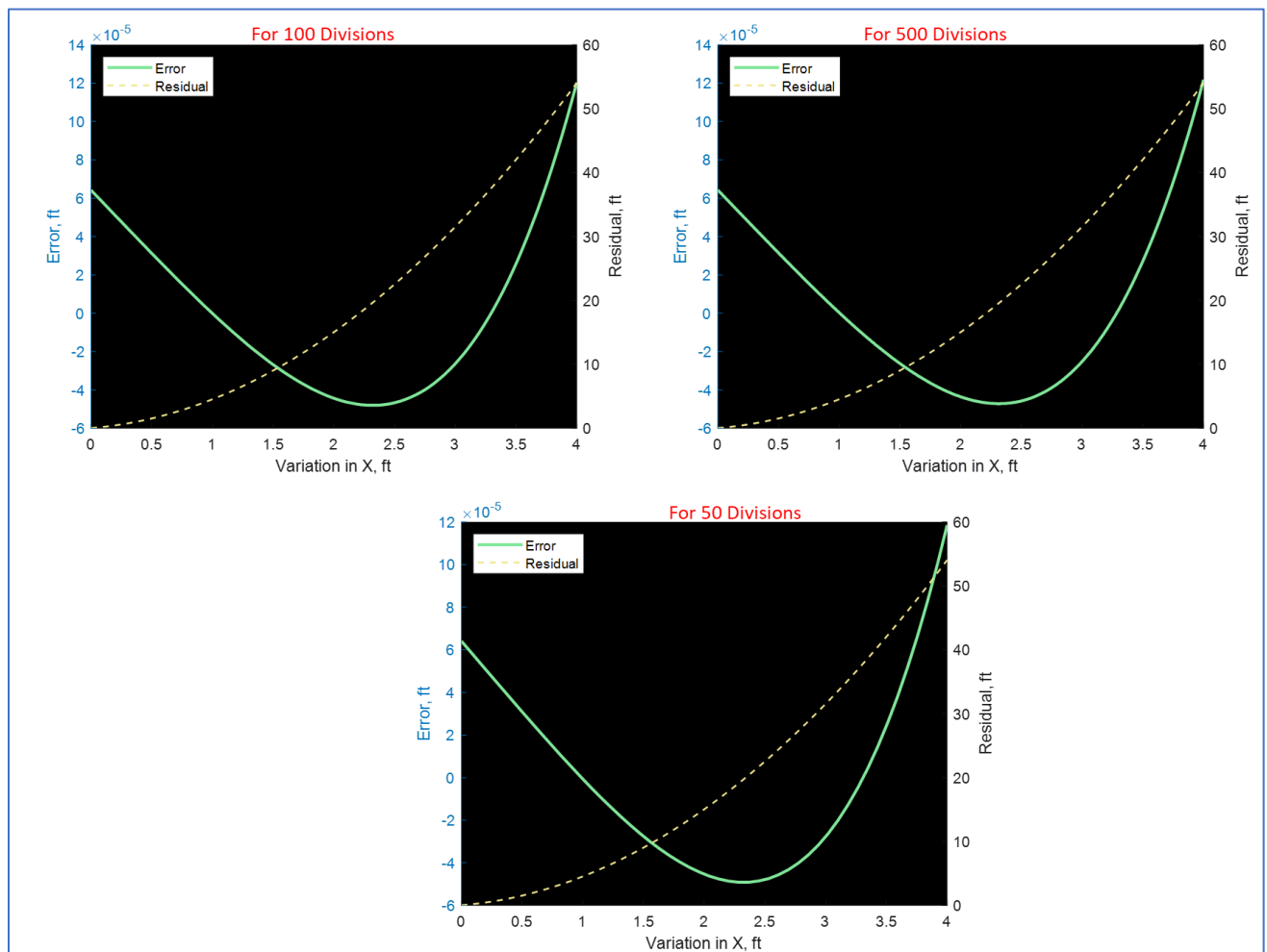


Figure 6. 13 Residual Plot for Axial Loading for 50, 100, and 500 Divisions

6.2 Time Based Assembly Process

The goal of the time-based solution is to produce the displacements with variation in time. As seen in chapter 5, the time-based solution was derived from the inverse Laplace transformation of the results of the partial differential equation. Here is how the simulation loop to produce results goes.

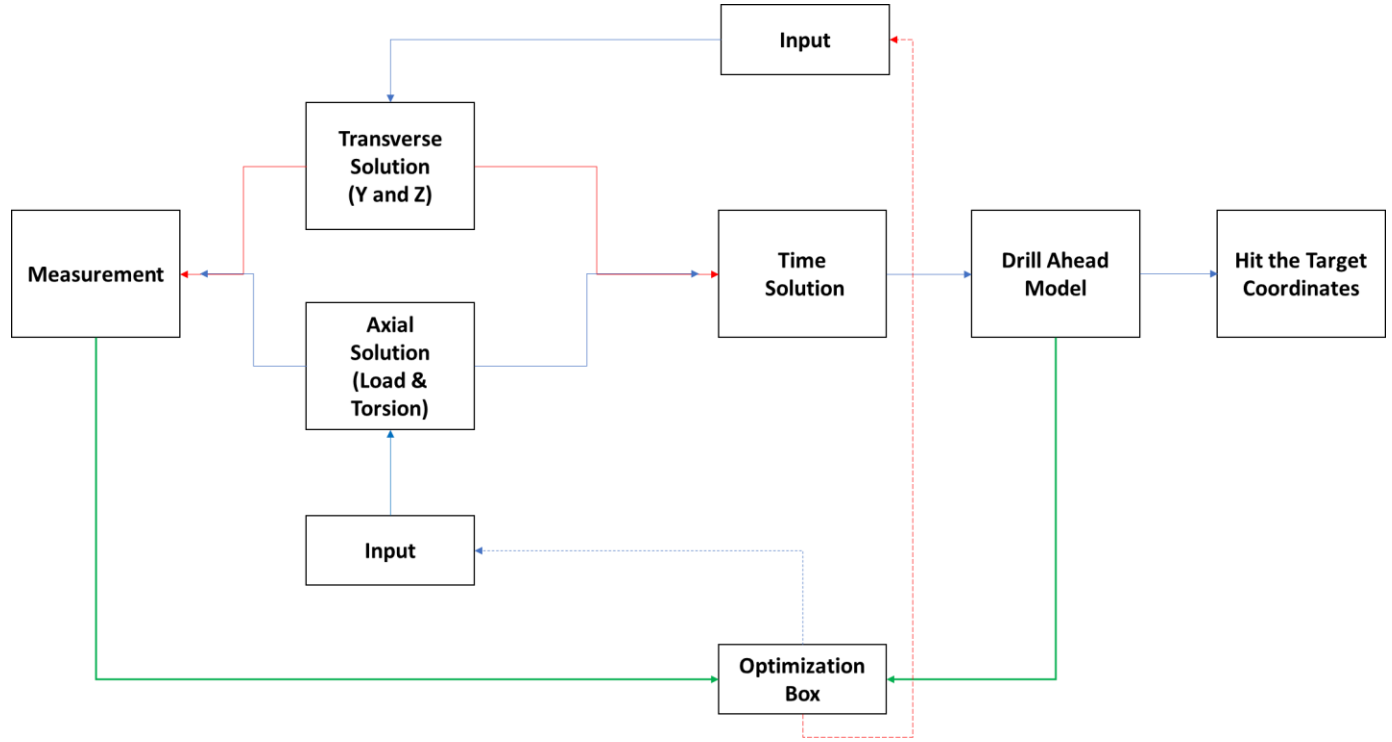


Figure 6. 14 The Drilling Simulation Process

The assembly is key to ensuring the whole simulation is specifically for drilling simulation. The assembly boundary conditions make the finite element directly for drilling processes. Forces, moments, and displacements of the same nodes add up. Three equations govern how element by element outputs are combined to make the assembly of beams.

$$\sum_{i=1}^n Axial_{displacement} = c_1 x_i^{c_2} + c_3 x_i^{c_4} + \dots c_0 x_i^0 \quad \text{Equation 6. 8}$$

$$\sum_{i=1}^n Transverse Y_{displacement} = c_1 y_i^{c_2} + c_3 y_i^{c_4} + \dots c_0 y_i^0 \quad \text{Equation 6. 9}$$

$$\sum_{i=1}^n Transverse Z_{displacement} = c_1 z_i^{c_2} + c_3 z_i^{c_4} + \dots c_0 z_i^0 \quad \text{Equation 6. 10}$$

Equation 6.8, Equation 6.9 and Equation 6.10 are generated every loop of simulation for each element and added up for the assembly. The space-based simulation of the transverse and axial

element motion lead to the determination of the stiffness matrix, mass matrix and damping matrix for each element. These n-by-n constants are inputs into the time-based simulation. Here is the proposed calculation process.

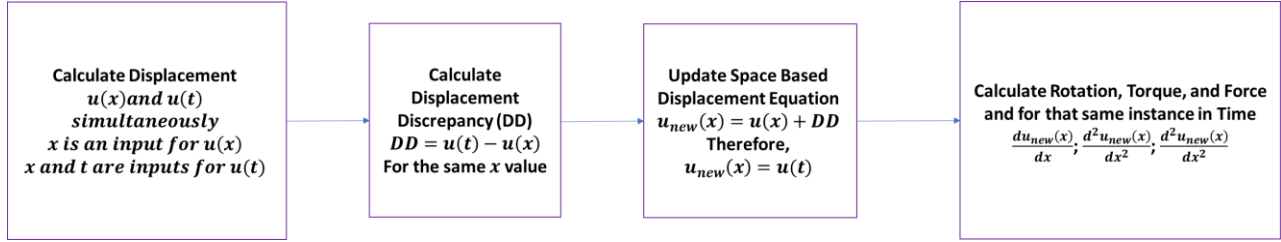


Figure 6. 15 Calculation of Rotation, Torque and Force

To fully incorporate the displacement discrepancy into the rotation, torque and force calculations, a new constant has to be calculated. Here are the adjusted displacements.

$$\sum_{i=1}^n Axial_{displacement} = c_1(x_i + n_{axial})^{c_2} + c_3(x_i + n_{axial})^{c_4} + \dots c_0(x_i + n_{axial})^0 = DD + c_1x_i^{c_2} + c_3x_i^{c_4} + \dots c_0x_i^0 \quad \text{Equation 6. 11}$$

$$\sum_{i=1}^n Transverse Y_{displacement} = c_1(y_i + n_{TransverseY})^{c_2} + c_3(y_i + n_{TransverseY})^{c_4} + \dots c_0(y_i + n_{TransverseY})^0 = DD + c_1y_i^{c_2} + c_3y_i^{c_4} + \dots c_0y_i^0 \quad \text{Equation 6. 12}$$

$$\sum_{i=1}^n Transverse Z_{displacement} = c_1(z_i + n_{TransverseZ})^{c_2} + c_3(z_i + n_{TransverseZ})^{c_4} + \dots c_0(z_i + n_{TransverseZ})^0 = DD + c_1z_i^{c_2} + c_3z_i^{c_4} + \dots c_0z_i^0 \quad \text{Equation 6. 13}$$

Since the values of DD , x_i , y_i and z_i are known, then the values of n_{axial} , $n_{TransverseY}$, and $n_{TransverseZ}$ can be easily calculated. The time step for each simulation is 2 seconds. This is because the simulation needs at least 3 rows to function excellently.

6.2.1 Movement Away from the Reference Point

The global system is the point of origin of the system. For movement to be appreciated, a reference point has to be defined before the movement starts. In the case of drill string simulation, the entire string does not move. This is where the boundary conditions for the assembly of the drill string becomes very key. Figure 6.16 shows key areas where the displacement of the drill string is zero. The restrictions are because of the constraints in the drill string structure. The reason for the lack

of movement in the Y and Z directions at the surface is the indicate the *holding in place* by the top drive. If any node touches the wall of the wellbore, it means:

$$\sqrt{u_y^2 + u_z^2} = D_{hole} - OD_{Component} \quad \text{Equation 6. 14}$$

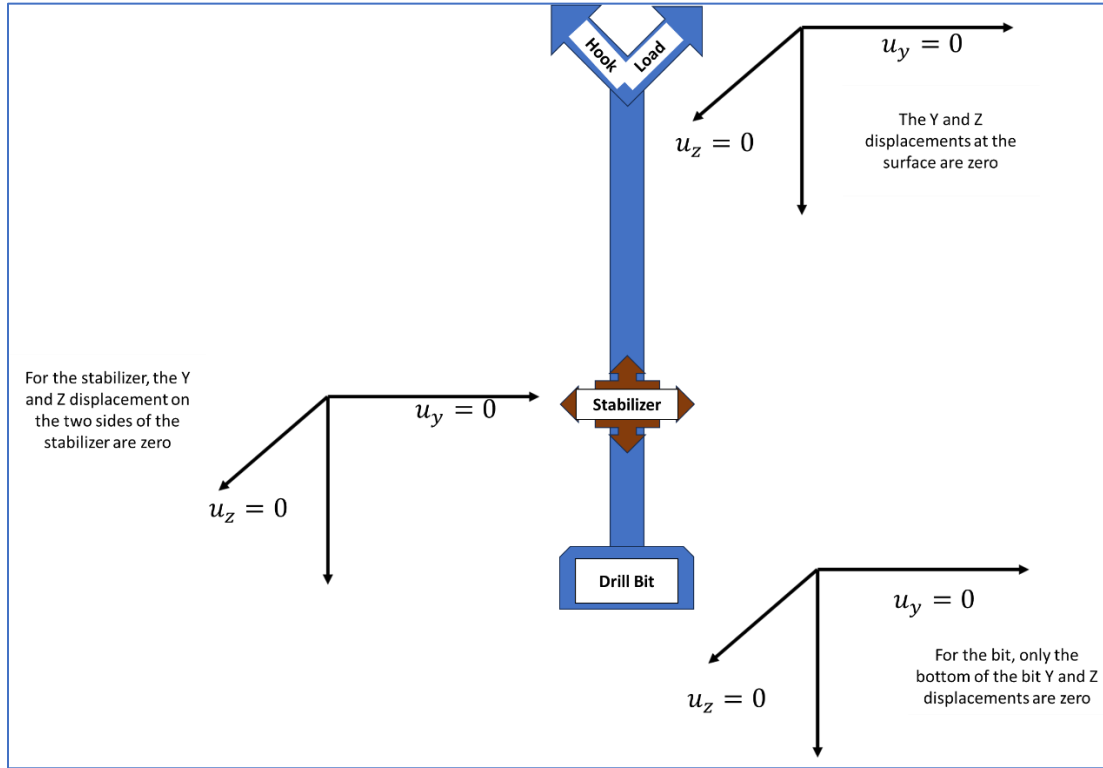


Figure 6. 16 Effect of The Assembly Boundary Conditions on Displacements

The stabilizer extends towards the walls of the wellbore, which is within its purpose, and this is why displacements at stabilizers is zero for the Y and Z directions. The boundaries at the bottom of the bit are a convention that appreciates the impact of the strength of the rock. The digging will most likely only allow axial movements where the power of the drilling ensures one direction movements. For this thesis, the reference point is at the surface of the drilling.

6.2.2 Pull of Interest

The transverse displacement comes in a pair of 4 by 4 matrix which signifies the arrangement in Equation 4.28 while the axial displacement comes in a pair of 2 by 2 matrix per time loop signifying the arrangement in Equation 4.52. This leads to the labelling for the displacement consequently.

$$u_y = \begin{bmatrix} u_{11}^e & u_{12}^e & u_{13}^e & u_{14}^e \\ u_{21}^e & u_{22}^e & u_{23}^e & u_{24}^e \\ u_{31}^e & u_{32}^e & u_{33}^e & u_{34}^e \\ u_{41}^e & u_{42}^e & u_{43}^e & u_{44}^e \end{bmatrix} \quad \text{Equation 6. 15}$$

Similarly for the Z direction,

$$u_z = \begin{bmatrix} u_{11}^e & u_{12}^e & u_{13}^e & u_{14}^e \\ u_{21}^e & u_{22}^e & u_{23}^e & u_{24}^e \\ u_{31}^e & u_{32}^e & u_{33}^e & u_{34}^e \\ u_{41}^e & u_{42}^e & u_{43}^e & u_{44}^e \end{bmatrix} \quad \text{Equation 6. 16}$$

In the same manner, the displacements for the X direction are identified.

$$u_{x_{load}} = \begin{bmatrix} u_{11}^e & u_{12}^e \\ u_{21}^e & u_{22}^e \end{bmatrix} \quad \text{Equation 6. 17}$$

However, for the transverse displacements, there are only 4 nodes meaning all displacements cannot be used at once. It then depends on what drilling process is taking place. There are key processes in drilling:

- Drilling and Slacking (downward movement)
- Pulling (upward movement)
- Rotating (round movement)
- Back reaming (round and up movement)

Usually, the initiating force comes from its own node, referring to u_{11}^e , u_{22}^e , u_{33}^e , and u_{44}^e . Here is the labelling.

$$u_y = \begin{bmatrix} \text{Process Type} & \text{Node 1} & \text{Node 1} & \text{Node 2} & \text{Node 2} \\ & y & z & y & z \\ \text{Pulling, Tripping} & \mathbf{u_{11}^e} & u_{12}^e & u_{13}^e & u_{14}^e \\ \text{Back Reaming} & u_{21}^e & \mathbf{u_{22}^e} & u_{23}^e & u_{24}^e \\ \text{Drilling/Slacking} & u_{31}^e & u_{32}^e & \mathbf{u_{33}^e} & u_{34}^e \\ \text{Rotation} & u_{41}^e & u_{42}^e & u_{43}^e & \mathbf{u_{44}^e} \end{bmatrix} \quad \text{Equation 6. 18}$$

$$u_z = \begin{bmatrix} \text{Process Type} & \text{Node 1} & \text{Node 1} & \text{Node 2} & \text{Node 2} \\ & z & y & z & y \\ \text{Pulling, Tripping} & \mathbf{u}_{11}^e & \mathbf{u}_{12}^e & \mathbf{u}_{13}^e & \mathbf{u}_{14}^e \\ \text{Back Reaming} & \mathbf{u}_{21}^e & \mathbf{u}_{22}^e & \mathbf{u}_{23}^e & \mathbf{u}_{24}^e \\ \text{Drilling/Slacking} & \mathbf{u}_{31}^e & \mathbf{u}_{32}^e & \mathbf{u}_{33}^e & \mathbf{u}_{34}^e \\ \text{Rotation} & \mathbf{u}_{41}^e & \mathbf{u}_{42}^e & \mathbf{u}_{43}^e & \mathbf{u}_{44}^e \end{bmatrix} \quad \text{Equation 6. 19}$$

$$u_{x_{load}} = \begin{bmatrix} & \text{Node 1} & \text{Node 2} \\ & x & x \\ \text{Pulling, Trip Out} & \mathbf{u}_{11}^e & \mathbf{u}_{12}^e \\ \text{Drilling, Trip in} & \mathbf{u}_{21}^e & \mathbf{u}_{22}^e \end{bmatrix} \quad \text{Equation 6. 20}$$

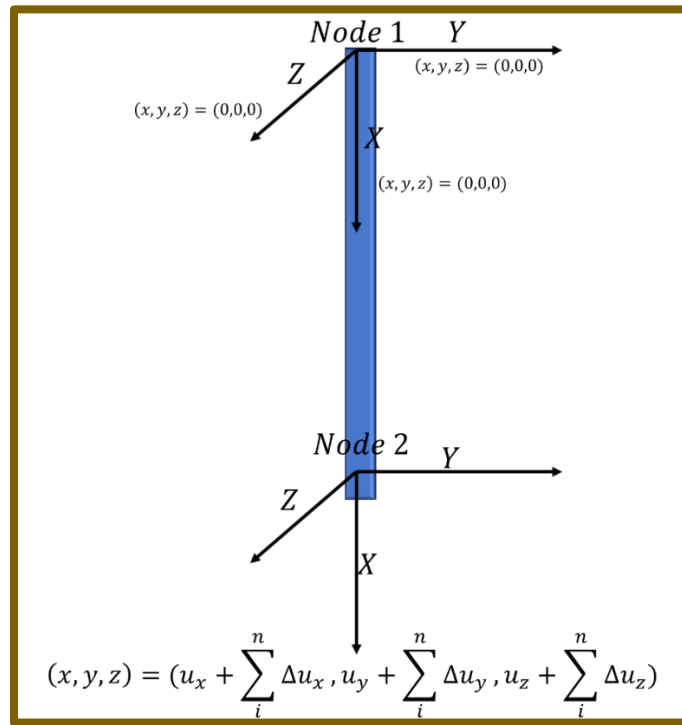


Figure 6. 17 Displacement from Reference Location

6.2.3 The Finite Element Simulation Flow

Figure 6.18 shows the flow of the simulation per element from break down of the drilling components till outputting important parameters. One element cannot lie on two drill components. The simulation for the transverse displacements and rotations, and the axial loading and axial torsions are obtained from Equation 4.2 to Equation 4.37 and Equation 4.38 to Equation 4.75. The three simulations can be done simultaneously. The time simulation takes the output from the finite element modeling and produces translation and rotation displacement with time variation.

Differentiating the expression once and twice in LaPlace domain will lead to results for velocity and acceleration. The displacements obtained from the time simulation are then used to adjust the displacement expressions for the transverse and axial simulations.

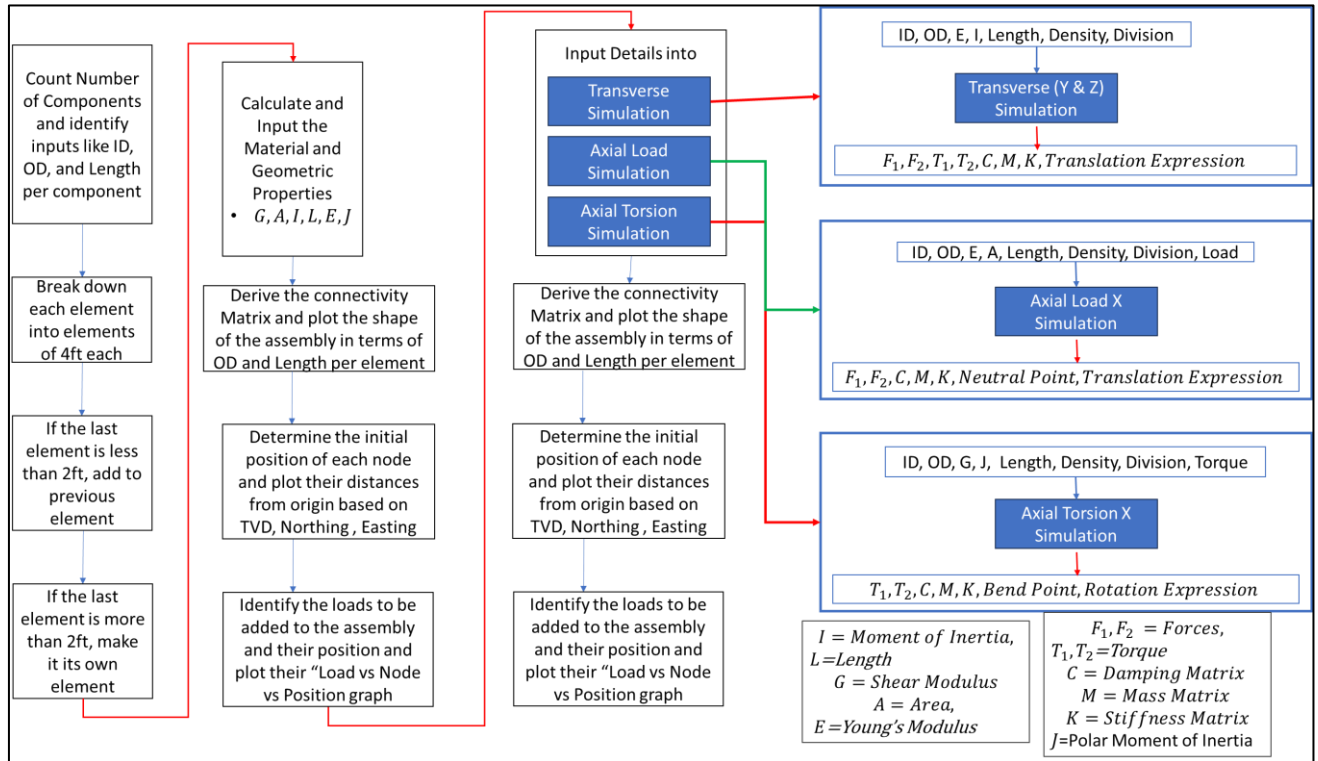


Figure 6. 18 Simulation Flow Chart for XYZ Finite Element Modeling

Now with the time simulation added to the loop, here are the adjusted displacements, torques and forces.

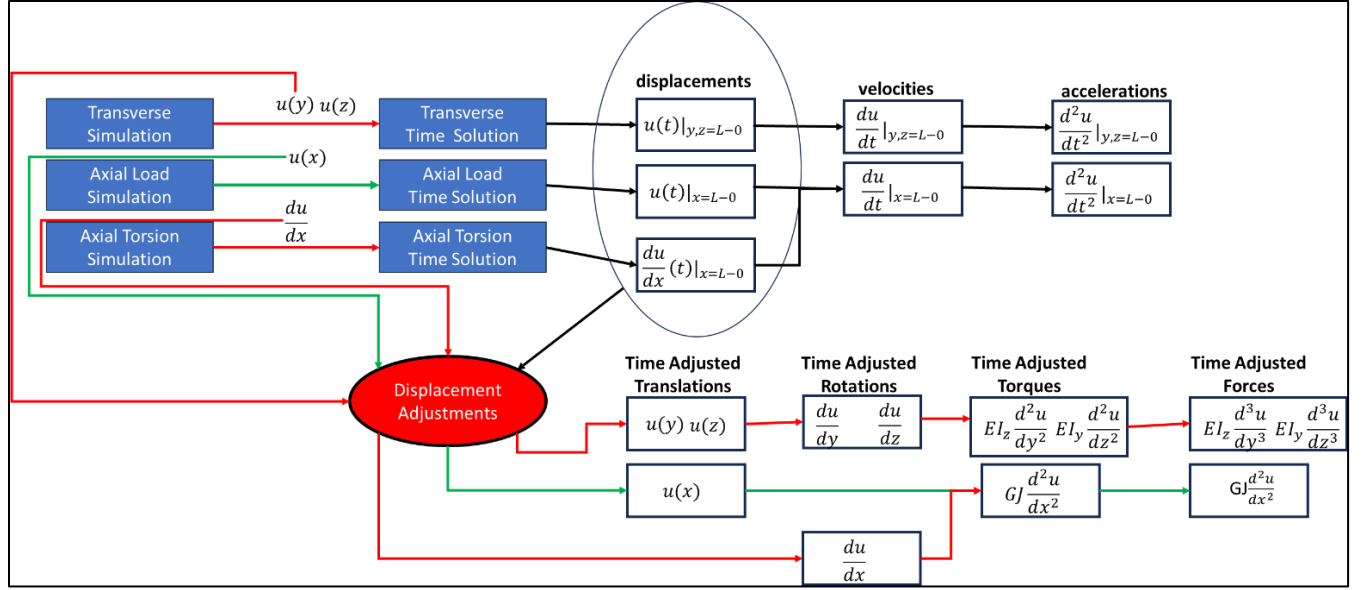


Figure 6. 19 Time Adjusted Displacements, Torques, and Forces

In terms of the elemental simulation, here is how the vital results for the displacements are obtained.

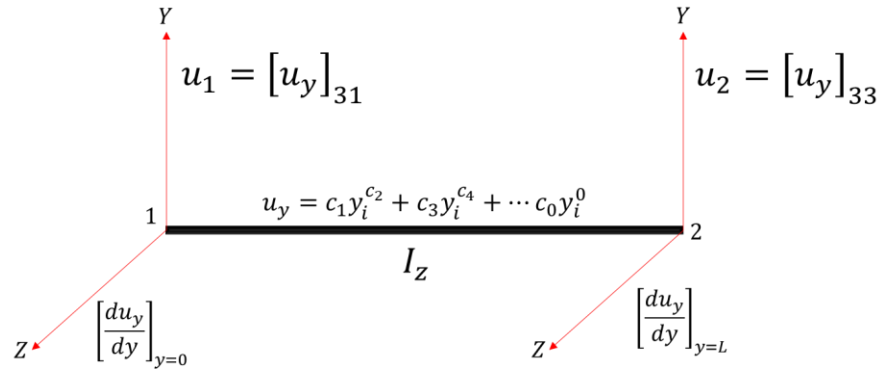


Figure 6. 20 Displacement Values for Transverse Y Direction

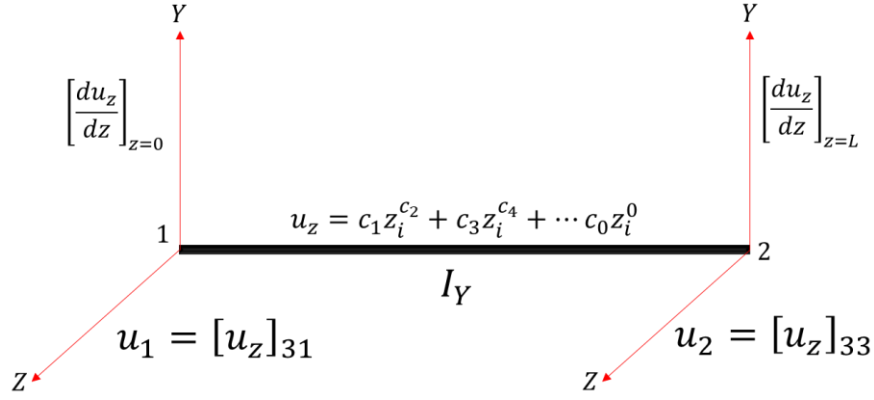


Figure 6. 21 Displacement Values for Transverse Z Direction

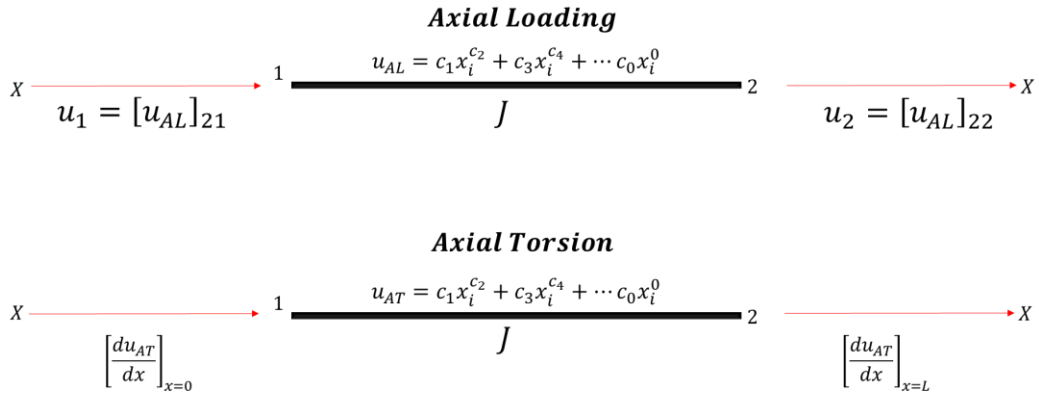


Figure 6. 22 Displacement Values for X Direction—Loading, Torsion

6.2.4 Important Assembly Results

The displacements, forces, torques, velocity and acceleration for nodes with the same number are added. Four Processes are going on in every loop of the assembly. They are all interconnected.

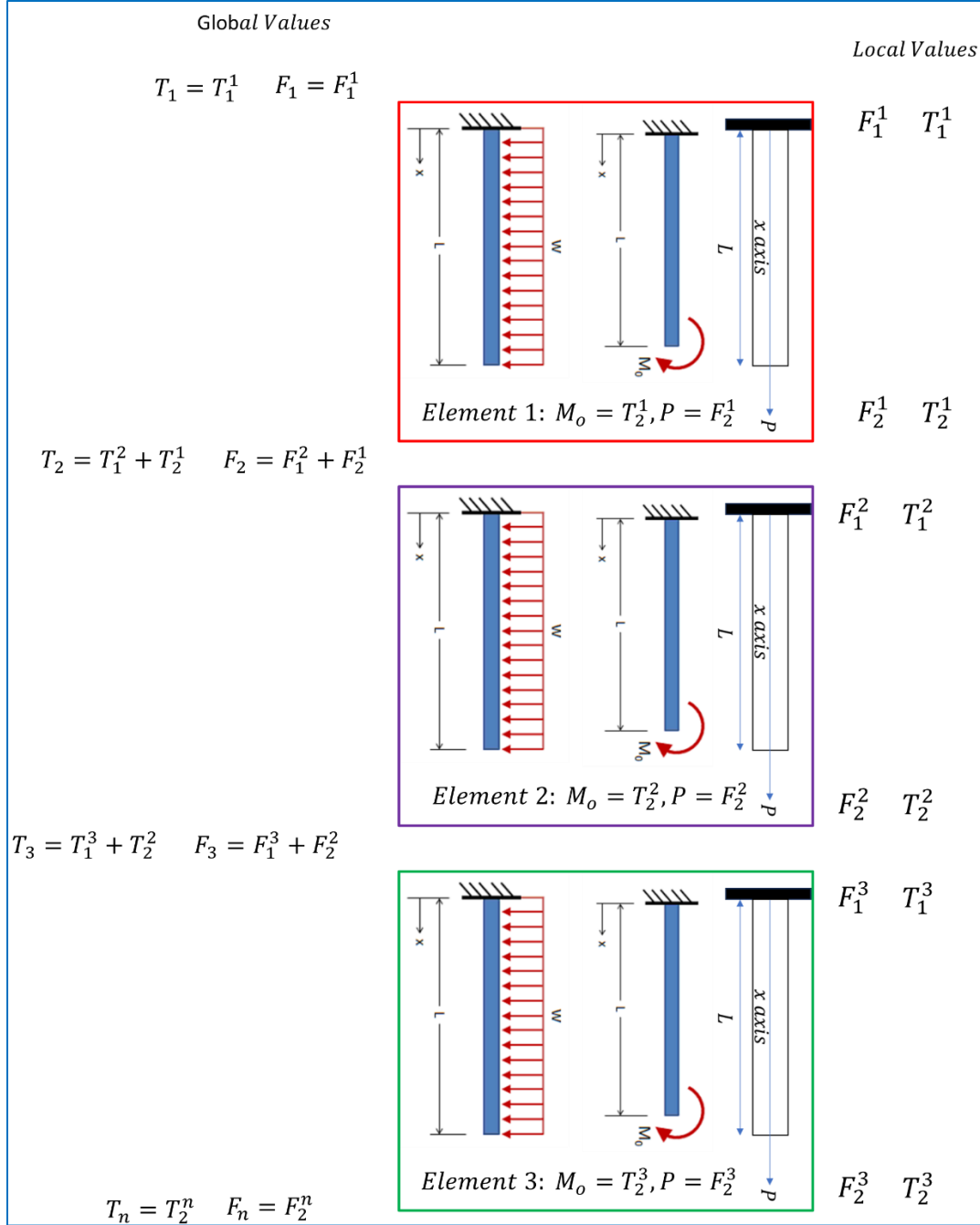


Figure 6. 23 Global Number of the Drill string

As shown in Figure 6.23, the four processes are cantilever uniform distributed load for both Y and Z directions, cantilever end moment for axial torsion and axial loading for X direction. The elements on top hold in place the elements below, the assumption is that the stimulus for each move is based on the torque on bit and the weight on bit below. In the interconnected phase, the

axial load P acts downward while the torque M_o causes the drill string to turn regardless of the resistance from the distributed weight of the drill string w .

6.2.5 Neutral Point of Tension/Compression and Neutral Point of Bending

At the neutral point of tension and compression, the axial loading force goes from tension to compression. This is better viewed as an assembly property to locate several points along the drill string where the neutral point could be found. When there are 2 or more neutral points of compression and tension, there lies a transition zone between two neutral points. In this thesis, positive axial forces mean tension while negative axial forces refer to compression.

At neutral point of tension and compression, $\sum_{i=1}^n \frac{d^3u}{dx^3} = 0$ *Equation 6. 21*

Therefore, the neutral points are the values of x the derivative expression is equated to zero. The neutral point of bending occurs when the torques during axial torsion are equal to zero.

At neutral point of tension and compression, $\sum_{i=1}^n \frac{d^2u}{dx^2} = 0$ *Equation 6. 22*

6.3 Drilling Parameter Validation

In order to compare drilling parameters from the simulation and the field results, a drill ahead action is carried out from based on the finite element modeling. The most important phenomenon in parameter comparison is scenario similarity. The simulated events have to mirror the reality.

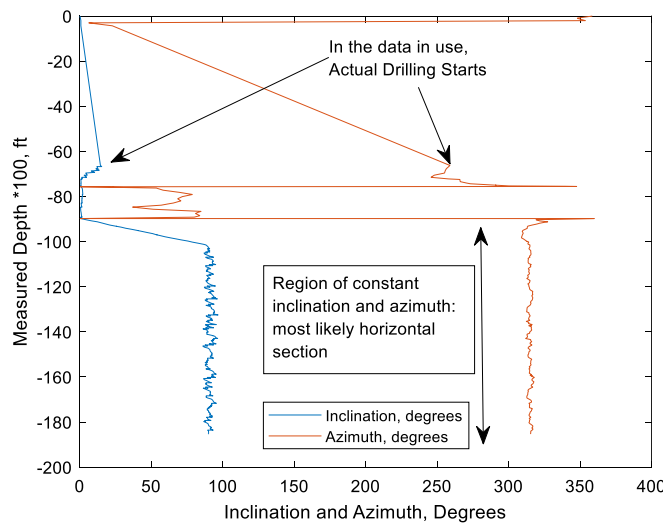


Figure 6. 24 Identifying Actual Drilling in Inclination Azimuth Plot

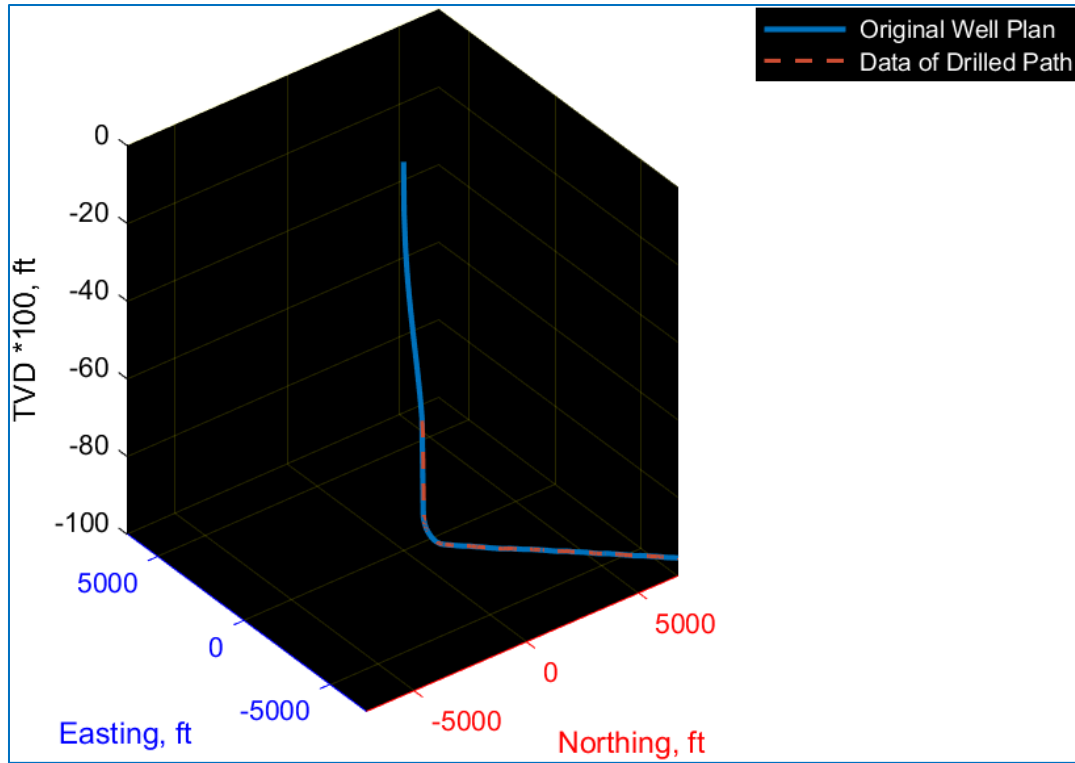


Figure 6. 25 Plot of Drilled Path vs Well Plan

Initiating the simulation to match the drilling process must be done accurately.

	A	B	C	D	E	F	G	H	I	J
1	Time sec	Top Drive RPM	ROP ft/hr	WOB klbs	GPM	Differential Pressure psi	HKLD klbs	Top Drive Torque (ft-lbs)	Bit Depth ft	Total Depth ft
2	0	39	137.2052	8.953398	109.9669	3107.46338	176.5779	6740	6624.502016	6624.502016
3	10	37	101.0944	8.973429	109.3745	3175.16284	176.6539	7220	6624.794274	6624.794274
4	20	38	100.0942	9.061846	90.64089	3079.29468	176.4919	5650	6625.086531	6625.086531
5	30	45	100.0942	9.014119	113.8085	2693.47119	176.6339	5240	6625.281347	6625.378755
6	40	37	98.51949	8.866555	111.7316	2755.17456	176.7849	6400	6625.573604	6625.573604
7	50	39	64.85971	8.960435	88.10793	3487.10962	176.8049	6060	6625.671013	6625.671013

Figure 6. 26 Initial Values of the Field Data

The parameters for comparison are Hookload, klbs, and Top Drive Torque, ft-lbs. The input data will be the weight on bit and the top drive RPM. Based on Figure 6.26, there is 6624.5 ft of the drill string already in the hole by the time the drilling begins. The initial values are:

$$WOB = 8.953398 \text{ klbs and Hookload} = 176.5779 \text{ klbs} \quad \text{Equation 6. 23}$$

$$\text{Surface RPM} = 39 \text{ rpm and Surface Torque} = 6740 \text{ ft lbs} \quad \text{Equation 6. 24}$$

Here are the general results. The first and most important result is the hook load because if the hook load is tracking too far wrongly then the load analysis of the entire system is faulty. From Figure 6.28, the tracking seems reasonable with a mean percentage error of 1.5971 percent. Since the weight on bit is the input into the system, the calculated hookload has the same kind of response to pull or push as the hookload obtained from the field.

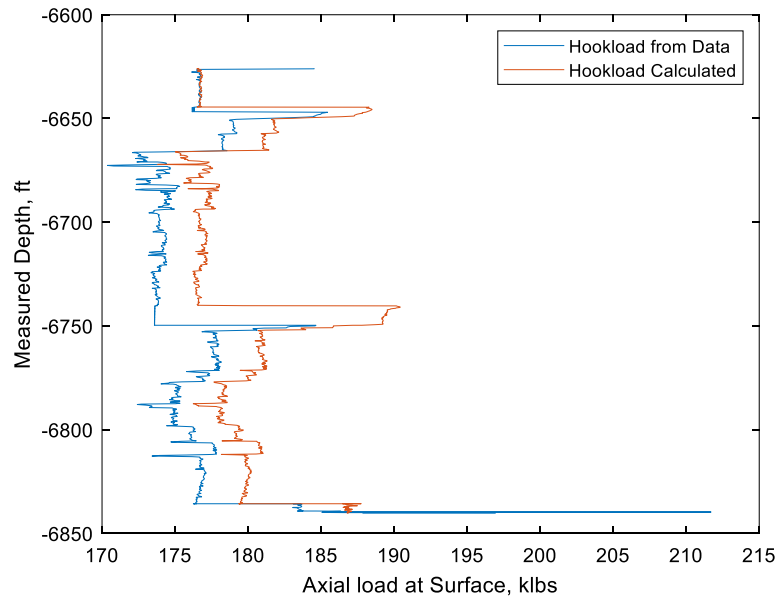


Figure 6. 27 Measured Hookload vs Calculated Hookload

From Figure 6.29, it can be seen that an increase in weight on bit led to decrease in hookload from both data and simulated, however, a decrease in weight on bit led to simultaneous increase in hookload.

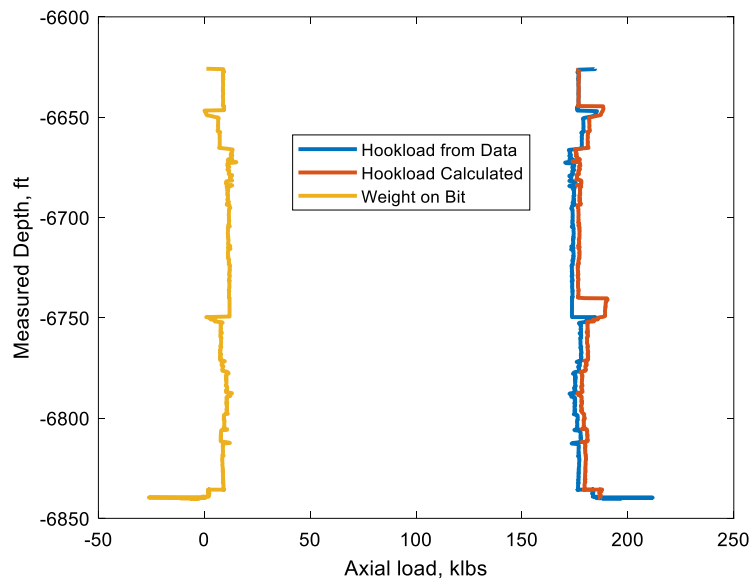


Figure 6. 28 Impact on Weight on Bit on Hook load during Simulation

The weight on bit and surface torque on the system were inputs into the system and torque per element and force per element were calculated for axial loading and here are the results.

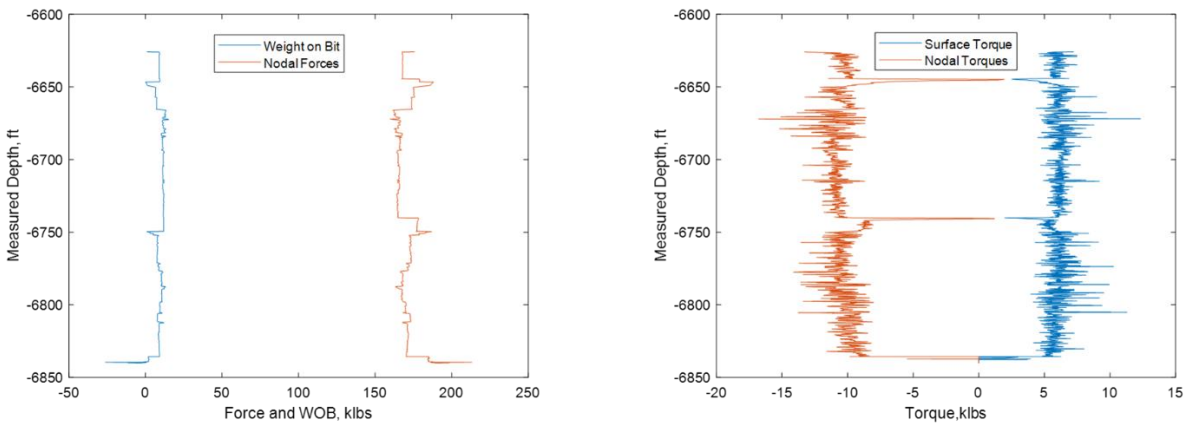


Figure 6. 29 Forces and Torques in Axial Nodes

Another parameter worthy of note is the rate of penetration. This is the ROP for the axial direction.

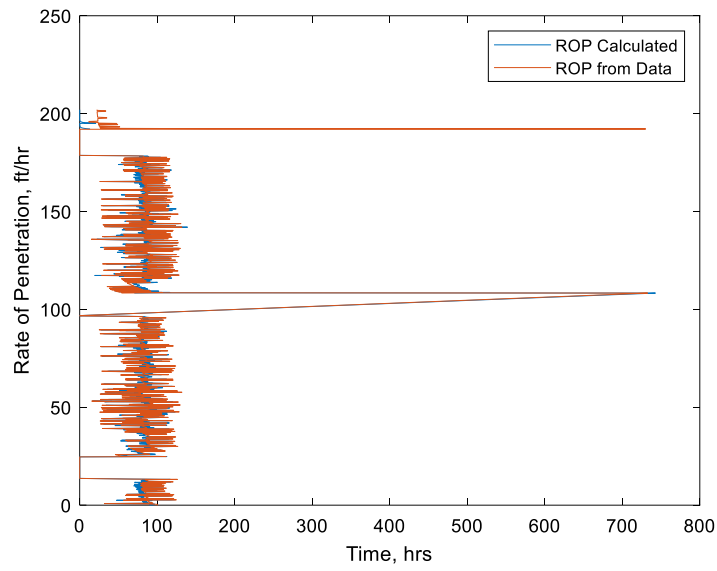


Figure 6. 30 ROP Calculated vs ROP Data

A look at the measured depth vs axial depth looks great as though the simulation was correct as shown in Figure 6.31.

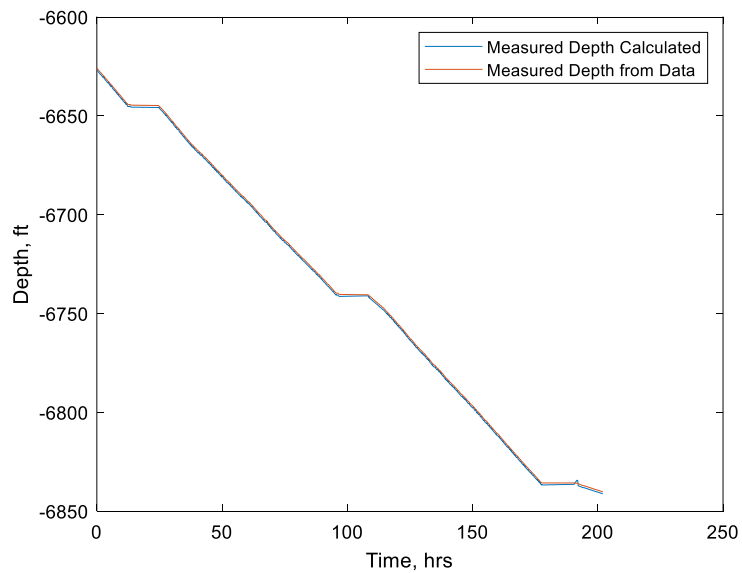


Figure 6. 31 Measured Depth from Data vs Axial Translation from Simulation

6.3 Downhole Measurement Validation

Based on the finite element modeling, downhole data can be calculated. In order to test the downhole measurement, some changes were made to back calculate surface torque based on changes to RPM while keeping weight on bit constant. The principle is to calculate the downhole torque by subtracting the summation of torques from the field surface torque but recalculate the surface torque and observe for an increase in surface torque when RPM is increased and lower surface torque when RPM is reduced.

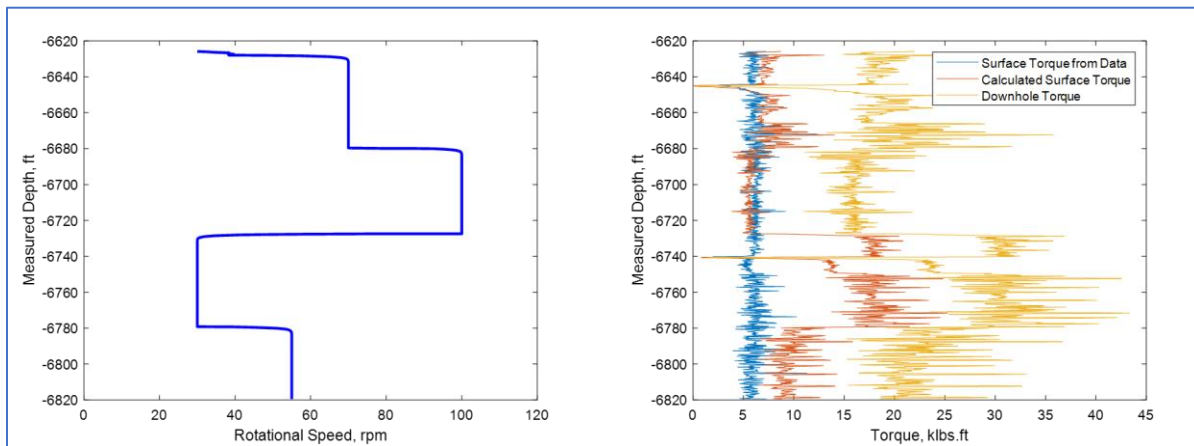


Figure 6. 32 Effect of Rotational Speed on Surface Torque

Based on the results, the simulation obtains surface torque equal to the torque from the field data when the RPM is continuously increased but at depths when the RPM is reduced drastically, the simulated surface torque varies from the field data significantly. One reason could be the fact that the surface RPM might not effectively affect all the components of the drill string as energy is lost along the string due to frictional loss and vibrations.

6.3.1 CCS Measurement

The data containing actual CCS values starts at 10,207.19 ft. Many factors affect the accuracy of the confined compressive strength based on findings from finite element model. The common thought would be an increase in rate of penetration would lead to lower CCS meaning the rock is easier to break into but on the contrary that fact may not be true all the time as a higher mud weight could also make the penetration faster if operation limits are not exceeded. Figure 6.33 shows regions where the CCS calculated and the CCS from the field data tally but yet again so many other factors can influence this result. The efficiency of the drilling and the bit coefficient of static

friction are other factors that can affect how the simulation CCS compares to the CCS from the field. Since, penetration rate plays a major part in the calculation done, therefore, massive variations in ROP will greatly affect the CCS values calculated hence the large variations shown in the plot.

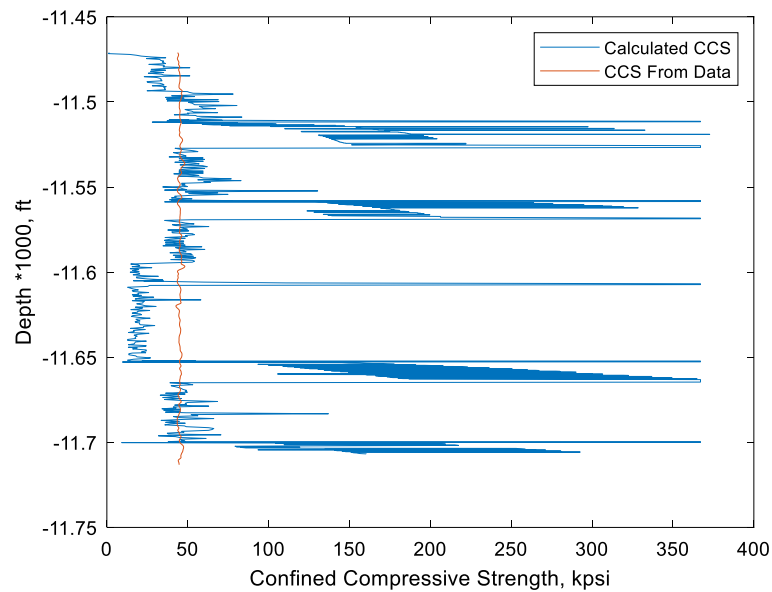


Figure 6.33 Calculated CCS vs CCS from Data

The mechanical specific energy is another parameter being monitored since it begins to inform the amount of energy needed for drilling and it prompts the intuition that energy has been lost across the drill string. As expected, MSE calculated responds similar to CCS because the MSE is part of the energy needed to break through the formation. CCS of higher values will require higher MSE to breakthrough. It all depends on the other factors that affect the SSC estimation.

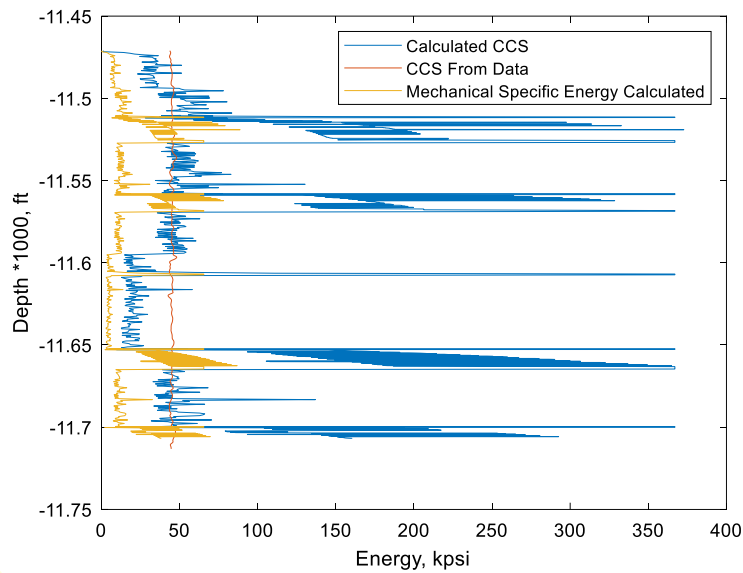


Figure 6. 34 MSE vs CCS vs Depth

6.4 Drilling Forecasting Validation

The key variables in forecasting are predicting the right inclination and azimuth. However, the input to Equation 5.98 and Equation 5.99 show that the resultant forces play an important role in calculating the next inclination and azimuth. The azimuthal changes in the original data as shown in Figure 6.35 are quite minimal but the inclination changes are significant.

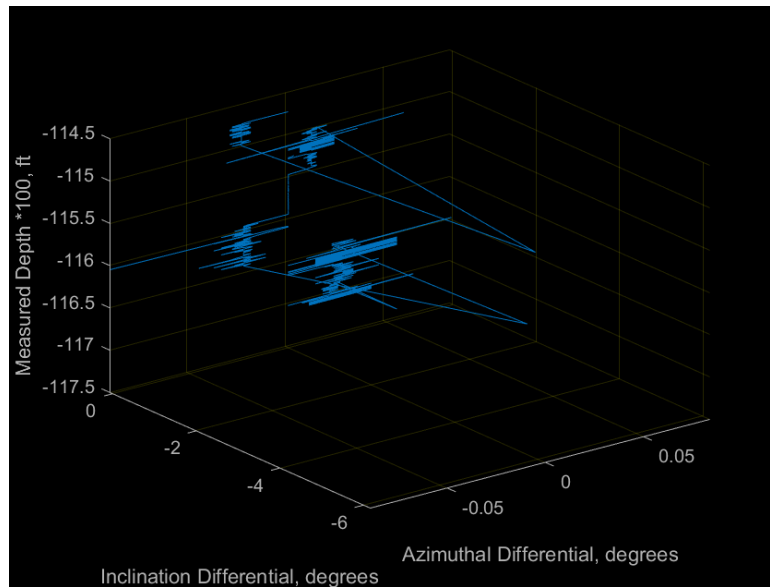


Figure 6. 35 Plot of Azimuth Differential vs Inclination Differential

Using the same data as was used in the CCS validation, the forces in the X, Y, and Z directions are investigated as shown in Figure 6.36. These forces can be better visualized when compared to the input weight on bit, Figure 6.37, which in this case was placed with a control system to ensure the CCS validation was as close as possible to the log CCS values.

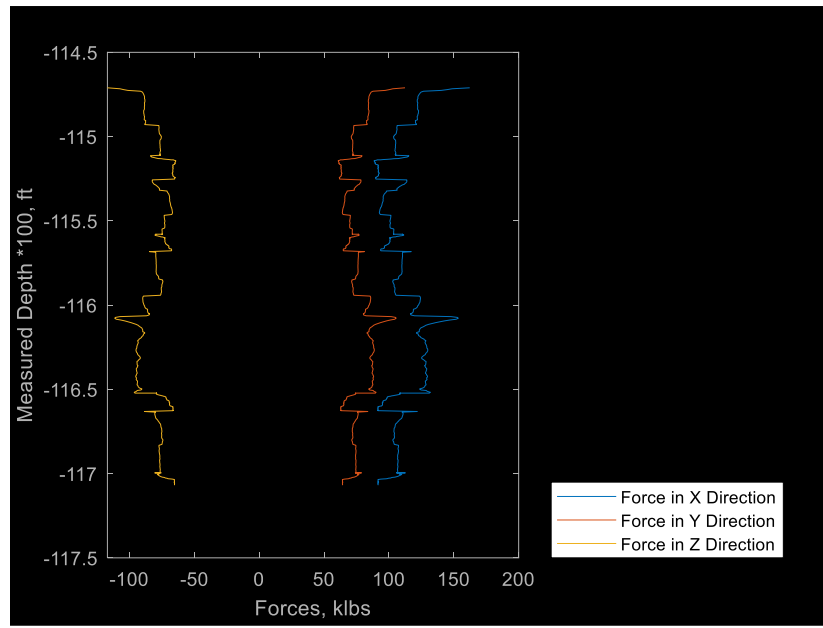


Figure 6. 36 Forces in X, Y, and Z Directions

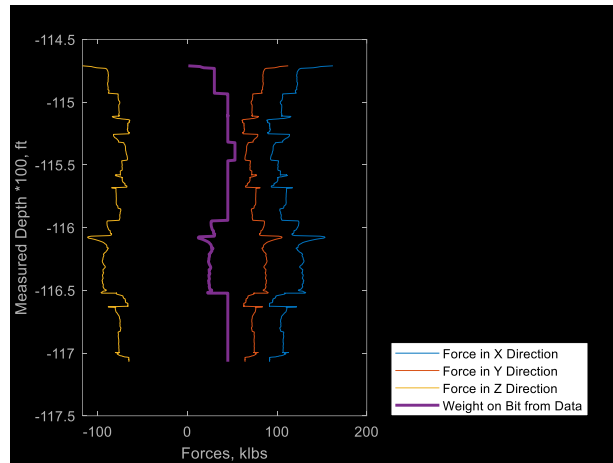


Figure 6. 37 Comparing XYZ Forces with WOB

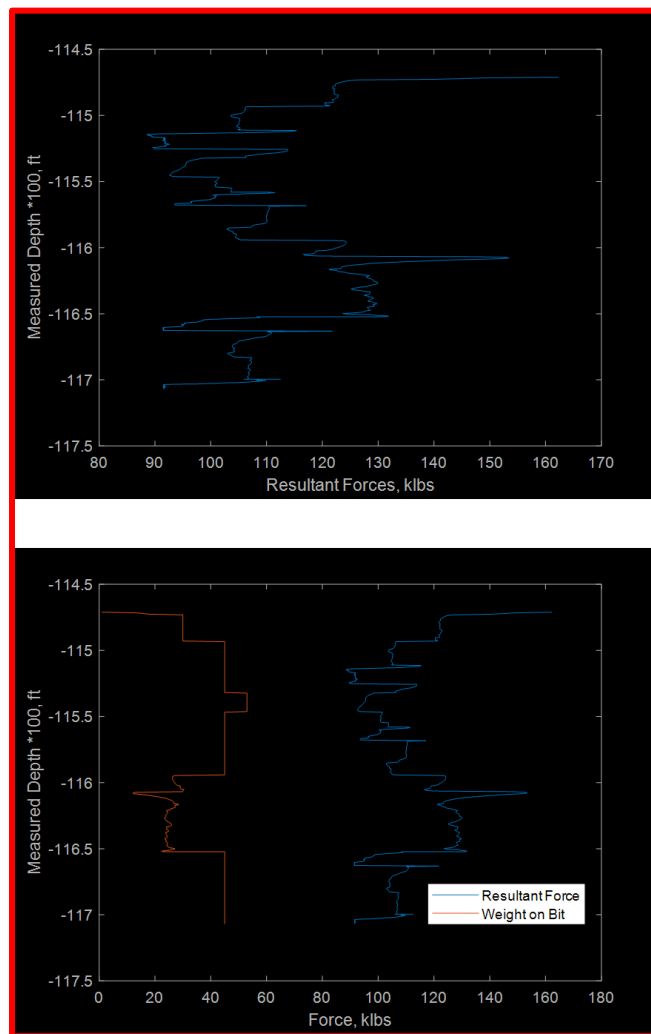


Figure 6. 38 Comparing the Resultant Force with WOB

Comparing the resultant force to the weight on bit shows that an increase in resultant force leads to a reduction in the resultant force. The explanation for this can be seen in the torque relationships.

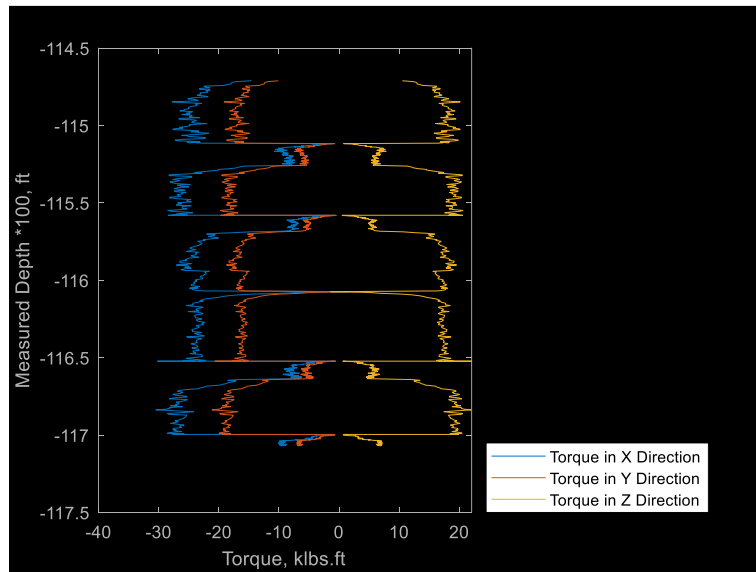


Figure 6. 39 Torques in X, Y, and Z Directions

In Figure 6.39, as torque is increased in the Z direction, there is a magnitude increase in torque in the X and Y directions. This can be appreciated when the surface torque is added into the plot.

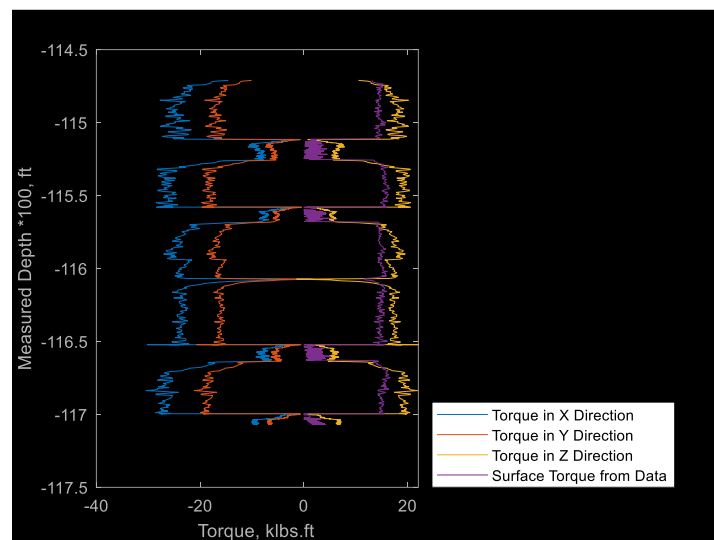


Figure 6. 40 Comparing XYZ Torques with Surface Torque

The first important point in Figure 6.40, is how surface torque is positive while the torques in the X and Y directions are negative. This indicates the phenomenon illustrated in Figure 5.5. String torques are the resistance to the applied surface torque. Since the Z direction torque tells a different story, it is better to visualize the comparison from the perspective of the resultant torque which is shown in Figure 6.41.

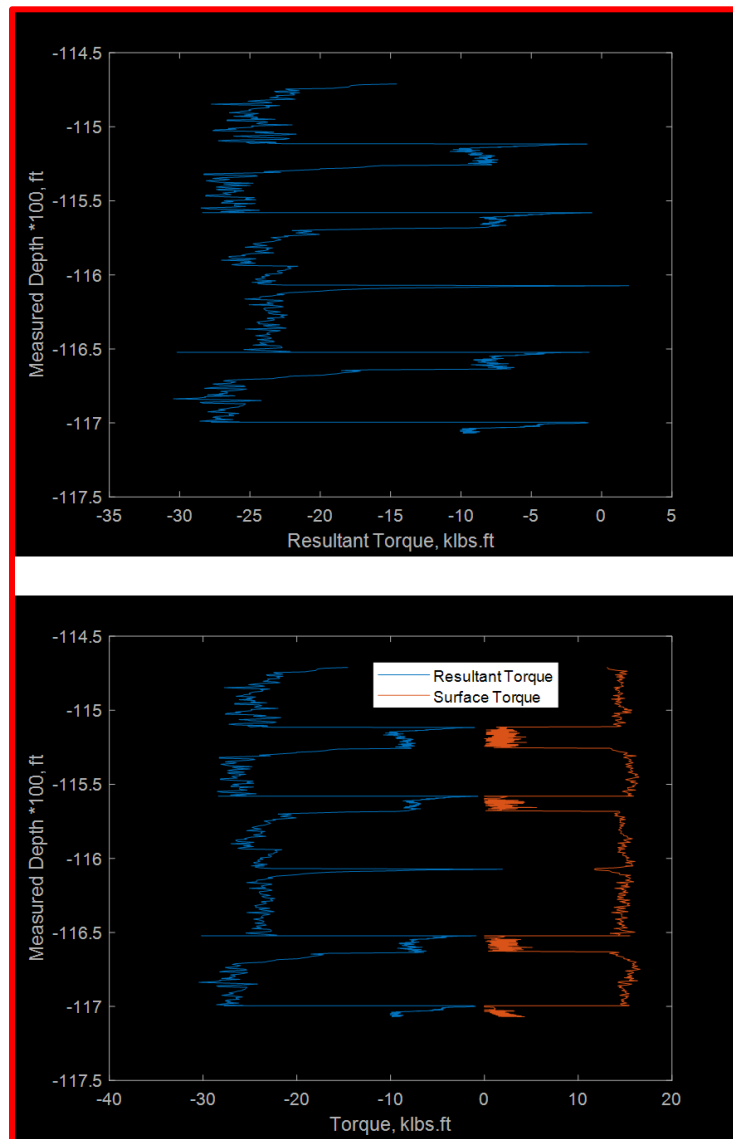


Figure 6. 41 Comparing Resultant Torque to Surface Torque

The decreases in surface torque are after breaking through a highly resistant rock. When the surface torque increases, there is a corresponding increase in the magnitude of the resultant string torque showing the resistance due to the formation of the intended rotation from the surface. The drill

ahead method will be correct if the right input is used. In this case, the prediction is 100 percent correct as shown in Figure 6.42 and Figure 6.43.

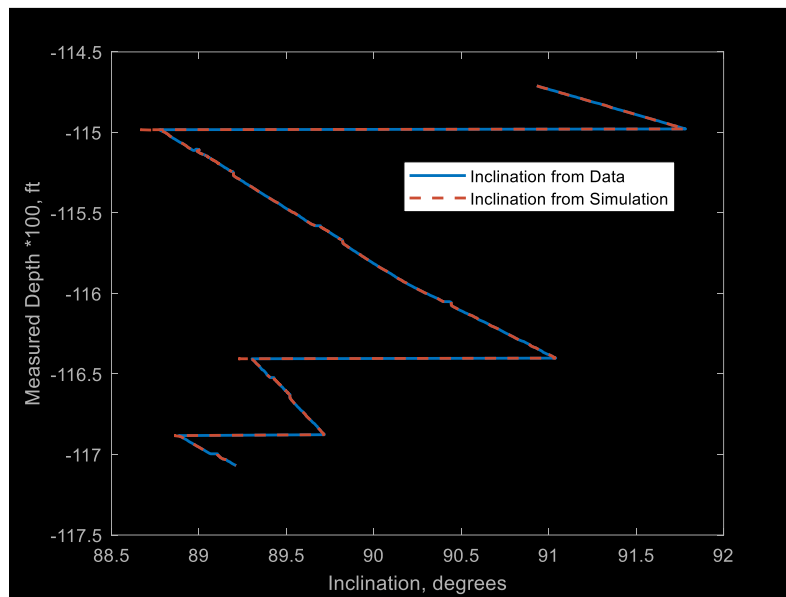


Figure 6. 42 Perfection of Inclination Predicted Compared with Field Data

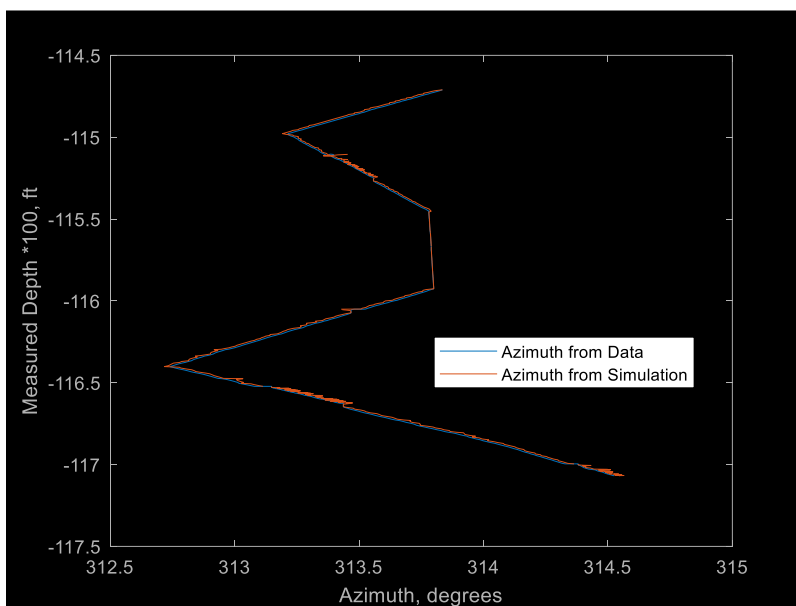


Figure 6. 43 Perfection of Azimuth Predicted Compared with Field Data

The azimuth prediction shows some minor differences but in general the prediction is correct.

6.5 Drilling Optimization Testing

Minimizing the mechanical specific energy (MSE) means reducing the amount of energy loss in the drilling process to unwanted events. More importantly, minimizing MSE means focusing the drilling energy on drilling through the rock in the specific direction to hit all targets.

$$\text{Since Area} = \frac{\pi * ID^2}{4} \quad \text{Equation 6. 25}$$

The MSE formula in Equation 5.113 can be rewritten as follows.

$$MSE = \frac{120 * Torque * RPM}{Area * ROP} + \frac{WOB}{Area} \quad \text{Equation 6. 26}$$

It is obvious that minimizing could either mean drilling with the minimum torque required, or minimum RPM required or with the minimum WOB required and lastly minimizing MSE could mean drilling with the maximum ROP required. These theories are based on their position on the equation. Just like with a car, human interaction exists at steering wheel and the gas pedal, also for drilling, making changes to the RPM (steering) and WOB (pedal) significantly affects the course of the drilling operations.

$$\text{Let } \frac{1}{Area} = K_a \quad \text{Equation 6. 27}$$

$$MSE = \left(\frac{120 * \pi * Torque * RPM}{ROP} * K_a \right) + (K_a * WOB) \quad \text{Equation 6. 28}$$

It is important at this point to specify the current units of the equation.

MSE is in psi

Torque is in lbs.ft

ROP is in $\frac{ft}{hr}$

WOB is in lbs

K_a is in $\frac{1}{in^2}$

RPM is in rpm (revolutions per minute)

Evaluating $\frac{RPM}{ROP}$ alone to get

$$\frac{RPM}{ROP} = \frac{rev}{min} * \frac{hr}{ft} * \frac{60*min}{1 hr} * \frac{1 ft}{12 inches} = \frac{5 rev}{in} = \frac{5 rev}{DOC} \quad \text{Equation 6. 29}$$

Where $DOC = \text{Depth of Cut in inches}$ Equation 6. 30

Rewriting Equation 6.28 and operating on a per rev basis to obtain a new expression for MSE.

$$MSE = \left((120 * \pi * Torque) * \frac{1}{DOC * (\frac{1}{5})} * K_a \right) + (K_a * WOB) \quad \text{Equation 6. 31}$$

$$MSE = \left(\frac{1884.9556 * Torque}{DOC} * K_a \right) + (K_a * WOB) \quad \text{Equation 6. 32}$$

Substituting for the values of axial Torque and WOB as indicated in Table 5.2

$$MSE = \left(\frac{1884.9556 * K_a}{DOC} * G * J * \frac{d^2 w}{dx^2} \right) + \left(K_a * G * J * \frac{d^3 w}{dx^3} \right) \quad \text{Equation 6. 33}$$

Simplifying the equation further gives the following.

$$MSE = K_a * G * J * \left(\left(\left(\frac{1884.9556}{DOC} \right) * \frac{d^2 w}{dx^2} \right) + \frac{d^3 w}{dx^3} \right) \quad \text{Equation 6. 34}$$

Based on the principle stated in Equation 5.114,

$$\frac{dMSE}{dx} = K_a * G * J * \frac{d}{dx} \left(\left(\left(\frac{1884.9556}{DOC} \right) * \frac{d^2 w}{dx^2} \right) + \frac{d^3 w}{dx^3} \right) \quad \text{Equation 6. 35}$$

In order to minimize MSE, the differential of MSE has to be equated to zero.

$$\frac{dMSE}{dx} = K_a * G * J * \frac{d}{dx} \left(\left(\left(\frac{1884.9556}{DOC} \right) * \frac{d^2 w}{dx^2} \right) + \frac{d^3 w}{dx^3} \right) = 0 \quad \text{Equation 6. 36}$$

Simplifying further gives the following expression.

$$\frac{d}{dx} \left(\left(\left(\frac{1884.9556}{DOC} \right) * \frac{d^2 w}{dx^2} \right) + \frac{d^3 w}{dx^3} \right) = 0 \quad \text{Equation 6. 37}$$

Consider the following boundary conditions in terms of the drilling process.

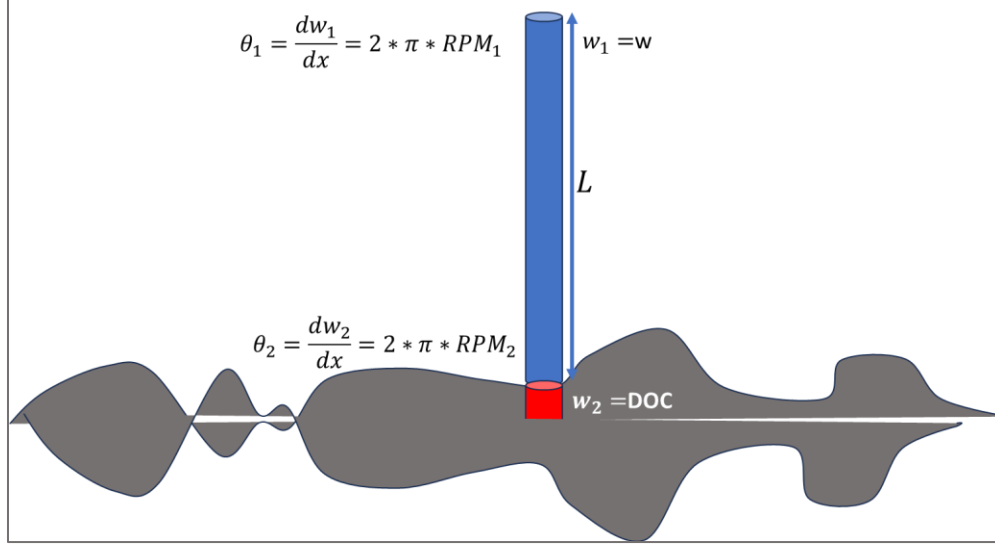


Figure 6.44 Boundary Conditions Illustration for MSE Minimization

Based on Figure 6.44, here are the boundary conditions for the business end of the MSE calculation.

$$w(0) = w_1 \quad \text{Equation 6.38}$$

$$w(L) = DOC \quad \text{Equation 6.39}$$

$$w'(0) = 2 * \pi * RPM_1 \quad \text{Equation 6.40}$$

$$w'(L) = 2 * \pi * \Delta RPM \quad \text{Equation 6.41}$$

After solving the differential equations with its four boundary conditions, the displacement at minimum MSE is obtained as the following.

$$w_{minMSE} = \left(\frac{23562Lw_1 - 25DOC^2 + 25DOC * w_1 * e^{-\left(\frac{47124L}{25DOC}\right)} + 23562L * w_1 * e^{-\left(\frac{47124L}{25DOC}\right)} + 25\pi DOC * L * RPM_1}{23562L - 25DOC + 25DOC * e^{-\left(\frac{47124L}{25DOC}\right)} + 23562L * e^{-\left(\frac{47124L}{25DOC}\right)}} \right) + \left(\frac{2x \left(23562DOC - 23562w_1 - 25\pi DOC * RPM_1 - 23562\pi L \Delta RPM + 23562L * RPM_1 \pi e^{-\left(\frac{47124L}{25DOC}\right)} + 25DOC * RPM_1 \pi e^{-\left(\frac{47124L}{25DOC}\right)} \right)}{23562L - 25DOC + 25DOC * e^{-\left(\frac{47124L}{25DOC}\right)} + 23562L * e^{-\left(\frac{47124L}{25DOC}\right)}} \right) - \left(\frac{25DOC e^{-\left(\frac{47124L}{25DOC}\right)} * (w_1 - DOC + \pi L * RPM_1 + \pi L * \Delta RPM)}{23562L - 25DOC + 25DOC * e^{-\left(\frac{47124L}{25DOC}\right)} + 23562L * e^{-\left(\frac{47124L}{25DOC}\right)}} \right) - \left(\frac{DOC * x^2 \left(23562DOC - 23562w_1 - 23562DOC e^{-\left(\frac{47124L}{25DOC}\right)} + 23562w_1 e^{-\left(\frac{47124L}{25DOC}\right)} - 25\pi DOC * REM_1 + 25\pi DOC * \Delta RPM - 47124\pi L \Delta RPM + 47124L * RPM_1 \pi e^{-\left(\frac{47124L}{25DOC}\right)} - 25 * DOC * \Delta RPM \pi e^{-\left(\frac{47124L}{25DOC}\right)} + 25DOC * RPM_1 \pi e^{-\left(\frac{45239L}{25DOC}\right)} \right)}{L \left(25e^{-\left(\frac{47124L}{25DOC}\right)} - 25 + 23562DOC * L + 23562 * DOC * L * e^{-\left(\frac{47124L}{25DOC}\right)} \right)} \right)$$

$$\text{Equation 6.42}$$

RPM_2 is the optimized rotary speed, $RPM_{optimized}$.

The generic form of w_{minMSE} is the following.

$$w_{minMSE} = \frac{C_1}{C_2} + \frac{C_3x}{C_2} - \frac{C_4e^{-C_5x}}{C_2} - \frac{C_6x^2}{C_7} \quad \text{Equation 6. 43}$$

However, the variable of interest is $RPM_{optimized}$. Making RPM_2 the subject of the formula in Equation 6.42 will help obtain an expression for RPM_2 which is also $RPM_{optimized}$.

$RPM_{optimized}$ will be key in resolving torsional vibration, also known as stick slip, thereby reducing torsional vibration energy loss.

$$\Delta RPM = \frac{AA}{BB} \quad \text{Equation 6. 44}$$

$$AA = w_{minMSE} - \left(\frac{23562Lw_1 - 25DOC^2 + 25DOC * w_1 * e^{-\left(\frac{47124L}{25DOC}\right)} + 23562L * w_1 * e^{-\left(\frac{47124L}{25DOC}\right)} + 25\pi DOC * L * RPM_1}{23562L - 25DOC + 25DOC * e^{-\left(\frac{47124L}{25DOC}\right)} + 23562L * e^{-\left(\frac{47124L}{25DOC}\right)}} \right) -$$

$$\left(\frac{2x \left(23562DOC - 23562w_1 - 25\pi DOC * RPM_1 + 23562L * RPM_1 \pi e^{-\left(\frac{47124L}{25DOC}\right)} + 25DOC * RPM_1 \pi e^{-\left(\frac{47124L}{25DOC}\right)} \right)}{23562L - 25DOC + 25DOC * e^{-\left(\frac{47124L}{25DOC}\right)} + 23562L * e^{-\left(\frac{47124L}{25DOC}\right)}} \right) +$$

$$\left(\frac{25DOC e^{-\left(\frac{47124L}{25DOC}\right)} * (w_1 - DOC + \pi L * RPM_1)}{23562L - 25DOC + 25DOC * e^{-\left(\frac{47124L}{25DOC}\right)} + 23562L * e^{-\left(\frac{47124L}{25DOC}\right)}} \right) +$$

$$\left(\frac{DOC * x^2 \left(23562DOC - 23562w_1 - 23562DOC e^{-\left(\frac{47124L}{25DOC}\right)} + 23562w_1 e^{-\left(\frac{47124L}{25DOC}\right)} - 25\pi DOC * REM_1 + 47124L * RPM_1 \pi e^{-\left(\frac{47124L}{25DOC}\right)} + 25DOC * RPM_1 \pi e^{-\left(\frac{45239L}{25DOC}\right)} \right)}{L \left(25e^{-\left(\frac{47124L}{25DOC}\right)} - 25 + 23562DOC * L + 23562 * DOC * L * e^{-\left(\frac{47124L}{25DOC}\right)} \right)} \right)$$

$$\text{Equation 6. 45}$$

$$BB = \left[\frac{25DOC * L * \pi}{23562L - 25DOC + 25DOC * e^{-\left(\frac{47124L}{25DOC}\right)} + 23562L * e^{-\left(\frac{47124L}{25DOC}\right)}} \right] -$$

$$\left[\frac{47124Lx\pi}{23562L - 25DOC + 25DOC * e^{-\left(\frac{47124L}{25DOC}\right)} + 23562L * e^{-\left(\frac{47124L}{25DOC}\right)}} \right] +$$

$$\left[\frac{DOCx^2 \left(47124\pi L - 25\pi DOC + 25DOC\pi e^{-\left(\frac{47124L}{25DOC}\right)} \right)}{L \left(25DOC^2 e^{-\left(\frac{47124L}{25DOC}\right)} - 25DOC^2 + 23562DOC*L + 23562*DOC*L*e^{-\left(\frac{47124L}{25DOC}\right)} \right)} \right] - \left[\frac{25DOC*L\pi e^{-\left(\frac{47124L}{25DOC}\right)}}{23562L - 25DOC + 25DOC e^{-\left(\frac{47124L}{25DOC}\right)} + 23562Le^{-\left(\frac{47124L}{25DOC}\right)}} \right]$$

Equation 6. 46

$$RPM_{Optimized} = RPM_1 + \Delta RPM$$

Equation 6. 47

To use the $RPM_{Optimized}$ for the purpose of minimizing the MSE, it has to be tested to have minimal properties. For a 6 ft component with initial RPM of 60 rpm and 10 ft displacement from origin will have an optimized RPM profile as follows.

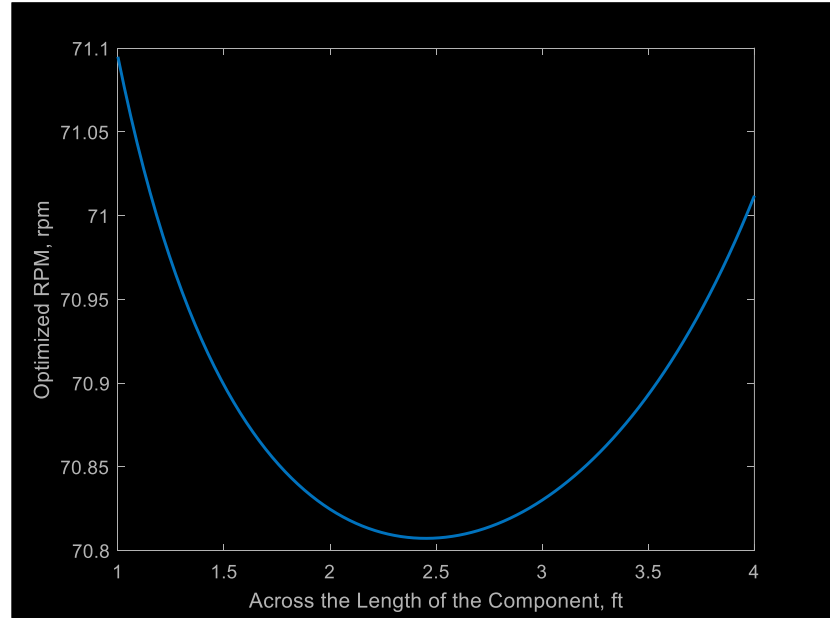


Figure 6. 45 Optimized RPM vs Length of BHA Component

For varying values of depth of cut, here are the corresponding optimized RPM.

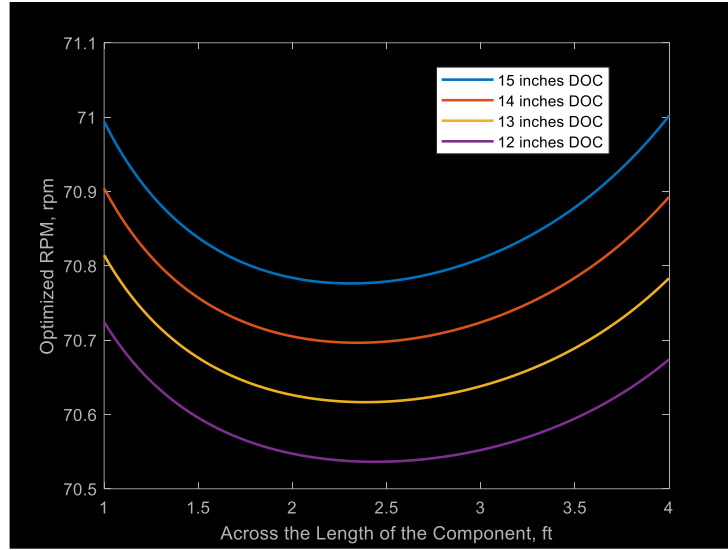


Figure 6. 46 Depth of Cut Effect on RPM

6.6 Identifying Minimum MSE Using Particle Swarm Optimization PSO

Stick slip can be accounted for in the optimized RPM by giving penalties to the objective function results when stick slip severity is high for a particular instance. Here is the severity table.

Lateral Acc		Lateral RMS Acc		Stick-Slip	
(g's)	Severity Level	(g's)	Severity Level	(-)	Severity Level
0-15	Normal	0-2.5	Normal	0-0.5	Low
15-35	Moderate			0.5-1	Moderate
35+	Severe	2.5+	Severe	1+	Severe

Figure 6. 47 Drilling Vibration Severity Snapshot (Dushaishi, Nygaard, Hoel, Andersen, & Hellvik, 2015)

A stick slip index from 0.5 and above has potential to increase the MSE thereby reducing energy available for actual drilling.

$$\text{Downhole Stick Slip Index, DSSI,} = \frac{\max(\text{RPM}) - \min(\text{RPM})}{2 * \text{mean}(\text{RPM})} \quad (\text{Etaje, 2018}) \quad \text{Equation 6. 48}$$

When $\text{DSSI} > 0.5$, the objective function, $\text{RPM}_{\text{Optimized}} = \text{RPM}_{\text{Optimized}} + 20$;

When $\text{DSSI} > 1$, the objective function, $\text{RPM}_{\text{Optimized}} = \text{RPM}_{\text{Optimized}} + 30$.

The challenge is to get data points that fit the exact criteria. A further understanding of the severity is needed which is shown in Figure 6.48.

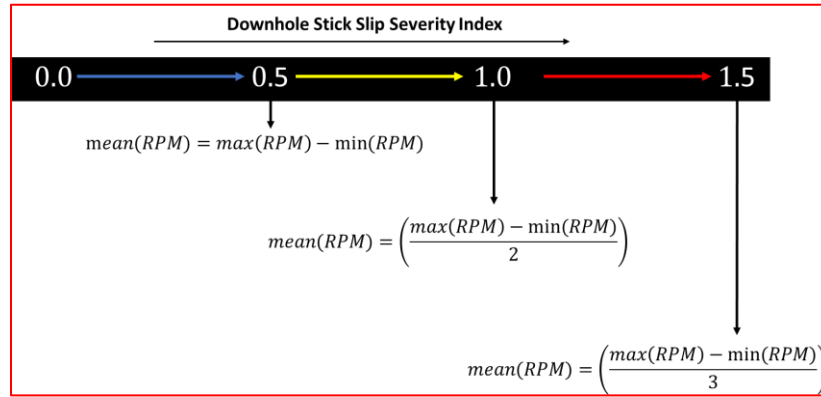


Figure 6. 48 Formula for Mean of Datapoints Per Stick Slip Severity

With the formula for mean RPM known, it is possible to generate the data points that reflect each of these regions of stick slip severity. Table 6.1 shows all the potential values of RPM combination for stick slip at severity level 0.5, 1.0 and 1.5. Multiplying each value by same number gives high RPM replica of the same scenario.

Table 6. 1 Simulation Baseline Downhole Stick Slip Severity

RPM for Low DSSI Level	RPM for Moderate DSSI Level	RPM for Severe DSSI Level
10	10	10
10	5	2
10	4	1
10	2	7
10	9	2
9	3	3
10	3	1
10	7	1
10	1	2
1	1	1

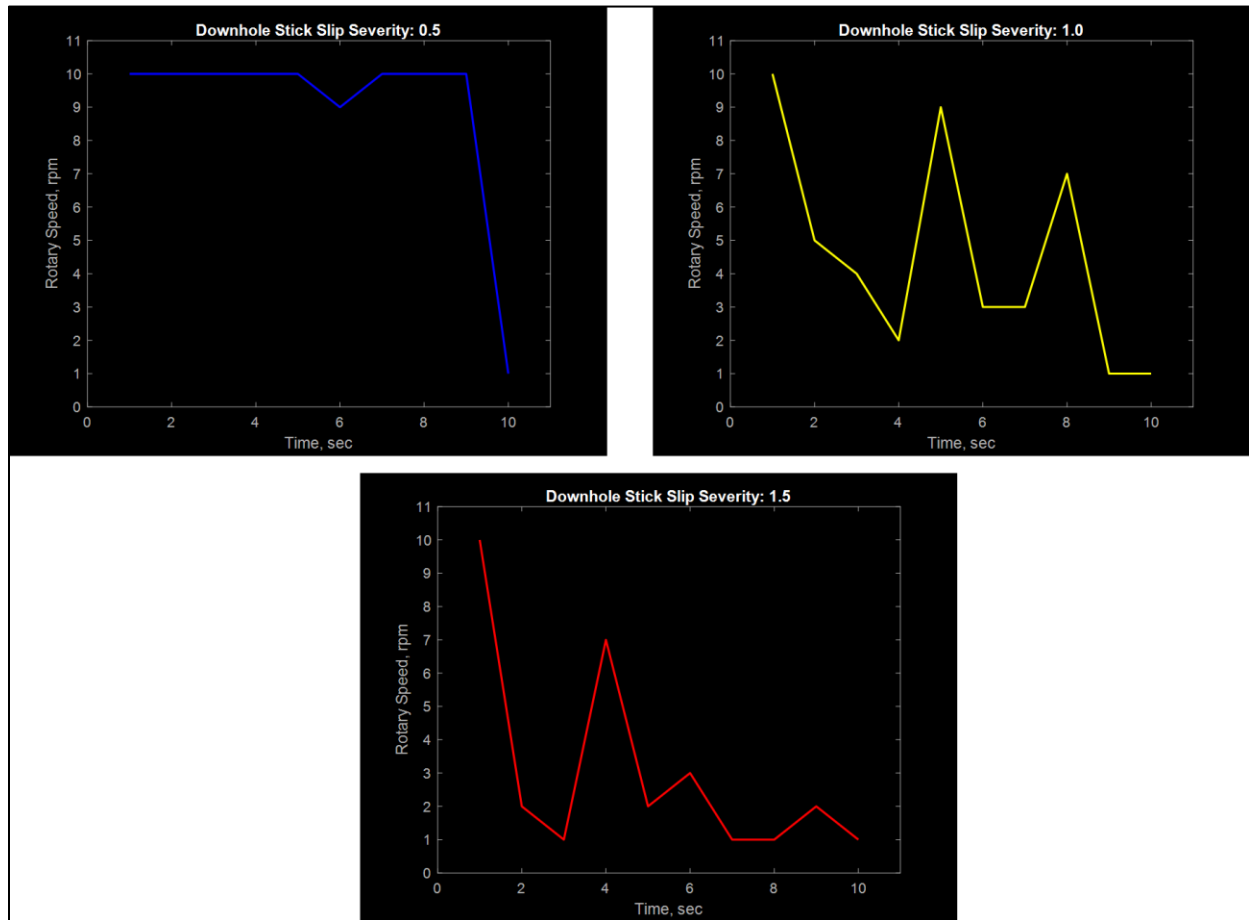


Figure 6. 49 Behavior of Stick Slip Severity at 0.5, 1.0 and 1.5 Levels

These levels have been programmed to end at the same RPM. Plugging them all into the RPM objective function would give the following results.

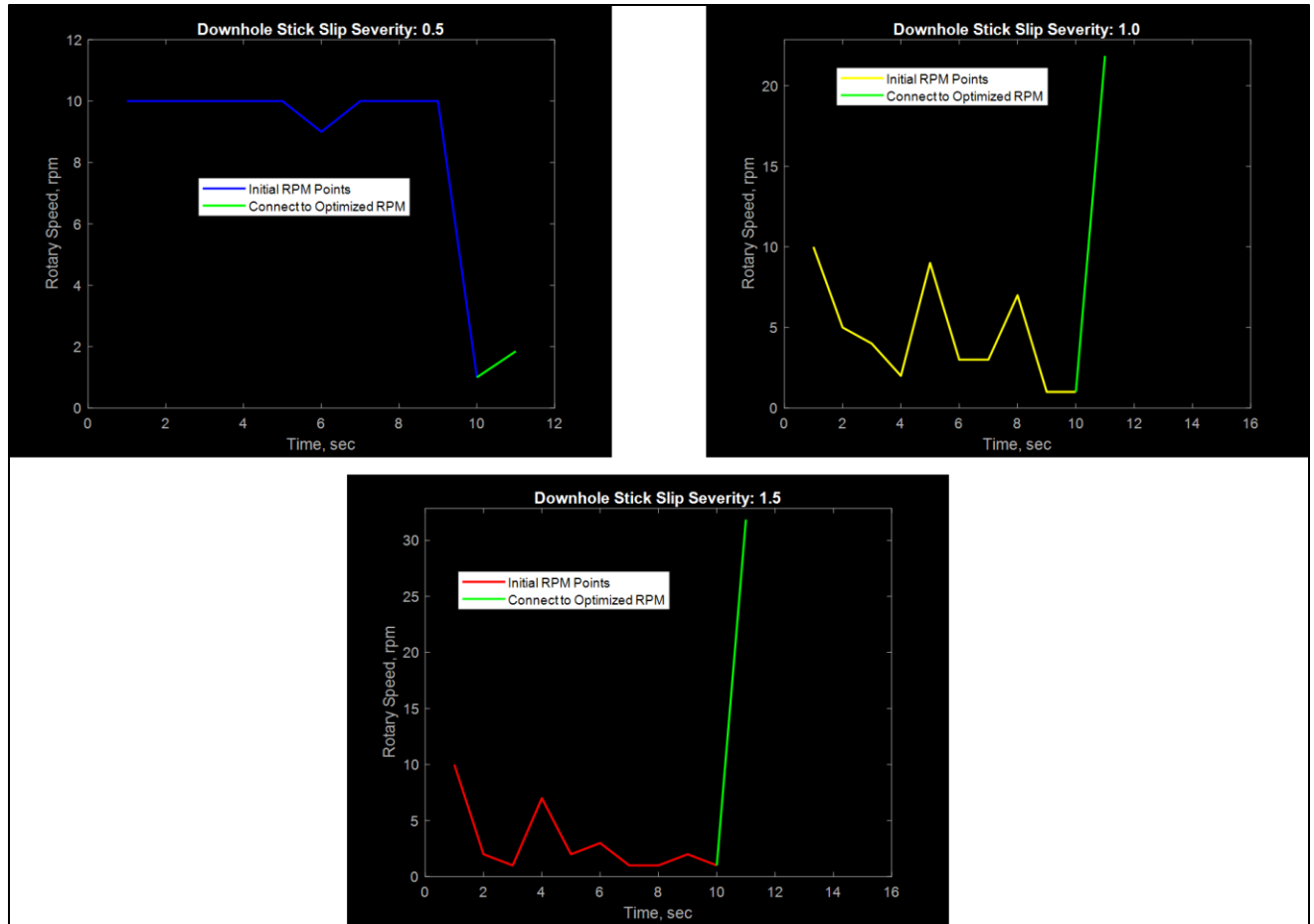


Figure 6. 50 Effect of Penalties in the Objective Function on Optimized RPM

The goal of Figure 6.50 is to show how the objective function penalizes an input group of RPM data corresponding to moderate or severe stick slip. That step automatically disqualifies that minimum from being the global minimum. Another study would be to vary the depth of cut and view the impact low depth of cut and high depth of cut.

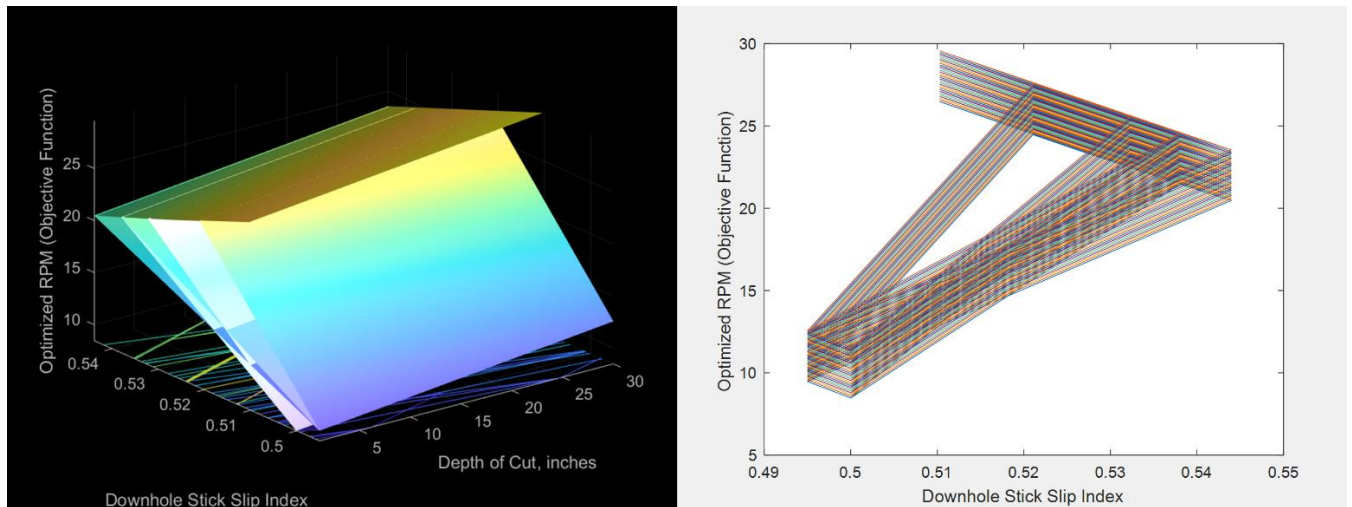


Figure 6. 51 Surface Plot of Optimized RPM and Stick Slip Index

The important value is to ensure that the result of the objective function does not lead to optimized RPM that harbors high stick slip index as shown in Figure 6.52 where uniform RPM data is inputted into the objective function. Even though the results show higher values as input RPM increases, a better interpretation would be to look at the data from previous time combined with the input RPM.

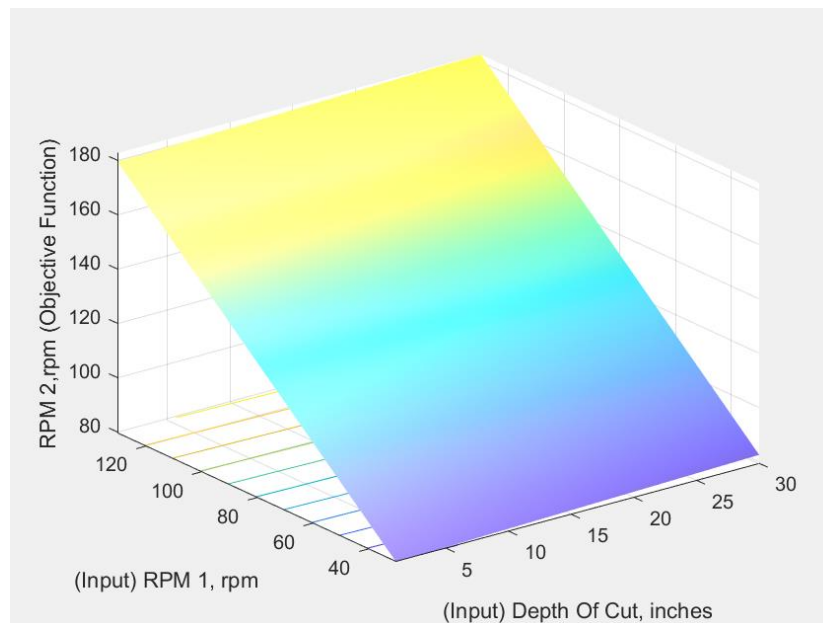


Figure 6. 52 Increasing Optimized RPM with Increasing RPM Input

In Figure 6.53, there is a sharp change in color as data moves from one level of stick slip severity to the next signifying the effect of the penalties added.

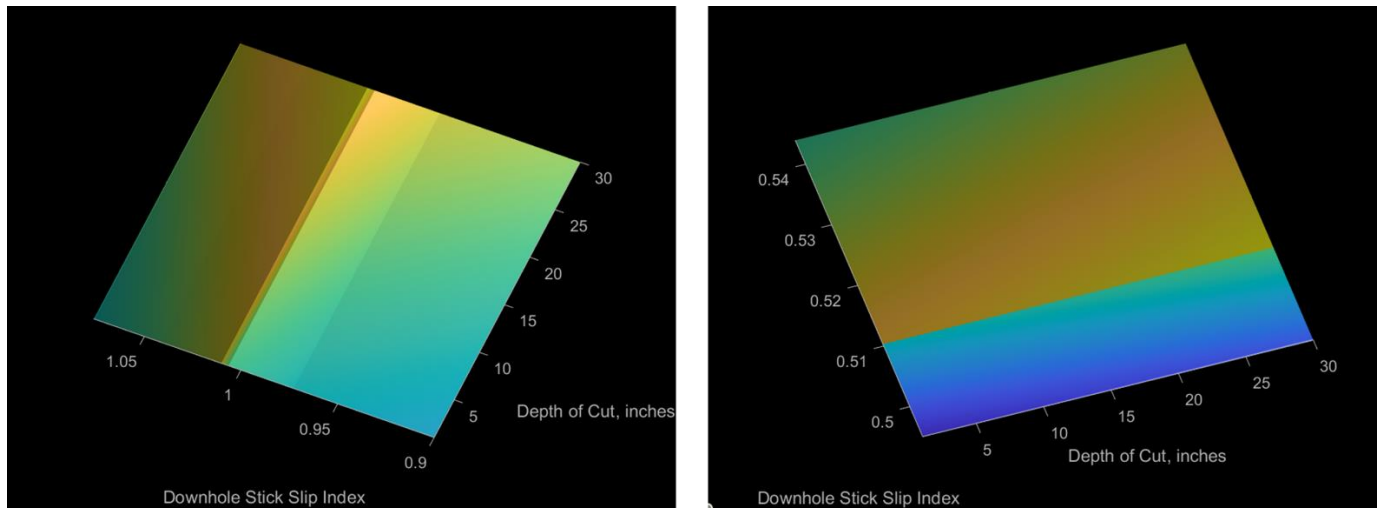


Figure 6. 53 Effect of Depth of Cut on DSSI

The PSO loops through the optimized RPM objective function as shown in

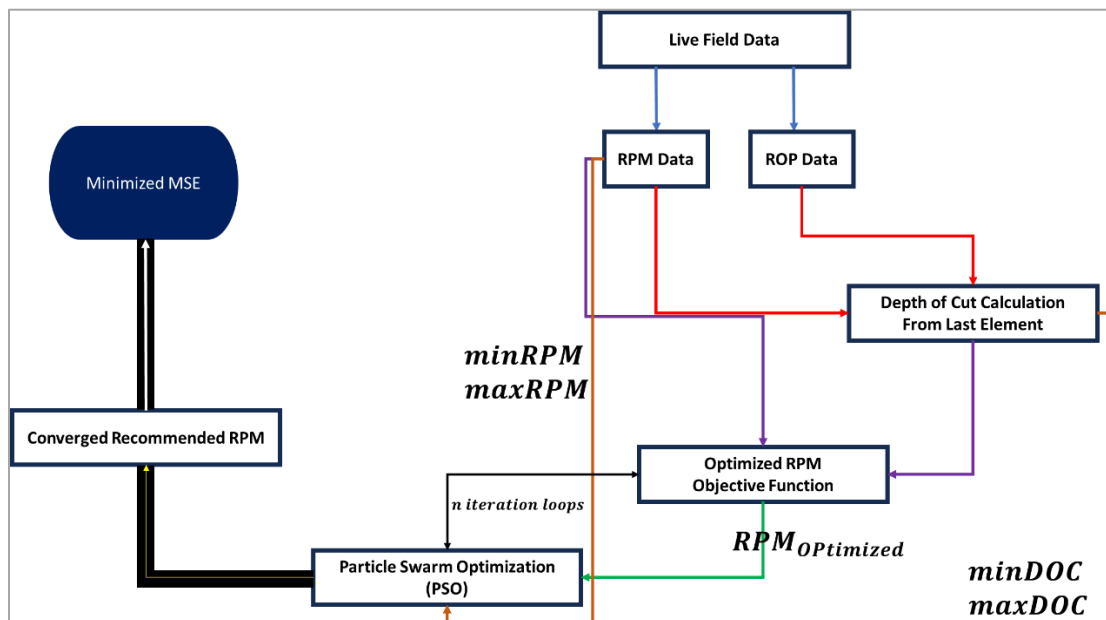


Figure 6. 54 Looping the PSO and the Optimized RPM Objective Function

The first step is to choose the number of particles, N , needed in the swarm to find the global minimum. Each particle represents a solution to the given problem. In this thesis, the problem is to find the minimum optimized RPM for a given set of drilling data. The current velocity, \vec{V}_i^t , of each particle is then multiplied by an inertia weight \vec{w} which is used to maintain the current direction. \vec{w} has values between 0.2 and 0.9. It is used to tune exploration and exploitation positions of the particle solution. The PSO algorithm in each loop updates the movement, direction, and speed of the current position of a particular particle using the next velocity vector \vec{V}_i^{t+1} . The next velocity vector \vec{V}_i^{t+1} depends on the current velocity, the tendency towards the personal best for that particle, \vec{P}_i^t , and the tendency towards the single global best (global minimum), \vec{G}_i^t . There is a need to specify maximum velocity V_{max} and maximum iteration Max_Iter . Each particle will go through Max_Iter iterations. Here is the pseudo code.

```

Initialize the controlling parameters ( $N$ ,  $c1$ ,  $c2$ ,  $Wmin$ ,  $Wmax$ ,  $Vmax$ , and  $MaxIter$ )
Initialize the population of  $N$  particles
do
  for each particle
    calculate the objective of the particle
    Update PBEST if required
    Update GBEST if required
  end for

  Update the inertia weight
  for each particle
    Update the velocity ( $V$ )
    Update the position ( $X$ )
  end for

while the end condition is not satisfied

Return GBEST as the best estimation of the global optimum

```

$$\vec{X}_i^{t+1} = \vec{X}_i^t + \vec{V}_i^{t+1}$$

$$\vec{V}_i^{t+1} = w\vec{V}_i^t + c_1r_1(\vec{P}_i^t - \vec{X}_i^t) + c_2r_2(\vec{G}_i^t - \vec{X}_i^t)$$

Figure 6. 55 Pseudo Code for Particle Swarm Optimization

With this process completed, the MSE optimized and minimized can be calculated.

$$MSE_{minimized} = \frac{120 * Torque * RPM_{recommended}}{Area * ROP} + \frac{WOB}{Area} \quad \text{Equation 6. 49}$$

This process was run on a data with MWD CCS data. It is important to have the CCS data for validation. The recommended RPM from the optimization process was used to recalculate MSE.

The results shown from Figure 6.56 to Figure 6.59 clearly indicate that the recommended RPM is lowered and steady which is an early sign for low stick slip index. The ROP based on the optimization is calculated by keeping depth of cut constant and calculating ROP from the recommended RPM and there are changes in ROP when compared to ROP from the data however, the resulting MSE is greater than MSE from the data.

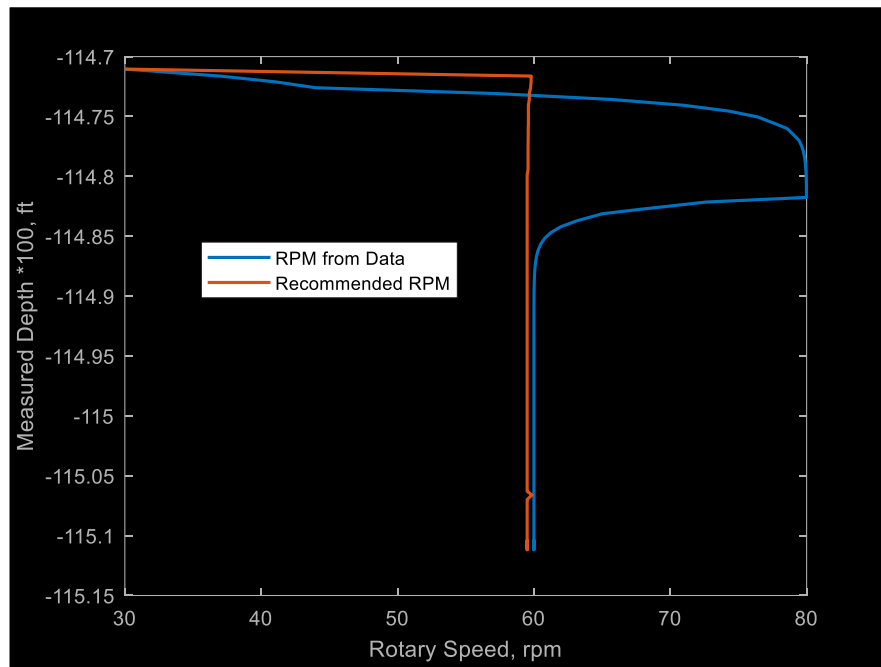


Figure 6. 56 Comparing RPM from Data to RPM Recommended by the Optimization Process

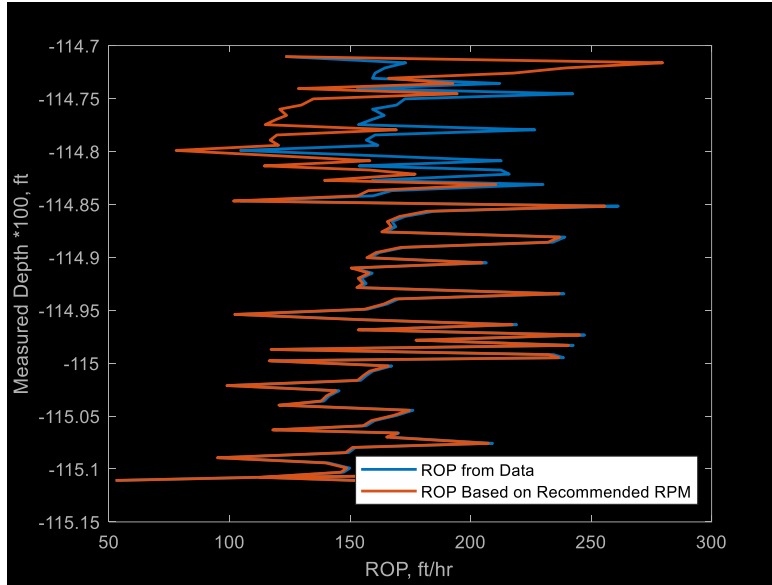


Figure 6. 57 Comparing ROP from Data to ROP from Optimization Process

The MSE from the optimization is greater even though minimization was the goal. On a case-by-case basis, it will be greater or lower depending on how much safe energy is used or unused. The MSE is not entirely based on the global minimum if that location is found to have higher stick slip severity. That means the lowest local minimum would be chosen by the PSO to achieve safe drilling.

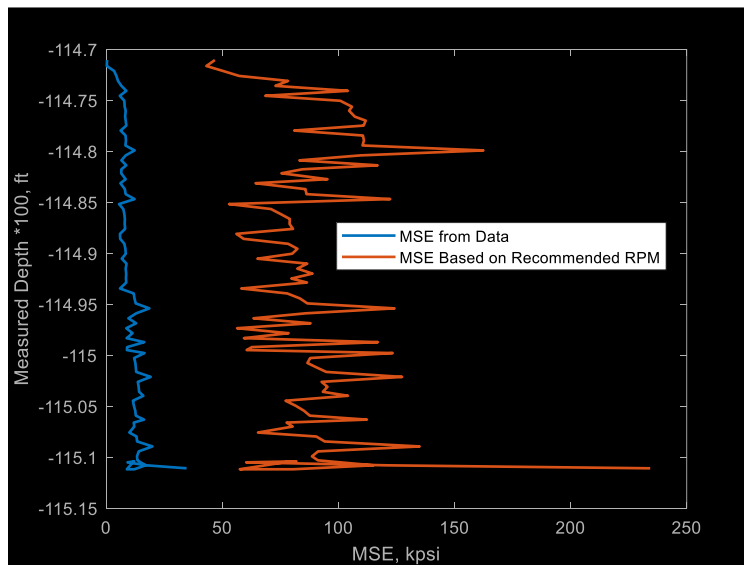


Figure 6. 58 Comparing MSE from Data and MSE from Optimization Process

The big achievement is the reduction in downhole stick slip index. There is a 28 percent reduction in downhole stick slip index.

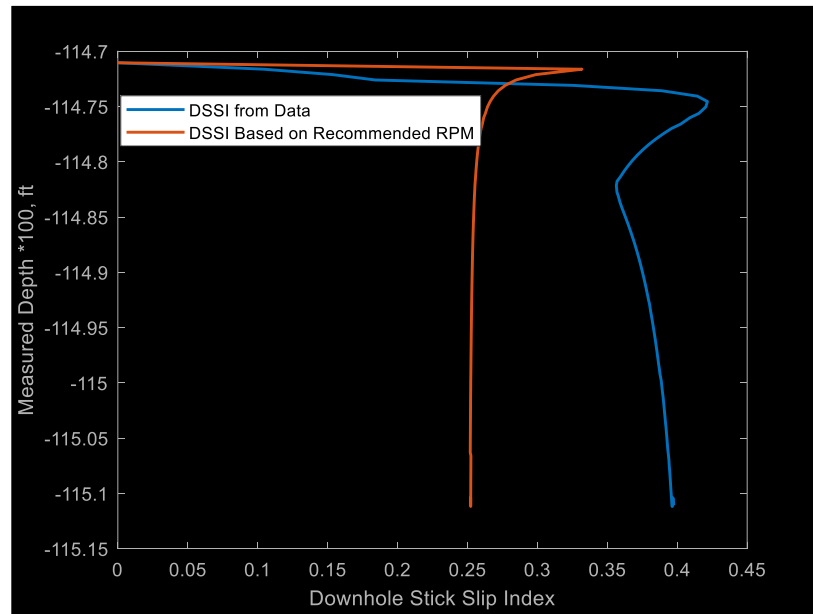


Figure 6. 59 Proof of Reduction in Stick Slip Vibration

6.7 Conclusion

It can be concluded that the MSE minimization process should rather be called MSE optimization process as the decision to raise or lower MSE should be based on the data supplied to the particle swarm optimizer since the objective function is built with constraints to lower drill string vibrations. When tested with field data, the objective function and optimizer built in this research was found to increase MSE but lower the downhole stick slip index by 28 percent. The downhole stick slip index was below 0.5. A total of 20 functions were created to actualize the results in this chapter as shown in Figure 6.60



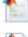
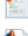











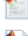


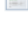

<input type="checkbox"/> Name	Date modified	Type	Size
 AxialLoadSolution	2023-07-30 12:55 AM	MATLAB Code	6 KB
 AxialTorsionSolution	2023-07-30 1:10 AM	MATLAB Code	6 KB
 ConvertStiffnessMassDamping	2023-07-31 5:23 PM	MATLAB Code	8 KB
 DiscretizeBHA	2023-08-02 7:51 AM	MATLAB Code	3 KB
 ElementFEMsimulation	2023-08-02 6:55 AM	MATLAB Code	5 KB
 findAzi	2023-08-01 10:50 AM	MATLAB Code	1 KB
 findDataPoints	2023-08-09 9:13 PM	MATLAB Code	1 KB
 findIncAzi	2023-08-01 10:45 AM	MATLAB Code	2 KB
 findMSE	2023-08-11 8:10 AM	MATLAB Code	1 KB
 findNET	2023-08-01 9:39 PM	MATLAB Code	4 KB
 findTurn	2023-08-01 10:52 AM	MATLAB Code	1 KB
 LandscapeforMSE	2023-08-10 4:33 AM	MATLAB Code	1 KB
 ObjectiveFunctionForMSEMinimization	2023-08-10 11:00 AM	MATLAB Code	3 KB
 PSOmse	2023-08-10 12:42 PM	MATLAB Code	3 KB
 RecommendRPM	2023-08-10 10:59 PM	MATLAB Code	3 KB
 StickSlip	2023-08-11 9:27 AM	MATLAB Code	1 KB
 TimeSolutionAxialLoad	2023-08-08 4:19 AM	MATLAB Code	2 KB
 TimeSolutionAxialTorsion	2023-08-04 10:00 AM	MATLAB Code	2 KB
 TimeSolutionTransverse	2023-08-04 9:59 AM	MATLAB Code	3 KB
 TransverseSolution	2023-08-08 4:25 AM	MATLAB Code	12 KB

Figure 6. 60 List of Functions Needed for Simulation and Testing

Chapter 7 Conclusion

There is no gap in importance between drilling simulation and drilling field trials as both processes co-exist to ensure new technologies are tested and validated before being launched as a new process or best practice. Figure 7.1 shows a high level of interactions between field trials and drilling simulation. In summary, drilling simulation, a set of physic-based models run through time or depth steps to mirror events in the drilling rig, is the backbone of all field testing of technologies or procedures. If a model has been validated using drilling simulation, the risk of wasted field trial is lowered significantly. This is why the formulation of models that make up drilling simulation is key and this what this thesis has focused on.

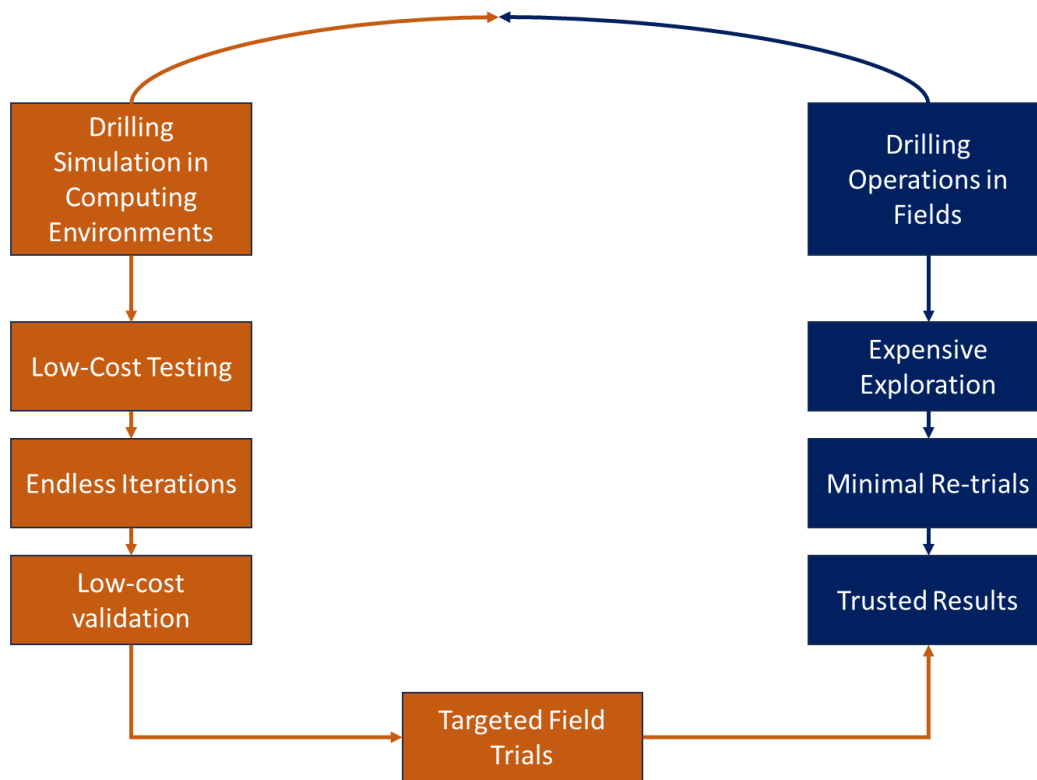


Figure 7. 1 Relations Between Drilling Simulation and Drilling Field Testing

7.1 A Review of Drilling Simulation

Based on the experience of conducting the research in this thesis, a better understanding of drilling simulation can be explained. The big question to answer is “why are things the way they are?” The only way to answer such a question is to first define the governing equations that surround the

scenario to be understood. When the equations are solved, the solution can then be tested to ensure the assumptions made were accurate and sufficient to replicate actual field scenarios.

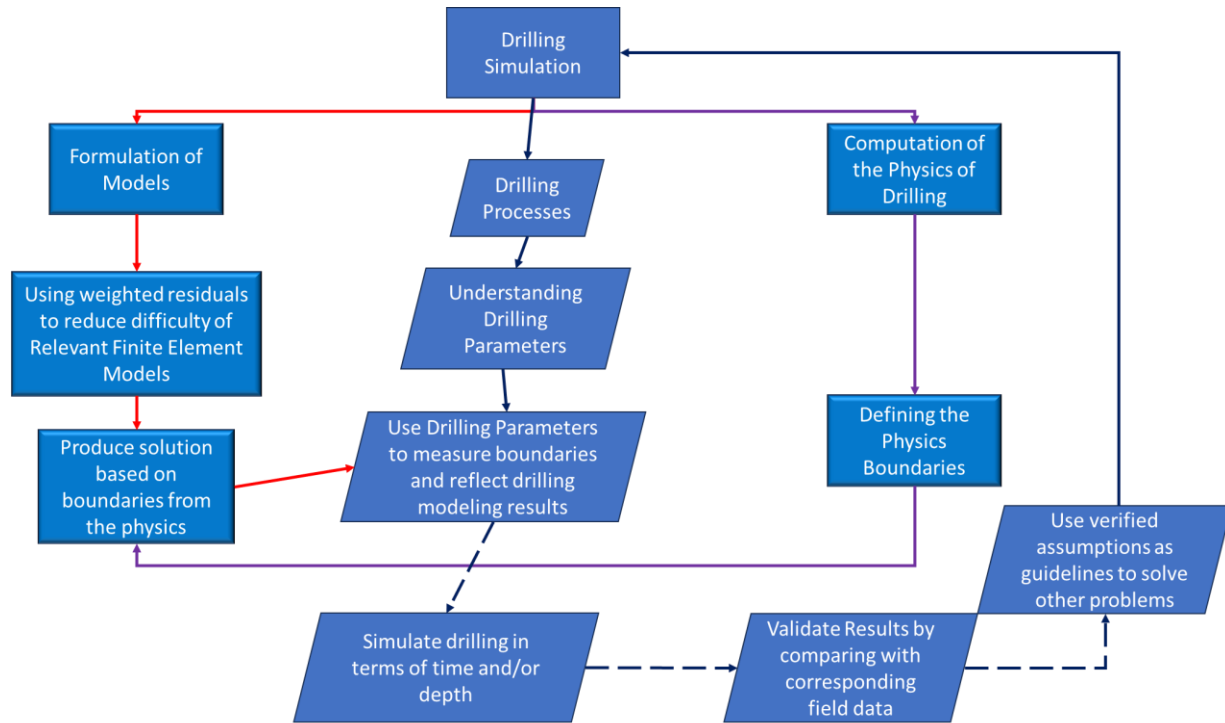


Figure 7. 2 An Overview of Drilling Simulation

Figure 7.2 gives the overview of the drilling process and how computation and modeling play a part in achieving validated results. The boundaries are set based on proven beam deflection equations. This is important to ensure reasonable boundaries are set. The four processes in need of boundaries in this thesis are axial loading, axial torsion, transverse bending in the Y direction and transverse bending in the Z direction.

7.2 Key Activities of the Research

20 functions were used to simulate the processes described in this research. Finite element formulation of space models linked with time-based models have been developed for the 2-node system in X (axial loading and axial torsion), Y (transverse bending of Z), and Z (transverse bending of Y) directions. Laplace transform was used to solve the time based partial differential equation paving way for the development of velocity, acceleration, force, and torque equations. Drill ahead modeling using build and walk relation to resultant forces was validated. Stick slip mitigation using the optimized RPM objective function was used to optimize the mechanical

efficiency of drilling. 28 percent reduction in stick slip was achieved during the test. Several plots of drilling parameters were done to display results of optimization, modeling conditions, trajectory of the drill string, and vibration occurrence via stick slip. An expression of the optimized RPM was developed and simulated with field data. Confined compressive strength from the field data was compared with the CCS obtained from the simulation but there was no perfect match yet. Further runs of the simulation would show more lessons as to how to improve the results.

7.3 Expanding the Research

It is a known fact that the error of the finite element model reduces as the order of the element increases. This thesis focused on linear nodal system, a two-node system. This means each element has only two nodes. This is potentially the reason why Figure 6.8 to Figure 6.13 show the residuals having errors above 20 % even though the solution has less than 2 percent error. A higher order nodal system is needed. This thesis has laid the groundwork to build more nodes in each element of the drill string. For instance, for a 6-node system with 36 degrees of freedom, the elementary equation for the interpolation functions will have the following expression for the transverse Y direction.

$$w^e|_y = \sum_{j=1}^{12} u_j^e \phi_j^e(y) = u_1^e \phi_1^e(y) + u_2^e \phi_2^e(y) + u_3^e \phi_3^e(y) + u_4^e \phi_4^e(y) + u_5^e \phi_5^e(y) + u_6^e \phi_6^e(y) + u_7^e \phi_7^e(y) + u_8^e \phi_8^e(y) + u_9^e \phi_9^e(y) + u_{10}^e \phi_{10}^e(y) + u_{11}^e \phi_{11}^e(y) + u_{12}^e \phi_{12}^e(y) \quad \text{Equation 7. 1}$$

Similarly, the transverse Z direction will have similar expression.

$$w^e|_z = \sum_{j=1}^{12} u_j^e \phi_j^e(z) = u_1^e \phi_1^e(z) + u_2^e \phi_2^e(z) + u_3^e \phi_3^e(z) + u_4^e \phi_4^e(z) + u_5^e \phi_5^e(z) + u_6^e \phi_6^e(z) + u_7^e \phi_7^e(z) + u_8^e \phi_8^e(z) + u_9^e \phi_9^e(z) + u_{10}^e \phi_{10}^e(z) + u_{11}^e \phi_{11}^e(z) + u_{12}^e \phi_{12}^e(z) \quad \text{Equation 7. 2}$$

The axial loading equation and axial torsion equation are shown below respectively.

$$u^e|_x = \sum_{j=1}^6 u_j^e \phi_j^e(x) = u_1^e \phi_1^e(x) + u_2^e \phi_2^e(x) + u_3^e \phi_3^e(x) + u_4^e \phi_4^e(x) + u_5^e \phi_5^e(x) + u_6^e \phi_6^e(x) \quad \text{Equation 7. 3}$$

$$\begin{aligned} \theta^e|_x &= \sum_{j=1}^2 \theta_j^e \phi_j^e(x_M) \\ &= \theta_1^e \phi_1^e(x_M) + \theta_2^e \phi_2^e(x_M) + \theta_3^e \phi_3^e(x_M) + \theta_4^e \phi_4^e(x_M) + \theta_5^e \phi_5^e(x_M) + \theta_6^e \phi_6^e(x_M) \end{aligned}$$

$$\text{Equation 7. 4}$$

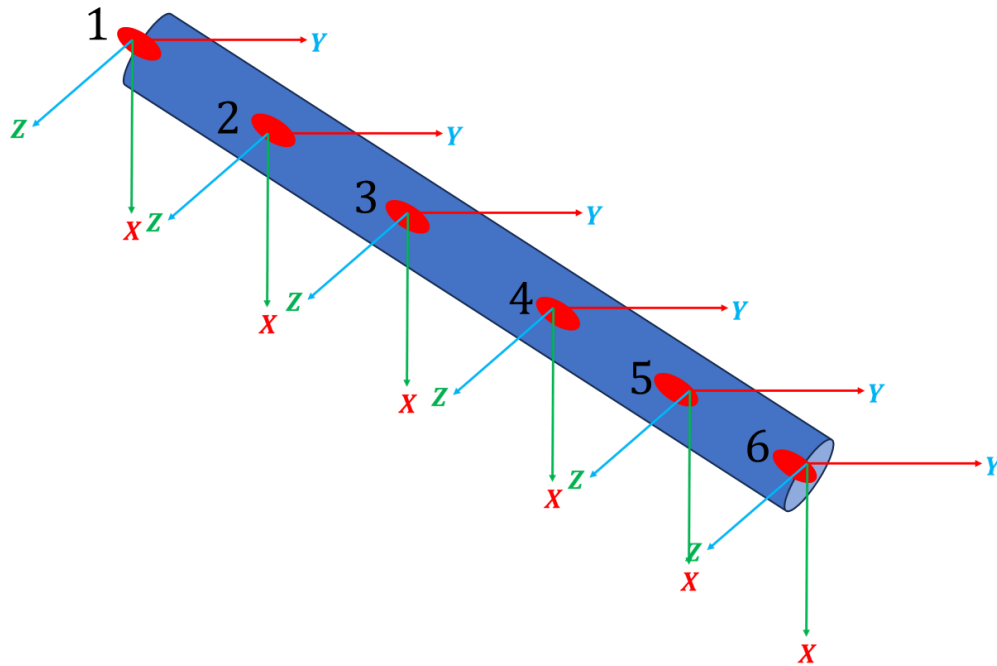


Figure 7. 3 Six Node System

The boundary conditions for the first and last node remain the same as that for a 2-node system. The challenge however is to find extra equations that will make it possible to calculate the extra constants in the equations. Since the 6-node system is a higher resolution into each element than the 2-node system, the expectation is that the error in the residuals for the 6-node system will drastically reduce compared to the 2-node system.

Another area of improvement would be the inclusion of whirling in the objective function for the optimized RPM. Whirling is a type of lateral vibration occurs when the drill string rotates disproportionately around the center line of the wellbore hole. There would be coupling of stick slip (torsional vibration) and whirling. According to interviews with drilling supervisors, whirling occurs more than 90 percent of the time and it is the main reason for tool damage. This thesis has setup a procedure to help mitigate stick slip. The same procedure can be followed to mitigate whirling in isolation or coupled with stick slip. The challenge in this is to fully model the behavior of the BHA as whirling occurs. A start point is to simulate the movement of the drill string from the perspective of the sensor placed on a position on the BHA.

References

- Aarsnes, Flø, U. J., Meglio, F. D., & Shor, R. J. (2018). Avoiding Stick Slip Vibrations through Intelligent Startup Trajectory Design. *Journal of Process Control*.
- Aryan, V. (2018). *Borehole Problems: Drilling Hydraulics*. Retrieved from Slideshare: <https://www.slideshare.net/Vvkr/borehole-and-drilling-problems>
- Ashfahani, A., Sulistiyo, S., & Hapsari, H. (2020). Dynamic Well Modeling, Where are We?: Mahakam Operation Experience for Well Diagnostics & Optimization . *SPE/IATMI Asia Pacific Oil & Gas Conference and Exhibition*. Bali, Indonesia: SPE.
- Beeh, H. A. (2017, Mrch 18). *Understanding Torque and Drag Models*. Retrieved from https://www.youtube.com/watch?v=Bv25XGkqHp4&t=1176s&ab_channel=PDPEgypt
- Bogaerts, M., Cardozo, j., Flamant, N., Giam, D., Villar, V., & Lehr, J. (2019). Novel 3D Fluid Displacement Simulations Improve Cement Job Design and Planning in the Gulf of Mexico . *Annual Technical Conference and Exhibition*. Calgary, Alberta, CA: SPE.
- Bradford, I. (2000). Drilling problems: Techniques aim at improving drilling performance. *Oil and Gas Journal*, 98, 22-23.
- Brekke, A. (2016). *Master's Thesis*. Retrieved from UiS : https://uis.brage.unit.no/uis-xmlui/bitstream/handle/11250/2408854/Brekke_Alexander.pdf?sequence=1&isAllowed=y
- Budynas-Nisbett. (2011). *Shigley's Mechanical Engineering Design*. New York : McGraw-Hill.
- Caicedo, Calhoun, & Ewy. (2005). Unique Bit Performance Predictor Using Specific Energy Coefficients As a Function of Confined Compressive Strength Impacts Drilling Performance. *18th World Petroleum Congress*. Johannesburg.
- Calhoun, W., Caicedo, H., & Ewy, R. (2008). *Method for predicting rate of penetration using bit-specific coefficients of sliding friction and mechanical efficiency as a function of confined compressive strength*. Retrieved from Google Patents: <https://patents.google.com/patent/EP1836509B1/en>

- Daireaux, B., Ambrus, A., Carlsen, L., Mihai, R., Gjerstad, K., & Balov, M. (2021). Development, Testing and Validation of an Adaptive Drilling Optimization System. *SPE/IADC International Drilling Conference and Exhibition*. Virtual: SPE.
- Depouhon, A., & Detournay, E. (2015). Stick-slip instabilities in rotary drilling systems. *49th US Rock Mechanics / Geomechanics Symposium*. San Francisco, CA, USA: ARMA.
- DrillingManual. (2017, November 05). *Drilling Torque & Drag | Drag Calculations*. Retrieved from Drilling Manual: <https://www.drillingmanual.com/drilling-torque-and-drag-calculations-excel-spreadsheet/>
- Dushaishi, Nygaard, Hoel, Andersen, & Hellvik. (2015). Post Well Vibration Analysis in the North Sea: A Tool to Understand Drilling Performance. *34th International Conference on Ocean, Offshore and Arctic Engineering*. ASME.
- Eland, C. (2021). *In Oil & Gas what is upstream and downstream?* Retrieved from Eland Cables: <https://www.elandcables.com/the-cable-lab/faqs/faq-what-are-upstream-and-downstream-works-in-the-oil-gas-industry>
- Etaje, D. (2018). *Identifying the Optimum Zone for Reducing Drill String Vibrations*. Calgary: University of Calgary PRISM Repository.
- Fabain, R. T. (1994). Confined compressive strength analysis can improve PDC bit selection. [Polycrystalline Diamond Compact]. *Oil and Gas Journal; (United States)*.
- Franca, L. F. (2011, July). *A bit-rock interaction model for rotary-percussive drilling*. Retrieved from International Journal of Rock Mechanics and Mining Sciences: <https://doi.org/10.1016/j.ijrmms.2011.05.007>
- Gilbert, W. (1954). Flowing and Gas-Lift Well performance. In *Drill. & Prod. Prac* (pp. 126–57). Dallas, Texas: API.
- Hanley, C., Stuart, S., Bass, C., & Garcia, A. (2012). Development of a Software System for Drilling Optimization using Surface and Downhole Drilling Data Modeling a Human Process for Drilling Optimization. *IADC/SPE Asia Pacific Drilling Technology Conference and Exhibition*. Tianjin, China: SPE.

- Hargrave, M. (2022, July 21). *Day Rate (Oil Drilling) Definition*. Retrieved from Investopedia: <https://www.investopedia.com/terms/d/day-rate-oil-drilling.asp>
- Harvey, B. (2018). Drilling Simulations Enhance Well Planning and Drilling Decisions. *Engineering Reality Magazine*, Vol. 8, 48-51.
- Hassanzadeh, H., & Pooladi-Darvish, M. (2007). Comparison of different numerical Laplace inversion methods for engineering applications. *Elsevier Inc.*
- Herbig, C., Christian, L., Reckmann, H., Hohl, A., Heinisch, D., Boyd, A., . . . Murphy, S. (2016). Reaming and Drilling Practice Optimization using Modeling and Simulation Techniques . *SPE Deepwater Drilling and Completions Conference*. Galveston, Texas, USA: SPE.
- Hossain, M. E. (2015). Drilling Costs Estimation for Hydrocarbon Wells. *J. Sustainable Energy Eng., Vol. 3, No. 1, September 2015*.
- Katsikadelis, J. T. (2020). *Dynamic Analysis of Structures*. Elsevier.
- Konstantin, P. (2013). Well Flow Dynamic Modelling – the Tool to Optimize Well Operations. *SPE Arctic and Extreme Environments Technical Conference and Exhibition*. Moscow, Russia: SPE.
- Liu, H., Shor, R., & Park, S. (2019). Intelligent Wellbore Path Estimation Using Multiple Integrated MEMS Sensors. *SPE/IADC International Drilling Conference and Exhibition*. The Hague, The Netherlands: Society of Petroleum Engineers.
- Liu, Y., Ma, T., Chen, P., & Yang, C. (2018). Method and apparatus for monitoring of downhole dynamic drag and torque of drill-string in horizontal wells. *Elsevier Journal of Petroleum Science and Engineering*, 320-332.
- Mach, J., Proano, E., & Brown, K. (1979). A Nodal Approach for Applying Systems Analysis to the Flowing and Artificial Lift Oil or Gas Well. *SPE*.
- Menand, S., Sellami, H., Tijani, M., Stab, O., Dupuis, D., & Simon, C. (2006). Advancements in 3D Drillstring Mechanics: From the Bit to the Topdrive. *IADC/SPE Drilling Conference*. Miami, Florida, USA: SPE.
- Morley, A. (1961). *Strength of Materials 11th Edition*. William Cloves and Sons.

- Najmi, N. F., Soh, A., Nair, D. G., Zaim, M. A., James, B., Subroto, B., & Omar, T. (2015). Advanced FEA Modeling Delivers Solution for Designing a Dual Hole Opening BHA for a Single Directional Run. *SPE/IADC Drilling Conference and Exhibition*. Society of Petroleum Engineers.
- Okpozol, P., Peters, A., & Okologume, W. (2016). DIRECTIONAL WELL TRAJECTORY DESIGN: THE THEORITICAL DEVELOPMENT OF AZIMUTH BENDS AND TURNS IN COMPLEX WELL TRAJECTORY DESIGNS. *Nigerian Journal of Technology*, 831-840. Retrieved from DOI:10.4314/njt.v35i4.18
- Pastusek, P., Payette, G., Shor, R., Cayeux, E., Aarsnes, U. J., Hedengren, J., . . . Liu, Y. (2019). Creating Open Source Models, Test Cases, and Data for Oilfield Drilling Challenges. *SPE/IADC International Drilling Conference and Exhibition*. The Hague, The Netherlands: Society of Petroleum Engineers.
- Pegasus Vertex. (2022). *Drilling Software*. Retrieved from Common Drilling Problems: www.pvisoftware.com/infographics
- Reddy, J. (2005). *An Introduction to the Finite Element Method*.
- Reza, M., & Alcocer, C. (1986). A Unique Computer Simulation Model Well Drilling: Part I - The Reza Drilling Model. *SPE California Regional Meeting*. Oakland, California: SPE.
- Richardson, T., Gernay, C., & Detournay, E. (2007). A simplified model to explore the root cause of stick-slip vibrations in drilling systems with drag bits. *Journal of Sound and Vibration*, 432-456.
- Sahal, A. R., & Al-Zubaidi, N. S. (2021). Analysis of Torque and Drag in Abu Ghirab Horizontal Well Using Landmark (WellPlan) Software. *Association of Arab Universities Journal of Engineering Sciences*.
- Sampaio, J. H. (2007). Planning 3D Well Trajectories Using Spline-in-Tension Functions. *Journal of Energy Resources Technology*, 289-299.
- Samuel, R., Kumar, A., Gonzales, A., Marcou, S., & Rød, A. M. (2016). Solving the Casing-Wear Puzzle Using Stiff-String Model . *JPT of Management*.

- Shor, R. (2019, September). *ENPE 627 L01 Fall 2019*. Retrieved from University of Calgary D2L: <https://d2l.ucalgary.ca/d2l/le/content/276679/fullscreen/3634074/View>
- SoftDrill NL. (2023). *Friction factors*. Retrieved from Softdrill NL Torque & Drag: <https://www.softdrill.nl/help/tdrag/index.htm?context=150>
- Sparks, C. (2007). *Fundamentals of Marine Riser Mechanics: Basic Principles and Simplified Analyses*. Tulsa, Oklahoma: Penn Well Corporation.
- StudentEnergy. (2022). *WHAT IS DRILLING?* Retrieved from Student Energy: <https://studentenergy.org/production/drilling/#:~:text=Oil%20Transport-,What%20is%20Drilling%3F,exploration%20purposes%20in%20new%20areas>.
- Wang, Y. (2022). Simulating Wellbore Integrity During Drilling in Gas Hydrate Bearing Sediments by Coupled THMD Model. *56th U.S. Rock Mechanics/Geomechanics Symposium*. Santa Fe, New Mexico, USA: ARMA.
- Williams, A. (2009). *Structural Analysis*. Retrieved from <https://engineering.stackexchange.com/questions/15040/how-to-determine-fixed-end-moment-in-beam>
- Wilson, J., & Heisig, G. (2015). Investigating the Benefits of Induced Vibrations in Unconventional Horizontals via Nonlinear Drill String Dynamics Modeling. *SPE/IADC Drilling Conference and Exhibition*. London, United Kingdom: Society of Petroleum Engineers.
- Xiaozhen, S. (2013). *Common Hidden Dangers and Remedies of Inside Blowout Preventers (IBOPs)*. Oxford UK: Elsevier.

Appendix

The appendix are the codes of 3 MATLAB functions used to interpolate well plan data.

Appendix 1 How to Interpolate Measured Depth, Inclination and Azimuth

```
function [I_x,A_x]=findIncAzi(MD,beti,inc,azi,Course_Factor)
% MD is one value 1 by 1 from the measured depth data. It is not in the
% well plan data so the corresponding inclination and azimuth values are
% not given
% beti, inc, and azi are the measured depth, inclination and azimuth data
% from the well plan
% Course_Factor is 100 for field units and 30 for SI units
% I_x and A_x are the corresponding inclination and azimuth for depth MD
% the simulation is used to calculate I_x and A_x for several values of MD
% it is better to start beti,inc,azi from the surface for more accurate
% results
[aa,pp]=find(beti<MD);
[aaa,ppp]=find(beti>MD);
szAA=size(aa,1);
szAAA=size(aaa,1);
if szAA>0
    MD11=beti(aa);
    In11=inc(aa);
    In1=In11(end,1);
    AZ11=azi(aa);
    AZ1=AZ11(end,1);
else
    MD11=0;
    In1=0;
    AZ1=0;
end
if szAAA>0
    MD22=beti(aaa);
    In22=inc(aaa);
    In2=In22(1,1);
    AZ22=azi(aaa);
    AZ2=AZ22(1,1);
else
    MD22=0;
    In2=0;
    AZ2=0;
end
MD1=MD11(end,1);
MD2=MD22(1,1);
% Build
Build2=(Course_Factor/(MD2-MD1))*(In2-In1);
Turn2=findTurn(Course_Factor,AZ1,AZ2,MD2,MD1); % findTurn is a function to calculate
Turn shown at the end of this function
if In1==In2 && AZ1==AZ2 % No Build No Turn
    I_x=In1;
    A_x=AZ1;
elseif In2>In1 && AZ1==AZ2 % Build Only
    I_x=In1+((Build2/Course_Factor)*(MD-MD1));
```

```

    A_x=AZ1;
elseif In2==In1 && AZ1~=AZ2 % Turn Only
    I_x=In1;
    A_x=findAzi(Course_Factor,AZ1,AZ2,Turn2,MD,MD1); % findAzi is a function to
    calculate the next azimuth shown at the end of this function
elseif In2<In1 && AZ1==AZ2 % Drop Only
    I_x=In1-((Build2/Course_Factor)*(MD-MD1));
    A_x=AZ1;
elseif In2>In1 && AZ1~=AZ2 % Build and Turn
    I_x=In1+((Build2/Course_Factor)*(MD-MD1));
    A_x=findAzi(Course_Factor,AZ1,AZ2,Turn2,MD,MD1);
elseif In2<In1 && AZ1~=AZ2 % Drop and Turn
    I_x=In1-((Build2/Course_Factor)*(MD-MD1));
    A_x=findAzi(Course_Factor,AZ1,AZ2,Turn2,MD,MD1);
end
end
%% Turn
function Turn_n=findTurn(Course_Factor,An_1,An_2,Mn_2,Mn_1)
% The goal is to calculate turn between two azimuth points given their
% corresponding measured depth
% An_1 is azimuth of first survey point
% An_2 is azimuth of second survey point
% Mn_1 is measured depth at survey point 1
% Mn_2 is measured depth at survey point 2
if An_2>An_1
    y1=abs(360-An_2);
    y2=y1+An_1;
    y3=An_2-An_1;
    if y2<y3
        difT=y2;
    elseif y2>=y3
        difT=y3;
    end
elseif An_2<An_1
    y4=abs(360-An_1);
    y5=y4+An_2;
    y6=An_1-An_2;
    if y5<y6
        difT=y5;
    elseif y5>=y6
        difT=y6;
    end
elseif An_2==An_1
    difT=0;
end
Turn_n=(Course_Factor/(Mn_2-Mn_1))*(difT);
end
% find Azimuth
function An_x=findAzi(Course_Factor,An_1,An_2,Turn_n,Mn_x,Mn_1)
% The goal is to find the interpolated azimuth between two azimuth in the
% well plan data
% An_1 is azimuth of point 1
% An_2 is azimuth of point 2
% Turn_n is the turn between point 1 and point 2
% Mn_x is the measured depth for which an azimuth is to be assigned

```

```

% Mn_1 is the measured depth of point 1
% Note that this function is used in a loop to calculate An_x...there may
% be conditions that does not need this function
difA=(Turn_n/Course_Factor)*(Mn_x-Mn_1);
if An_2>An_1
    y1=abs(360-An_2);
    y2=y1+An_1;
    y3=An_2-An_1;
    if y2<y3
        if difA>An_1
            An_x=360-(difA-An_1);
        elseif difA<=An_1
            An_x=An_1-difA;
        end
    elseif y2>=y3
        An_x=difA+An_1;
    end
elseif An_2<An_1
    y4=abs(360-An_1);
    y5=y4+An_2;
    y6=An_1-An_2;
    y7=360-An_1;
    if y5<y6
        if difA>=y7
            An_x=difA-y7;
        elseif difA<y7
            An_x=An_1+difA;
        end
    elseif y5>=y6
        An_x=An_1-difA;
    end
elseif An_2==An_1
    An_x=An_1;
end
end

elseif y5>=y6
    An_x=An_1-difA;

end

elseif An_2==An_1
    An_x=An_1;

end
end

```